BIOMECHANICS OF THE KNEE JOINT: HIGH TIBIAL OSTEOTOMY SURGERY

by

Denis J. DiAngelo, M. Eng., B.A.Sc.

A Thesis

Submitted to the School of Graduate Studies

in Partial Fulfilment of the Requirements

for the Degree

Doctor of Philosophy

McMaster University

March, 1993

BIOMECHANICS OF THE KNEE JOINT: HIGH TIBIAL OSTEOTOMY SURGERY

Dedicated to my wife Sue
and children Nicholas and Emily.

Doctor of Philosophy (1993)
(Mechanical Engineering)

McMASTER UNIVERSITY
Hamilton, Ontario

TITLE: Biomechanics of the Knee Joint:
High Tibial Osteotomy Surgery

AUTHOR: Denis J. DiAngelo, B.A.Sc. (University of Waterloo)
M. Eng. (McMaster University)

SUPERVISOR: Professor W.R. Newcombe

NUMBER OF PAGES: xx, 329

ABSTRACT

Alignment deformities at a knee joint having unicompartmental osteoarthritis increase the stress level of the affected compartment and the progression of the disease. The biomechanical integrity of the knee joint can be restored through osteotomy surgery of the proximal tibia, and is believed to retard the advancement of the disease.

This research attempted to quantify the biomechanics of high tibial osteotomy surgery for correction of a varus knee deformity. Both elements of analytical and experimental modelling were completed. A two dimensional trigonometric model of the lower extremity was formulated that provided a more precise method of analyzing and forecasting the changes to the knee and limb orientations following osteotomy surgery.

The experimental work resulted in two novel and original contributions: 1) the design of a direct measurement system for local dynamic contact pressures in the knee joint and 2) the retrofitting of an existng (non-operative) joint simulator. Measurement of the contact area and pressure patterns of the medial compartment was determined for three different knee alignment configurations (neutral, varus and post-osteotomy). Alterations to the joint alignment did not affect the contact area patterns of the medial compartment. Comparison of the contact pressure patterns showed that simulation of a varus deformity increased loading on the medial compartment, whereas the simulated post-osteotomy alignment increased loading along the intercondylar eminence, by redirecting the load inward, towards the joint centre.

ACKNOWLEDGEMENTS

I would like to express my appreciation to the following individuals who have contributed to the completion of this research:

- Professor W. Roy Newcombe of the Mechanical Engineering Department at McMaster University, for his continued guidance and supervision throughout the course of this work,
- Joe Verhaeghe, an electrical technician with the Mechanical Engineering Department at McMaster University, for without his expertice and knowledge of electronics, the joint simulator would have most likely remained in a nonoperative state.
- Dr. Ian J. Harrington of the Toronto East General and Orthopaedic Hospital for the opportunity to utilize the joint simulator in this research,
- Dr. Trevor C. Hearn of the Sunnybrook Health Science Centre for access to the Biomechanics Research Laboratory at Sunnybrook,
- Dr. Albert Schopfer and Dr. Mark Vrahas for their assistance in the retrieval and preparation of the knee joint specimens, and for the assessment of the joint pathology,
- Lastly, to my wife, Sue, and children Nicholas and Emily, whose continued understanding, support and care provided the incentive to complete this research.

TABLE OF CONTENTS

Table of Contents (continued) PAGE

Table of Contents (continued) PAGE

Table of Contents (continued) PAGE

Table of Contents (continued) PAGE

LIST OF TABLES

List of Tables (continued) PAGE

LIST OF FIGURES

List of Figures (continued) PAGE

List of Figures (continued) PAGE

List of Figures (continued) PAGE

List of Figures (continued) PAGE

List of Figures (continued) PAGE

List of Figures (continued) PAGE

GLOSSARY OF MEDICAL TERMS

Arthritis: inflammation of a joint, usually accompanied by pain, and frequent changes to its structure.

Arthroplasty: surgical formation or reformation of a joint.

Articular cartilage: hyaline or translucent matrix of connective tissue that covers the mating surfaces of bone.

Biomechanics: the knowledge and methods of mechanics applied to structure and function of the living biological system.

Distal: furthest from the point of attachment or centre of body.

Femur: bone that extends from the hip joint to the knee joint, and is the longest and strongest bone in the skeleton.

Gait: manner of walking.

Goniometer: apparatus used to measure joint movements and angles.

In vitro: test done in the laboratory rather than in a living organism.

In vivo: in the living body or organism.

Lateral: pertains to the side of the body, ie. furthest from the centre line of the body.

Medial: nearer to the body of attachment, centre of the body or point of reference.

Morphometry: measurement of forms of organisms.

Orthopaedics: branch of medical science that deals with prevention or correction of disorders involving locomotor structures of the body.

Osteoarthritis: chronic degenerative joint disease, characterized by the destruction of the articular cartilage, with overgrowth of bone and impaired joint function.

Osteophytes: outgrowth of bone or loose bodies.

Osteotomy: the operation for cutting through bone.

Proximal: nearest the body of attachment, centre of the body or point of reference.

Glossary of Medical Terms (continued)

Radiograph: x-ray photograph, produced on a photographic plate or film by the action of roentgen rays or radium.

Subluxation: a partial or incomplete dislocation.

Synovial: lubricating fluid of the joints.

Tibia: the inner and larger bone of the lower leg connecting the knee joint and ankle joint.

Tibiofemoral: relationship between the tibia and femur bones.

Valgus knee deformity: inward displacement of the knee relative to the hip and ankle joints, producing a knee - knocking appearance.

Varus knee deformity: outward displacement of the knee relative to the hip and ankle joints, producing a bow - legged appearance.

CHAPTER 1.0

INTRODUCTION

Osteoarthritis, OA, is a chronic, degenerative joint disease characterized by the destruction of the articular cartilage and overgrowth of bone at the joint surfaces. Approximately ten million people in the United States experience pain related to arthritis and at least ninety percent of the people over sixty years of age exhibit signs of OA [46]. Any malalignment of adjacent limb segments will increase the stress distribution at the affected compartment surface, and is thought to enhance the progress of OA.

Osteoarthritis of the knee joint is affected by the malalignment between the tibia and femur, and ranks third in frequency to that of the spine and hip [85]. A successful surgical technique carried out to correct an alignment deformity at the knee joint is the high tibial osteotomy. This procedure is suitable for knee joints having severe unicompartmental arthritis with some degree of angular deformity. It has been hypothesized that the osteotomy realigns the segments and redistributes the loads across the joint surface, thereby allowing the cartilage to regenerate and return the joint to a more normal, healthy state [22,33,34,60,69,81,82,83,103].

Current research on knee joint biomechanics has established contact area patterns of the tibial plateau surface for static loading and complete knee extension orientations. Minimal information is available on the dynamic behaviour of the knee joint, other than that

obtained from gait laboratory studies [58,73,115].

Knee simulators have been designed to test artificial implants for component failure. However, the equipment has not been employed to investigate the mechanics of high tibial osteotomy surgery. Furthermore, simulation studies of total knee replacements can not provide any information on the contact behaviour at the level of the articular cartilage surface, nor can they analyze the effects of a knee alignment deformity.

The objective of this work will be to carry out an investigative study which will help to quantify the functionality of the high tibial osteotomy. This will involve both experimental work and analytical modelling. The modelling phase involves the formulation of a trigonometric model of the lower extremity that analyzes the effect of osteotomy surgery on knee alignment and kinematics. The model provides a more precise method of analyzing and forecasting the changes to the joint and limb orientations, as well as, any changes made to the limb lengths. The aim is to have the orthopaedic surgeon utilize the model during the preoperative planning stages of osteotomy surgery and increase the post - operative success rate.

Any limitations in the outcome of the surgery or errors associated with the use of conventional surgical methods can be identified and resolved with the model. Finally, the model will calculate the correct size and location of the bone wedge to be removed in order to maximize the area of contact and maintain proper joint alignment. Two case studies are carried out to demonstrate the model, and involve the close wedge and dome osteotomy procedures.

The experimental phase requires the development and implementation of a measurement system that will monitor the transient pressure distribution patterns between the articulating surfaces of the knee, and identify the contact area zones on the medial compartment, for known applied external forcing functions and knee motion patterns. Three different knee alignment conditions are simulated: neutral alignment, 20° varus tibiofemoral alignment, and post - osteotomy alignment.

To simulate the dynamic motion of the leg during walking, an existing test apparatus was selected, but required extensive modifications and further development of the equipment to provide the controlled joint kinematics, and apply a time varying load across the joint. The control system for the test equipment consisted of a microcomputer, two dedicated microprocessors, and three stepper motors with translators. A computer software package permited specification of limited knee motion patterns. However, unforeseen controller problems and shortage of funds prevented tests previous to this work from being carried out. To resolve these problems, modifications to the existing computer software and hardware systems were completed.

Tests were carried out on cadaveric knee specimens for prescribed knee motion patterns. The different knee alignment configurations will be simulated by altering the orientation and position of the femur and tibia. The proposed trigonometric model is used to determine the necessary adjustments to the limb orientation and position. Review of the contact area and pressure patterns associated with the different knee alignment configurations is performed to

determine if a relationship exists between the lower limb alignment and the response characteristics at the articular surface.

CHAPTER 2.0

THE KNEE JOINT

2.1 Anatomical Description

The knee can be classified as a synovial weight-bearing joint consisting of two articulating surfaces: the femoral condyles and tibial plateaus. Figures 2.1 and 2.2 illustrate the anterior and posterior views of the knee joint, respectively. The mating surfaces are covered with articular cartilage interposed by the menisci. Articular cartilage is a biphasic material consisting of a solid matrix (≅ 20% by weight), and an interstial fluid phase (≅ 80%), comprised mostly of water (Guilak et al. [55]). Articular cartliage also exhibits a stress relaxation behaviour, where the thickness of the cartilage will vary with time and rate of loading (Kwan, [93]).

The menisci have a fibrocartilage structure with the fibres mainly oriented circumferentially (Bullough [20]) to better resist hoop or circumferential stresses. Injury to the menisci typically involves separation of these fibrils. The medial meniscus has a semilunar shape, with a larger radius of curvature than the lateral one. The lateral meniscus is circular in appearance and covers a greater portion of the lateral compartment. Both mensici attach to the tibia along the periphery of the joint and at the base of the intercondylar eminence. Besides filling the gap generated by the convexity of the femoral condyles, the menisci protect the wall of the joint capsule against impingement between the articulating bones and serve to distribute the

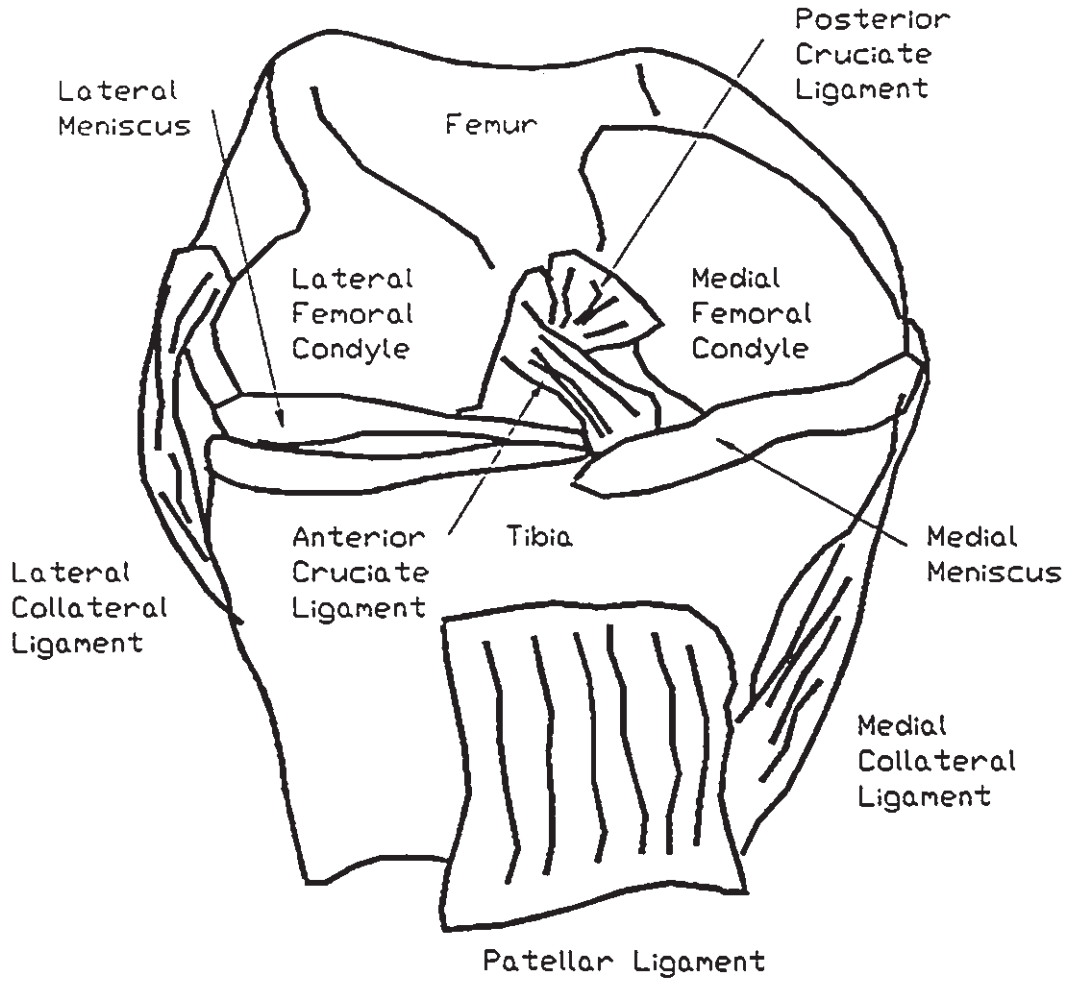

Figure 2.1 Anatomical features of the knee joint: Anterior view.

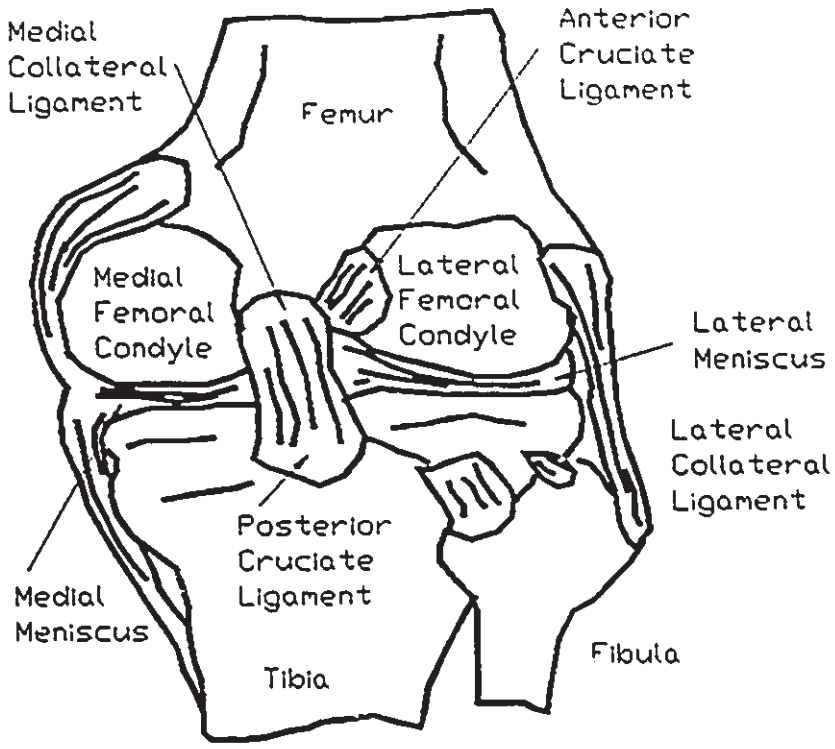

Figure 2.2: Anatomical features of the knee joint: Posterior view.

loads across the joint surface.

The biomechanical integrity of the joint is maintained by the surrounding musculature and ligamentous structure. The main muscle groups are the quadriceps, gastrocnemius and hamstrings, and the ligament groups are the medial and lateral collateral ligaments and anterior and posterior cruciate ligaments.

2.2 Morphometrical Anatomy of the Knee

Morphometrical measurements of knee geometry are an integral part of establishing design criteria for total knee replacements, and to identify surgical cutting planes for lower limb osteotomy surgery (Elias et al. [40], Erkman and Walker [47], Kurosawa et al. [92], Rehder [133], Yoshioka et al. [174]). Relevant anatomical data was collected from the knee specimens employed in this study , as well as data referenced in the literature. A partial listing is provided in tables 2.1 and 2.2, and illustrated in figure 2.3.

Engelbrecht et al. [42], Erkman and Walker [47], and Kurosawa et al. [92] measured cadaveric knee specimens to determine an average range of sizes suitable for prosthetic knee design, based on the width and depth of the tibial plateau, and the width, depth and height of the femoral condyles. Data extracted from their studies are detailed in table 2.2, and correlated well with similar measurements taken from the cadaver knee specimens used in this study.

Elias et al. [40] suggested modelling the posterior femoral condyles as spheres of radius 21 mm, and was found to be accurate to within 1-2 mm over 90°of knee flexion. Values of 21 mm and 19 mm,

respectively, were determined by Kurosawa and Walker [92] for the same parameters, and also estimated the centre to centre distance between tibial compartments to be 46 mm.

Recent trends in analytical modelling of the knee have also used this data to analyze the kinematic and dynamic behaviour of the joint, as well as to establish a range of average or normal values of the alignment of the lower limb. Furthermore, many of the surgical procedures for corrective alignment surgery and implant surgery require information on the lower limb alignment.

In this research study, the morphometrical data will be included in both the experimental work and the analytical modelling analysis. An estimate of the size and shape of the medial tibial plateau surface will be required in order to design a new measurement device that can be inserted into the joint capsule and monitor the contact behaviour. The modelling analysis will require information on the limb alignment to predict the spatial differences between a neutrally aligned joint and a malaligned joint, as well as the new position of the joint following osteotomy surgery.

Table 2.1: Morphometrical Measurements of the Knee Joint: Cadaveric Specimens used in this Study

Specimen Number/ Gender	Tibial Plateau* Measurements (mm)					Femoral Condyle* Measurements (mm)										
	1	2	3	4	5	1	2	3	4	5	6	7	8	9	10	11
1 / M	40	33	78	54	47	22	24	11	31	31	25	24	80	91	56	3
2 / M	42	32	78	55	46	23	27	11	31	31	25	24	80	89	61	3
3 / M	39	27	79	58	49	25	24	11	28	29	22	23	79	87	65	3
4 / M	39	31	77	56	48	22	26	10	31	29	25	23	79	91	62	3
5 / F	37	29	71	46	45	26	22	11	27	26	22	22	70	84	55	2.5
6 / F	36	30	70	46	44	18	23	12	27	25	20	21	69	76	54	2.5
7 / M	37	25	74	51	49	20	25	10	27	27	21	20	71	79	55	3
8 / M	39	23	75	49	47	20	26	10	27	27	25	22	69	79	56	3
Average	1	2	3	4	5	1	2	3	4	5	6	7	8	9	10	11
Male	39	29	77	54	48	22	25	11	29	29	24	23	76	86	59	3
Female	37	30	71	46	45	22	22	12	27	26	21	22	70	80	55	2.5

* Legend numbering corresponds to Figure 2.3 with values rounded off to the nearest mm, except for the cartilage thickness, ie. (11): ± 0.5 mm.

M: Male; F: Female

Table 2.2 : Morphometrical Measurements of the Knee Joint:
Referenced Data from Other Studies

Specimen Number/ Gender	Tibial Plateau* Measurements (mm)					Femoral Condyle* Measurements (mm)										
	1	2	3	4	5	1	2	3	4	5	6	7	8	9	10	11
[40]	na	na	na	na	na	na	na	na	na	na	21	24	na	na	na	na
[42]	na	na	na	43	47	na	na	na	25	23	na	na	81	na	na	na
[47]/M	30	na	75	44	44	23	23	na	na	na	30	27	na	na	64	na
[47]/F	26	na	66	39	39	20	21	na	na	na	28	25	na	na	58	na
[92]											21	19	92			
[174]/M	na	na	na	31	32	na	na	na	na	na	na	na	83	90	72	na
[174]/F	na	na	na	28	27	na	na	na	na	na	na	na	72	80	65	na

* Legend numbering corresponds to Figure 2.3 with values rounded off to the nearest mm, except for the cartilage thickness (11): ± 0.5 mm.

na: data not available.

M: Male; F: Female

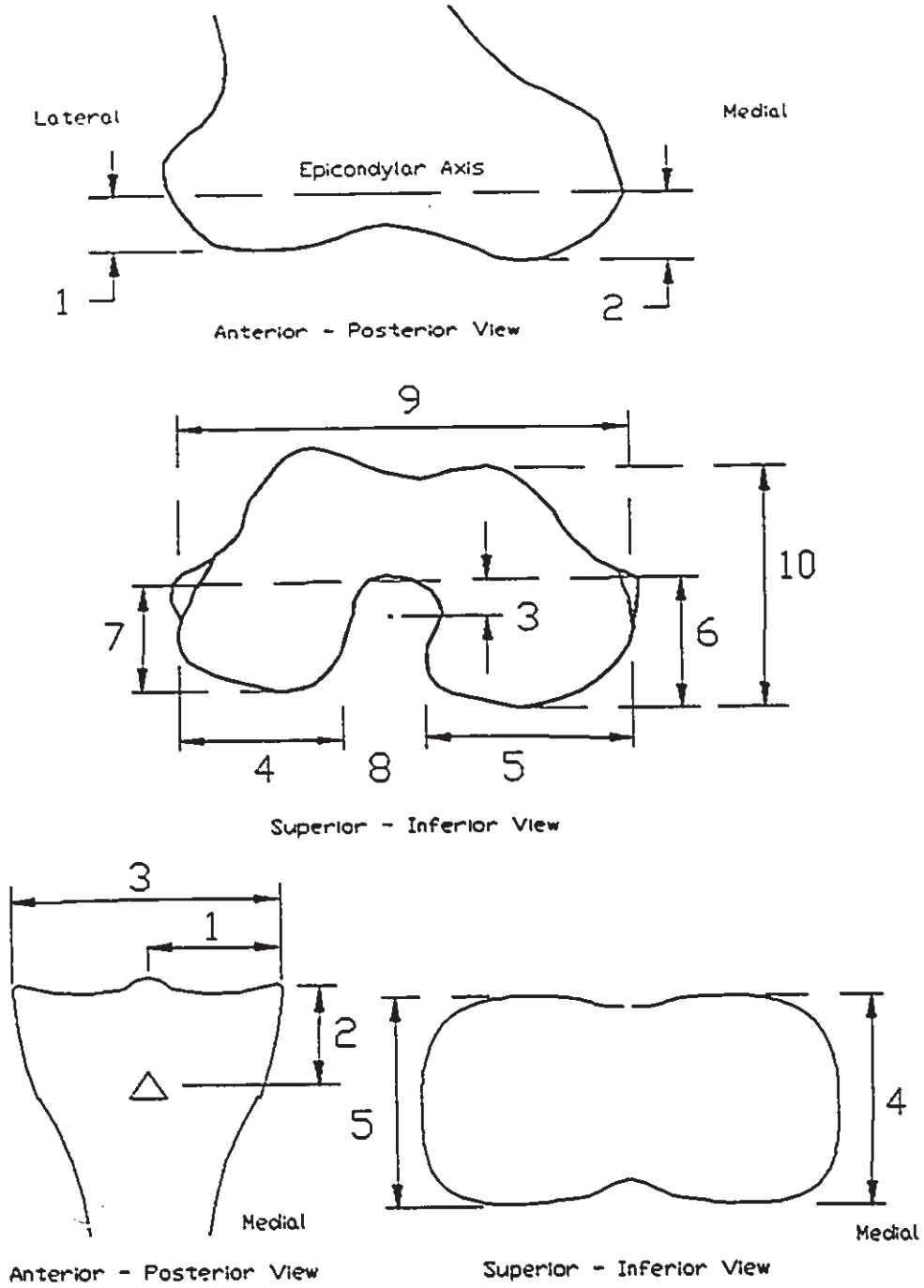

Figure 2.3: Morphometrical measurements of the femoral condyles and tibial plateau. Reference numbers correspond to dimensions given in Tables 2.1 and 2.2.

2.3 Knee Joint Pathology

Various forms of knee joint pathologies exist. Some of the more common types are listed below.

1. Rheumatoid Arthritis is a systemic disease of unknown cause characterized by inflammatory changes in the joint and related structures.
2. Osteochondritis involves the inflammation of bone and cartilage, and can be caused by loose bodies inside the joint capsule.
3. Osteomyelitis is also characterized by inflammation of bone, especially the bone marrow, and is caused by a pathogenic organism.
4. Osteoarthritis is a chronic disease affecting the synovial joints and is characterized by the destruction of the articular cartilage, overgrowth of bone with lipping and spur formation and impaired joint function.
5. Angular Deformity of the lower limb segments alters the joint alignment and zones of contact area between the articulating surfaces. This can create conditions of overstressing or understressing of the cartilage and bone. Severe deformity can also reduce the joint stability and range of motion.

High tibial osteotomy surgery is often recommended for knee joints having a combined angular deformity and unicompartmental OA.

2.3.1 Osteoarthritis

Osteoarthritis is a noninflammatory degenerative disease of the weight-bearing synovial joints and can be considered as one of man's oldest and most common diseases [46]. The disease is predominant in

aging adults and is associated with abnormal joint mechanics, injuries, excessive cartilage wear due to high stress at the joint and certain metabolic disorders that affect articular cartilage. Osteoarthritis can be classified as either primary or secondary; primary or idiopathic OA has no apparent cause, whereas secondary OA occurs in joints with preexisting abnormality. Pain is the primary sympton for both forms, however, the magnitude of pain is not always related to the degree of damage in the joint. Secondary OA can also show the following signs : 1) joint enlargement or bone spur formation, 2) loss of joint mobility and/or stability due to osteophytes or loose bodies, 3) incongruity between mating surfaces and 4) joint deformity causing subluxation, bone cysts, bony overgrowth or subchondral bone loss.

2.3.2 Angular Deformity

Whether OA is a result of a mechanical alignment problem or a biological imbalance remains undecided. Nevertheless, researchers agree that joint malalignment contributes to the advancement of OA [31,32,60,73,81,85,105,132]. Coventry [33] stated that if the primary cause of unicompartmental arthritis of the knee joint was due to changes in the normal tibiofemoral alignment and excessive loading at the joint, then the treatment must involve mechanical principles. Furthermore, the osteotomy does not cure the arthritis, but it does improve the biomechanical integrity of the joint by transferring the load from the diseased portion to the relatively healthy portion [32].

Once degeneration of the articular cartilage starts, the knee alignment can change, and thus create an abnormal distribution of forces

on the medial or lateral tibial plateaus. The affected side will be subjected to higher magnitudes of stress than that occurring in the normal situation and will lead to further degeneration of that side, plus further angular deformity. This forms a continuous open cycle which can only be controlled by mechanically altering the joint geometry.

When reviewing the various surgical techniques employed to correct a malalignment, one must understand the axis system used to describe the deformity. The anatomical and mechanical axes of the lower extremity are the most common reference systems employed to describe the biomechanical alignment. The anatomical axis of the femur consists of a line through the centre of the femoral shaft passing through the knee centre, whereas the the anatomical axis of the tibia passes through the knee centre down the centre of the tibial shaft. At the intersection of these axes is the anatomical tibiofemoral angle. This angle becomes difficult to estimate because of curves along the length of the bone shafts and cannot account for any malunions or abnormalities in the proximal femur, along the femoral and tibial shafts, or at the ankle joint [132,162].

The mechanical axes of the femur and tibia do, however, account for these abnormalities. The femoral axis is defined as a line passing between the centre of the femoral head and the centre of the femoral condyles, whereas the tibial mechanical axis joins the centre of the tibial plateau to the centre of the ankle joint. At the intersection of the mechanical axes is the mechanical tibiofemoral angle. The two different axes systems are shown in figure 2.4, along with the two

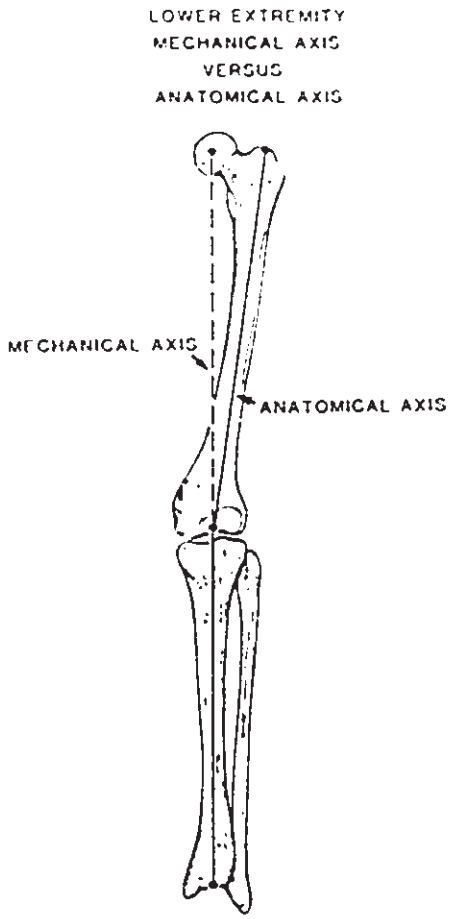

Figure 2.4: Lower extremity anatomical axes versus mechanical axes [105].

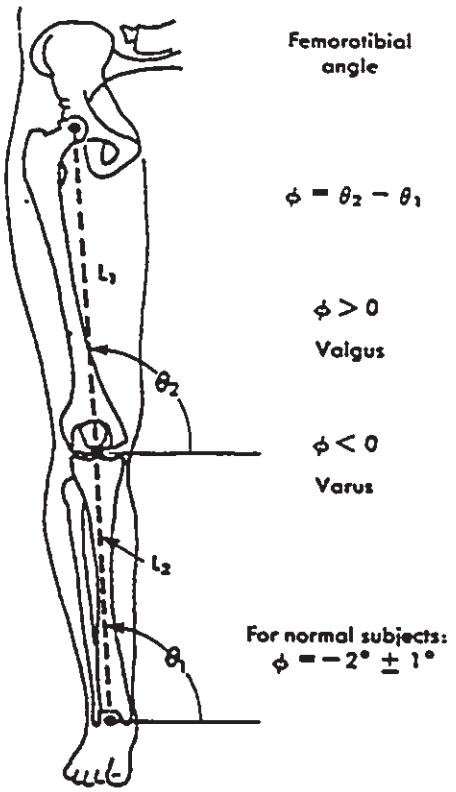

Figure 2.5: Definition of mechanical tibiofemoral angle [25].

definitions of the tibiofemoral angle. A normally aligned knee joint has a 0° offset between the mechanical axes of the femur and tibia. As well, a deviation of 5° to 7° typically exists between the anatomical and mechanical axes of the femur.

An alternate technique of quantifying the lower limb alignment was given by Chao [25]. An angle , ϕ, was defined as the difference between the angle enclosed between a horizontal datum line and the mechanical axis of the femur, θ_2 in Figure 2.5, and a second angle formed between the horizontal datum line and the mechanical axis of the tibia, θ_1. The advantage of this technique was that the lower limb alignment could be compared relative to the ground reaction force vector and centre of gravity of the body.

Using the notation in figure 2.5, a varus angulation described a bow legged deformity, and occurred when $\phi = \theta_2 - \theta_1 < 0^{\circ}$. For the static case, an increase in the loading of the medial compartment of the knee joint and tension in the lateral collateral ligament resulted. Similarly, a valgus deformity ($\phi > 0^{\circ}$) shifted the contact force laterally and increased tension in the medial collateral ligament. This represented a knee knocking deformity; both types of deformity are illustrated in Figure 2.6. Using the notation given by Chao [25], the anatomical tibiofemoral angle varied between 0° and 2° varus.

Note that the knee joint alignment was recorded in the A-P plane only. Consideration should have also been given to the angular deformity in the M-L plane, which represented the angular tilt of the tibial plateaus. Figure 2.7 shows that the tibial plateaus slope posteriorly 10° to 15° with the normal knee joint. This angular offset

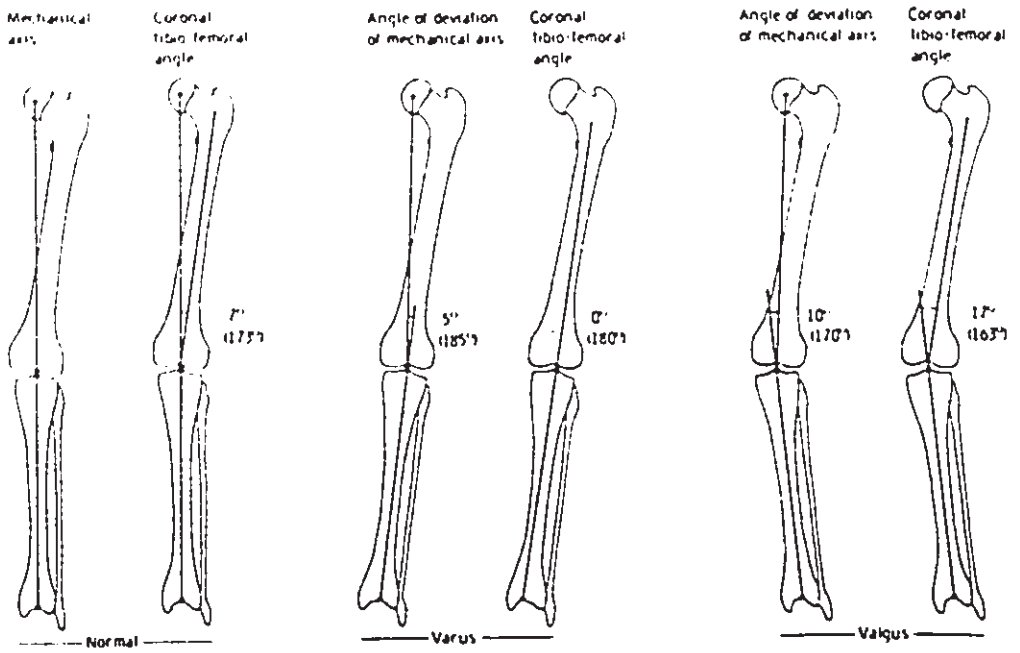

Figure 2.6: Normal, varus and valgus angulation of the knee [162].

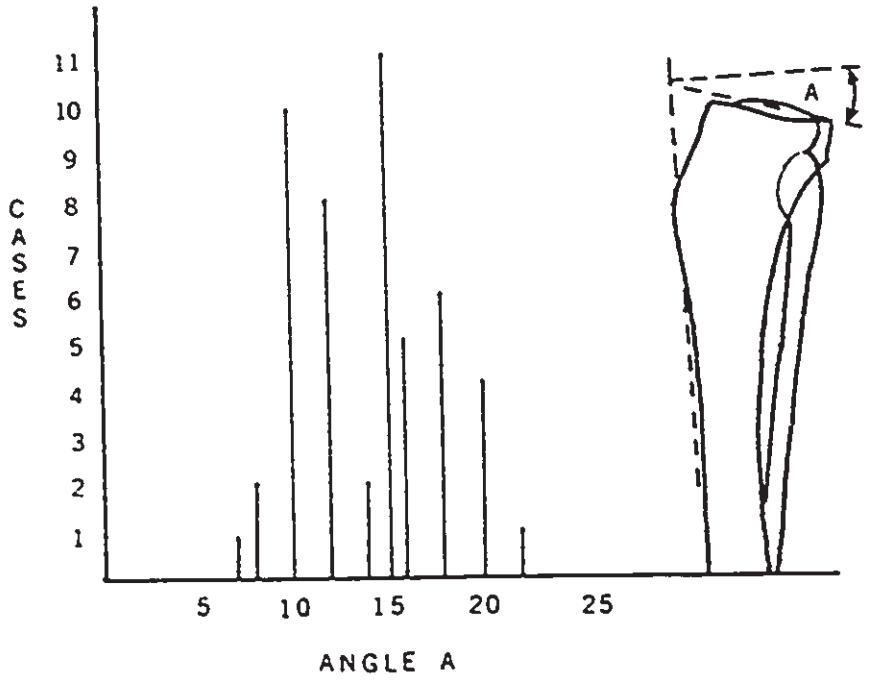

Figure 2.7: Angular tilt of tibial plateau in medial-lateral plane [107].

can also promote a flexion deformity [107,128]. A deteriorating flexion deformity will increase the contact stress because the greatest area of contact between the tibia and femur occurred with the knee in full extension and decreased with flexion [85,98]. The peak contact stress is further augmented by the increased muscle action required to maintain knee stability in a flexed position. Messieh et al. [106] recommended A-P radiographs with the knee flexed 30° in order to adequately examine the state of arthritis of the articular cartilage.

A third rotational offset occurs about the longitudinal axes of the femur and tibia and is commonly referred to as internal or external rotation. Changes to the angle will affect the alignment of the foot and the contact area at the knee joint; the latter will be especially noticeable during knee flexion. Flexion and rotation aberrations of up to 10° were found to introduce less than 2° of apparent axial alignment error (Jiang et al. [71], Krackow et al. [88], Wright et al. [172]). However, an occurrence of 15° or greater flexion contracture created an artifactual deformity of 2.8° to 5.5° for 10° to 20° of rotation. Figure 2.8 demonstrates how a flexion contracture results in shortening of the standing leg length, when defined as the distance between the hip and ankles joints viewed in the A-P plane. When a flexed knee is complimented with some degree of external rotation, an apparant varus offset at the knee will occur in the A-P view. This becomes critical when osteotomy or total replacement surgery is employed to correct a varus/valgus alignment deformity that has both a flexion contracture and an external rotational deformity greater than 10°. It is important to note that two orthogonal radiographs will enable determination of the

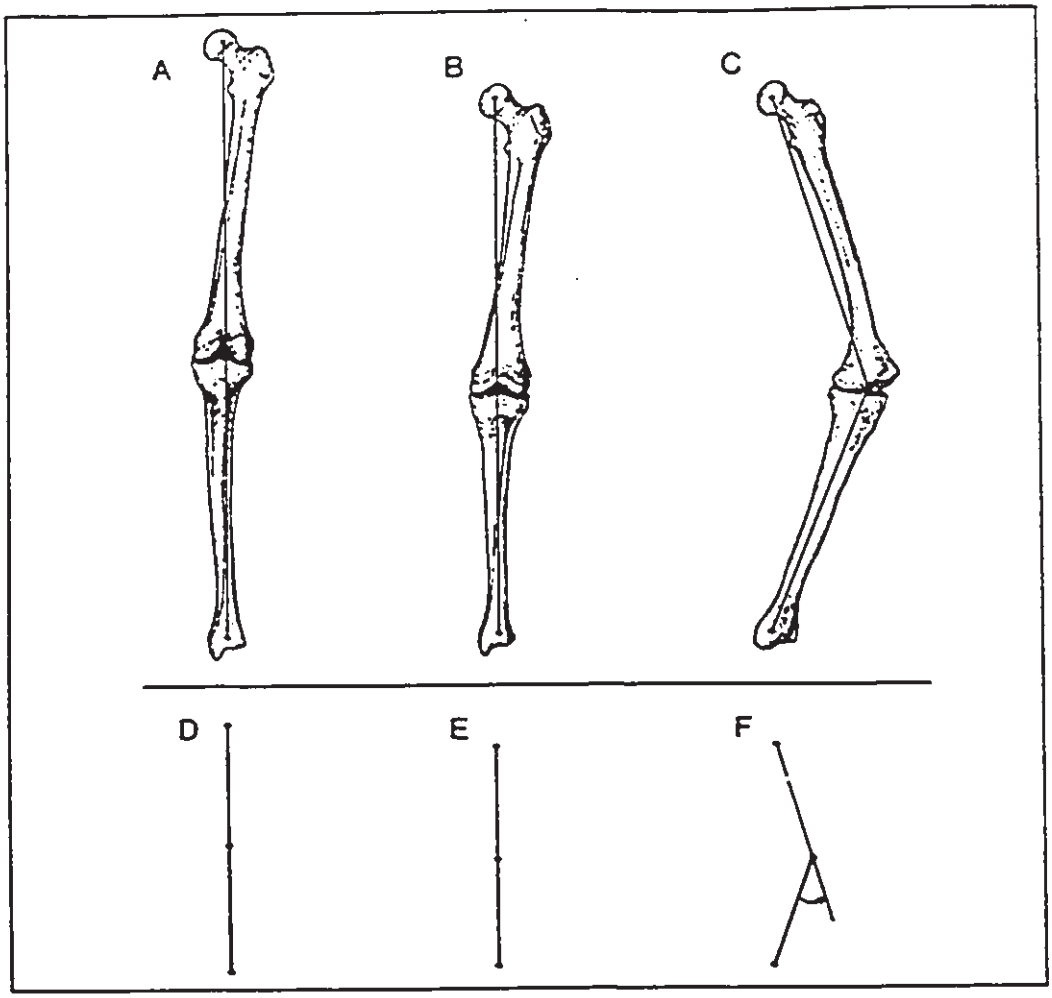

Figure 2.8: Effects of knee flexion and external rotation on the apparent varus alignment in the A-P plane [88].

A: Neutral alignment of mechanical tibiofemoral Angle.

B: Effect of knee flexion on tibiofemoral angle.

C: Effect of knee flexion and external rotation at the hip and ankle.

D: Mechanical axes of tibia and femur are aligned with each other.

E: Similar situation as in Figure D:, in addition to an apparent shortening of the overall limb length.

F: Similar situation as in Figure E:, in addition to an apparrent varus deformity.

true angular deformity between the femur and tibial mechanical axes, but can not be used to estimate the rotational deformities (Barr and Breitfuss [9]). However, if a flexion contracture exists, a method described by Krackow et al. [88] can be implemented to estimate the relative change in the apparent and true varus/valgus angular offset that can occur, and requires an initial estimate of the axial offset for neutral alignment. That is, for a given axial alignment at a predefined neutral position, any additional rotational offset will exaggerate the true varus/valgus angle at the knee. The difference between the apparent and true angular offset can be separated out to give the true varus/valgus angle.

Although a two dimensional kinematic model employing the mechanical or anatomical axes of the lower extremity can be used to define the knee joint alignment, it should not be used to estimate the loading status at the knee during walking. This was noted by Harrington [58] who stated that for the static case the location of the knee centre depended primarily on the inclination of the tibial plateaus in the coronal plane and not the tibiofemoral angulation. No correlation was found to exist between the angular deformity measured on the radiographs and the force distribution in the joint, which suggested that individuals could modify the force transmission by adopting mechanisms that resulted in unloading the knee joint. For dynamic conditions, the location of the joint force was not clearly predictable, and hence it was claimed that a simple osteotomy to correct clinical deformity without elaborate mathematical analysis was satisfactory. This is partly due to insufficient experimental data necessary to quantify and

describe the effects of high tibial osteotomy surgery on knee joint mechanics, due to the inability to measure contact loads and pressure before and after osteotomy surgery. Harrington also stated that until transducers were available that were capable of measuring joint loads directly, such information could only be obtained from gait studies.

Contrary to these suggestions of not using the tibiofemoral angle, the procedure followed by Chao [25] and others will give the same results if one assumes the tibial plateau to be perpendicular to the long axis of the tibia, and regardless whether the force analysis is static or dynamic, any alteration in the mechanical alignment of the knee joint will affect the loading pattern on the tibial plateaus. The difficulty arises in estimating the loads transmitted across the knee while considering the relative spatial motion between the femur and tibia. It should also be noted that the analytical model used by Harrington [58] assumes that the tibial plateau is at right angles to the long axis of the tibia and the joint force acting on it is a single force at some point on a predefined line in a direction parallel to the long axis of the bone and located one-quarter of the width from the knee centre. These assumptions do not support the previous claims denouncing the use of the tibiofemoral angle nor do they incorporate the true angular offset of the tibial plateau in the coronal plane.

The experimental work undertaken here will measure the contact pressure variations along the tibial plateau surface for two knee alignment configurations, malaligned and post-osteotomized realignment, and compare the results with that for a normal neutrally aligned knee. The experimental set-up will attempt to simulate the dynamic motion that

occurs at the knee during the early stance phase of walking. Averaged values of the anatomical and geometrical shapes and sizes of the tibia and femur are included in the analysis, as well as the effects of meniscal contributions.

2.3.3 Remodelling of the Osteoarthritic Surface

The purpose of the high tibial osteotomy is to restore the knee joint alignment and retard any further advancement of the disease. Clinical and radiological evidence exists that indicates high tibial osteotomy surgery can relieve the effects of osteoarthritis through a remodelling process of the articular surface and involves the formation of new bone and fibrous tissue. Figure 2.9 shows where new bone has formed on top of the original cartilage surface of an osteoarthritic femoral head. The mechanism leading to this is currently unknown, however, Meachim and Brooke [105] provided the following suggestions that support osteotomy : 1) the osteotomy interrupted the blood supply which decreased the vascular engorgement, 2) the osteotomy increased the surface contact area, thereby reducing the amount of surface wear , and hence lessen the quantity of debris released into the joint cavity and 3) laboratory examination and radiological evidence sometimes showed that the region of tissue destruction has been completely re-covered by new bone or tissue. The formation and maintainance of cartilage depended on the magnitude of the local compressive stresses [98]. Pauwel [125] stated that bone was even more sensitive than cartilage to the magnitude of stresses. A decreased stress condition led to bone resorption and an increased stress stimulated formation of bone

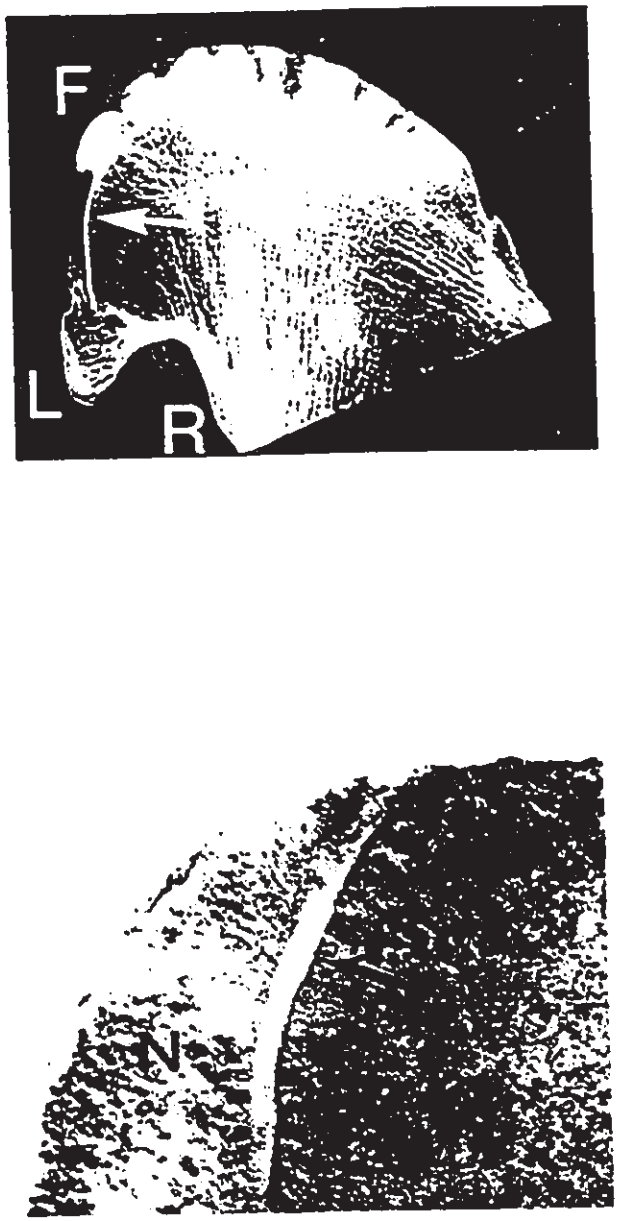

Figure 2.9: Formation of bone regrowth on an osteoarthritic head [105].

[33,105,132].

The distribution of stresses at the knee joint was confirmed using radiographs to show that the bone density underlying the tibial plateaus has a symmetrical outline when the articular surfaces were congruent [73,98]. Joint malignment and incongruent surfaces combined to produce excessive joint stresses which enhanced the level of osteoarthritis. To control the stress levels at the knee joint, the contact area must be maximized through realignment of the limb segments.

2.4 Surgical Techniques Employed to Correct a Knee Deformity

2.4.1 Rationale and Types of High Tibial Osteotomy Surgery

Osteoarthritis of a knee joint with a lower limb angular deformity can be treated with a high tibial osteotomy. The osteotomy involves cutting the bone shaft and realigning the segments to achieve a more normal joint alignment, plus improve the loading conditions. Preference for the type of osteotomy is dictated by the degree of the deformity, state of the arthritis and the surgical procedures commonly practiced by the surgeon. Routine surgical approaches are the (i) open wedge, (ii) closed wedge and (iii) dome osteotomies. A brief review of each method is provided next; a complete assessment of the technical content of the close wedge and dome methods are carried out in Chapter 4.0.

2.4.2 Open Wedge Osteotomy

The open wedge osteotomy involved making a cut through the

proximal tibia parallel to the plateau surface, spreading the two segments apart, and adding a wedge of bone to fill the gap. Some open wedge osteotomy procedures recommended cutting the fibula as well. The rotational correction made between the two segments attempted to restore the knee alignment to a neutral position or one of slight valgus. This is demonstrated in figure 2.10.

2.4.3 Close Wedge Osteotomy

The close wedge osteotomy surgery is illustrated in figure 2.11 and involved removal of a wedge shaped piece of bone from the tibia. The bone wedge was created by making a cut in the proximal tibia parallel to the plateau surface. A second cut, distal to the first, was produced at a prescribed orientation from the first. The angle subtended by the two cuts represented the final amount of angular correction, and usually attempted to restore the tibiofemoral angle to either a neutral or slightly valgus alignment. The two cut surfaces were held together with fixation plates or staples to keep the fracture stable and under compression.

2.4.4 Dome Osteotomy

If the proximal tibial osteotomy required a correction of more than 15°, a dome osteotomy was considered. The dome osteotomy had a series of small holes drilled along a curved line drawn across the proximal tibia. The holes were close together and ran perpendicular to the long axis of the tibia [99,152]. The procedure is illustrated in figure 2.12 and shows how the correct alignment is achieved through

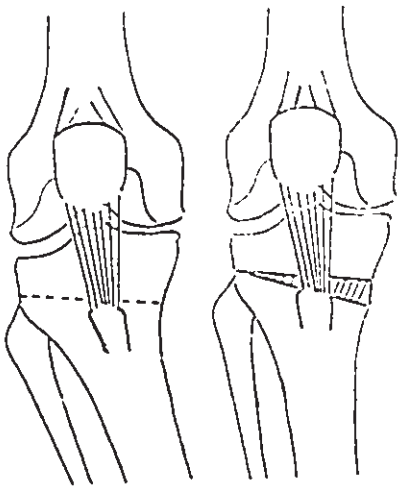

Figure 2.10: Open wedge osteotomy [60].

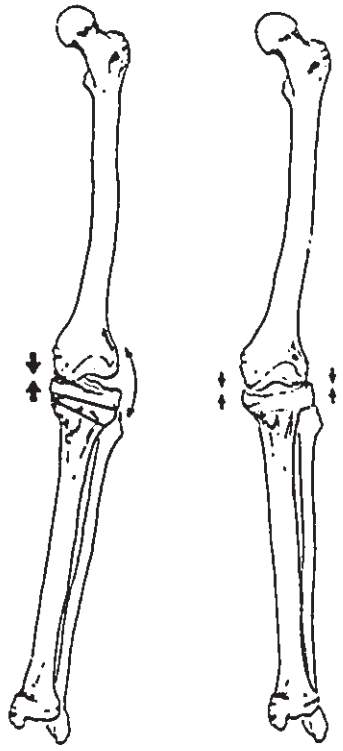

Figure 2.11: Close wedge osteotomy [103].

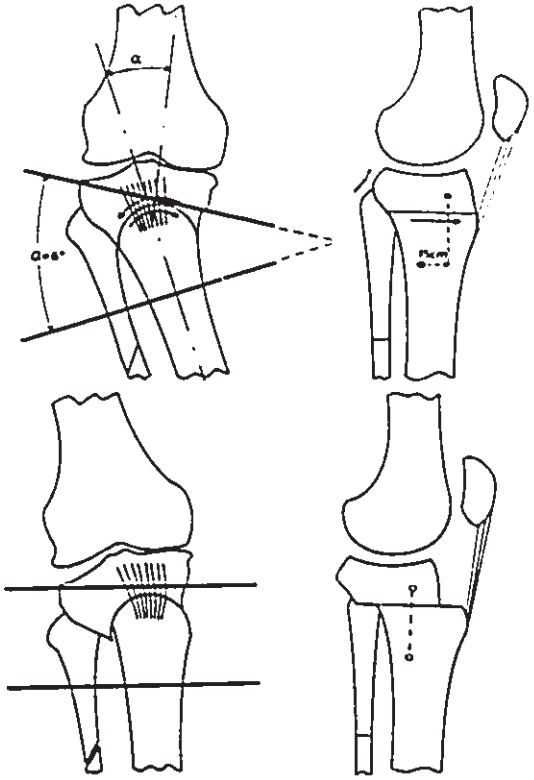

Figure 2.12: Dome osteotomy [98,99].

rotation of the two segments. The recommended amount of alignment correction was that necessary to restore the knee joint to either a neutral or slightly vaglus alignment. Maquet [98,99] has defined a separate set of axes for the femur and tibia, to be used to establish the required amount of angular correction. It is important to know the different terminology employed to describe the overall alignment of the lower extremities, especially when it is used to rate the success of the surgery.

As well, with the dome osteotomy, the lower part of the tibia can be displaced forward relative to the femur. This would reduce the compressive force transmitted between the patella and femoral condyle surface, and also enlarge the contact area, thereby reducing the contact stress.

2.5 Limitations and Patient Selection of Osteotomy Surgery

The original state of health of a patient considered for a high tibial osteotomy will largely affect the success rate of the operation and can help to explain why poor results and complications arise. Some of the contra-indications for osteotomy are [1,32,33,34,46,69,82,162] : 1) excessive bone loss from the tibial plateaus, greater than 1/2 cm, 2) evidence of internal derangement caused by a meniscal tear or osteophytes, 3) severe ligament instability and ligamentous laxity, 4) excessive subluxation of the tibia on the femur, 5) tibiofemoral deviations greater than 15° often restrict open or close wedge osteotomy; dome or distal femoral osteotomies should be considered, 6) lack of knee flexion beyond 80° and flexion contracture greater than

15°, 7) vascular insufficiency, 8) for unicompartmental osteotomy, the opposite compartment must be in a state of good health, and 9) older, less active patients.

Kettalkamp and Colyer [85] and Kettalkamp et al. [81] recommended a close wedge or dome osteotomy for treatment of a valgus deformity of less than 10° and a distal femoral osteotomy for a deformity greater than 10°.

Maquet [99] stated that, as a rule, any varus deformity must be dealt with a barrel vault osteotomy of the proximal tibia. Overcorrection of 3° to 6° was recommended and added to the angular offset noted on the Anterior - Posterior (A-P) radiograph of the lower leg. A femoral osteotomy was recommended for treatment of a severe valgus deformity.

Ogata [117] modified the close wedge osteotomy of the proximal tibia to treat varus deformities in children by creating an interlocking effect between the osteotomized bone segments. A valgus stress and medial rotation were applied to the distal segment in an attempt to increase the contact area and stability at the osteotomy site.

Coventry [32,33,34] stated that osteotomy of the proximal tibia was a reasonable method of treatment of unicompartmental arthritis of a knee with a valgus deformity. Osteotomy of the supracondylar region of the femur was preferred for valgus angulation in excess of 12°.

Coventry [32,33,34] also stated that the biomechanical alignment and tilt of the tibial plateau in the A-P plane must be checked before performing a high tibial osteotomy. If the medial wedge removed was too large, the tibial articular surface slanted exccessively downward from

the horizontal plane. This introduced shear forces on the plateau surface. Coventry limited this angulation to 10°, whereas Insall et al. [69] suggested 10° to 15° and Kettalkamp et al. [83] placed an upper limit of not more than 10° to 15°. Femoral osteotomy or arthroplasty should be considered for larger deviations. Some researchers [31,46,69,99] also consider over-estimating the degree of correction. This was thought to compensate for the loss of correction that was noted to have occurred postoperatively.

2.6 Short and Long Term Follow-up Studies of High Tibial Osteotomy Surgery

The most practical way of judging the success of the osteotomy is by evaluating such properties as decrease in pain, ability to walk, joint mobility, joint instability and joint alignment. Pain relief is the most critical. Table 2.3 provides a list of short and long term follow-up studies carried out on different types of osteotomies; included in the table are the recommended anatomical tibiofemoral angles. The tabulated success rate is a combination of the joint motion, joint stability and freedom of pain. Excellent to good results were observed postoperatively and continued for approximately three years on average. Between three to five years postoperatively, the success rate dropped to fair.

Table 2.3: Success Rates of High Tibial Osteotomy Surgery

Follow-up Period (months)	Number of Osteotomies	Type	Recommended Angle (Degrees)	Success Rate %	Reference
120	139	close	5	64	[1]
24	88	close	10	94	[22]
60	88	"	"	87	"
120	"	"	"	69	"
32	23	close	5 - 7	80	[39]
12	20		7	57	[41]
12	11	dome		76	[46]
12	6	close		"	"
60	93	open	5	90	[60]
120	"	"	"	45	"
24	95		10	97	[69]
60	"		"	85	"
108	"		"	63	"
38	37	close	5	66 < 5^{o}	[83]
38	11	dome		42 > 5^{o}	"

Table 2.3: Success Rates of High Tibial Osteotomy Surgery

Follow-up Period (months)	Number of Osteotomies	Type	Recommended Angle (Degrees)	Success Rate %	Reference
12	40	close	5 - 7	86	[103]
36	40	"	"	64	"
60	40	"	"	50	"
108	40	"	"	28	"
36-60	128	close	9.8	83	[137]
72-108	"	"	"	79	"
>120	"	"	"	74	"
60	89	close	10	58	[139]
57.6	105	dome	7	75	[152]
192	213	close	10	60	"

CHAPTER 3.0

REVIEW OF EXPERIMENTAL RESEARCH

3.1 Knee Joint Mechanics

Experimental research on knee joint mechanics has included measurement of the kinematic and dynamic motion of the joint, estimates of the contact area and pressure distribution patterns at the articular surfaces for specific knee orientations, and quantification of the function and activity of the ligaments and muscle structures surrounding the knee.

3.1.1 Kinematic Analysis

Direct measurement of planar and three dimensional kinematics of the knee can be achieved using stereometric techniques or electromechanical - mechanical devices. Stereometric techniques have the measuring instrument isolated from the body and record the coordinates of three non-colinear points at two different body positions. Sonic digitizers, cineradiography and cinematography are all forms of stereometric techniques. Most planar motion studies employ cinematography to record movement of a body segment; this method is also predominent with gait laboratory investigations [98,113,114,118,145,151]. Selection of appropriate reference points constitutes the greatest error with these methods. Scherrer and Hillberry [140] used sonic digitizers as a measurement system which worked on the principle of accoustic transmission. Huiskes et al. [64]

introduced an analytical stereophotogrammetric procedure to measure the three dimensional geometry of the articulating surfaces in vitro. More recently, Kärrholm et al. [78] measured in vivo the active knee motion after cruciate ligament rupture with a roentgen stereophotogrammetric analysis and considered the method to be superior to the previous methods of electrogoniometry and high speed photography.

Mechanical and electromechanical techniques have the measuring instrument physically attached to the body. This may hinder the movement and influence the resultant motion to take on an alternate path. The most common type of instrumented linkage is the electrogoniometer, which can measure up to six degrees of freedom. Townsend [157] analyzed the knee joint kinematics with a special external linkage device that permitted transfer of data in terms of the helical axis kinematic parameters. Shiavi et al. [147] carried out in vivo motion studies of the knee with a six degree of freedom goniometer and applied helical motion analysis to analytically model the resultant motion. Although instrumented linkages are generally more accurate than radiographic methods, any loose motion in the linkages and initial estimates of the linkage parameters contribute to the errors with this method. Sommer and Miller [150] employed an optimization routine to minimize linkage measurement error, and Suntay et al. [153] discussed the errors associated with spatial linkage devices used to measure knee motion.

3.1.2 Dynamic Analysis

Gait studies combine cinematography methods with force platform

techniques to assess the mechanics of a joint [51,58]. However, this approach requires numerous assumptions to be made [58,113,118,145], and can only monitor the external forces acting on a system. Despite this, Harrington [58] and Johnson et al. [73] still recommend that gait studies be employed to analyze the effects of the high tibial osteotomy on knee joint loading, rather than the static approach which uses weight bearing radiographs. They are not, however, suggesting that radiographs can not be employed to measure the angular deviation between two bone segments.

In vitro analysis of knee joint mechanics requires the use of specialized testing equipment. Instron or Machine Testing System (MTS) equipment, special loading devices and simulators have all been designed to reproduce the static or dynamic load and movement patterns that occur at the knee during weight bearing stance or walking. The equipment permits measurement of either the resultant kinematic motion to a given external loading environment, or subsequent load response to a given movement pattern [3,43,46,49,68,146,154]. However, these studies have not included any indepth analysis on the biomechanics of osteotomy surgery, nor have they completed any extensive review of the dynamic response characteristics at the knee due to changes in the lower extremity alignment.

3.2 Review of Experimental Models of Osteotomy Surgery

Chao [25] classified the mechanics of the tibial osteotomy by histological factors and biomechanical factors. The histological factors consisted of regeneration of damaged cartilage, retardation of

bone sclerosis and cyst formation, prevention of ligament laxity, decreasing pain and reduction of vascular pressure as a source of pain. The biomechanical factors included correction of knee deformity in the A-P plane, realignment of the load bearing axis, increasing joint stability and altering patellofemoral mechanics. At present, there is a need to quantify these factors through experimentation.

Kettelkamp and Chao [81] analyzed the two dimensional loading conditions at the knee joint using full length standing radiographs and attempted to correlate the varus/valgus offset to the load transmission at the joint. This procedure could be included as part of the preoperative planning stages of high tibial osteotomy surgery [33,34,69,83,85,103]. The approach does not, however, represent the maximum loading state that occurs with a flexed knee during the stance phase of walking.

Engin [46] studied, in vitro, the effects of knee alignment on static load transmission across the joint using a bone strain gauge method. The experimental results could then be used to predict the joint load pattern at the articular surface, and included the effects of realignment surgery on contact load. Furthermore, the concept of overcorrecting the lower limb alignment could be reviewed, with the intent to redirect more load to the unaffected compartment. However, malalignments of only 2.5° and 5° varus or valgus were included in their study, and the equipment was unable to reproduce the physiological joint malalignment.

Prodromos et al. [129] carried out a series of gait studies to observe the clinical changes following high tibial osteotomy. The study

concluded that the moment tending to adduct the knee during gait was predictive of the postoperative clinical results and those patients classified with a high adductor moment postoperatively had a higher recurrence of knee deformity following surgery. The study also indicated that static alignment of the knee alone could not predict the dynamic load present during walking, and thus, could not be correlated with the clinical results. Johnson et al. [73] indicated a need to combine radiological diagnosis with gait analysis to ensure a more successful outcome of a tibial osteotomy. The results from gait analyzes showed that a greater load was borne on the medial plateau, regardless of the knee alignment. During normal gait, a horizontal force component existed at the knee that tried to displace the tibia medially relative to the femur. This had the effect of increasing the adductor moment, as noted by Prodromos et al. [129] and also increased the medial plateau force. Similar comments were brought forward by Harrington [58], who recommended the use of gait studies to properly assess the effects of knee alignment on load transmission.

3.3 Contact Area and Pressure Distribution Patterns of the Knee

Measurement of contact area and pressure patterns at the knee surface would help to quantify the biomechanics of high tibial osteotomy surgery. Previous studies on the measurement of contact area patterns of the knee joint have been carried out under conditions of static loading or stance weight bearing, while maintaining a constant joint orientation.

Similarly, measurement of the contact pressure has also been

limited to a fixed knee angle. An indirect approach used to estimate the contact pressure along the articular surface is to combine the measured contact area values with the applied load [2,3,49]. Unfortunately, this will only generate an overall average estimate of the pressure. Few studies have been able to analyze the dynamic case. This is largely due to the inability to design and develop adequate transducers to be inserted in the joint, and is also compounded by the fact that articular cartilage exhibits a nonelastic, time-dependent behaviour [2,86]. If such a device was available, the effects of joint alignment on load transmission could be assessed, and would enable a comparison between the knee mechanics of a neutrally aligned knee joint to that of a malaligned or post-osteotomy realigned knee.

3.3.1 Contact Area Patterns

Kettalkamp and Jacobs [80] used a radiographic technique to determine in vitro the tibiofemoral weight bearing area. Knee specimens were mounted between two plexiglass plates and placed under a load not greater than 80 N. A radiolucent medium was injected into the joint cavity and radiographs outlining the joint surface were taken in the transverse plane. Estimates of the contact area are given in table 3.1 and were found to be 7.7 cm^2 at 0° knee fexion. Knee flexion was restricted to 35° or less to prevent the apparatus from subluxing the joint. Since the applied loads were minimal, a realistic representation of the in vivo loading conditions at the knee was not attainable. This procedure was also unable to distinguish between the loads sustained by the menisci and the remaining cartilage covering the centre portion of

Table 3.1: Knee Surface Contact Area Patterns

MEDIAL		LATERAL		Total Area (cm^2)	Load (N)	Number of Specimens	Reference
With Menisci	Without Menisci	With Menisci	Without Menisci				
				12.	2688	18	[3]
				12.	1000		"
				2.11[a]	1200	14	[17]
6.4	3.0	5.1	2.2	5.2[a]	1000	7	[49]
				11.5			"
7.4	3.7	4.5	2.4	6.1[a]	30-80	5	[80]
				12.9			"
4.7		3.0		7.7	30-80	14	"
10.0		9.5		20.1[b]	2000-	10	[97]
				11.6[c]	2500		"
7.5		5.2		12.7	1200	12	[134]
	1.6		2.1	3.7[a,b]	1500	1	[159]
	1.8		1.5	3.3[a,c]	1500		"

a = without menisci

b = complete extension

c = 90° flexion

each compartment.

A casting method was employed by Walker and Hajek [159] to determine in vitro the location and size of the load bearing area in cadaver knee specimens. Each specimen was placed in an Instron machine at a predesired amount of knee flexion and compressed to 1500 N for 5 s. A cast of the joint cavity was produced with self curing bone cement. Measurement of the contact area patterns are given in table 3.1, and do not include the menisci; Walker and Hajek [159] also stated that the menisci do not support any of the applied load and removal would result in a limiting case. The results were also complimented with an analytical model that used deformation theory to calculate the contact area. The cartilage was modelled as an elastic layer bonded to a rigid half space and deflected into itself with minimum bulging at the outer boundary. However, articular cartilage behaves viscoelastically, and to include this in the study would require in vivo measurements.

Studies with the menisci intact were carried out by Walker and Erkman [160] for loads between 0 to 1500 N. A casting technique was employed to generate the outline of the contact surface , and the approach required a loading time of 5 s.

Maquet et al. [97] measured the contact area with a radiographic method where coloured water was injected into the joint cavity and then placed under a load of 2200 N for 30 s . A series of radiographs were taken at various knee orientations to provide an outline of the articular surface. The contact area was 20.13 cm^2 at 0° flexion and 11.6 cm^2 at 90°. These values along with those recorded for menisectomies, are also included in table 3.1. The observed patterns

are shown in figure 3.1 and were similar to those obtained during previous studies at loads of 900 N or more.

Fukubayashi and Kurosawa [49] measured the contact area with a casting technique and analyzed the contact pressure distribution patterns using a pressure sensitive colour forming transducer. Measurements of the contact area with and without the menisci are given in table 3.1 . For a load of 1000 N, the contact area was 11.5 cm^2 with the menisci and 5.2 cm^2 without. The testing procedure involved loading the knee in an Instron machine and applying a constant strain rate up to desired load, followed immediately by a stoppage of the strain application.

A plastic micro-indentation transducer was designed by Ahmed and Burke [3] to measure in vitro the static pressure distribution and contact area patterns on the tibial plateau surface. Values ranging from 21 cm^2 at 0° flexion and 2668 N to 12 cm^2 at 0° flexion and 1000 N were obtained. The results from their investigation are included in table 3.1. The measuring device required a minimum pressure of 0.035 Pa and a loading duration of 120 s, and had an associated error of approximately 10%. This method provided information for static conditions only, and was far too elaborate and sophisticated to be easily implemented by others.

Riegger et al. [134] used a densitometer with the prescale film to estimate the contact area of an osteoarthritic knee. Values of 7.5 and 5.2 cm^2 were calculated for the medial and lateral compartments, respectively, and were for a loading of 1200 N. Brown et al. [17] also used the prescale film, but employed an Eyecom II scanner to estimate

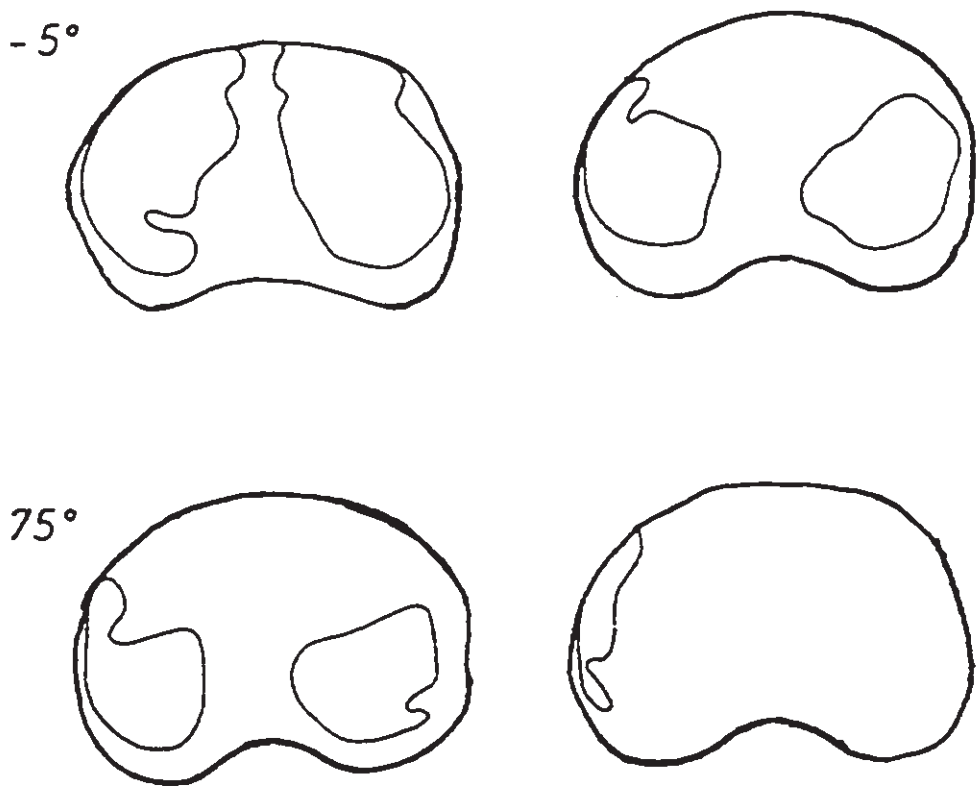

Figure 3.1: Topical view of tibial plateau surface illustrating variations in the contact area patterns for different degrees of knee flexion [97].

the contact area. The scanner determined an 8-bit staining intensity (ie. 256 gray levels) for each pixil in a 640 x 480 view field. An overall contact area of 2.11 cm^2 was estimated from 14 lateral knee compartments, post - menisectomy.

3.3.2 Contact Pressure Distribution Patterns

Maquet [97] estimated the average contact pressure by combining the resultant contact area values with the applied loads; joint pressures varied between 3 kg/cm^2 and 19.3 kg/cm^2. However, this approach assumed the stresses were uniformly distributed over the entire weight bearing surface and did not consider the high local stress conditions that were present during the onset of osteoarthritis.

Fukubayaski and Kurosawa [49] measured the pressure distribution across the tibiofemoral joint directly with a pressure sensitive film. Peak pressure at 1000 N was 3 MPa with the menisci intact and 6 MPa without the menisci. Contour pressure plots were generated as shown in figure 3.2.

Ahmed and Burke [3] measured the pressure distribution on the tibial plateaus using a micro indentor transducer. Results of pressure patterns for four knee specimens are given in figure 3.3 and correspond to a compressive load of 890 N.

All of these techniques for measuring contact pressure have been for static loading only, except for the method by Maquet et al. [97], and are detailed in table 3.2. More recently, Inabi and Arai [68] developed a technique to measure the dynamic contact pressure on the tibial plateaus; six cadaver knee specimens were tested. Small holes

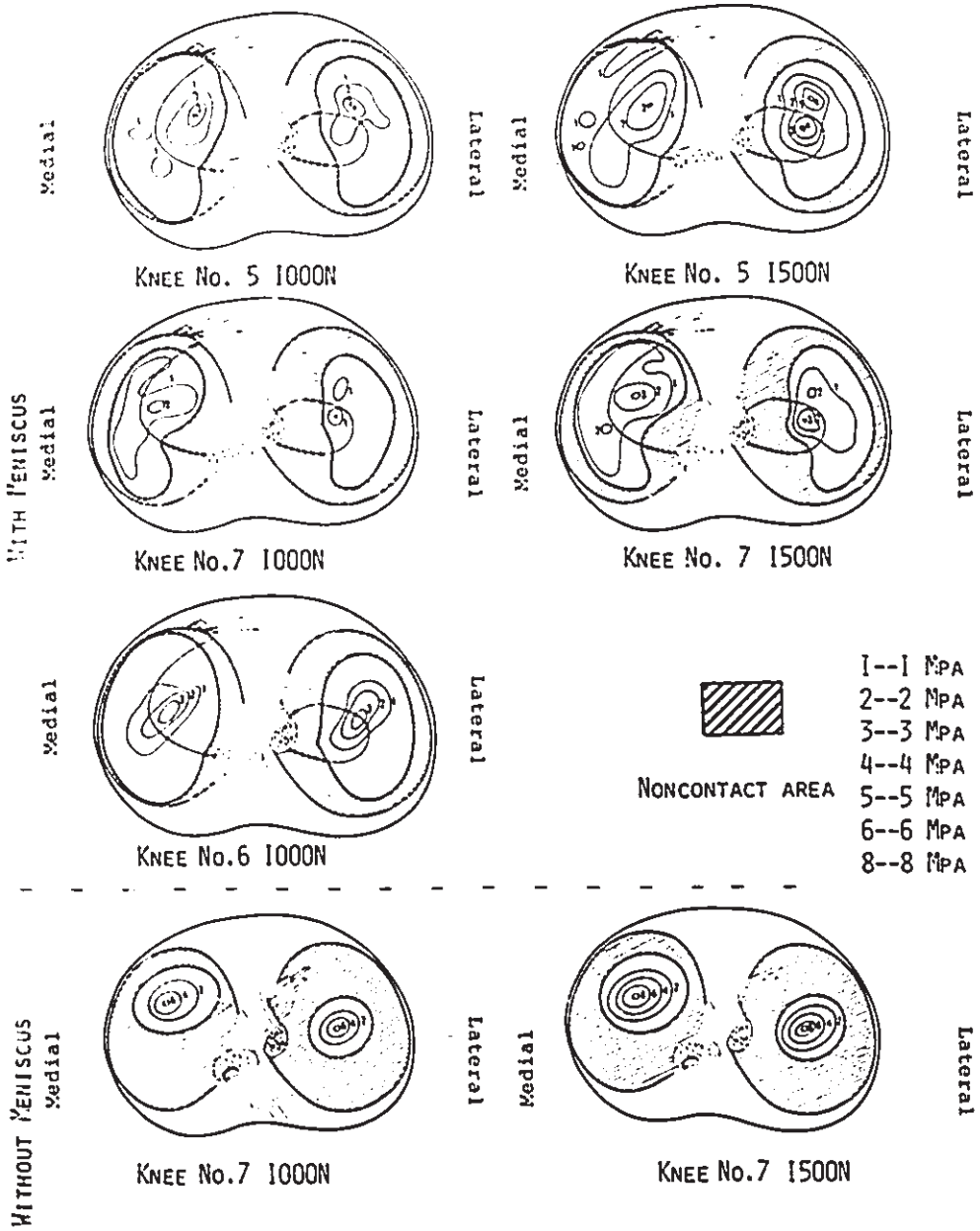

Figure 3.2: Pressure distribution patterns on the tibial surface with and without the menisci [49].

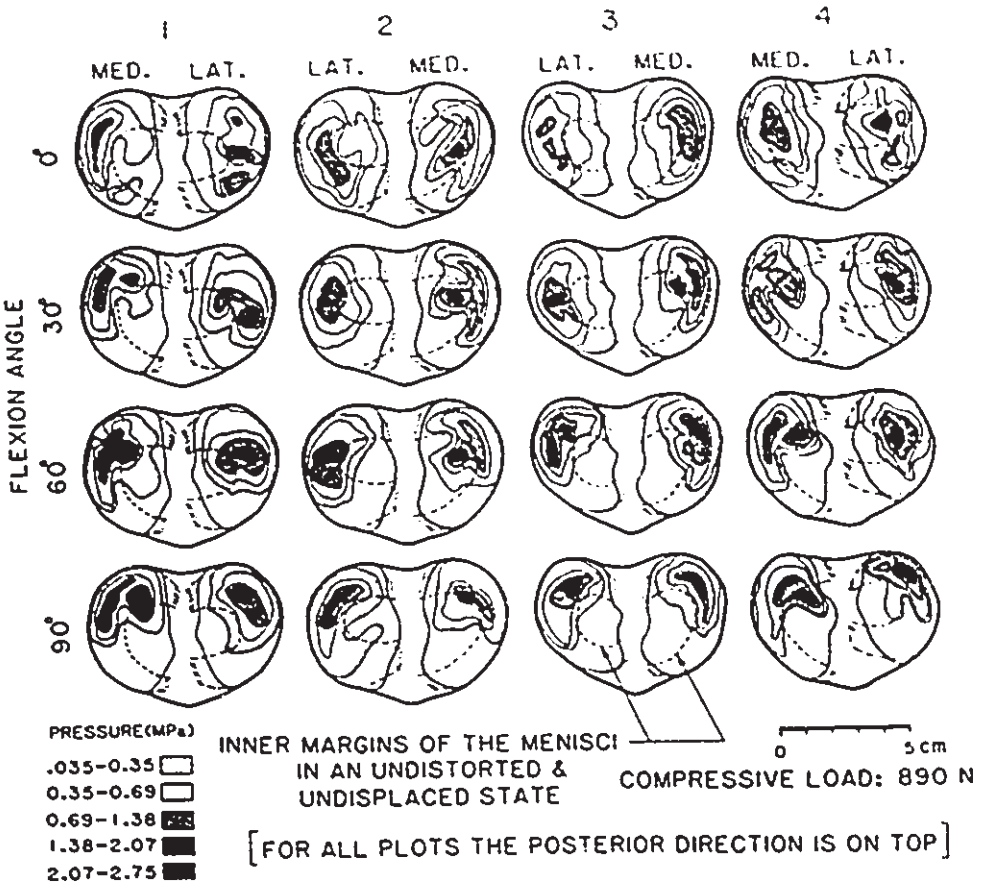

Figure 3.3: Pressure distribution patterns on the tibial plateau surface [3].

Table 3.2: Knee Surface Contact Pressure Patterns

Average Contact Stress Mpa/kN load		Peak Contact Stress Mpa/kN load	Load (N)	Number of Specimens	Reference
0.54		2.0	450-1800	18	[3]
2.36[a]		3.8[a]	1200	14	[17]
0.86		3.10			[18]
0.7		2.5	1000	7	[49]
	M	1.47	2700	6	[68]
	L	0.54	"	"	"
	M	1.90	"	"	"
	L	2.09	"	"	"
	M[a]	2.36	"	"	"
	L	2.80	"	"	"
0.5			2400	10	[97]
M 1.27		3.01	1958	12	[134]
L 1.98		4.69	"	"	"
M 1.63		3.52	5° varus	"	"
L 1.53		3.67	alignment		
M 1.12		2.55	5° valgus	"	"
L 2.45		5.76	alignment		
M 1.43		3.01	5° close wedge	"	"
L 2.04		4.56	osteotomy		
M 0.99			800	6	[142]
L 1.13			"	"	"
4.06			1500	4	[159]
	M	3.2	1000 @	4	[160]
	L	1.3	30° flexion		"

All data for neutral alignment, unless otherwise indicated.
a = without menisci; M = medial compartment; L = lateral compartment

were drilled at various locations on the tibial plateau and connected to a transister pressure transducer. The experimental apparatus is shown in figure 3.4, and the results of contact pressure patterns for various loading configurations are given in figure 3.5. Peak pressures of 4MPa, 6 MPa, and 8 MPa were recorded for a knee specimen with menisci, after partial menisectomy and following complete menisectomy, respectively. Variations in pressure patterns with angular position are illustrated in figure 3.6. These results agreed with those from previous studies; however, this procedure is also not a true dynamic investigation, but rather a quasi-static one, as it does not include the relative sliding motion between the femoral condyles and the tibial plateaus, and involves loading frequencies much less than those associated with walking.

Schmotzer et al. [142] implanted six dynamic pressure transducers on the top surface of both the medial and lateral tibial compartments of six cadaveric knees and investigated the effects of varus/valgus alignment on contact pressure. The mean pressure from all six transducers was averaged and normalized to the applied load; ie. approximately 80 kg for their study. This resulted in estimates of 0.90 Mpa laterally and 0.74 MPa medially for an normal, neutrally aligned knee. The average mean medial pressure doubled for a 10° varus alignment with complete unloading laterally. A 5° valgus knee alignment increased the lateral compartment pressure to 1.24 MPa and also unloaded the opposite compartment. Of interest, the range in local pressure measurements on the medial compartment varied between 0.5 and 3.3 MPa, which translates to a factor of 6.6 between the lowest and highest

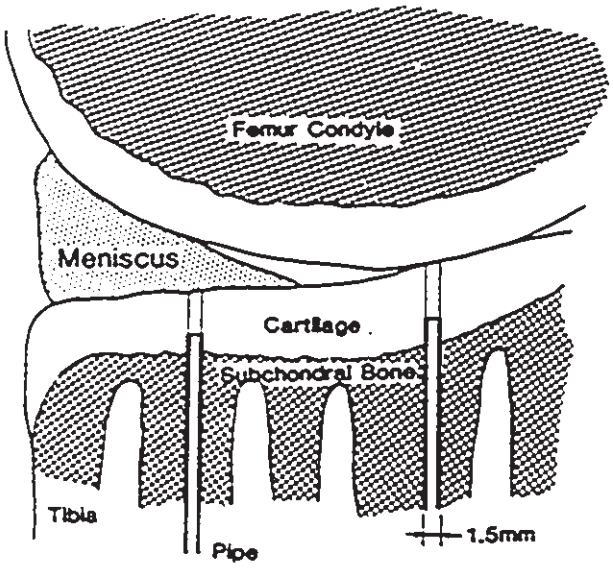

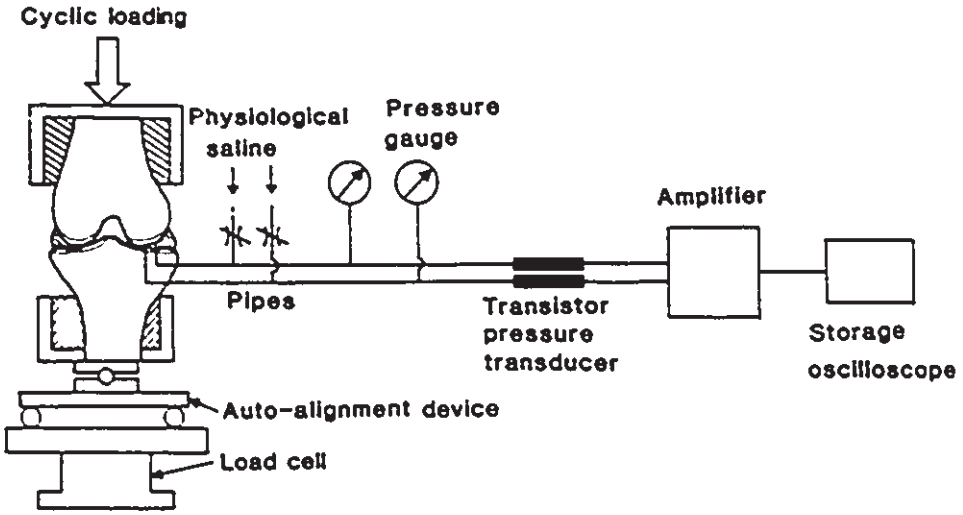

Figure 3.4: Schematic diagram of pressure measurement apparatus employed by Inaba and Arai [68].

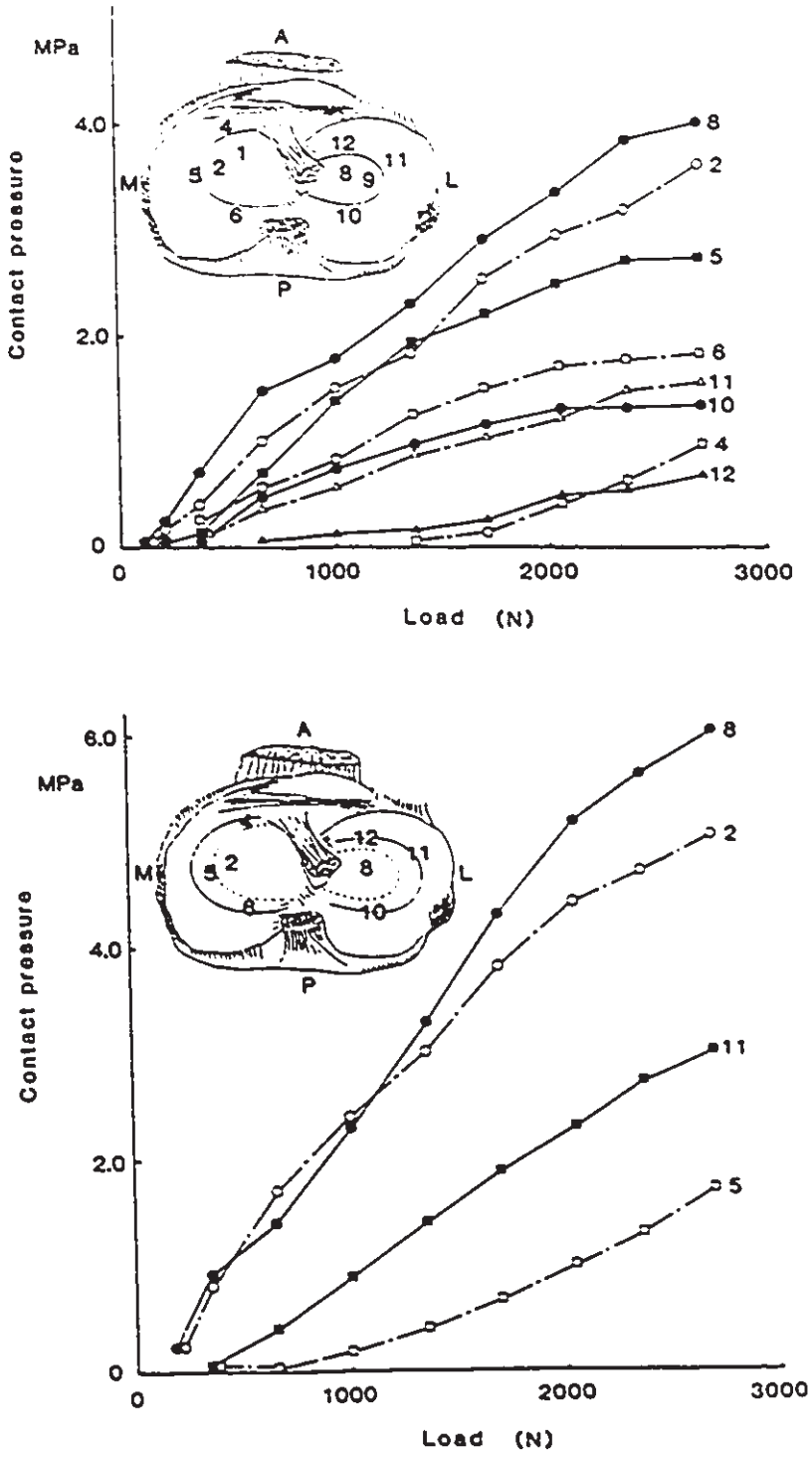

Figure 3.5: Contact pressure patterns for various loading conditions [68].

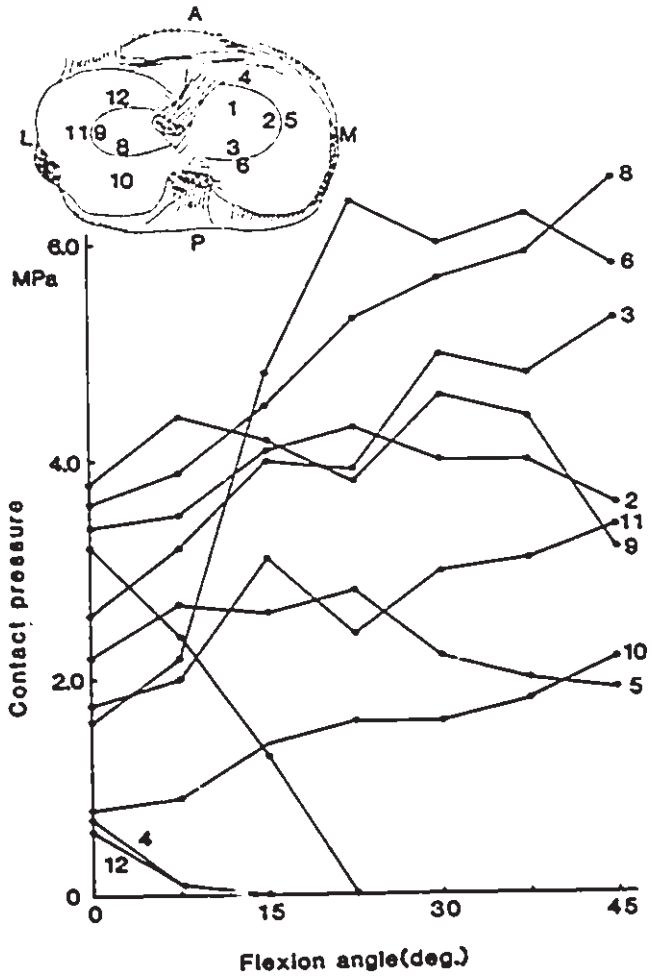

Figure 3.6: Contact pressure patterns versus knee flexion [68].

pressure readings. Although the transducers record the dynamic behaviour, the test setup was quasi-static at best, since the joint orientation remained constant and a non physiological load was applied.

Brown et al. [17] investigated the effects of step off fractures on contact stress aberrations that simulated tibial plateau fractures. For a 3 mm step off level, peak local pressures averaged 75% greater than those prevailing anatomically. Fuji prescale film and an eye comm II scanner had been used to estimate contact pressures. Knee flexion was held to 20° for all tests. Average and peak pressures were 2.36 and 3.1 MPa/kN load, respectively, and are provided in table 3.2 for a 1200 N load and knee flexion of 20°. Previous work by Brown and Shaw [18] had estimated average and peak contact pressures to be .86 and 3.1 MPa/kN of load, respectively.

Riegger et al. [134] compared the variations in contact pressure and area patterns for varus and valgus knee malalignments with those for a neutrally aligned knee joint. Average and peak contact pressures (MPa/kN of load) for the neutrally aligned knee were 1.27 and 3.01 medially, and 1.98 and 4.69 laterally; values for the malaligned cases are included in table 3.2. The effectiveness of a close wedge osteotomy to reduce the contact pressure on the medial tibial plateau was also investigated. Their study found that a five degree realignment may not be sufficient to alter medial contact pressures. This should not have been too surprising, as load variations between the neutral and 5° malalignment configurations would alter the peak applied force by less than a 1/2 percent. Any variations would thus be largely dependent on changes due to the conformity of the mating surfaces.

CHAPTER 4.0

MODELLING ANALYSIS

4.1 Analytical Modelling of the Knee Joint

Numerous mathematical models of the knee joint have been developed to analyze the kinematic and dynamic motions of the joint, quantify ligament and muscle functions, and assess the overall alignment of the lower extremity. Each model requires a method of formulation, method of solution, as well as comprehension and assessment of the results. It must also be understood that validation of the theoretical models is primarily accomplished through experimentation; hence the advancement of knee joint models depends on the success of experimental research on the knee joint.

Few investigators have employed these models to analyze the biomechanics of high tibial osteotomy surgery [81,109]. Furthermore, most clinical research is limited to subjective evaluation of the pre- and post-operative stages of the surgery, and involves minimal biomechanical analysis. For example, the pre-operative planning stages of high tibial osteotomy surgery typically employ a graphical technique to describe the surgical approach. Unfortunately, the methodology of the surgery is not without limitations or errors that will directly affect the outcome of the surgery.

There is a need for a precise method of analyzing and forecasting the changes in the joint angles and limb lengths following osteotomy surgery. Thus, a two dimensional trigonometric model of the

lower extremity is formulated here for the first time to help quantify the effects of osteotomy surgery on the lower-limb alignment and kinematics at the knee, as well as, identify the limitations and errors involved with conventional methods.

4.2 Modelling Osteotomy Surgery of the Proximal Tibia

Realignment of the lower limb segments through angular correction of the tibia is thought to reduce the contact pressure at the articular surface of the affected knee, and thus retard the advancement of osteoarthritis. This may in turn alleviate the joint pain and improve joint function (Hsu [66], Maquet [98]). Two of the more common types of knee osteotomy surgery, which will be reviewed, are the close wedge and dome osteotomies. The goal of osteotomy surgery is to restore the overall alignment of the lower extremity. However, there is no common agreement as to how the optimal correction angle for the close wedge osteotomy should be determined; similarly, the amount of rotational correction required with the dome osteotomy to restore the alignment.

The most common technical error limiting the outcome of this surgical method has been under-correction of the deformity [1,37,51,52]. As a result, some degree of over-correction is typically recommended in order to achieve long term clinical success. Yet, there is a general lack of objective criteria that supports the theoretical justification of the different procedures, and is believed to be due to the limitations of the surgical methodology, and a lack of reliable normal data.

Therefore, the proposed model will be employed to accomplish the following objectives.

1) Establish a method of standardizing the way in which the tibiofemoral alignment is measured. Conventional methods use two different systems to define the lower limb alignment. Since the success of the surgical methods is based on the resultant alignment, a standardized parameter would allow comparison between success rates for the different surgical methods.

2) Redefine the terminology of over-correction or under-correction of the tibiofemoral alignment so as to relate to the neutral tibiofemoral orientation, TF = 0°.

3) Review the methodology of the close wedge and dome osteotomy procedures and identify the limitations and errors associated with each.

4) Determine the appropriate technical steps necessary to overcome these limitations and reduce the associated errors. This can be accomplished in two parts. The first is to carry through the osteotomy surgery as described in the literature, and determine the difference in the actual and desired tibiofemoral angles. The second is to redefine the preoperative steps so that the desired tibiofemoral angle is achieved. This is elaborated at greater length in the following sections.

5) Record changes to the lower extremity that occur following osteotomy surgery. This would include the preferred tibiofemoral angle, overall limb length, amount of angular compensation required at the hip and ankle joints, and the expected orientation of the tibial plateau surface relative to the ground or a horizontal datum line.

6) Determine the changes in the position and orientation of the knee

joint centre relative to the hip and ankle joints for different tibiofemoral alignments. That is, to determine the location of the knee centre relative to the weight bearing axis for a malaligned and neutrally aligned joint, as well as with a post-osteotomy realigned configuration. This information can also be used to estimate the location of the external force vector on the tibial plateau surface.

4.2.1 Two Dimensional Model of the Lower Extremity

Full length A-P radiographs of the lower limb are necessary to adequately determine the alignment of the femur and tibia, and should include views of the hip and ankle centres (Cooke et al. [29], Hsu et al. [66], Wright et al. [172]). The lower limbs are typically placed with the tibial tuberosity facing forward and the knee fully extended. Various techniques are employed to acquire the radiographs, and each method attempts to reduce any associated errors with the measurement technique. If a flexion contracture exists along with a torsional angular deformity, then a lateral radiograph is also required. This is necessary to account for the difference in the true and apparant angulations at the knee.

Standard measurements used to quantify the overall lower limb alignment and knee geometry in the frontal plane are the hip, knee and ankle joint locations and orientations, and the lengths of the femur and tibia. The hip centre (H) can be estimated on the radiograph using a set of circular templates. The knee centre (K) is taken as the mid point of the tibial spines halfway between the intercondylar notch. The ankle centre (A) is the mid point between the malleoli and one-half the

height of the talus. The anatomical and mechanical axes of the femur and tibia can now be identified using these anatomical landmarks, and are shown in figure 4.1. To carry out any biomechanical analysis of the lower limb, the mechanical axes should always be employed. Unfortunately, this parameter is not always employed in the methodology of osteotomy surgery of the proximal tibia.

The mechanical axes of each limb can also be referenced relative to a horizontal datum line to establish an overall alignment of the lower extremity. The mechanical axis of the femur passes through the hip and knee centres, and the length of the femur is taken as the distance between the joint centres along the mechanical axis. The overall length and mechanical axis of the tibia are defined by the knee and ankle joint centres. Using the notation of Chao [25] outlined in Chapter 2.0, and referring to figure 4.1, the tibiofemoral alignment is given by ϕ = FMAO - TMAO. A varus alignment occurs when ϕ is negative. Likewise a positive value indicates a net valgus offset. Some individuals use the anatomical axes to define the lower limb alignment; however, when considering osteotomy surgery the mechanical axes should always be used. This improves the accuracy in approximating the lower limb alignment. For the proposed model, the mechanical tibiofemoral angle is used to describe the lower limb alignment, and all remaining references to the tibiofemoral angle (<TF) are equivalent to the mechanical tibiofemoral angle, unless stated otherwise.

Two additional parameters to measure are the angular offset at the articular surface between the femoral condyles and the tibial plateau, labelled AS in figure 4.1, and the displacement offset of the

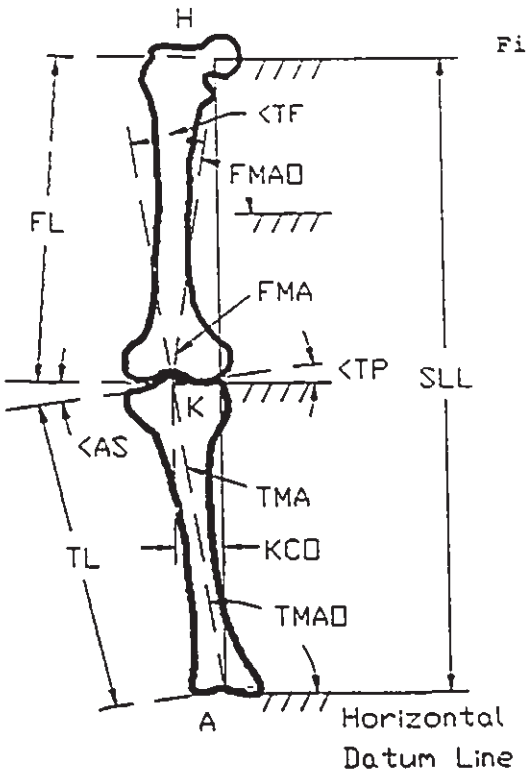

Figure 4.1: Propose model of the lower extremity.

PARAMETERS:

Femoral Length: FL
Tibial Length: TL
Standing Leg Length: SLL
Knee Centre Offset: KCO
Femoral Mechanical Axis: FMA
Tibial Mechanical Axis: TMA
FMA Offset: FMAO
TMA Offset: TMAO
Articular Surface Angle: <AS
Tibiofemoral Angle: <TF
Tibial Plateau Tilt: <TP
Condylar Angular Offset: <CO
Plateau Angular Offeset: <PO

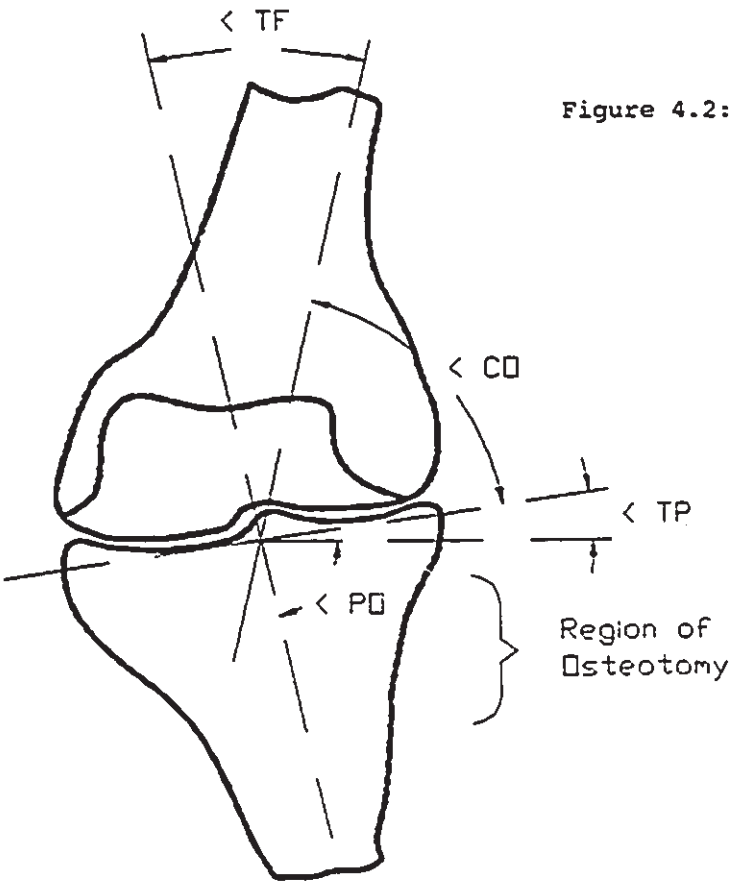

Figure 4.2: Initial set-up of knee joint model.

Articular surface component reduced to zero (<AS = 0).
Tibial plateau tilt dependent on over - all lower limb alignment.
(Different for single and double legged stance.)

knee centre (KCO) relative to the hip-ankle line (HA). A non-zero value of the articular surface component would represent single compartment loading. In the case of a varus deformity, where AS is not equal to zero, a lateral compartment liftoff is indicated, which requires tension in the lateral collateral ligaments to maintain joint stability. When ligament tension is increased, as well as an increase in the quadriceps activity, lateral compartment contact will occur. To determine the smallest amount of angular offset between the articular surfaces, or if two compartment contact can be achieved, non weight bearing radiographs with the lower limb in a supine position are recommended (Hernigou et al. [60], Ogata et al. [122]). It should be noted that the angular offset (AS) should be corrected passively, and should not be considered as part of the osteotomy correction. In the proposed model AS = 0°, and it was assumed that loading of both compartments was possible, and that in the neutral orientation, the knee centre laid on the weight bearing line, ie. KCO = 0. These are illustrated in figure 4.2.

The two dimensional model will now be used to review the methodolgy of the close wedge and dome osteotomy procedures. A varus tibiofemoral alignment was selected to illustrate the surgical approaches and to quantify the differences between each method.

4.2.2 Close Wedge Osteotomy

The close wedge osteotomy involved making two separate cuts through the proximal tibia, removing the bone wedge and repositioning the distal segment. The suggested amount of rotational correction was set equal to the existing tibiofemoral angle. This is illustrated in

figure 4.3a) for correction of a varus malalignment. Following removal of the bone wedge, the post-operative alignment of the tibia, and subsequent reoriented position of the knee, is shown in figure 4.3b).

Upon examination, the tibiofemoral alignment was not restored to a neutral position, but rather, a slight varus offset was created, and represented a condition of under-correction, UC. The angular difference, UC, was due to the fact that the surgical method assumed the correction occurred about the knee centre, but it actually occurred at the apex of the two cut surfaces, point C in figure 4.3b).

The ankle joint was repositioned to the location A', and did not intersect the extension of the hip-knee line (HA), as was intended, but rather, laid approximately 1° to 2° off HA. In order to obtain a neutral orientation, an additional amount of rotation was required (AC). This amount could be estimated using a graphical technique, or more accurately with the analytical model. Although the graphical approach illustrates the limitation of the surgical approach, it was unable to quantify the amount of additional correction required. To accomplish this, the model was modified to determine a relationship between the angular offset of the wedge and the resultant tibiofemoral angle. Additional parameters were identified that described the location of the osteotomy, as well as the knee joint angle and lower limb lengths.

The location and size of the osteotomy is illustrated in figure 4.4. The first osteotomy cut was typically between 1.5 cm and 2.5 cm below the tibial plateau surface (d) [69,82,103,129], yet could be as much as 3.5 cm [60] to 7 cm [139]. The width of the cut surface (WC) in the frontal plane was slightly less than the width of the tibial plateau

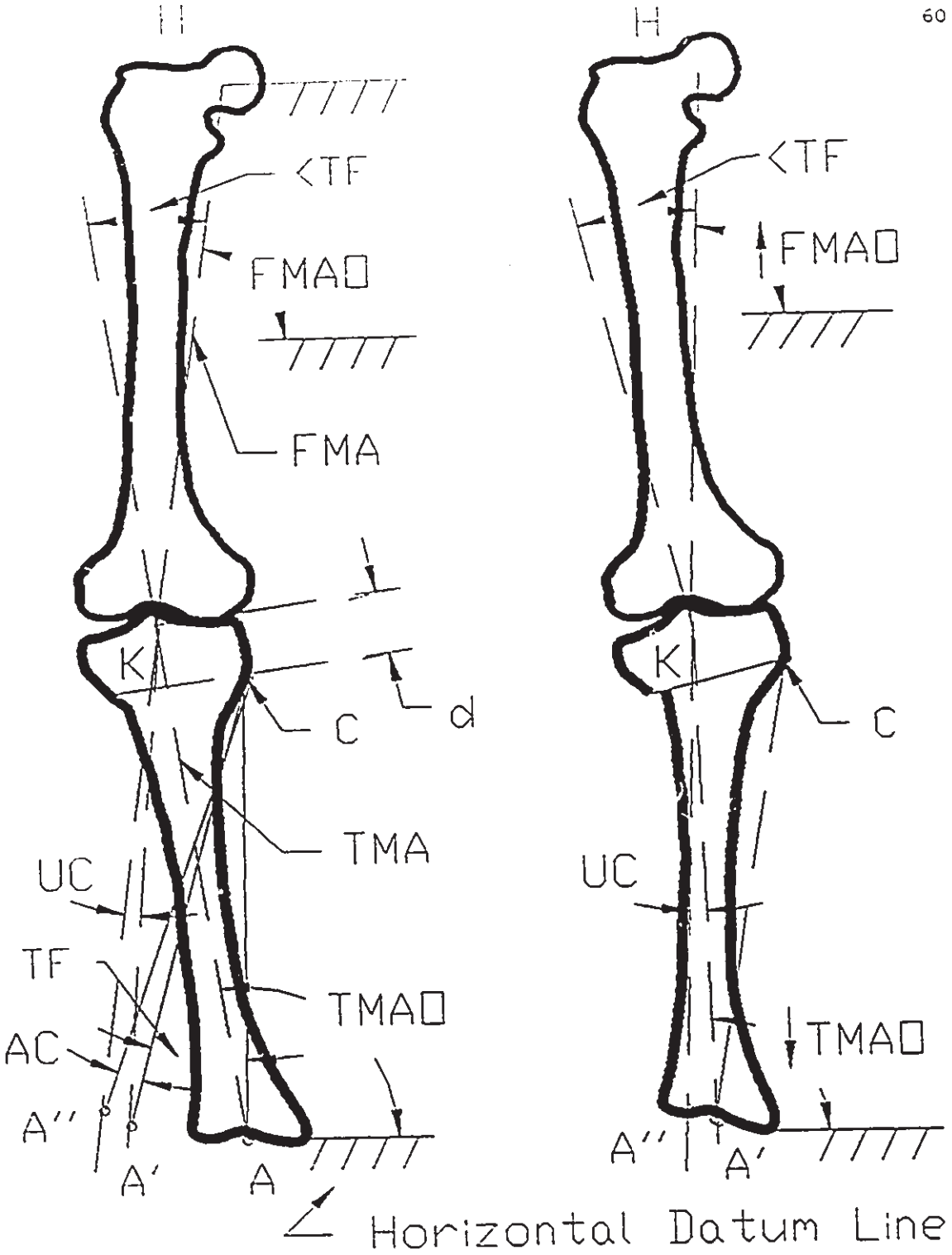

a) Initial alignment parameters for close wedge osteotomy.

b) Resultant alignment following conventional approach.

Figure 4.3: Modelling the surgical procedure of the close wedge osteotomy.

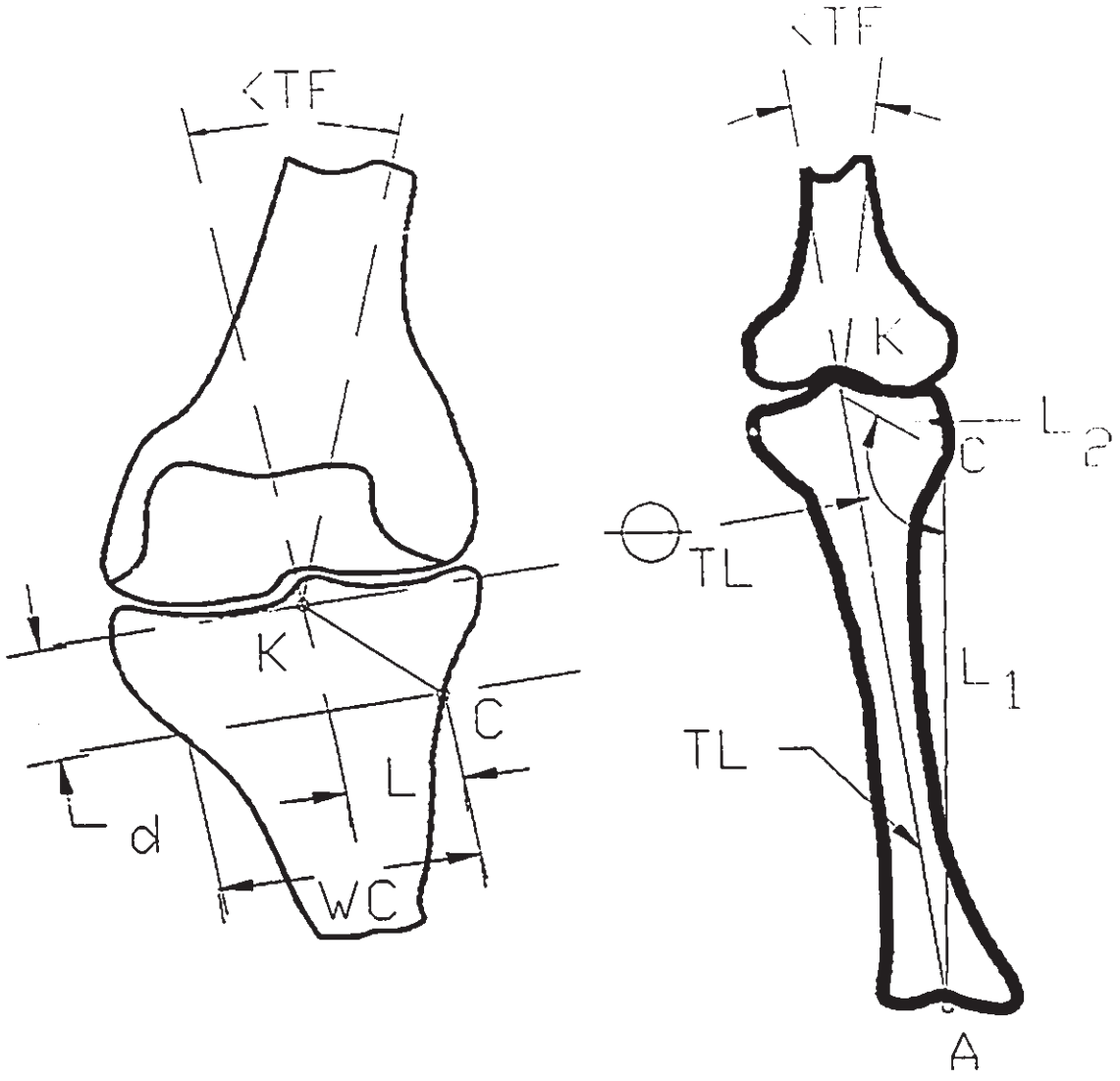

a) Identification of surgical cutting plane relative to the knee centre.

b) Relationship between the knee and ankle joint centres and the point of rotation of the osteotomy.

Figure 4.4: Identification of the model parameters for the close wedge osteotomy.

surface (WP). Morphometrical data on these parameters were collected from the knee specimens used in this study and were presented in Chapter 2.0. Values of WP were, on average, 85 +/- 9mm and 73 +/- 7mm, for male and female subjects, respectively, and reduced approximately 5% to 10% at a level 2.5 cm distal to the plateau surface. For the model, WC = 0.95 WP, but could be easily changed to accommodate a range of different knee sizes. Referring to figure 4.4, a right angle triangle was formed, with a hypotenuse (L_2) between points K and C, with the two remaining sides defined by the level of the first osteotomy cut and the mechanical axis of the tibia. For a given depth of cut, d, the following trigonometric expressions were derived, for the initial setup conditions, AS = 0° and L = WC/2.

$$\theta_1 = \tan^{-1}\{ L / d\} \qquad (4.1)$$

$$L_2 = d / \cos\theta_1 \qquad (4.2)$$

A second triangle was formed by points K, C and A, (see figure 4.4b), with sides L_1, L_2 and TL. Using the cosine law, the following expressions were derived.

$$L_1 = \{ L_2^2 + TL^2 - 2 * L_2 * TL * \cos\theta_1\}^{1/2} \qquad (4.3)$$

$$\theta_{TL} = \cos^{-1}\{ (L_1^2 + L_2^2 - TL^2) / (2 * L_1 * L_2) \} \qquad (4.4)$$

These values could now be used to define the orientation and

position of the tibia prior to and following osteotomy surgery. Three separate cases were reviewed: 1) determination of the tibiofemoral alignment associated with the conventional method, and the subsequent amount of undercorrection, 2) determination of the exact amount of rotational correction required to achieve neutral alignment, and 3) if an overall valgus tibiofemoral alignment was preferred, determine the rotational correction required to produce the desired alignment.

4.2.2.1. Case 1): Conventional Method - Neutral Alignment

The wedge size (θ_W) was set equal to TF and subtracted from θ_{TL}, as shown in figure 4.5. The new position of the tibia was defined by KA', and the corresponding change to the tibiofemoral alignment is given below.

$$\theta_W = \theta'_{TL} = \theta_{TL} - |TF| \tag{4.5}$$

$$TL' = \{ L_1^2 + L_2^2 - 2 * L_1 * L_2 * \cos\theta'_{TL} \}^{1/2} \tag{4.6}$$

$$\theta'_1 = \cos^{-1}\{ (TL'^2 * L_2^2 - L_1^2) / (2 * TL' * L_2) \} \tag{4.7}$$

The relative change to the tibial alignment (θ_{TMA}) created a new mechanical axis, TMA', that directly affected the tibiofemoral angle.

$$\theta_{TMA} = \theta'_1 - \theta_1 \tag{4.8}$$

$$TF' = \theta_{TMA} - |TF| \tag{4.9}$$

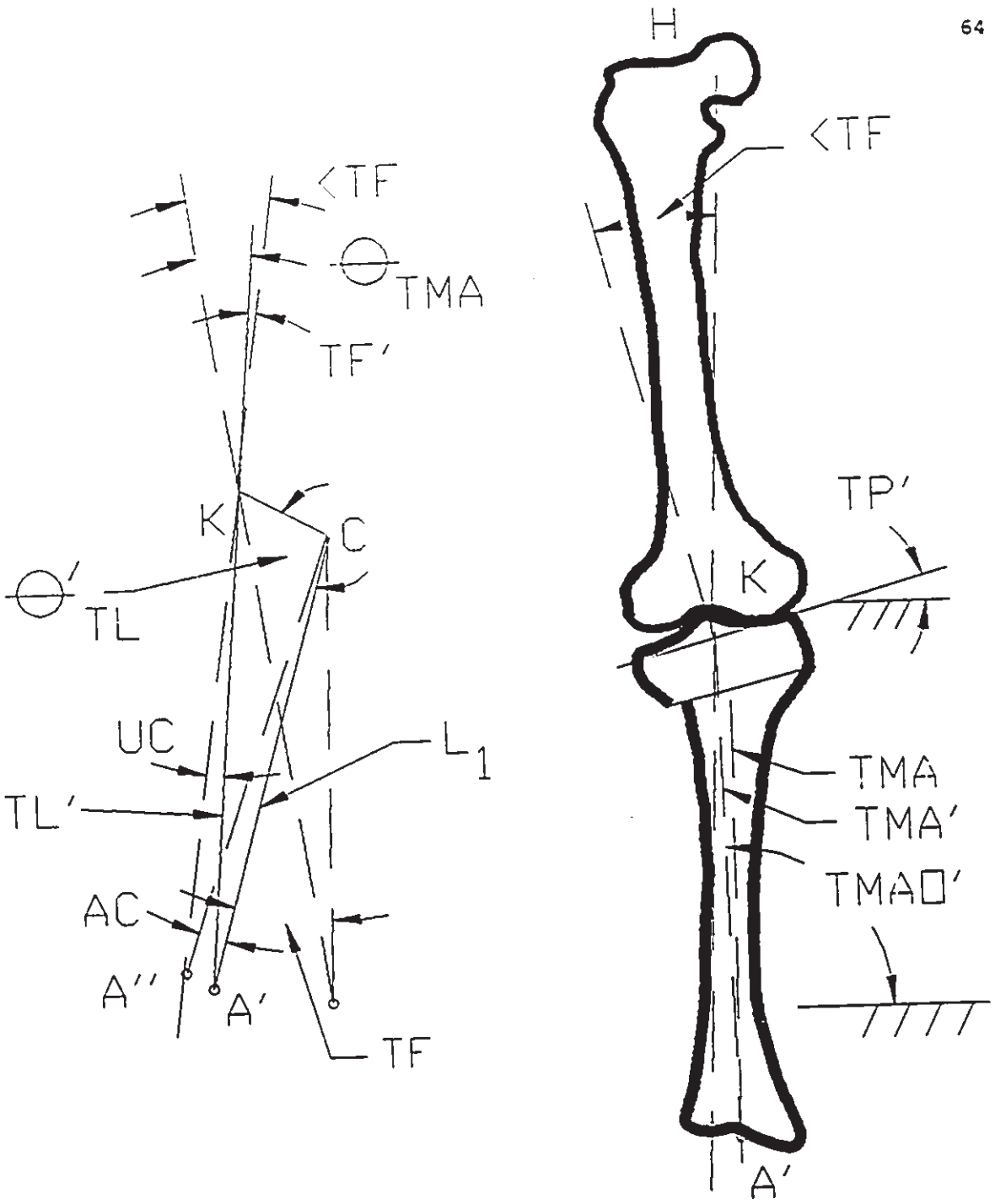

a) Relationship between the knee and ankle joint centres following rotational correction about point C.

b) Resultant alignment reveals an undercorrected/varus condition.

Figure 4.5: Case 1: Review of the conventional approach of the close wedge osteotomy.

A negative value of TF' represented a varus or under-corrected tibiofemoral alignment; likewise a positive value indicated an over-corrected or valgus tibiofemoral alignment.

$$UC = - TF' \quad \text{and} \quad OC = + TF' \tag{4.10}$$

4.2.2.2 Case 2): Modified Method - Neutral Alignment

One approach to calculating the amount of additional correction was to complete the second option and determine the wedge size necessary to obtain a neutral knee orientation. This is illustrated in figure 4.6, where angle θ_1 was increased by TF and the necessary wedge size was given by θ_w''.

$$\theta_1'' = \theta_1 + TF \tag{4.11}$$

$$L_1^2 = TL''^2 + L_2^2 - 2 * L_2 * TL'' * \cos\theta_1'' \tag{4.12}$$

Rearrange in the form $Ax^2 + Bx + C = 2$ and solve for the positive root of TL''.

$$TL''^2 + (-2 * L_2 * \cos\theta_1'') * TL'' + (L_2^2 - L_1^2) = 0 \tag{4.13}$$

$$TL'' = \left\{ \frac{2 * L_2 * \cos\theta_1'' + \{(-2 * L_2 * \cos\theta_1'')^2 - 4 * (L_2^2 - L_1^2)\}^{1/2}}{2} \right\}$$

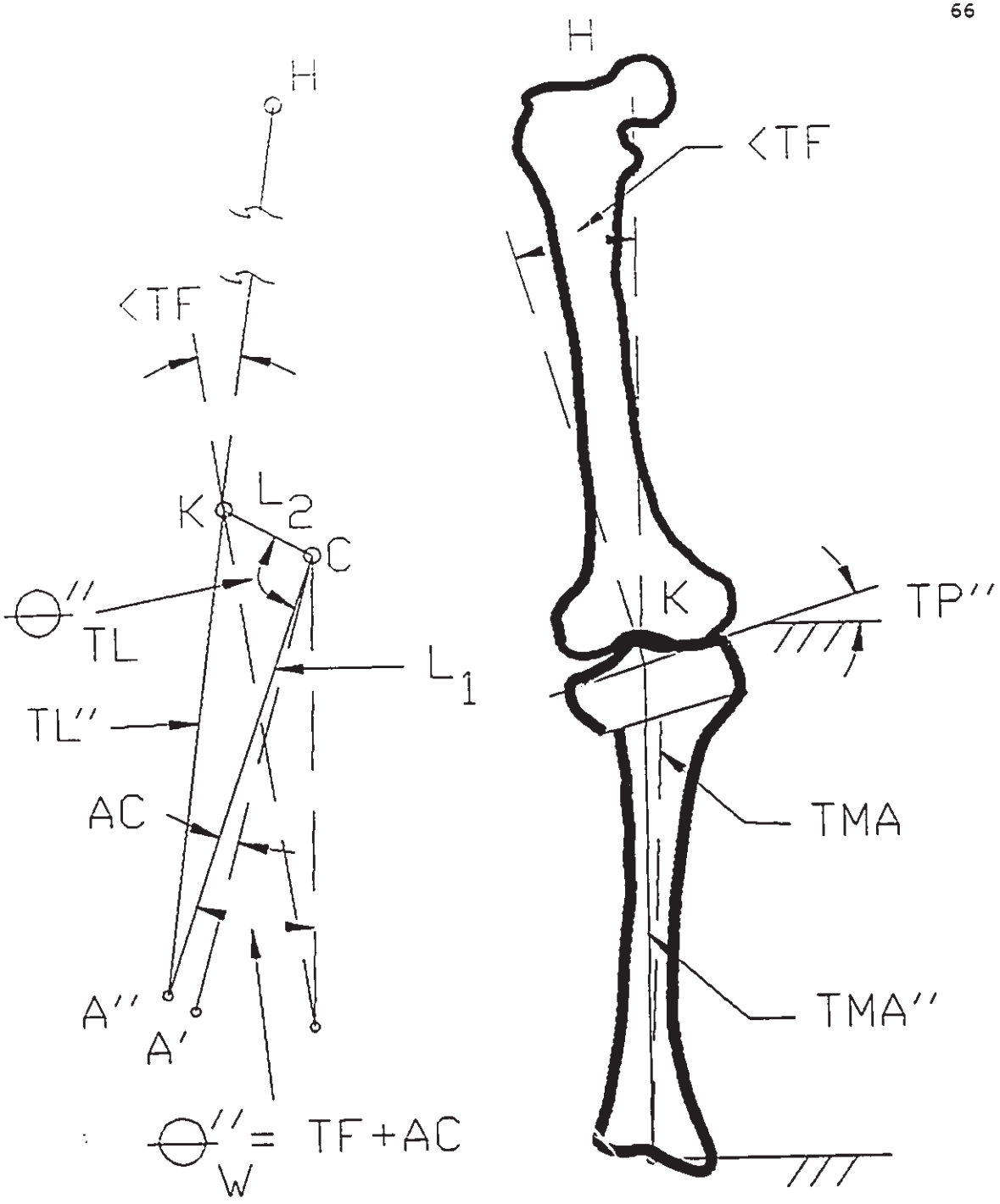

a) Realignment of the lower limb to a neutral orientation.

b) Identification of parameters corresponding to the neutral position.

Figure 4.6: Case 2: Modified approach to the close wedge osteotomy.

$$\theta''_{TL} = \cos^{-1} \{ (L_1^2 + L_2^2 - TL''^2) / (2 * L_1 * L_2) \} \qquad (4.14)$$

The actual degree of wedge correction was equal to θ''_w.

$$\theta''_w = \theta_{TL} - \theta''_{TL} \qquad (4.15)$$

and thus, the amount of additional correction (AC) required from case 1) was:

$$AC = \theta''_w - \theta_w \qquad (4.16)$$

Any alterations to the knee alignment directly affected the existing alignment at the adjacent joints, as well as the overall standing length of the lower extremity. The original limb length is given below as:

$$SLL = LF * \sin(FMAO) + LT * \sin(TMAO) \qquad (4.17)$$

Following correction to a neutral orientation, ie. case 2), the standing leg length becomes,

$$SLLP = LF + TL'' \qquad (4.18)$$

This could also be expressed as an increase or decreasae relative to the original length.

$$SLL\% = (SLL - SLL'') / SLL * 100 \qquad (4.19)$$

The angular changes required at the hip and ankle joints were calculated for the neutral orientation. Note that the final rotational adjustment at the ankle joint corresponds to the final wedge correction and new tibial mechanical axis (TMA'').

$$\text{delta } \theta_H = |FMAO - 90^\circ| \tag{4.20}$$

$$\text{delta } \theta_A = \theta''_W - \text{delta } \theta_H \tag{4.21}$$

Finally, the relationship of the tibial plateau surface relative to a horizontal datum line was equal to,

$$TP'' = TP + \text{delta } \theta_H \tag{4.22}$$

4.2.2.3 Case 3): Modified Method - Over-corrected Alignment

Many surgeons recommend a valgus tibiofemoral alignment, or an over-corrected condition (OC). To accomplish this with the model, equations (4.11) to (4.15) in case 2) were used, except the alignment correction became $\theta'''_1 = (\theta_1 + TF + OC)$. This is illustrated in figure 4.7; note the incremented labels for TL''' and θ'''_W. Calculation of the new hip and ankle joint orientations and standing leg length involved the use of the following equations.

$$SLL''' = \{FL^2 + TL'''^2 - 2 * FL * TL''' * \cos(180 - OC)\}^{1/2} \tag{4.23}$$

$$SLL\% = (SLL''' - SLL) / SLL * 100 \tag{4.24}$$

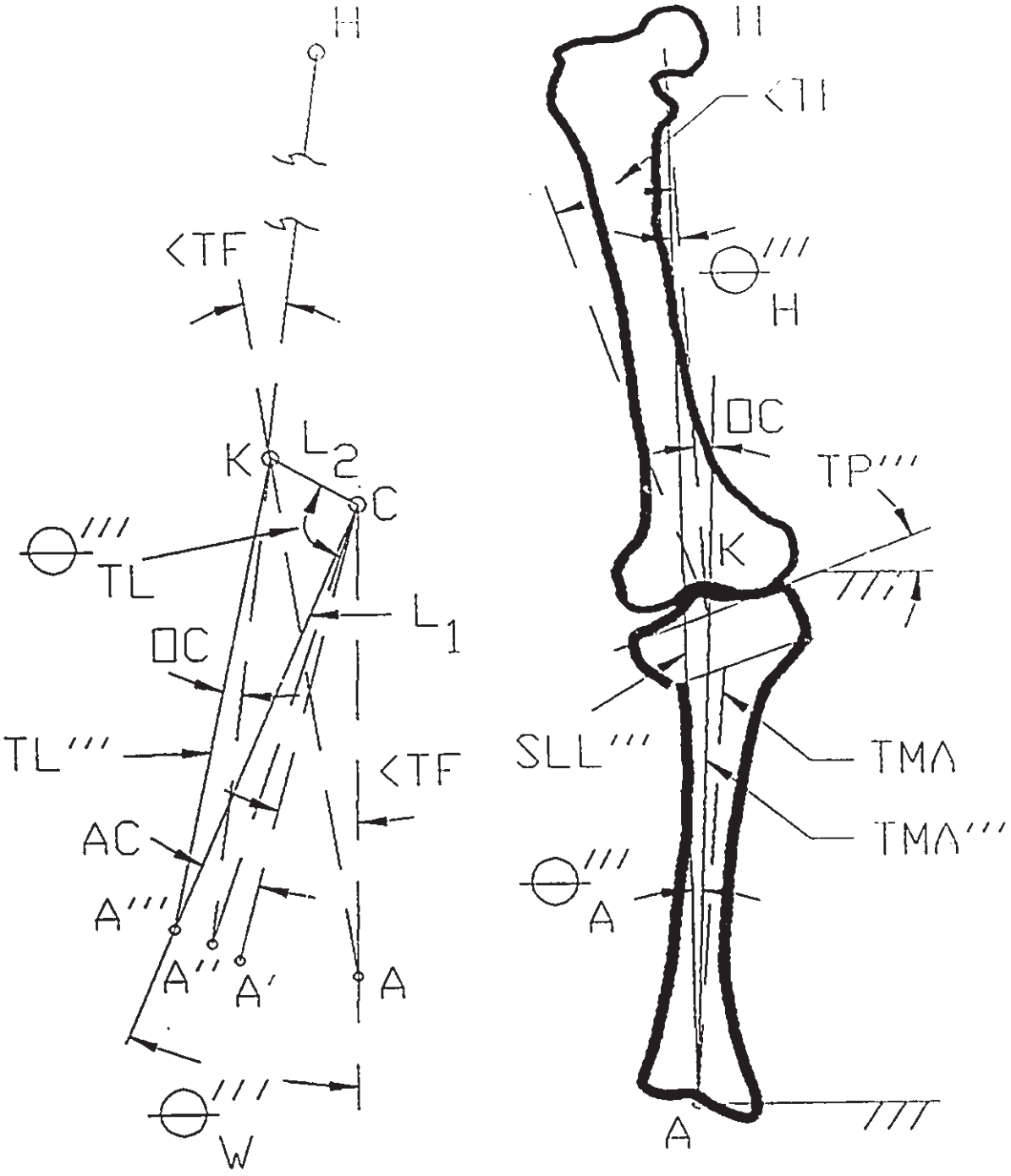

Figure 4.7: Valgus or over-corrected tibiofemoral alignment with a close wedge osteotomy.

$$\theta_H''' = \cos^{-1}\{(SLL'''^2 + FL^2 - TL'''^2) / (2 * SLL''' * FL)\} \quad (4.25)$$

$$\theta_A''' = OC - \theta_H''' \quad (4.26)$$

$$\text{delta } \theta_H' = \text{delta } \theta_H + \theta_H''' \quad (4.27)$$

$$\text{delta } \theta_A' = \theta_W''' - \text{delta } \theta_H' \quad (4.28)$$

$$TP''' = TP + \text{delta } \theta_H + \theta_H''' \quad (4.29)$$

4.2.2.4 Shift in Weight Bearing Axis across Tibial Plateau Surface

An alternate way to measure an over-corrected alignment was to measure the the location of the hip-ankle line (HA) relative to the knee centre during stance. In the case of over-correcting a varus malalignment, one may want to know at what point the weight bearing axis intersects the lateral compartment, and determine the corresponding wedge size necessary to obtain that condition. Ogata [122] recommends that the weight bearing axis be located at a distance of 70% of the tibial plateau width from the medial margin. Referring to figure 4.8a, HA should therefore intersect the tibial plateau at point I, located 70% of WP from the medial marign or 20% of WP from the knee centre. The model could be used to determine the location of I, for a selected amount of over-correction. The same equations used in case 3) were used again to calculate the standing leg length (SL'''), tibial axis length (TL'''), and θ_H'''. Figure 8b) shows the relationship between the amount of over-correction of the tibiofemoral axis and the location of the weight

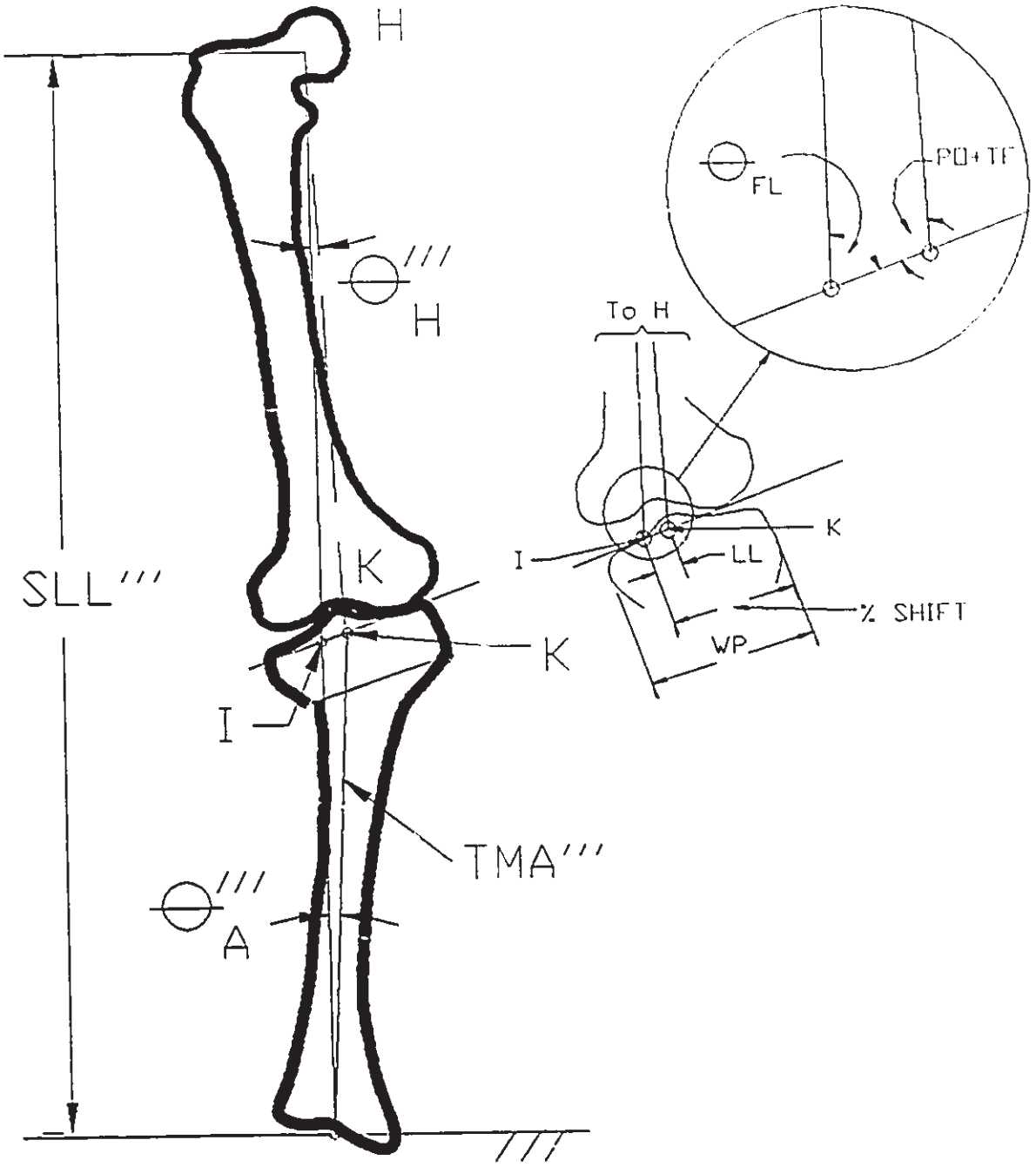

Figure 4.8: Location of weight bearing axis on tibial plateau for an over-corrected knee alignment.

bearing axis on the lateral compartment. A second triangle was formed with sides parallel to the tibial plateau surface (LL), extension of the hip-ankle line (LXT) and the new mechanical axis of the tibia (FL''').

$$\theta_{FL} = 180 - (PO + TF + \theta'''_{H}) \tag{4.30}$$

$$LL = \sin\theta'''_{H} * FL / \sin\theta_{FL} \tag{4.31}$$

The percent lateral shift of the weight bearing axis from the medial margin of the tibia is given below. For the neutral alignment case, LL = 0 and % shift = 50.%.

$$\% \text{ shift} = (LL + WP/2) / WP * 100 \tag{4.32}$$

4.2.3 Dome Osteotomy

The proposed model was also used to review the methodology of the dome osteotomy, as prescribed by Maquet [98,99]. The surgical procedure involved creating a curved fracture through the proximal tibia, then rotating the two segments to achieve a preferred knee joint alignment. The centre of the curved fracture was marked point D in figure 4.9, and was typically placed 4 to 6 cm below the plateau surface, with a fracture radius (r) of 2 or 2.5 cm. Maquet [98] defined two separate axes for the femur and tibia that were different than the conventional mechanical axes. The femoral axis was defined by a line between the hip centre and the midpoint of the cross section at the level of the osteotomy; point C in figure 4.9. Note that point C always

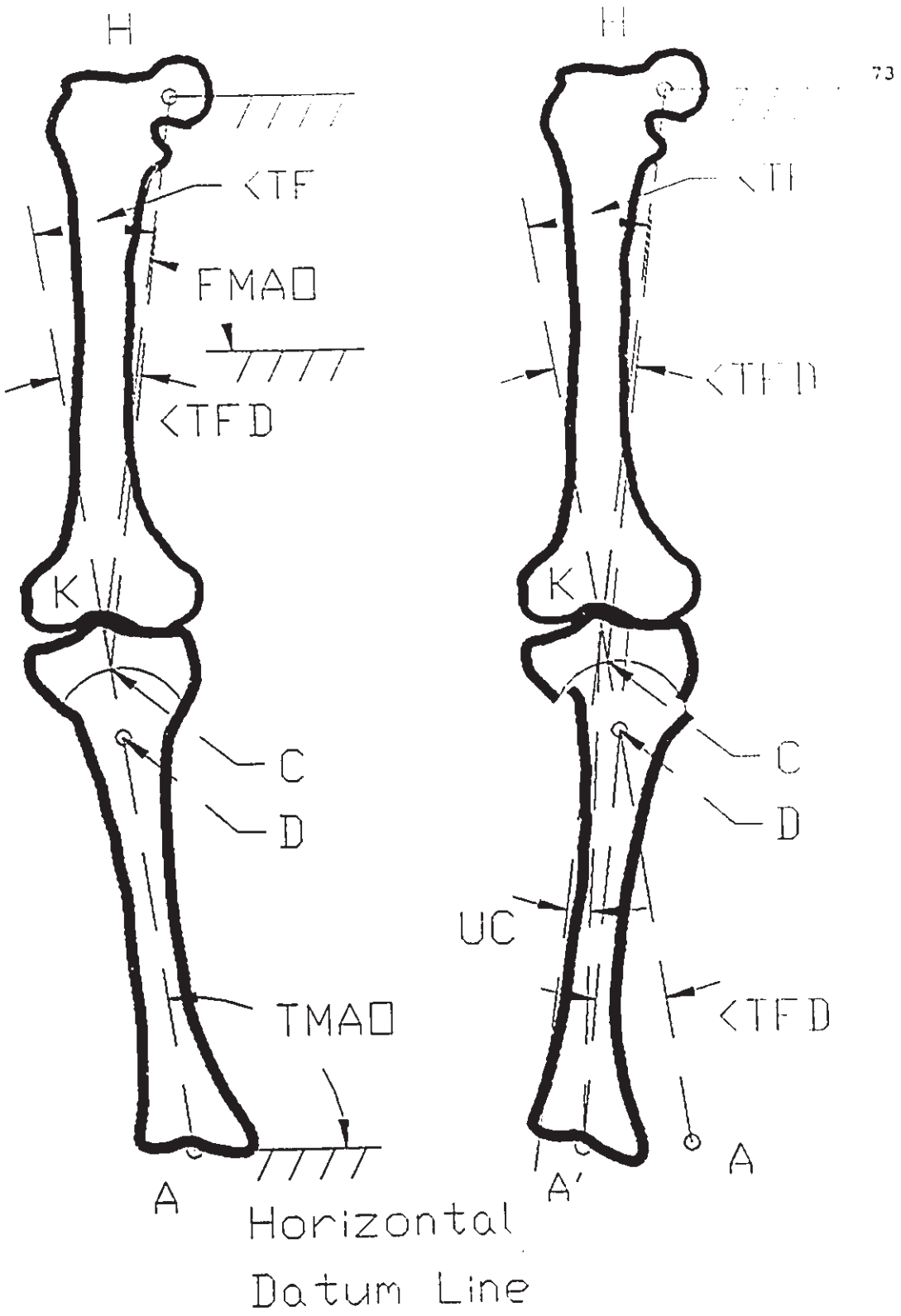

a) Initial alignment parameters for dome osteotomy.

b) Resultant alignment following conventional approach.

Figure 4.9: Modelling the surgical procedure of the dome osteotomy.

laid on the line KD at the level of the osteotomy cut. Another line drawn from the level of the osteotomy cut to the centre of the ankle represented the axis of the tibia. The alignment of the knee was then described by the angle subtended by these two lines, θ_{TFD}. Note that this angle was not the same as the mechanical tibiofemoral angle, TF. A relationship between them is derived below and illustrated in figure 4.10. The angle subtended between the mechanical axes of the femur and tibia is given by θ_4. Letting $\beta = 0$, the following relationships were derived.

$$\theta_4 = 180 - |TF| \tag{4.33}$$

$$d_4 = \{d_F^2 + d^2 - 2 * d_F * d * \cos\theta_4\}^{1/2} \tag{4.34}$$

$$\theta_{TFD} = \cos^{-1}\left\{\frac{d^2 + d_4^2 - d_F^2}{2 * d_4 * d}\right\} \tag{4.35}$$

Alignment correction was carried out by having the two bone segments rotated relative to each other an amount equal to $(\theta_{TFD} + \beta)$, where β varied between 3° and 6°, and was referred to by Maquet as an amount of over-correction. However, their definition of over-correction was different from that defined previously, and was not relative to the mechanical axes of the lower extremities, but rather relative to the axis system identified with the surgical procedure itself. To avoid any confusion, the term over-correction will now refer to the difference

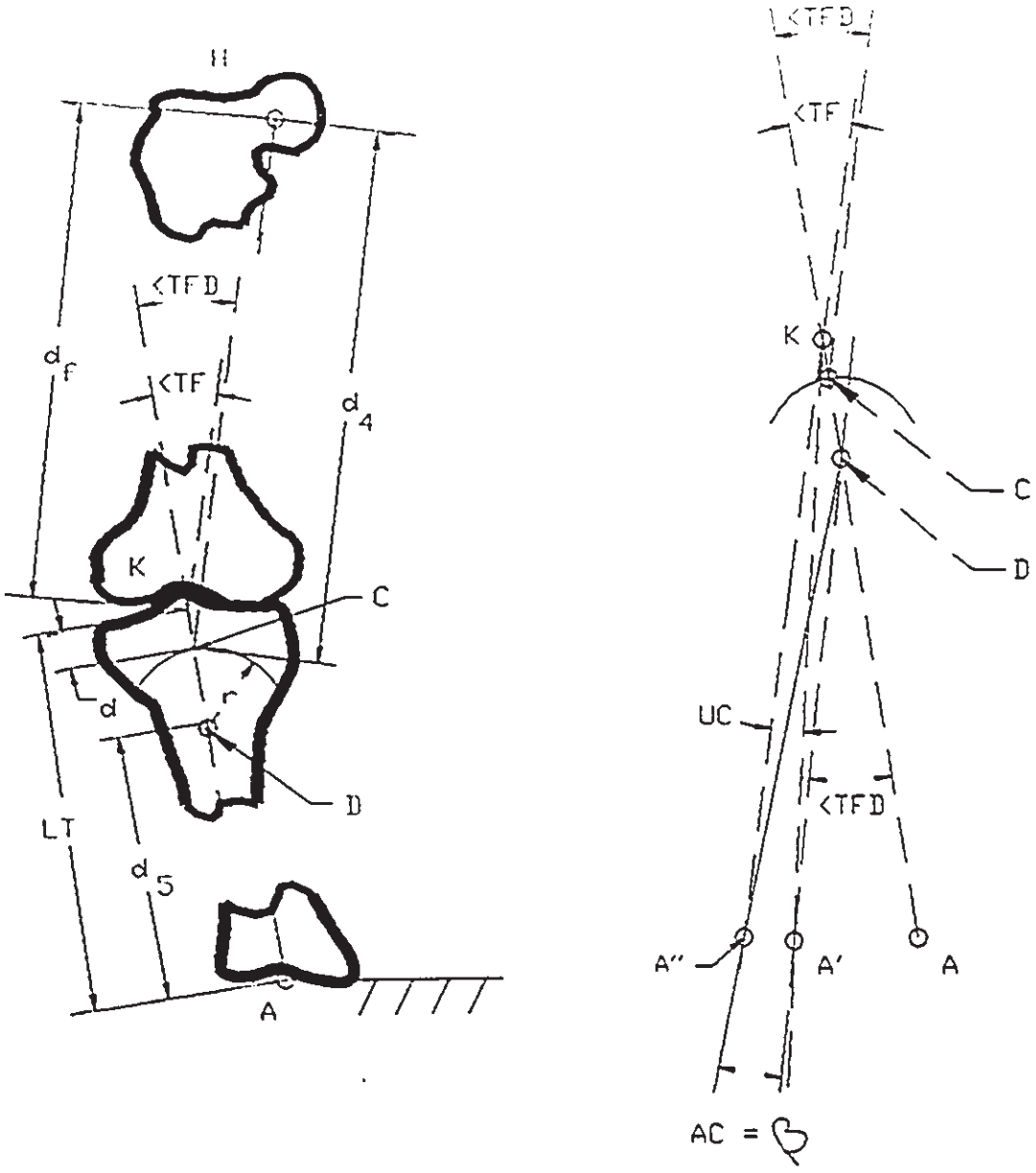

a) Relationship between the mechanical axes of the lower limb and the axes system used with the dome osteotomy.

b) Identification of β - term representing degree of over correction.

Figure 4.10: Identification of the model parameters for the dome osteotomy.

between the mechanical axes of the femur and tibia, called the tibiofemoral alignment (TF); a neutral orientation would have TF = 0°.

The model was then used to demonstrate the procedure, and to quantify its limitations. Two different approaches to the surgical procedure were reviewed in order to determine: case 1) the tibiofemoral alignment associated with the conventional method, and quantify any under/over correction of the tibiofemoral angle, and case 2) the additional amount of rotational correction required to achieve a neutral alignment. The value of β was initially set to zero, and thus, any amount of additional correction (AC) of the tibia between cases 1) and 2) was equilvalent to the β term referred by Maquet, ($3^{\circ} \leq \beta \leq 6^{\circ}$).

4.2.3.1 Case 1): Conventional Method - Neutral Alignment

Initially the axis of the distal tibial segment was aligned with the tibial mechanical axis, ie. $\theta_5 = 0^{\circ}$ and $\theta_6 = 180^{\circ}$. The tibia was then realigned by subtracting an amount equal to θ_{TFD} from θ_6. The new alignment of the tibia (KA') is shown in figure 4.11, while the corresponding change to the tibiofemoral alignment was marked TF'. The new alignment of the lower extremities is given below.

$$d_5 = LT - d - r \tag{4.36}$$

$$\theta'_6 = 180^{\circ} - \theta_{TFD} \tag{4.37}$$

$$d'_6 = \{(d+r)^2 + d_5^2 - 2 * (d+r) * d_5 * \cos\theta'_6\}^{1/2} \tag{4.38}$$

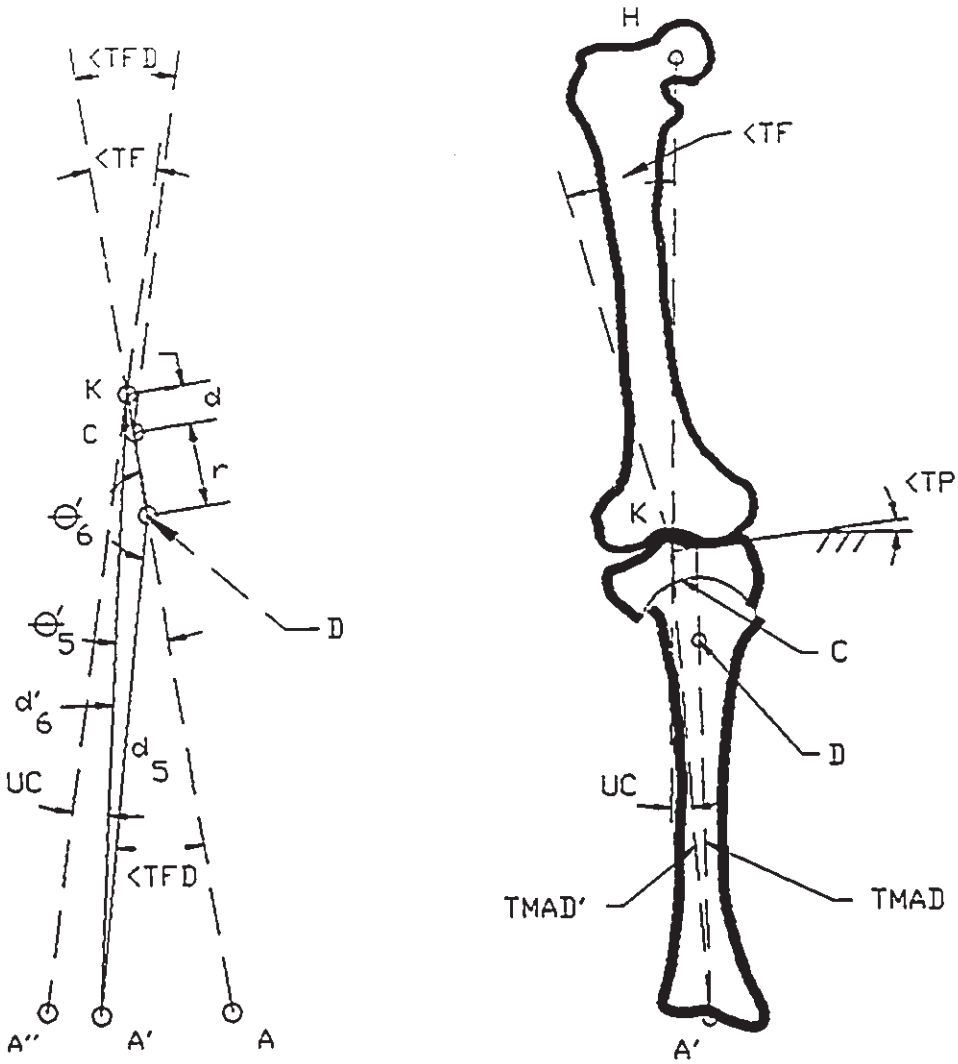

a) Relationship between the knee and ankle joint centres and the point of rotation of the osteotomy.

b) Resultant alignment reveals an undercorrected/varus alignment when β = 0.

Figure 4.11: Case 1: Review of the conventional approach of the dome osteotomy.

$$\theta_5' = \cos^{-1}\{ ((d+r)^2 + d_6'^2 - d_5^2) / (2 * (d+r) * d_6') \} \quad (4.39)$$

The rotational correction was applied to the tibia and changed the angle of the mechanical axis of the tibia by an amount TMAD, which in turn, altered the tibiofemoral angle.

$$TMAD = \theta_5' \quad (4.40)$$

$$TF' = TMAD - |TF| \quad (4.41)$$

As observed with the close wedge osteotomy, a condition of under-correction occurred, as illustrated in figure 4.11, and was equivalent to the resultant tibiofemoral angle, ie. UC = $|TF'|$.

4.2.3.2 Case 2): Modified Method - Neutral Alignment

The modified approach was implemented to calculate the amount of rotational correction necessary to restore the knee to a neutral orientation, ie. TF = 0°, and to estimate the amount of additional rotation required when the conventional method was used. This is illustrated in figure 4.12, where angle θ_5 was set to the value of TF, and the tibial rotation necessary for neutral alignment equalled θ_D''.

$$\theta_5'' = TF \quad (4.42)$$

$$d_5^2 = d_6''^2 + (d+r)^2 - 2 * d_6'' * (d+r) * \cos\theta_5'' \quad (4.43)$$

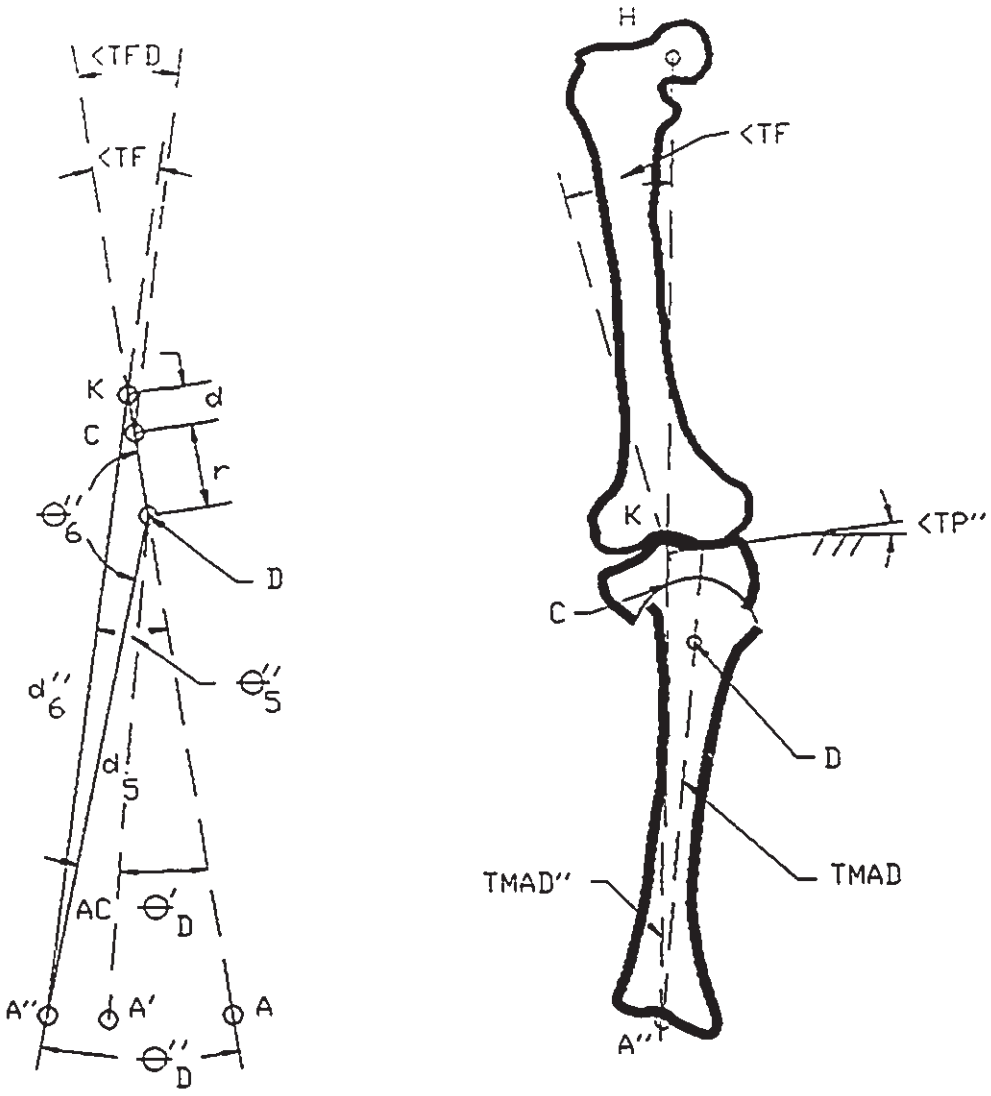

a) Realignment of the lower limb to a neutral orientation.

b) Identification of parameters corresponding to the neutral position.

Figure 4.12: Case 2: Modified approach to the dome osteotomy.

rearranging in the form $Ax^2 + Bx + c = 0$ and solving for d_6'',

$$x1 = -2 * (d+r) * \cos\theta_5''$$

$$x2 = 4 * ((d+r)^2 - d_5^2)$$

$$d_6'' = (-x1 + (x1^2 - x2)^{1/2}) / 2 \qquad (4.44)$$

$$\theta_6'' = \cos^{-1}\{(d_5^2 + (d+r)^2 - d_6''^2) / (2 * d_5 * (d+r))\} \qquad (4.45)$$

and the actual rotation required by the osteotomy (θ_D'') is

$$\theta_D'' = \theta_6 - \theta_6'' \qquad (4.46)$$

Referring back to figure 4.11, the amount of additional correction (AC) required to obtain a neutral orientation with case 1) was equal to:

$$AC = \theta_D'' - \theta_{TFD} \qquad (4.47)$$

As observed with the close wedge ostoetomy surgery, alterations to the knee alignment changed the existing alignment at the adjacent joints, as well as the overall standing length of the lower extremity. Correction to a neutral alignment changed the standing leg length. The resultant length could also be expressed as a percent increase or reduction in the original length.

$$SLL = LF * \sin(FMAO) + LT * \sin(TMAO) \quad (4.48)$$

$$SLL'' = LF + d_6'' \quad (4.49)$$

$$SLL\% = (SLL'' - SLL) / SLL * 100 \quad (4.50)$$

The corresponding angular changes required at the hip and ankle joints were calculated for the neutral orientation.

$$\text{delta } \theta_{HD} = |FMAO - 90^\circ| \quad (4.51)$$

$$\text{delta } \theta_{AD} = \theta_D'' - \text{delta } \theta_{HD} \quad (4.52)$$

Lastly, changes to the tibial plateau surface were measured in relationship to a horizontal datum line.

$$TP'' = TP + \text{delta } \theta_{HD} \quad (4.53)$$

4.2.3.3 Case 3): Modified Method - Over-corrected Alignment

When a valgus tibiofemoral alignment was preferred, the amount of over-correction (OC) was directly added to the overall tibial correction. That is, equations (4.42) to (4.46) in case 2) were repeated, except the alignment correction became $\theta_5' = |TF| + OC$. The resultant lower limb alignment is illustrated in figure 4.13, and involved changes to the limb length, hip and ankle orientations, and the tilt of the tibial plateau surface.

$$SLL''' = (FL^2 + d_6^2 - 2 * FL * d_6 * \cos\theta_{SLL'''})^{1/2} \quad (4.54)$$

$$\theta'''_{HD} = \cos^{-1}\{ (SLL'''^2 + FL^2 - d_6'''^2) / (2 * SLL''' * FL) \} \quad (4.55)$$

$$\theta'''_{AD} = OC - \theta'''_{HD} \quad (4.56)$$

$$\text{delta } \theta'_{HD} = \text{delta } \theta_{HD} + \theta'''_{HD} \quad (4.57)$$

$$\text{delta } \theta'_{AD} = \theta'''_{W} - \text{delta } \theta'_{HD} \quad (4.58)$$

$$TP''' = TP + \text{delta } \theta_{HC} + \theta'''_{HD} \quad (4.59)$$

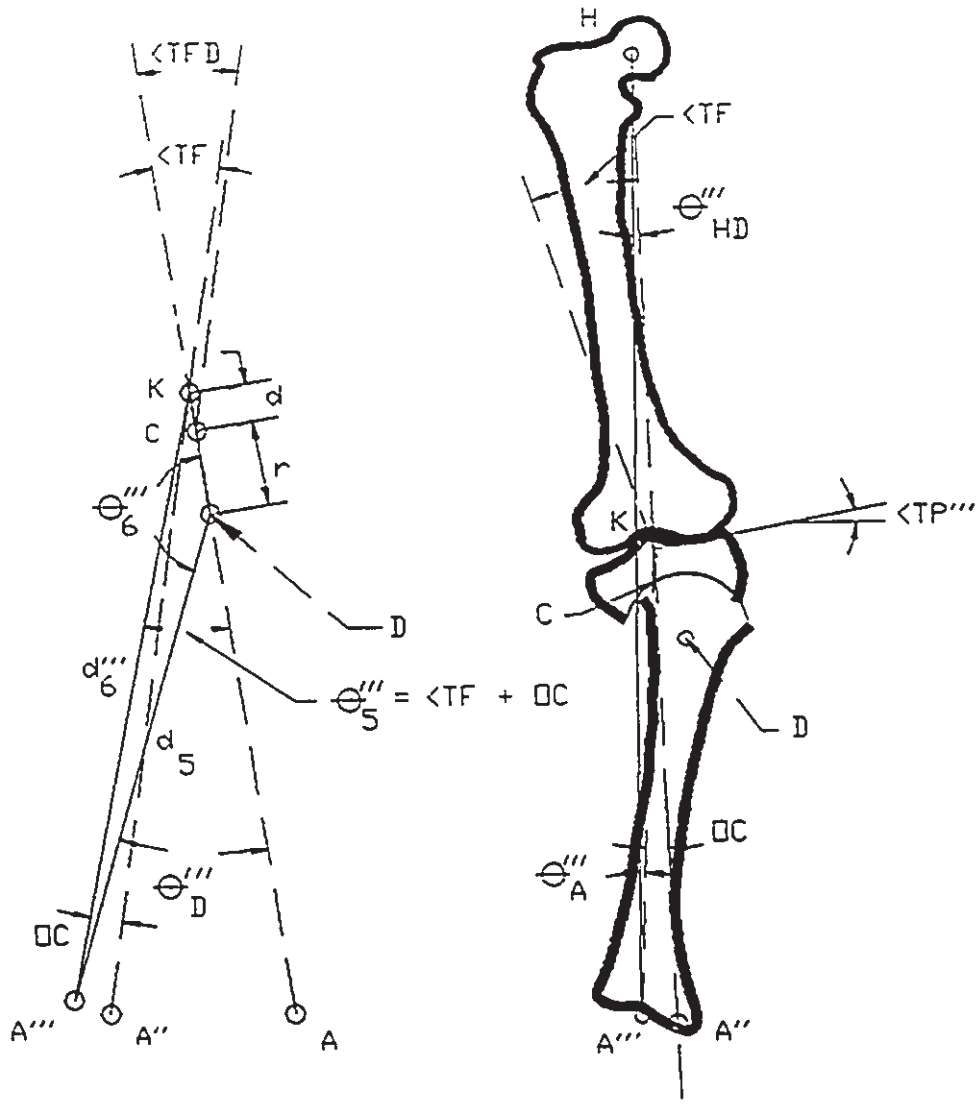

Figure 4.13: Valgus or over-corrected tibiofemoral aligment with a dome osteotomy.

4.3 Application of Model

A Fortran 77 computer program was written that executed the previously delineated equations on modelling the surgical methodology of the close wedge and dome osteotomies. The program is included in Appendix A and is completely interactive. A set of parameters must be defined that describes the alignment of the lower extremity. Application of the program is demonstrated in a sample problem and provided in the following section.

It is foreseen that this program would be made available to surgeons, and after obtaining malalignment information from full-length radiographs, they would easily and more accurately be able to determine the type, location and dimensions of the correctional cuts to be made.

4.3.1 Computational Results of Sample Problem

4.3.1.1 Initial Parameters

A sample problem was carried out using the trigonometric model to evaluate the steps involved in the surgical procedures. The initial alignment of the lower extremity is illustrated in figure 4.14.

A 15° varus tibiofemoral deformity was selected for the sample problem. Both the close wedge and dome procedures were analyzed, and included assessment of the conventional and modified techniques, as well as correction to a 5° valgus tibiofemoral angle. The 15° varus alignment consisted of a femoral offset of FMAO = 83° and a tibial offset of TMAO = 98°, relative to a horizontal datum line. Femoral and tibial lengths of 432 and 381 mm, respectively, were selected on the

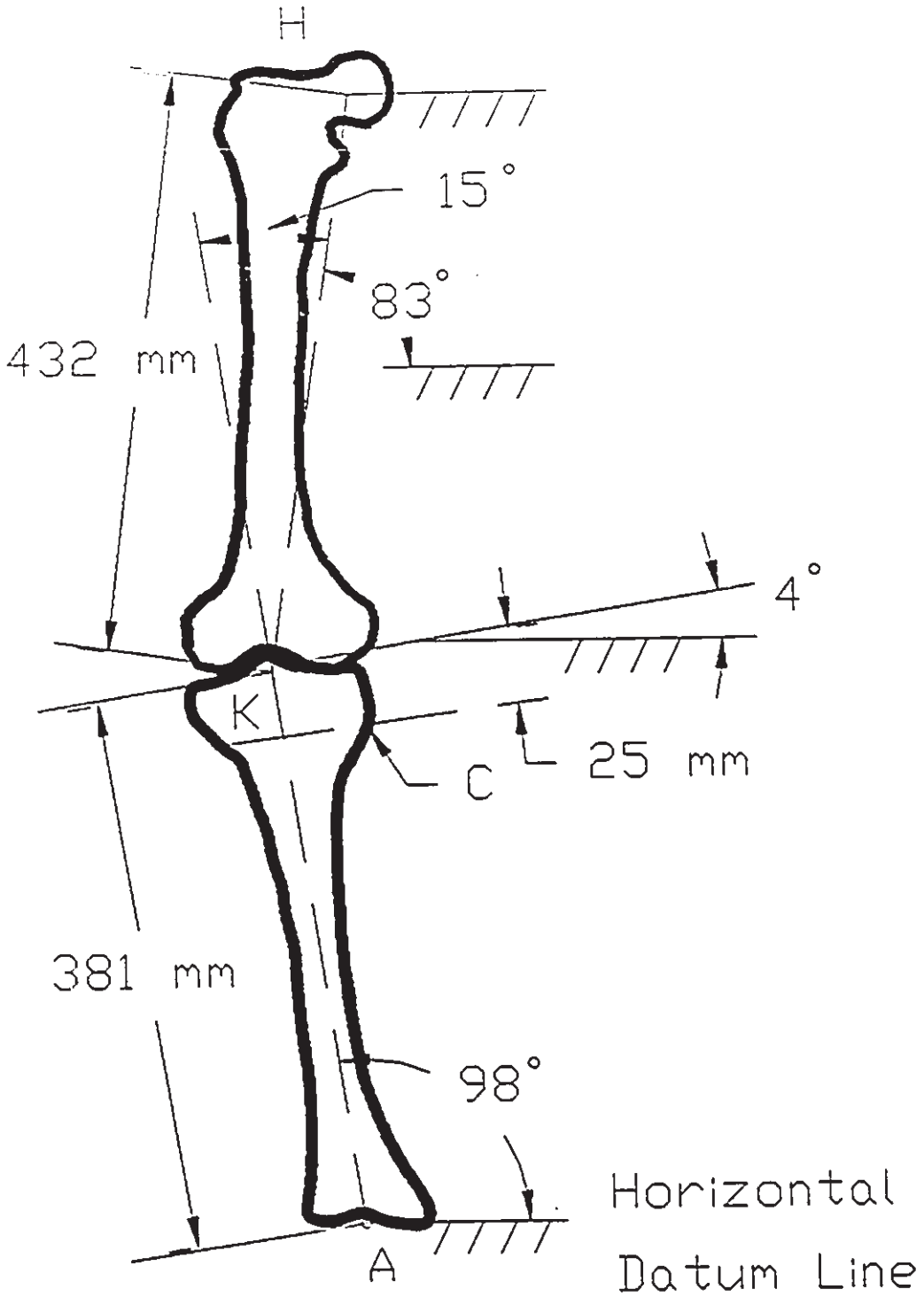

Figure 4.14: Varus alignment of lower extremity used in sample problem.

basis of previous anatomical measurements of the lower extremity provided in the literature (Cooke et al. [29], Winter [168]). This information would typically be obtained from existing full length radiographs of the lower extremity, using techniques decribed in Chapter 2.

The computational results from the program are included in the following sections for the close wedge and dome osteotomy models. Rotational adjustments required at the hip and ankle joints were also determined, along with the final changes made to the standing leg length and tilt of the plateau surface.

4.3.1.2 Close Wedge Osteotomy

The close wedge osteotomy was simulated by two cuts, one placed 25mm below the plateau surface and a second cut offset distally 15° from the first. The width of the tibial bone at the level of the first cut was set to 80mm (WC).

For case 1), a 15° wedge correction created a tibiofemoral angle of 14.2°, or a slightly under-corrected alignment. To achieve a neutral alignment, the results from case 2) indicated a wedge of 16° was required. The standing leg length (HA) decreased by approximately 5mm, relative to the original length. These values are illustrated in figure 4.15, and provided in table 4.1. Included in the table are the the net rotations that the hip and ankle joints must undergo to create the final limb alignment. It is important to understand that any angular correction at the knee joint directly affected the angulation of the hip and ankle joints. To achieve a neutral orientation, rotations of 7° and

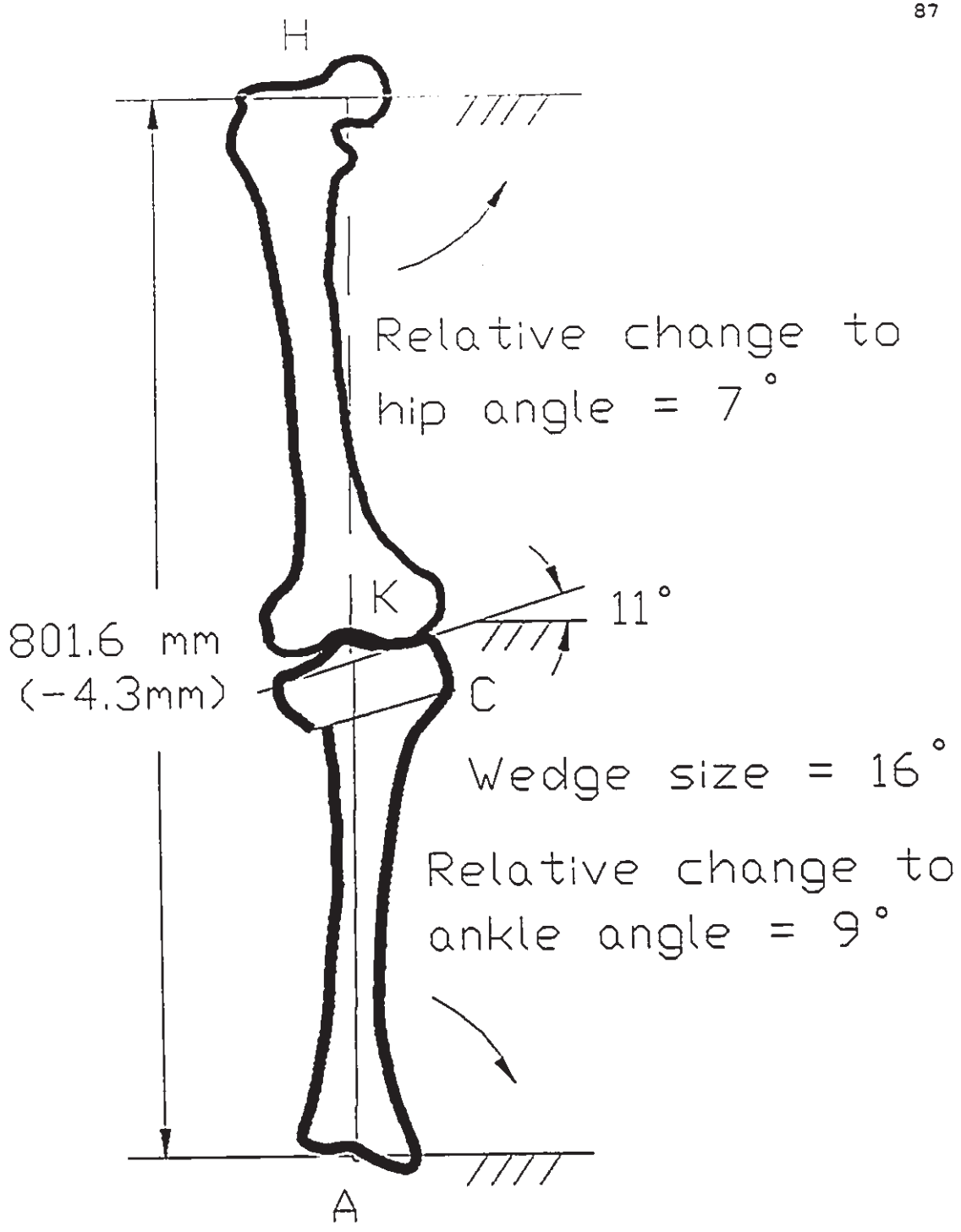

Figure 4.15: Resultant alignment of the lower extremity following correction of a 15° varus deformity using a close wedge osteotomy.

Table 4.1 Computational Results for Sample Problem: Correction of a 15° Varus Tibiofemoral Deformity using a Close Wedge Osteotomy.

INITIAL PARAMETERS:

Linear Measurements			Angular Measurements	
Length of femur	FL:	432mm	AS:	0°
Length of Tibia	TL:	381mm	TP:	4°
Standing Leg Length	SLL:	805.9mm	PO:	86°
Tibial Plateau Width	WP:	100mm	FMAO	83°
			TMAO	98°
			TF = FMAO - TMAO =	-15°

Close Wedge Osteotomy: WC = 80mm; d = 25mm

	Neutral Orientation		5° Valgus Tibiofemoral Angle	
	Case 1):	Case 2)	Case 1)	Case 3)
	$\theta_W = 15^{\circ}$	$\theta''_W = 16^{\circ}$	$\theta_W = 20^{\circ}$	$\theta'''_W = 21^{\circ}$
	TMA = 14.2°		TMA = 19°	
	TF' = -0.8°		TF' = -1°	
	UC = 1°	AC = 1°	UC = 1°	AC = 1°
	Relative change to Hip Angle	7°		9.3°
	Relative change to Ankle Angle	9°		11.7°
	Resultant Leg Length	801.6mm		796.1mm
	Increase (+) or Decrease (-) in Leg Length	-4.3mm		-9.8mm
	Tibial Plateau Tilt	11°		13.3°
	%Shift			69.%

9° were required at the hip and ankle joints, respectively. Thus, prior to the surgery, the range of motion of the adjacent hip and ankle joints should be checked by passively rotating each to ensure that the new position can be achieved. If the individual has a stiff joint and can not attain the required rotation, or the reoriented position brings about an increase in the level of pain at the joint, then a successful outcome of the osteotomy surgery is less likely.

The angular change at the hip joint also represented that amount of additional inclination of the tibial articular surface in the coronal plane. For the model, the plateau surface was initially offset 4° from the horizontal datum (ie. TP = 4°). Following the osteotomy, the tibial plateau offset increased to 11°, ie. TP = (4° + 7°) = 11°. This angulation should be kept to a minimum to control the shearing forces across the plateau surface, as they act to sublux the joint.

For a valgus tibiofemoral alignment of 5°, the conventional method produced an under-corrected tibiofemoral angle, requiring an additional angular correction of 1°, ie. a wedge of 21° was required. The standing leg length reduced by 10 mm, while a hip rotation of 9.3° and ankle rotation of 11.7° were required. Finally, the plateau surface laid 13.3° off the horizontal datum, and brought about a shift in the weight bearing axis (HA) equal to 69% of the plateau width, measured from the medial margin.

4.3.1.3 Dome Osteotomy

The dome osteotomy was modelled with a 25mm radius cut (r), with an origin (point D) located 50mm distal to the plateau surface.

For the conventional method (case 1), the resultant tibiofemoral angle was under-corrected by 2.7°. When the modified method was implemented, a rotational correction of 17.3° was required to obtain a neutral orientation (ie. TF = 0°). Remember that for both cases, β was set to zero in the model in order to quantify the amount of under/over correction of the tibiofemoral angle that occurred between the two cases. This also allowed for the calculation of the additional correction that was required to regain the desired tibiofemoral alignment. Here an additional correction of 3.1° was necessary to obtain a neutral alignment. The standing length of the lower extremity actually increased by 5mm for case 2), while hip and ankle rotations of 7° and 10.3° , respectively, were necessary. All of the calculated values for the neutral alignment of the simulated dome osteotomy are illustrated in figure 4.16, and listed in table 4.2.

When a tibiofemoral alignment of 5° valgus was preferred, the conventional method suggested a rotational correction of $14.2^{\circ} + 5^{\circ} = 19.2^{\circ}$, where $\beta = 5^{\circ}$. The model predicted a tibiofemoral angle of 1.7° valgus, which was 3.3° less than the intended amount. When case 2) was implemented, the required tibial correction ($\theta_{TFD} + \beta$) measured 23°; representing an additional rotation of 8.8°, ie. ($23^{\circ} - \theta_{TFD} = 8.8^{\circ}$). The difference in β between the two cases, here 3.8°, demonstrates the subjective limitations with this surgical technique.

4.3.1.4 Comparison Between the Conventional and Modified Methods

Limitations and errors associated with the conventional surgical method were identified by establishing a relationship between a

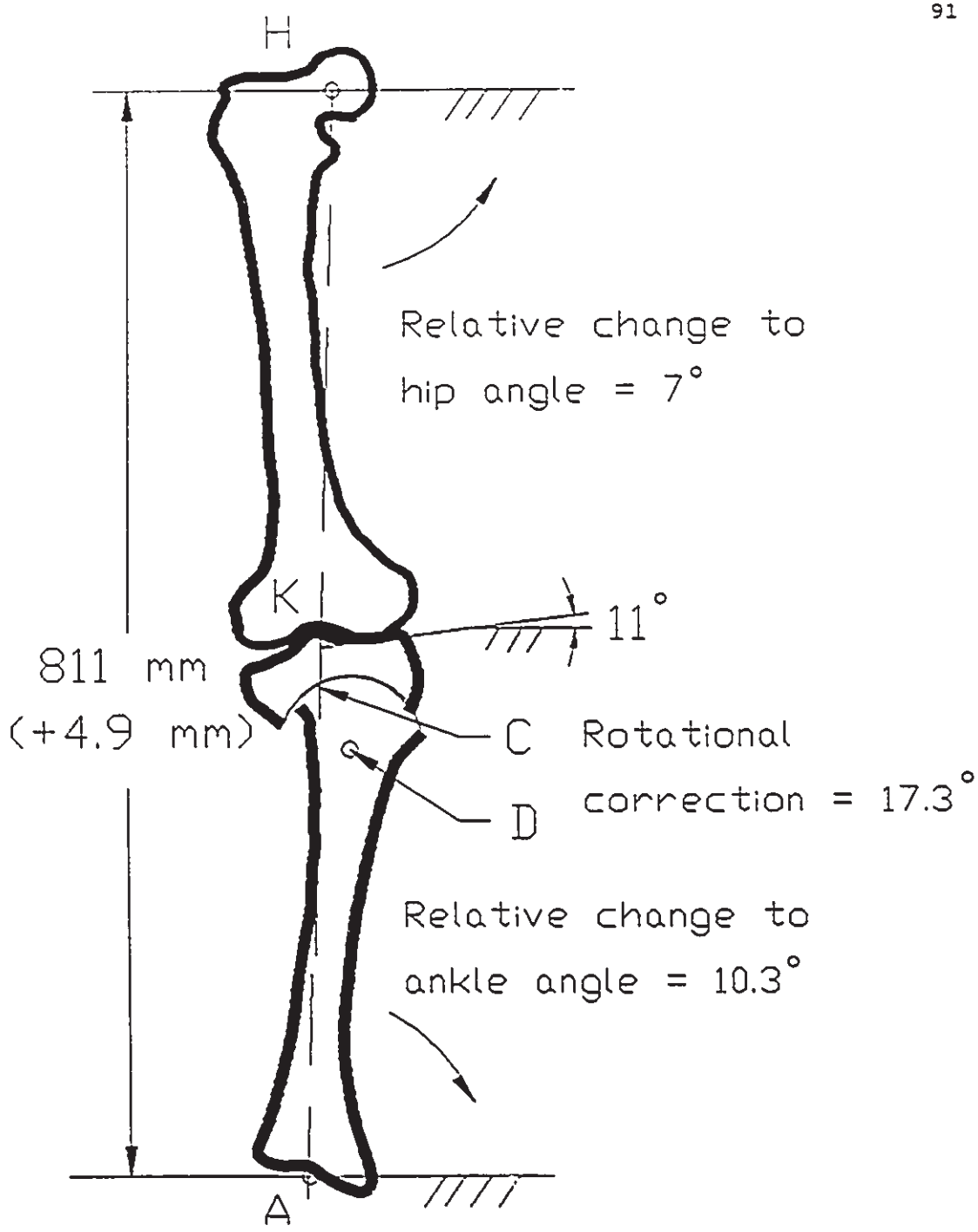

Figure 4.16: Resultant alignment of the lower extremity following correction of a 15° varus deformity using a dome osteotomy.

Table 4.2: : Computational Results for Sample Problem: Correction of a 15° Varus Tibiofemoral Deformity using a Dome Osteotomy.

INITIAL PARAMETERS:

Linear Measurements			Angular Measurements	
Length of femur	FL:	432mm	AS:	0°
Length of Tibia	TL:	381mm	TP:	4°
Standing Leg Length	SLL:	806.1mm	PO:	86°
Tibial Plateau Width	WP:	90mm	FMAO	83°
			TMAO	98°
			TF = FMAO − TMAO =	-15°

Dome Osteotomy: WC = 80mm; d = 25mm; r= = 25mm; TFD = 14.2°

	Neutral Orientation		5° Valgus Tibiofemoral Angle	
	Case 1):	Case 2)	Case 1)	Case 3)
	$\theta_D = 14.2^{\circ}$	$\theta_D'' = 17.3^{\circ}$	$\theta_D = 19.2^{\circ}$	$\theta_D''' = 23^{\circ}$
	TMAD = 11.5°		TMAD = 18.3°	
	TF′ = -3.5°		TF′ = 1.7°	
		UC = 2.7°		UC = 3.3°
	AC = 3.1°		AC = 3.8°	
Relative change to Hip Angle		7°		9.3°
Relative change to Ankle Angle		10.3°		13.6°
Standing Leg Length		811.0mm		808.8mm
% Increase or Decrease		+4.9mm		+2.7mm
Tibial Plateau Tilt		11°		13.3°
%Shift				70.%

preselected tibiofemoral malalignment and the resultant correction angle. This was accomplished by using the program to calculate the under-corrected angle (UC) and degree of additional rotation (AC) required to achieve a neutral tibiofemoral orientation, for varying degrees of malalignment.

In the case of the close wedge procedure, as the alignment deformity increased, the additional correction angle also increased. This is illustrated in figures 4.17 a) and b). Similarly, the amount of under-correction that occurred between the desired and resultant tibiofemoral angles increased as the alignment deformity increased. Figure 4.17 b) shows that the required rotational wedge correction was always greater than the actual alignment deformity. Furthermore, the amount of additional correction increased when an over-corrected tibiofemoral angle was selected.

When implementing the close wedge osteotomy, the user needs to select the location of the osteotomy cut (d) relative to the tibial plateau surface. This should be done with some consideration of the length of the tibia (TL) and width of the tibia plateau (WP). To better understand the relationship between them, the effects of each on the resultant tibiofemoral alignment are illustrated in figure 4.18. Values of AC and UC are plotted against the ratio (d/WC). Similarly, the effects of depth of the osteotomy cut to the tibial length (d/TL) and are compared in figure 4.19.

As the depth of the osteotomy cut was increased, the amount of under-correction increased, as well as the amount of additional correction needed to regain a neutral alignment. Figue 4.19 shows that

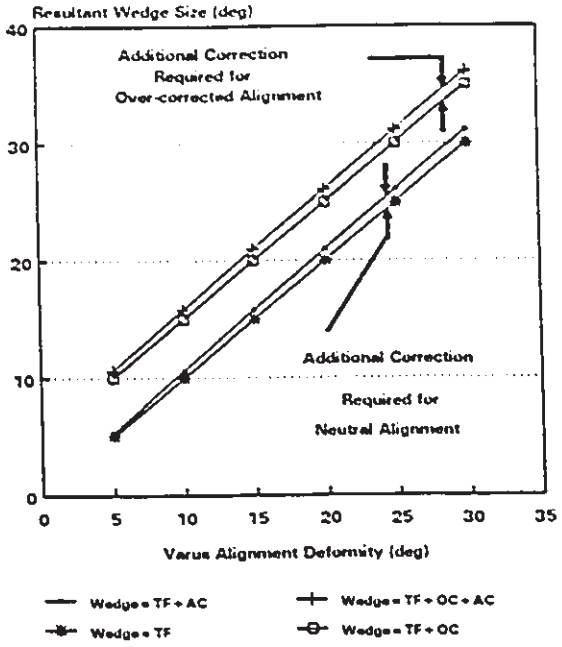

a) Required wedge correction for different varus alignment deformities.

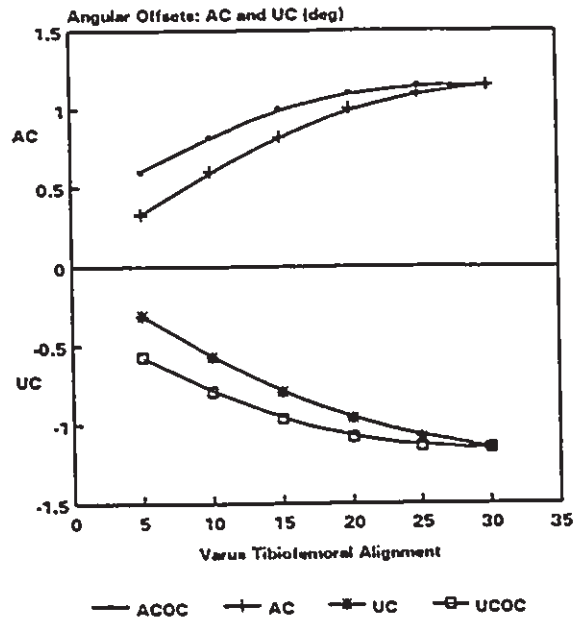

AC: Additional-correction
UC: Under-correction
OC: Over-correction

b) Relationship between the angular offsets (AC) and (UC) and a preferred tibiofemoral alignment.

Figure 4.17: Computational results of the close wedge osteotomy model.

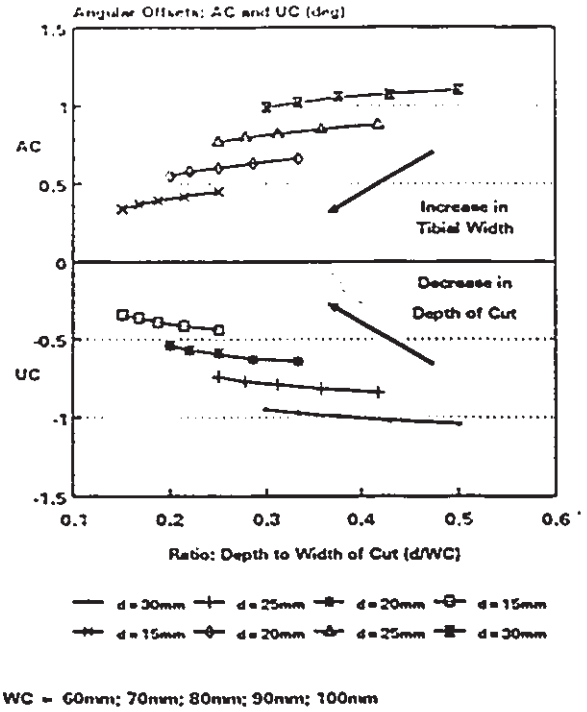

Figure 4.18: Effects of the depth of the osteotomy cut and width of the tibial plateau on the resultant tibiofemoral alignment.

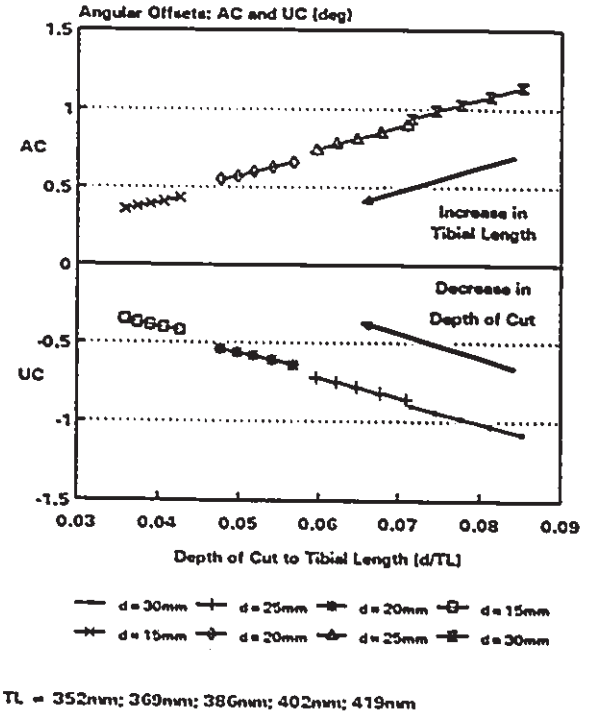

Figure 4.19: Effects of the depth of the osteotomy cut and length of tibia on the resultant tibiofemoral alignment.

the variations in the location of the cut surface had a greater effect on the resultant alignment than the width of the tibial plateau.

Upon review of the methodology of the dome osteotomy, as the varus malalignment increased, the additional angular correction (AC) also increased, as well as the amount of the under-correction (UC) associated with the conventional method. Figure 4.20a) shows that the necessary rotational adjustment of the distal tibia always exceeded the measured knee malalignment.

The conventional approach of the dome osteotomy, suggests an amount of over-correction should be added to the final rotation (referred to as β), ranging between 3° and 6°. However, for the sample problem, the model predicted an additonal 3.1° was necessary just to achieve a neutral alignment. This would correspond to a condition of $\beta = 0^{\circ}$, or no over-correction. This relative difference continues to increase as the alignment deformity increases.

When a 5° valgus tibiofemoral alignment was selected, the model predicted an additional 8.8° was necessary, ie. OC = 5° plus AC = 3.8°. In both cases, the final tibiofemoral alignment was always less the measured alignment deformity and produced an under-corrected tibiofemoral alignment. This is demonstrated in figure 4.20b).

When implementing the dome osteotomy, the user needs to select the location of the osteotomy cut (point C). This should be done with some consideration of the length of the lower extremity. To illustrate the effect of the depth of cut and limb length on the resultant alignment, the program was used to compare the additional correction (AC) and under-corrected values (AC) to the ratio of depth of cut per

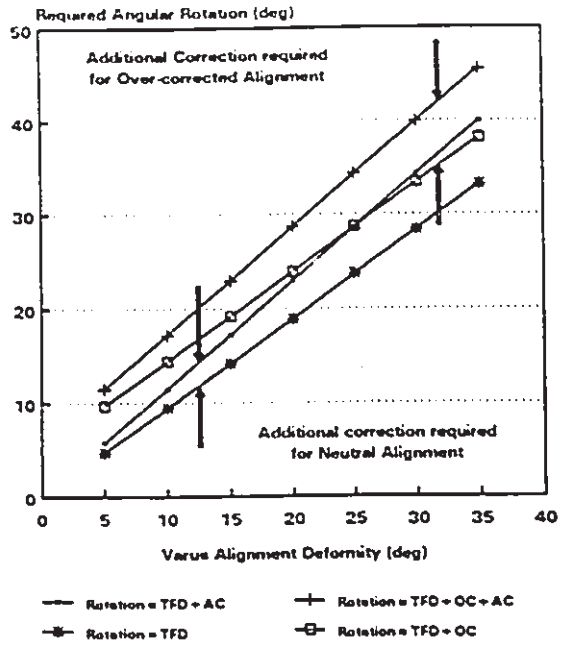

a) Required rotational correction of the distal bone segment (θ_w) for different varus alignment deformities.

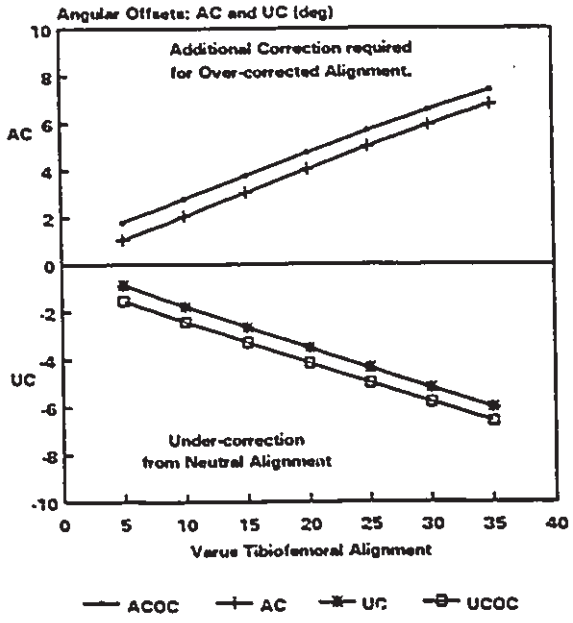

AC: Additional-correction
UC: Under-correction
OC: Over-correction of 5 degrees valgus

b) Relationship between the angular offsets (AC) and (UC) and a preferred tibiofemoral alignment.

Figure 4.20: Computational results of the dome osteotomy model.

tibial length (d/TL). The results are plotted in figure 4.21. Tibial lengths were set to 352 mm, 369mm, 386mm, 402mm, 419mm and 475mm, while d varying between 15 and 30 mm in increments of 5mm. As d increased, the required rotational correction increased, as well as the amount of under-correction. As the tibial length increased, however, minimal reduction was noted in the required rotational correction.

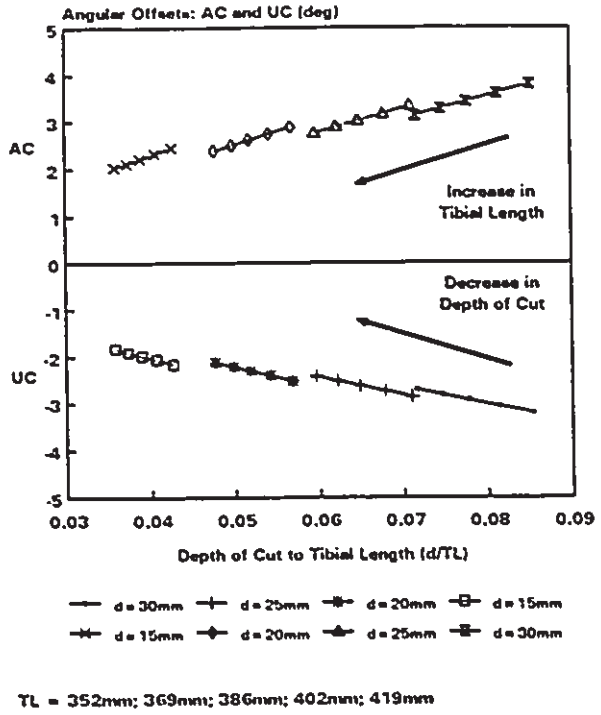

Figure 4.21: Effects of the depth of the osteotomy cut and length of tibia on the resultant tibiofemoral alignment for the dome osteotomy.

CHAPTER 5.0

MATERIALS

5.1 Introduction

The rationale for high tibial osteotomy surgery was to realign the tibia and femur in order to maximize the available contact surface area of the knee joint. By increasing the contact area, the joint articular pressure and stress state of the articular cartilage was reduced. This action has been shown to lessen the progress of osteoarthritis in the knee joint by enabling regeneration of the damaged cartilage. However, limited experimental evidence existed that supported this phenomenon. This was partly due to the state of available experimental equipment, as few mechanical devices exist capable of directly measure the dynamic contact behaviour between the articular surfaces of a cadaveric joint. Furthermore, without the experimental work, prediction of the optimal degree of alignment correction with osteotomy surgery remains uncertain.

The proposed experimental investigation attempted to quantify the biomechanics and functionality of the high tibial osteotomy, and reviewed the effects of knee malalignment conditions, in terms of contact area and contact pressure at the joint articular surface. Figure 5.1 is a schematic flow diagram of the proposed study and highlights the main topics of experimentation. The experimental phase also incorporated the results from the analytical modelling analysis, as described in Chapter 4 and shown in figure 5.1.

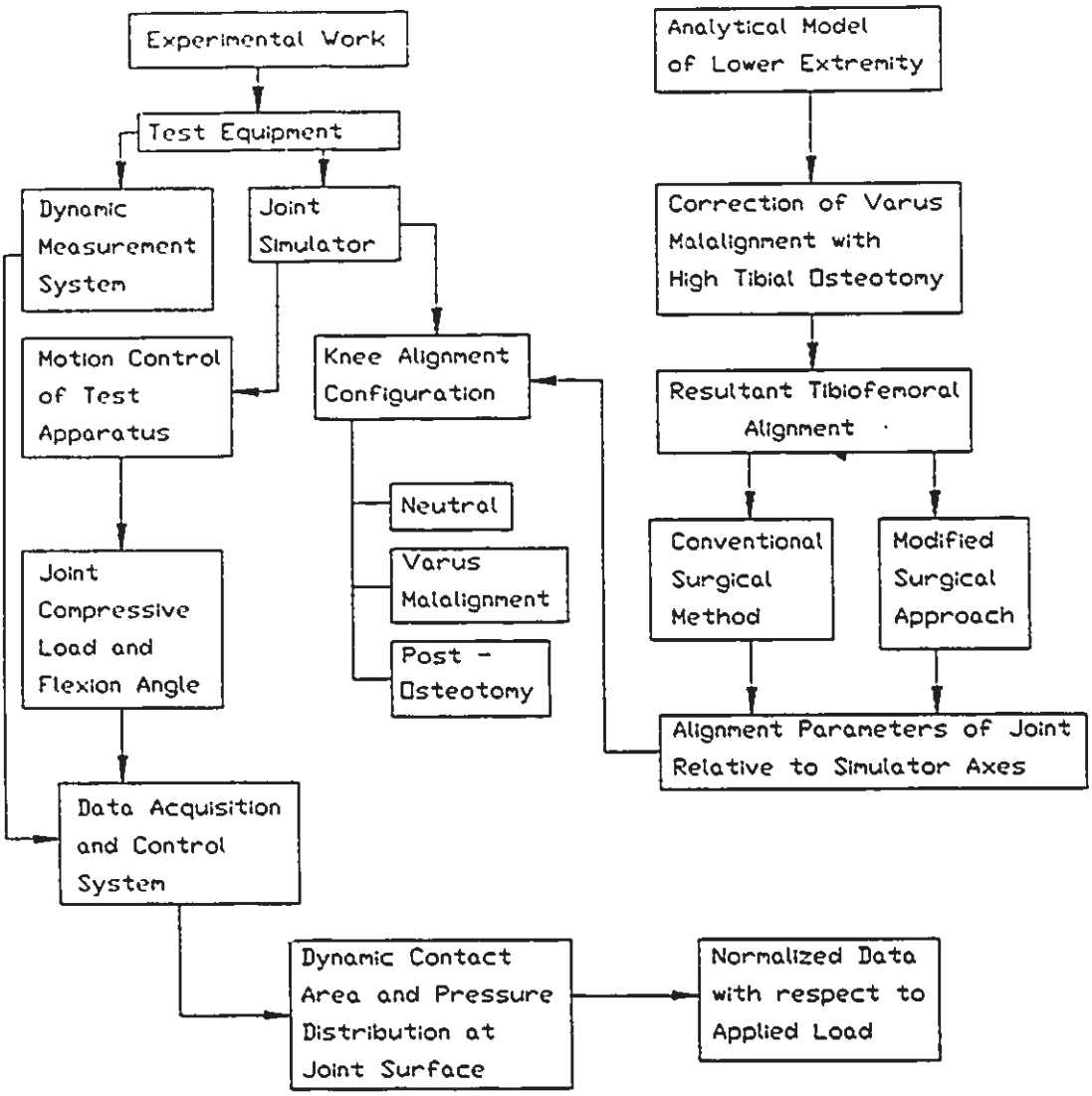

Figure 5.1: Arrangement of experimental and analytical work.

To carry out the proposed experimental work, three distinct and major contributions were required: 1) design and development of a dynamic pressure measurement system, 2) design and layout of a mechanical testing apparatus, and 3) the design and layout of a dedicated data acquisition system.

5.2 Dynamic Measurement System

An innovative measurement device was essential to monitor the in vitro dynamic contact pressure patterns between the articular surfaces of the knee. This would enable proper assessment of the effects of knee alignment , and high tibial osteotomy, on joint contact pressure when subjected to physiological load and movement conditions. The sensor material must also compensate for the viscoelastic deformational characteristics of the articular cartilage and menisci.

Measurement of the dynamic contact pressure behaviour at the joint surface proved to be a formidable task, often limited by the available measurement equipment. Many of the current techniques were described in section 3.3.2, and included the pressure sensitive Prescale film, used by Fukubayashi and Kurosawa [49], and the pressure transistor transducer designed by Inaba and Arai [68]. These systems are, however, limited to a quasi-static analysis at best, and typically have the knee orientation fixed while an oscillating load was applied across the joint. The measurement technique developed by Ahmed and Burke [3] could only analyze the static case, and could not be easily implemented in the laboratory.

More recently, Manouel et al. [95] developed a piezoelectric

polymer transducer for in vitro measurement of the dynamic contact stress distribution in the patellofemoral joint. The transducer consisted of a piezoelectric film sandwiched between two stainless steel electrodes and encapsulated with a teflon sheet. Final dimensions of the transducer were 3 mm in diameter and 0.7 mm thickness. Each transducer was cemented into a predrilled pilot hole located in the articular cartilage surface. The device circuitry required a charge amplifier for signal processing. Preliminary studies have been carried out on the contact pressure behaviour of the patellofemoral joint; no experimental work was carried out on the tibial plateau surface of the knee.

The following design criteria have been identified as part of any dynamic pressure measurement system.

1. The measurement pad must satisfy a dimensional constraint on the maximum allowable thickness. The sensor pad must be thin enough to be insertable into the knee joint cavity causing minimal alteration to the alignment, yet not disturb the menisci or surrounding ligament and muscle structures.

2. Properties of the sensing material must include the ability to respond to the dynamic nature of articular cartilage, meniscus and host bone.

3. The outer surface must be durable enough to withstand the continuous wear and frictional loads transmitted at the articular surface.

4. The measurement pad must be pliable enough to conform to the surface contour of the tibial plateau.

Such a device would permit in vitro measurement of the contact

pressure distribution patterns at the articular surface. From this, an estimate of the zones of contact area for various degrees of knee flexion and different arrangements of knee alignment would be possible.

Development of a new measurement system was thus undertaken, and utilized a polymeric piezoelectric material (Pennwalt Corp. [127]). The sensing material consists of a polymeric piezoelectric film having polyvinylidene flouride, PVFD, as a base resin. It is a long chain semicrystalline polymer of the repeated unit (CH_2CF_2). The material can be fabricated in sheet form to produce a flexible, tough and light weight material. Piezofilm is a dynamic material that develops an electrical charge proportional to a change in mechanical stress. The electrical charge will decay with time and depends on the dielectric constant and internal resistance of the material, as well as the input impedence of the interface electronics. Piezofilm also behaves as a pyroelectric transducer, as it is susceptible to temperature fluctuations, but can be controlled through proper sensor design [127]. The wide dynamic range of the material (.005 to 10^9Hz) and high elastic compliance make it ideal for measuring the transient contact behaviour of the viscoelastic articular cartilage.

Finally, piezomaterials are anisotropic, as their electrical. mechanical and electromechanical properties differ for electrical and mechanical excitation, along different directions of the film. That is, the material responds differently to pulling (tensile load) or bending of the piezofilm compared to the response for a purely compressive load applied across the film thickness. The compressive loading characteristics of the film were implemented in the design of the

measurement pad.

Prelimenary tests were carried out on a sample product of the piezofilm to evaluate its dynamic response characteristics. The sensor film was mounted in an MTS machine between two wooden blocks and placed under a cyclic load, and the output force from the sensor material was compared to the output signal from the MTS force transducer. Following signal integration and amplification, the signal response from the piezofilm was found to closely match the transducer output for load ranges between 100 and 4500 N. The sample material was fabricated on sheets 100 microns thick, which also made the material suitable for this study.

Although the entire surface area of the sensor is active, the output response does not differentiate between the total and actual areas under contact. Any unloaded area will lower the output voltage and cause substantial loss of the signal. This occurs because the unstressed area is the equivalent of a capacitor which shunts the electric charge produced by the sensing element. This is more prominent at higher frequencies. Fortunately, the proposed application operated at low frequency levels, thereby reducing signal loss. Thus, at best, estimates of average contact pressures were possible. When doing this, it was assumed that the total surface area was under contact. However, by reducing the active surface area of the sensor, local measurements of the contact pressure were available. This enabled estimations of the contact zones on the medial compartment for varying degrees of knee flexion. The concept of a multi-sensored measurement pad is considered superior to moving a single element across the tibial surface area. The

manufacturers of the film product recommend a minimum element circular diameter of 3.8 mm; thus a multi-element pad is feasible. The final number of sensor elements will depend on the availabe surface area of the medial compartment and the minimum element diameter size.

5.2.1 Design, Development and Fabrication of a Dynamic Multi- Element Measurement Pad

The steps employed in the design and fabrication of a new measurement system, for in vitro measurement of the dynamic contact stress distribution in the knee joint, are outlined below, and involve the use of the piezofilm product. Furthermore, design of the proposed measurement system was completed without any prior knowledge of the transducer work done by Manouel et al. [95].

Estimations of the surface area of the medial compartment were established from computer images of cadaver specimens, and provided an estimate of the active surface area available for the measurement pad. The final size and shape of the measurement device was selected to permit easy insertion into the joint capsule, yet not interfere with the joint alignment and stability, nor disturb the menisci or surrounding ligament and muscular structures.

The plateau surface of a cadaveric knee specimen is shown in figure 5.2. A digitized image of the same view is shown in figure 5.3; included in the pictures are the menisci and main ligament groups. The predominant area of contact on the medial compartment, as defined by previous researchers, is also included in figure 5.4. The overall

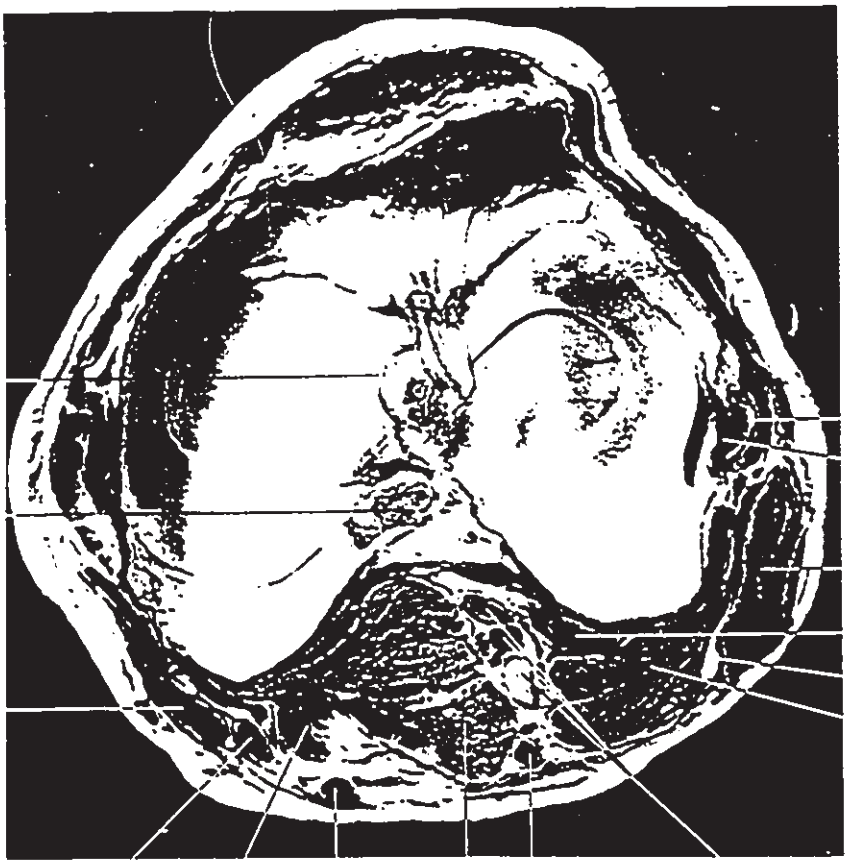

Figure 5.2: Cross-sectional view of proximal tibia [114].

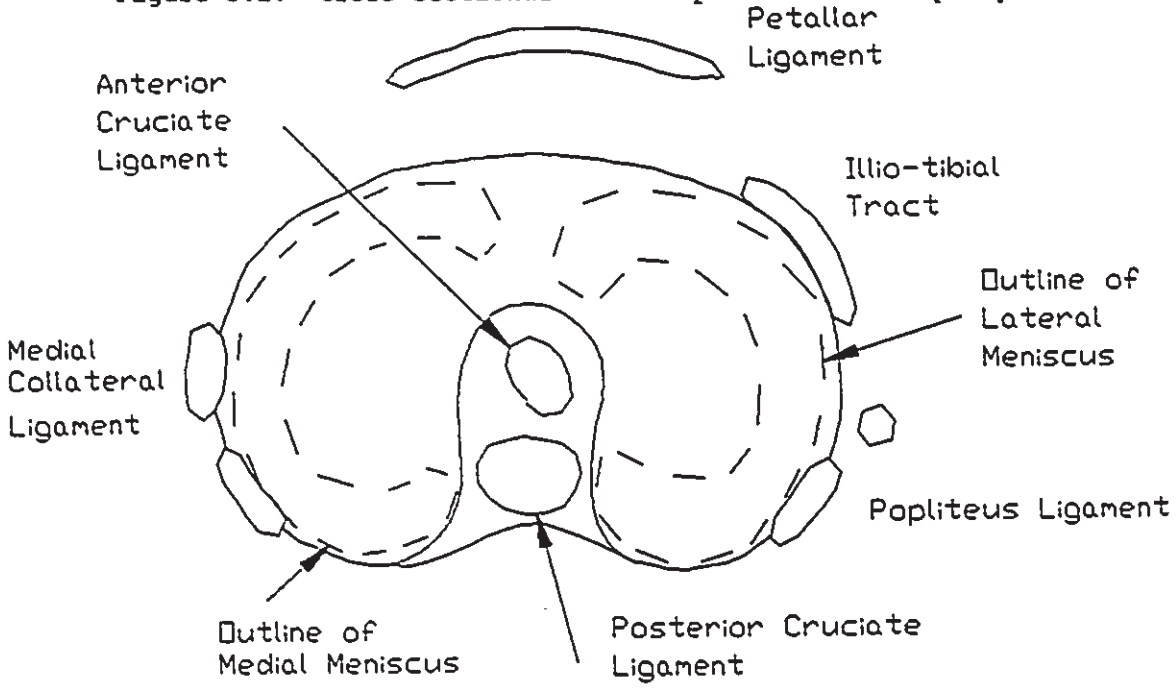

Figure 5.3: Digitized image of the proximal tibia.

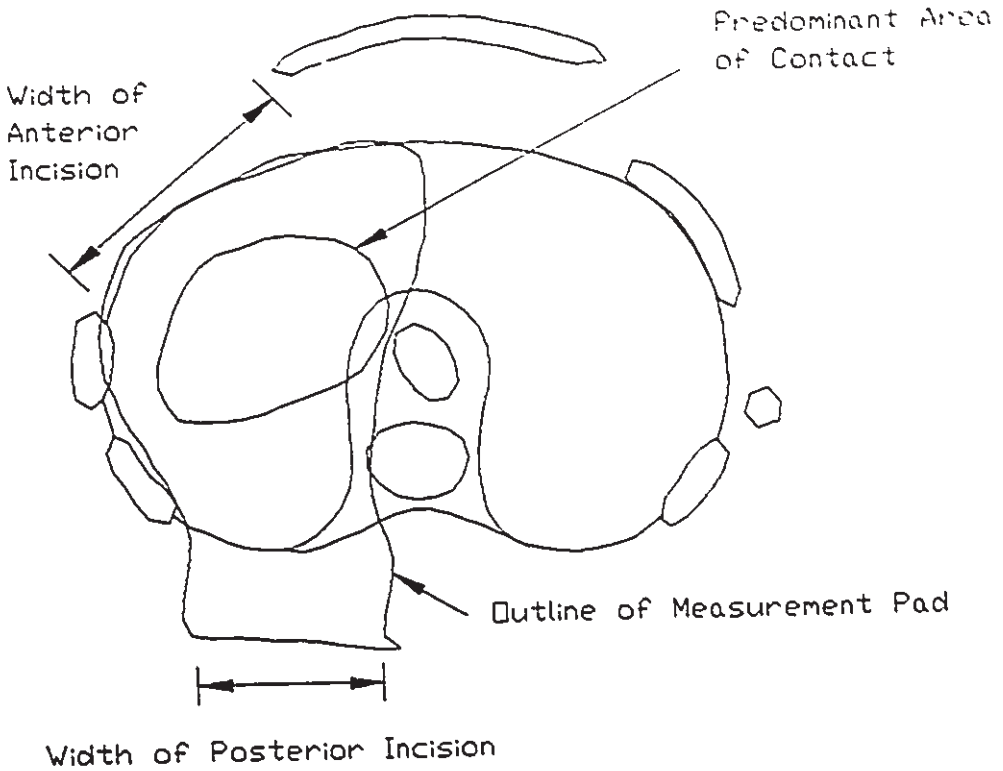

Figure 5.4: Location of sensor pad on medial tibial compartment.

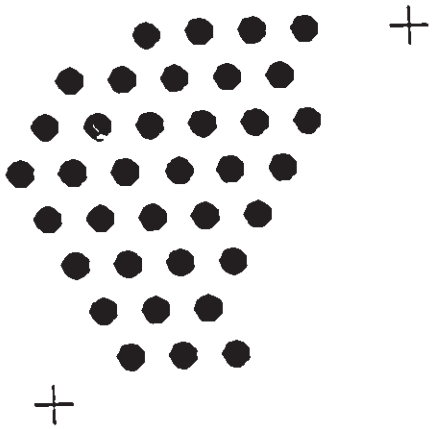

Actual Size of Measurement Pad

Figure 5.5: Sensor element arrangement of prototype measurement pad: Inner Sheet

construct of the measurement pad consisted of three layers of material sandwiched together. The middle layer included the piezofilm with the final array of sensor elements on it, and the outer layers were used to provide the two electrical connections to each element. Two separate array patterns were required: one for the piezofilm and a second for the wire tracings on the outer layers.

The actual pattern for the sensor elements was limited by the smallest element size (3.8 mm) and the size and shape of the medial compartment. The arrangement of the lead wire tracings provided the electrical connection between each element and the signal conditioning hardware (a standard 25 pin RS-232 cable connector). The following design constraint was placed on the wire tracings: a line width of 20 thousands of an inch ($\cong$ 0.5 mm).

Access to the articular surface was obtained via incisions through the joint capsule, as described later in section 5.9. The minimal length of the cut depended on the final width of the measurement pad. Conversely, the the final width of the measurement pad had to lay between the boundaries outlined by the perimeter of the joint capsule. The anterior length of the cut was estimated as the distance between the patellar tendon and the anterior part of the medial collateral ligament, and the posterior length of the cut by the distance between the posterior part of the medial ligament and the A-P centreline of the joint. These are identified in figure 5.4. To help reduce the width of the pad at these sections, the wire tracing separations were compressed to a centre line to centre line distance of .050 inches (1.27 mm). This required a special RS-232 connector, as most commercial connectors have

.10 inch centre line to centre line separations.

The last step in optimizing the layout of the wire tracing required that half of the connections on each outer sheet share a common ground. This reduced the number of active tracings extending out to the circuit board. By staggering the adjacent lead wires between ground and positive signals, signal interference and signal cross talk was reduced, since the ground tracings essentially acted as an electrical shield.

Numerous layouts of different element array patterns and wire tracings were generated on the computer before an optimal configuration was produced. The final prototypes were tested on embalmed knee specimens in the anatomy laboratory to validate the design. The optimal layout is shown in figure 5.5 and was comprised of a matrix of thirty-six individual sensor elements, uniformly distributed over the medial compartment.

The manufacturing process for the outer sheets was similar to that incorporated in flexible circuit board technology. Figure 5.6 shows the arrangement of the wire tracings. The lead wires extend out from the sensor elements and are aligned to mate with the connectors on the circuit board. A cross sectional view of the final measurement pad design is shown in figure 5.7. Fabrication of the measurement pad involved securing the outer and middle layers of material with double sided tape (.125 mm). In the original design, the tape isolated the wire tracings from touching the piezofilm. A later design modification had a layer of insulating material painted over the wire tracings to prevent any electrical short between the tracing signal and the piezofilm elements.

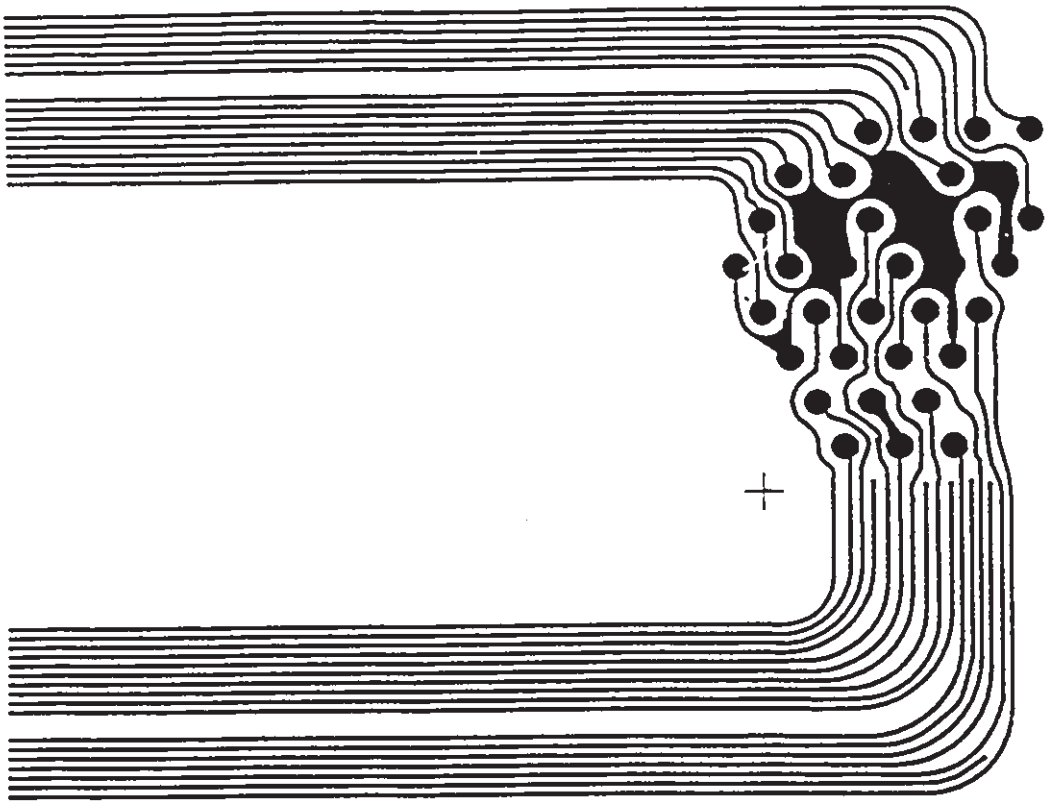

Figure 5.6: Wire tracing pattern on prototype measurement pad: Outer Sheet.

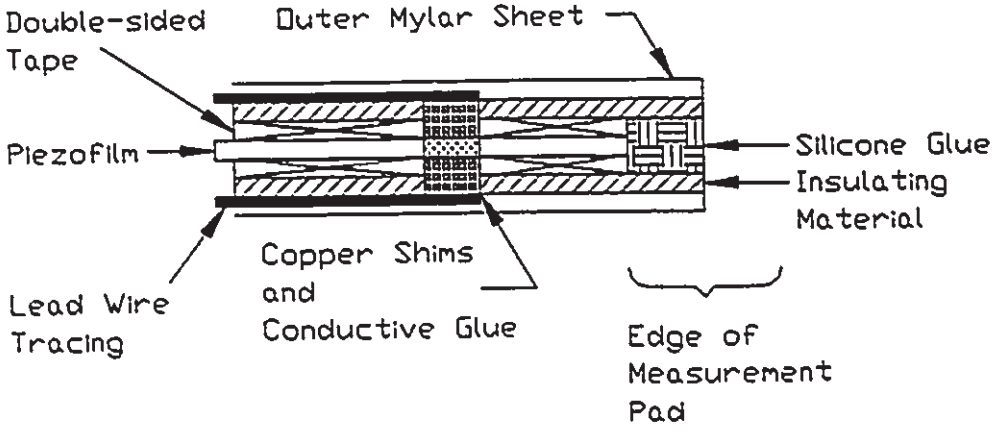

Figure 5.7: Cross - sectional view of measurement pad.

Introduction of a silicone glue along the outer perimeter of the measurement pad provided resistance to fluid penetration. This was necessary, as a generous supply of water (pseudo joint lubricant) was injected into the joint capsule at the level of the articular surface. The water was added between each trial run, helping reduce the friction and shear loads that occur across the top of the sensor element.

In order to place the sensor element under direct compression, ten copper shims (each .003 inches) were stacked together and positioned at the junction between the piezofilm and mating lead wire connections on the outer sheets; an electrical connection was maintained by a few drops of conductive epoxy. Care was taken to ensure the shims were positioned and held flat as the glue cured. The copper shims were of a slightly larger diameter than the sensor elements which caused the applied load to act over the entire circular surface area of the sensor element and reduced the effects of element bending. This was beneficial as the material was more responsive to a bending mode than pure compression. The measured output signal from each sensor now included the electrical resistance produced by the shims, epoxy and lead wires, as well as the piezomaterial.

It should be noted that the piezofilm itself has a common ground side and active positive side. Thus when mating all three sheets together, some elements will connect the positive side of the piezofilm to a positive tracing, while the remaining positive element connections will mate with a negative wire tacing. The same is true for the ground side of the piezofilm. This produced two types of signal patterns: positive-negative connection (type I) that generated a positive voltage

from the sensor for a compressive load and a positive-positive connection (type II) which generated a negative voltage for a compressive load. The two groups are illustrated in figure 5.8.

Since the material was also responsive to bending, two more loading configurations were included in the analysis. With the measurement pad inserted in a left knee, two types of element bending could occur: upward (a concave profile) or downward (convex profile). For a type I convex load arrangement the signal response was similar in polarity to that for the compressive mode. The only difference between the two modes of loading is the amplitude of the signal. A type I concave arrangement has a signal response opposite in polarity to that for the compressive mode. Thus, if the signal response from a particular element has the opposite polarity to that for the compressive mode, some degree of element bending must have occurred. The concept of like and opposite polarity responses can be used to identify the mode of loading of each element. Figure 5.8 also includes the voltage respones that are associated with element bending. When the sensor pad is flipped over, as is the case when going from a left knee to a right knee, the signal response for concave and convex profiles are reversed; a left knee - type I - concave profile has an opposite polarity response, whereas in a right knee this would be a like-polarity response.

The signal response from the piezofilm, when a compressive load was applied across the film thickness, was much lower than that when the film was pulled or bent. As a result, the amplitude of the signal could be used to differentiate between the mode of loading. It is unlikely

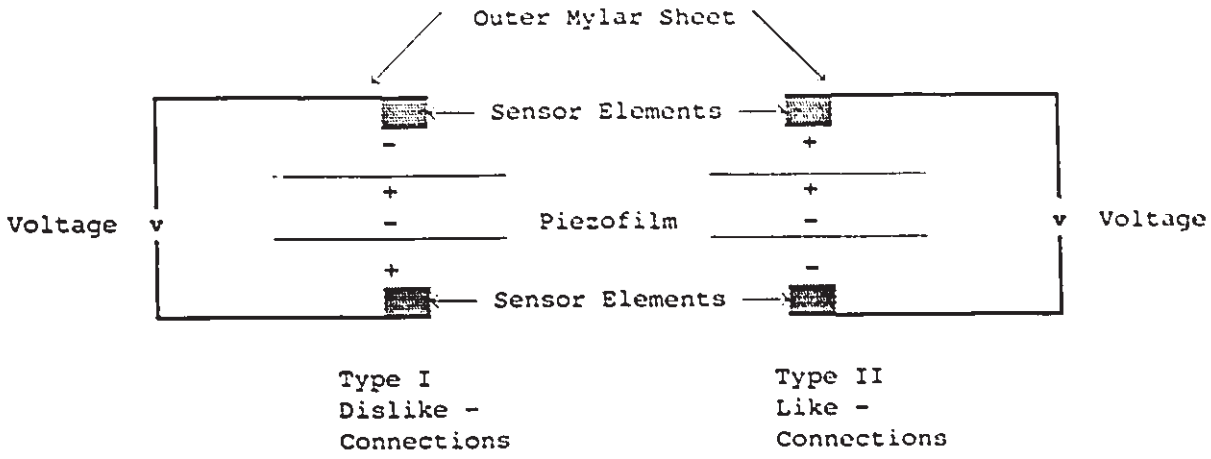

a) Sensor Element connections.

Type of Loading	Left Knee		Right Knee	
	Type I	Type II	Type I	Type II
Compression	+	-	+	-
Concave Profile	-	+	+	-
Convex Profile	+	-	-	+

b) Output voltage response patterns.

Figure 5.8 Sensor element connections and response patterns.

that all of the external load is carried by one particular sensor element. Thus, if the output signal calibrated for a compressive mode exceeds a percentage of the external applied load (10 to 15 percent), then a component of bending was presumed to be present. This was easy to determine by having the output normalized to the peak external load. This simple approach proved to be quite accurate and reliable in distinguishing between the modes of loading.

Although the measurement pad was designed to reduce bending of an element by adding copper shims, some degree of bending was unavoidable. This included those elements located near the inner edge of the meniscus or along the base of the intercondylar eminence. These were areas were the surface profile had a high radius of curvature relative to the element size. Figure 5.9 shows how elements in these regions can be placed under bending.

Preliminary tests with the first prototype resulted in mechanical problems of peeling and cracking of the ink tracings. A modified version of the measurement pad was fabricated using higher curing temperature ink which provided greater resistance to breakdown. A layer of non-conductive material was also deposited on top of the silver ink tracings, except at the sites where connection was made with the sensor element. The insulating layer provided EMI shielding, as the piezofilm is susceptible to low frequency noise (60 hz flourescent lights) and higher frequency interference (radio waves). The insulating material eliminated cracking and peeling of the tracings and prevented the tracings from making direct contact with the fixture hardware used to clamp the measurement pad. The final design of the pressure

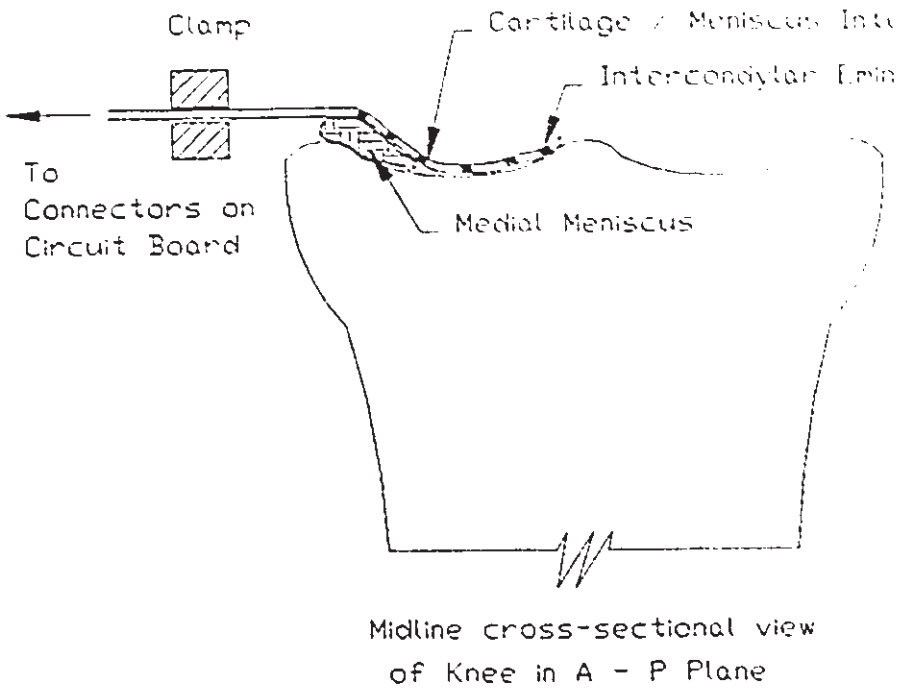

Figure 5.9: Surface regions where element bending can occur.

Figure 5.10: Final prototype of the measurement pad.

measurement pad is shown in Figure 5.10.

Unfortunately, difficulty was experienced in obtaining knee specimens for testing in this study, and two knees were sacrificed during the developmental stages of the prototype measurement pad and circuit board. This left four pair of knee joints available for testing. In addition, testing of the first pair of knees was done with the original prototype measurement pads, which had experienced some mechanical problems with the wire tracings.

5.2.2 Design of Signal Conditioning Hardware

The piezofilm employed in the sensor matrix is a dynamic material that produces an electrical charge proportional to a change in applied mechanical stress. The electrical response developed by the film decays with a defined time constant that is a function of the dielectric constant and internal resistance of the film, as well as the input impedance of the interface hardware. The interface electronics were required to process the signal prior to data acquisition. Here four groups of nine separate channels had to be recorded per trial to accommodate the thirty-six elements.

A schematic of the processing hardware required for a single channel is shown in figure 5.11. The analog circuit consists of a differential amplifier and RC loop used to set the cut-off frequency, fc, and a unity gain buffer and op-amplifier that will establish the circuit gain. Signal gains of either 10 or 100 could be selected for each element. Bench testing of the circuit design was initially performed exclusive from the testing apparatus. It was hoped that any

additional interference on the output signal, created by the mechanical testing equipment, could be isolated and removed.

After satisfactorily processing a single channel, a printed circuit board was laid out that could monitor all thirty-six sensor elements. The above circuit was repeated nine times, and a four-way switch was added plus a series of multiplexer chips. This enabled sampling of four different groups of channels. The layout for the printed circuit board was drawn using the commercial AUTOCAD drafting package and is shown in figure 5.12. Fabrication of the board was carried out with the assistance of the department technician. The necessary component hardware consisted of standard off the shelf items; the completed circuit board is shown in figure 5.13.

5.2.3 Modifications to the Basic Circuit Design

Satifactory operation of the analog circuit was achieved only after the following modifications were added to the design of the circuit hardware.

1. Use of piezoelectric materials often require a charge amplifier to integrate, amplify and filter the signal response. Static measurements required a charge amplifier, as the piezofilm produced a change in voltage output to a change in the applied stress. The present circuit hardware required nine amplifiers to service the thirty-six channels; unfortunately this was not feasible. In addition, the proposed concept of automatically switching between four groups of nine different channels was not possible, as a finite amount of time was required to let each channel stabilize.

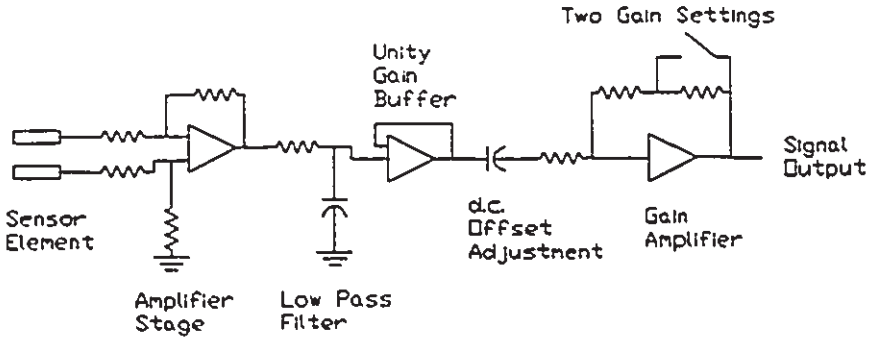

Figure 5.11: Signal Processing Circuitry for each sensor element.

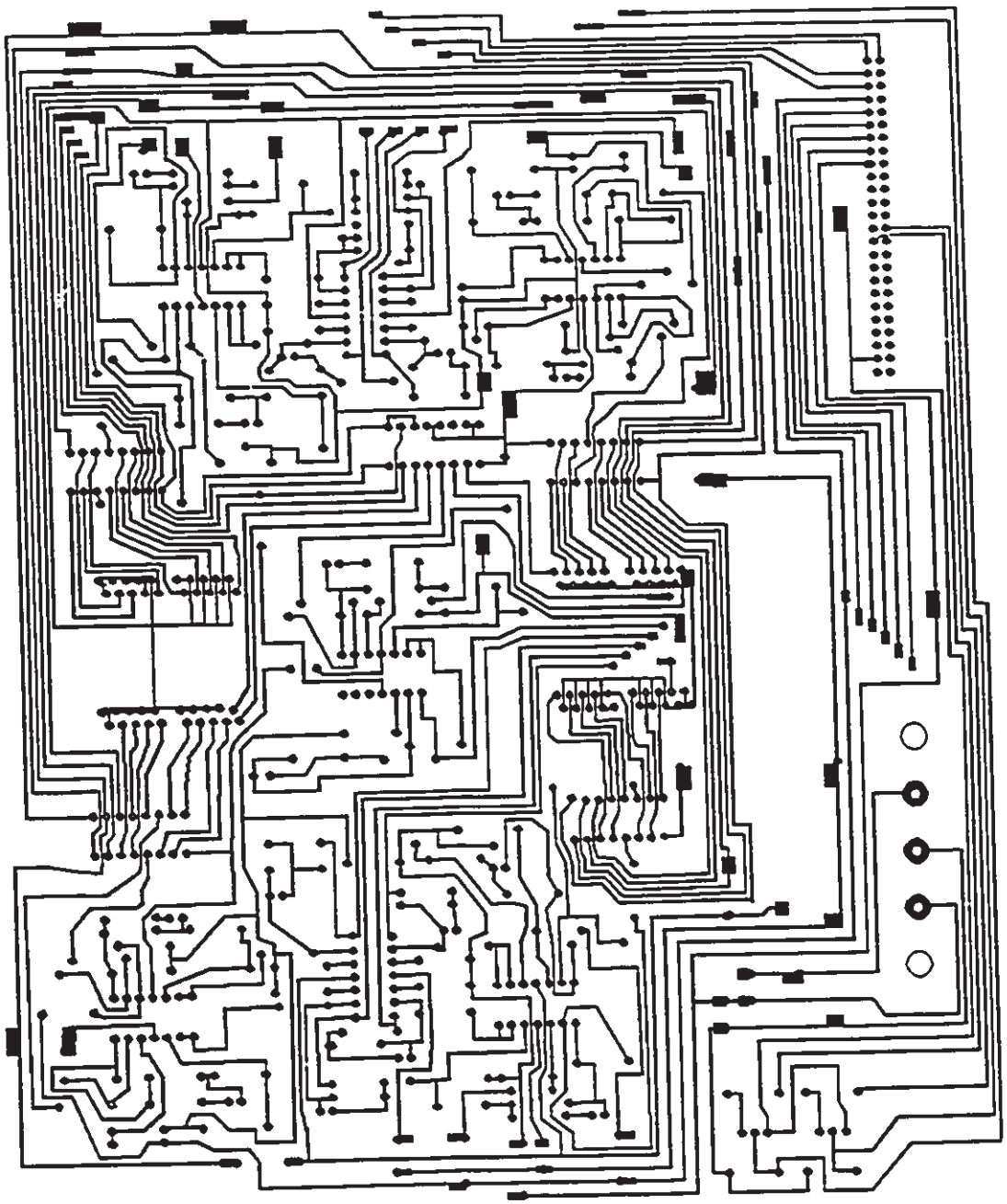

Figure 5.12: Layout drawing of the printed circuit board for the signal conditioning hardware.

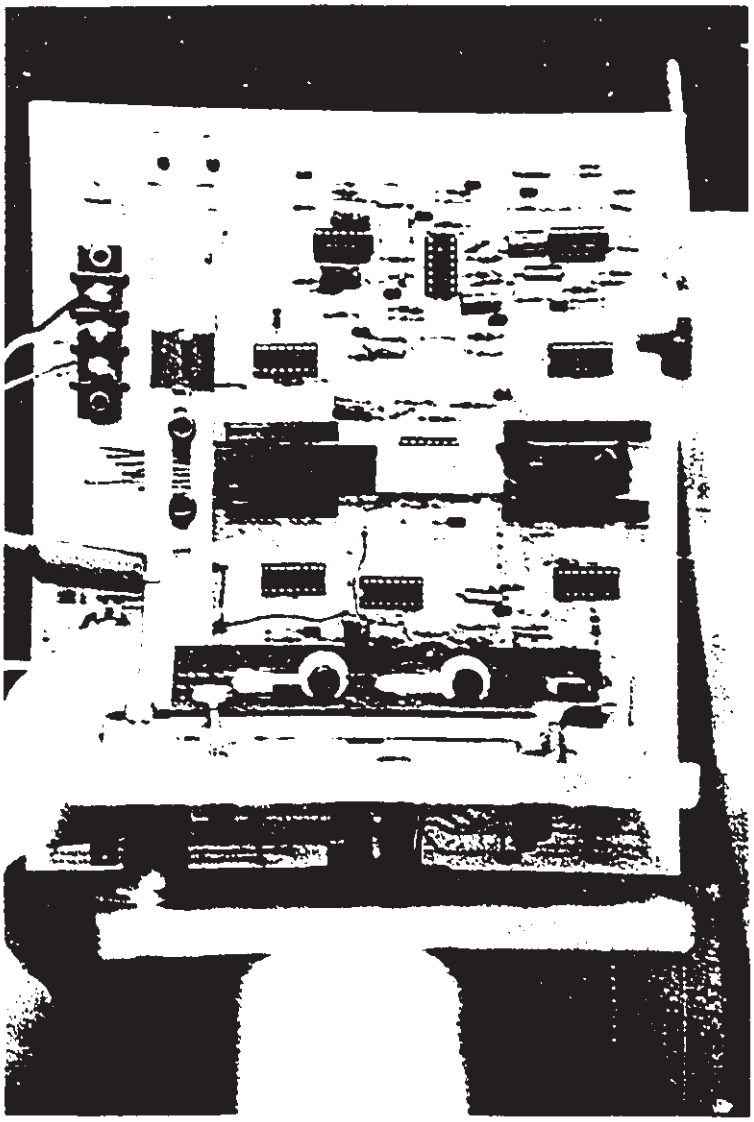

Figure 5.13: Custom designed signal processing circuit board.

Since this study focused on the dynamic response characteristics of the articular surface to alignment and load changes at the knee joint, charge amplifiers were not necessary. As a result, no static analysis was possible. Signal integration was done using computer software after the signal was sampled and stored. Amplification and filtering of the signal was carried out prior to data collection. Although the signal decayed with time without a charge amplifier, the sampling time and load frequency were much shorter in duration than the time over which signal decay occurred, and reduced any signal loss.

2. The electrical response from the piezofilm had an associated d.c. offset that increased due to the circuit amplification, but did reduce the operating voltage range of the A/D board. Installation of a capacitor between the buffer and gain op-amplifiers removed 95% of the d.c. offset and did not reduce the signal amplitude nor create any notible phase delay on the signal response.

The following four remaining modifications to the circuit design were necessary to accommodate the noise associated with the testing apparatus. A detailed discussion on the test apparatus itself is provided in the next section.

3. Due to the nature of stepper motors on the test equipment, a distinct jerky motion is produced with each step. A cut off frequency, fc, of 10 Hz was necessary to eliminate the mechanical noise from the displacement motors, and an fc of 10 to 30 Hz when the force motor was active. The noise created by the stepper motors contributed to the mechanical vibrations of the equipment and the limitations in the motor control software during acceleration and deceleration periods of the

trolley; the final fc was set to 5 Hz.

4. Preliminary tests were carried out with the pressure measurement pad inserted in an artificial knee joint mounted in the simulator. A test cycle comprising an external load of zero to 450 N and simultaneous flexion/extension phase of 0 to 45° was employed. Cycle times of one and three seconds were used. No notable difference was observed in the signal response pattern for sampling rates between 1 Hz and 1 MHz. Since no sudden voltage spikes had occurred, a low sampling rate could be used and was measured and found to be at least 10 Hz. The sampling rate was set to 100 Hz for all tests, but this could easily be changed with the data acquisition software.

5. An earth ground connection to the simulator chassis was necessary to eliminate the presence of a 50 Hz white noise that would randomly appear on the output signal.

6. The final modification required the building of a support clamp to hold the sensor pad and circuit board. Figure 5.14 shows the placement of the sensor pad in the knee joint. The pad is held rigidly in space with a clamping apparatus. The position of the clamp can be adjusted in an upward/downward, forward/backward and side to side motion to adjust to the final position of the knee in the simulator. After the sensor pad is clamped into position, the ends of the sensor are inserted into the connectors on the circuit board. For optimal operation of the sensor, the circuit board should be placed as close to the sensor pad as possible. This is essential to help minimize the effects of line losses and noise within the system.

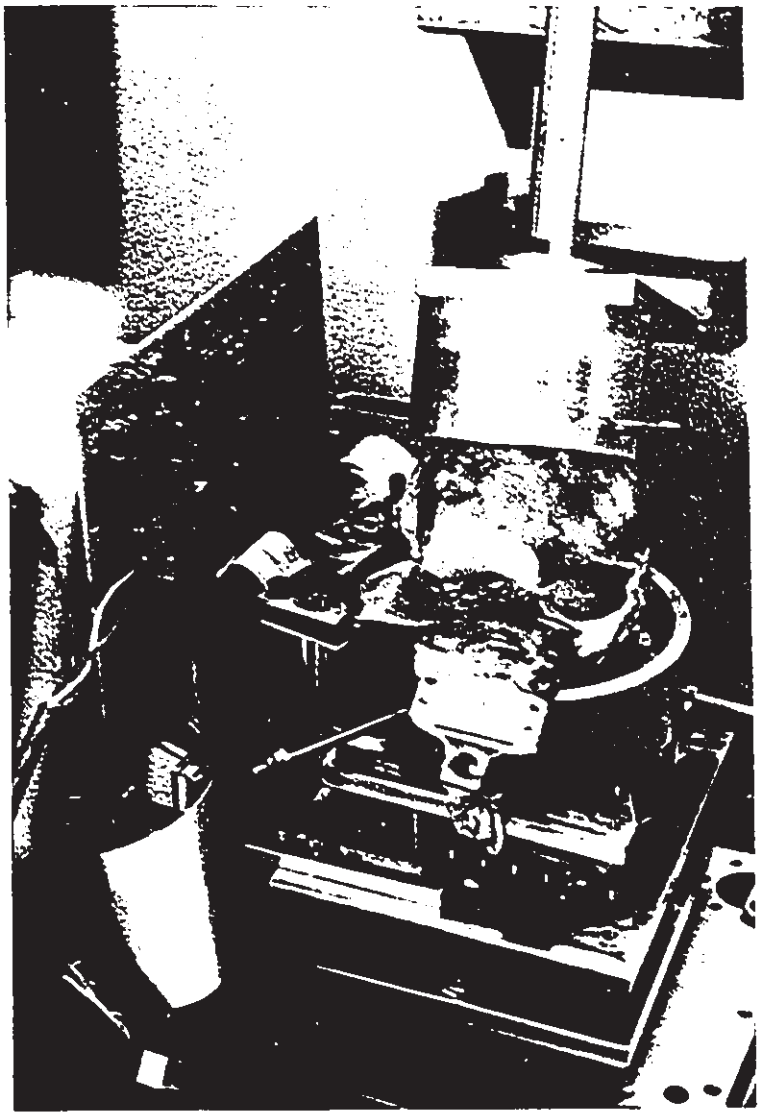

Figure 5.14: Support clamp for measurement pad and customized circuit board.

5.2.4 Calibration of Sensor Elements and Sources of Error

The measurement pad was inserted into the joint capsule, connected to the circuit board and clamped into position. Signal output from all elements was checked prior to testing by applying a load across the joint; confirmation of circuit hardware and A/D data acquisition software and hardware was also carried out at this time. Testing began after all elements were actively responding to the applied load. Final calibration of each element was done in situ at the completion of the tests and involved disarticulating the femur from the tibia, and removing it and all proximal components from the simulator. The top of the measurement pad was now exposed, yet remained connected to the circuit board.

A hand held rubber-tipped indenter, with a surface area slightly larger than that of each sensor element, was used to apply a normal force to the element. The actual force was recorded by the load cell on the simulator; both load cell and signal responses were collected and stored on the computer for later retrieval. Each sensor signal was integrated to convert the output in terms of voltage and compared to the the load cell value. A calibration factor equating signal output to load cell output for all sensor elements was estimated from five successive load applications and averaged out to give the final calibration ratio. This represents the sensitivity of the sensor element / amplifier circuit. Typical output curves from a sensor element and the corresponding load cell signal are shown in figure 5.15. Only that portion of signal where the compressed load increased was used to calculate the calibration constant. A consistant response pattern

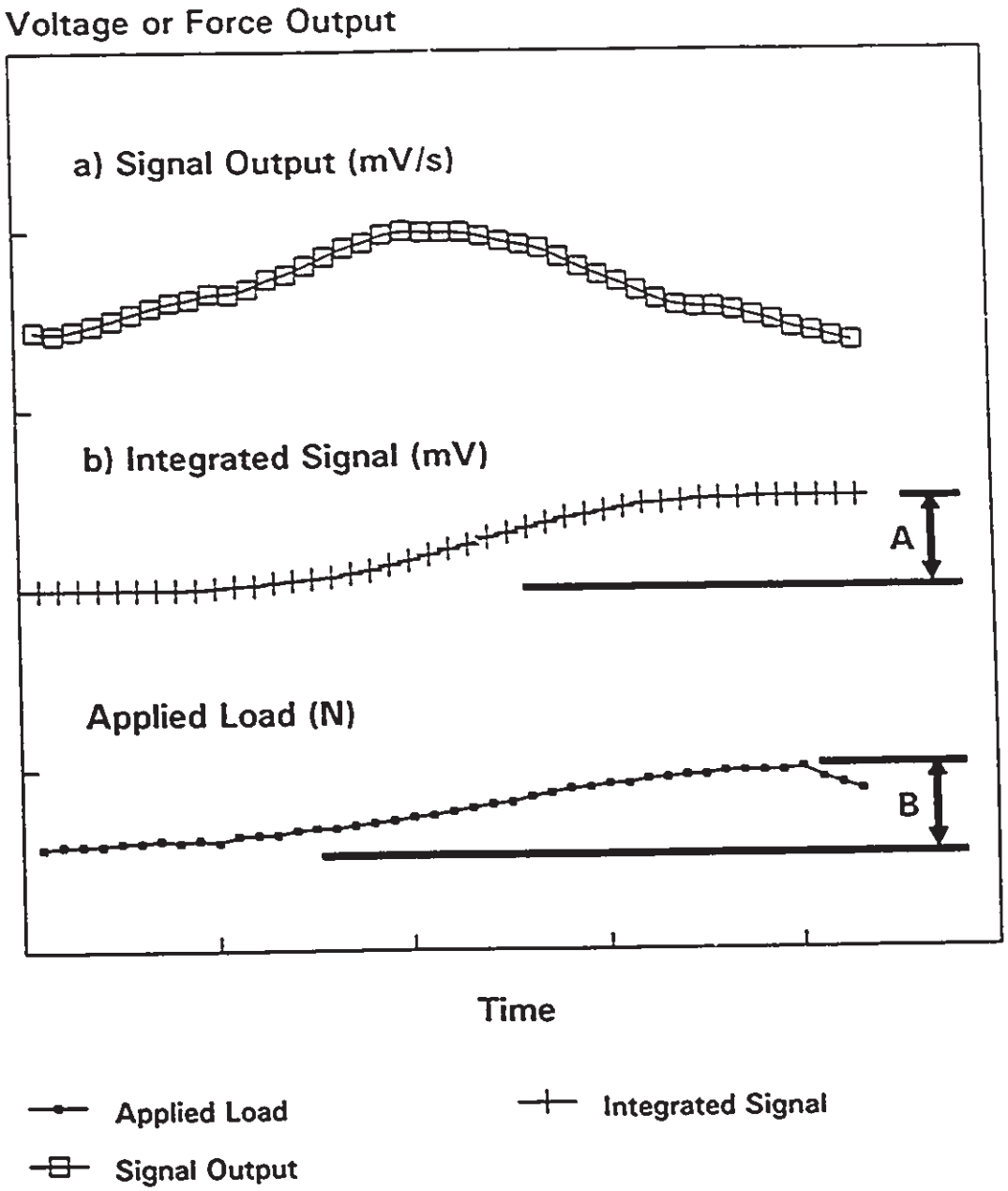

a) Typical signal pattern from sensor element prior to integration.

b) Integrated signal response pattern: calibration constant = A/B (mV/N)

Figure 5.15: Typical calibration curves of signal output patterns.

was obtained despite difficulties to ensure that the hand held indenter was absolutely perpendicular to the sensor surface on repeated trials. Since the tolerances of the resistors in the circuit were +/- 1% for two and +/- 5% for another two, the four stage amplifier circuit could be expected to have a maximum possible error of 27% ($1.05^2/.95^2*1.01^2/.99^2$).

5.3 Design of Mechanical Testing Equipment

The next phase of the experimental design addresses the need for a specialized testing apparatus capable of reproducing in vitro the dynamic motion of a knee specimen. The unusually high complexity of knee motion has previously limited satisfactory design of such a device. This research focuses on the effects of knee alignment (including the high tibial osteotomy) on the dynamic contact behaviour at the articular surface. Although the knee contributes to a multitude of different movement tasks (stair climbing, running, walking, etc.), the simulation of the joint motion during level walking will only be considered. Motion of the leg during each walking step comprises two distinct phases: the stance (support) phase and the swing (nonsupport) phase [154]. Figure 5.16 illustrates the typical sagittal motion of the knee joint during walking activities. The stance phase consitutes approximately 50% of the step cycle time, while the remaining time was devoted to swinging the lower - limb. During the stance phase, the knee rotates from an almost completely extended orientation to approximately 20 degrees flexion. By mid-stance, the knee begins to extend until just prior to heel-off where knee flexion returns to initiate push-off and

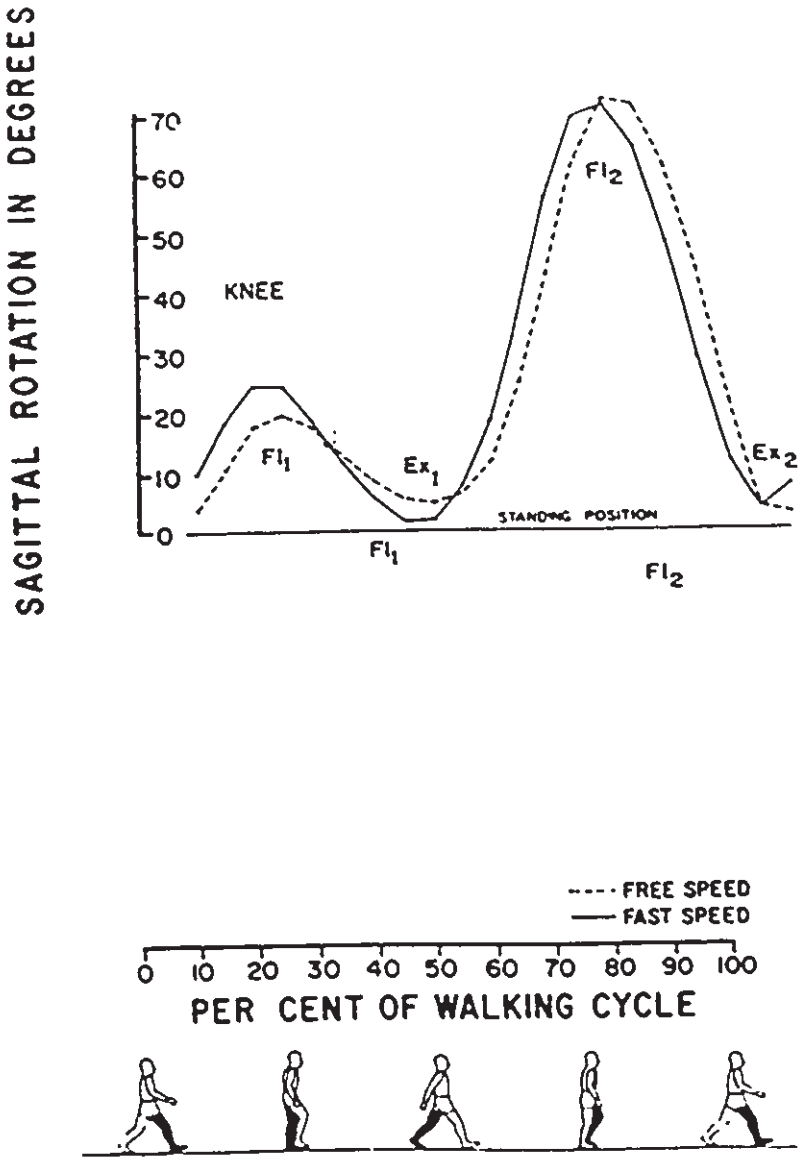

Figure 5.16: Sagittal plane kinematics of the knee joint for two walking speeds [115].

early swing. Load transfer at the knee, as determined from previous gait studies [58,113], is maximal during the stance phase and predominantly compressive in nature. Typical knee joint loading curves encountered during walking are displayed in figure 5.17, and include the compressive, A-P shear and M-L shear forces.

During the swing phase, the knee undergoes 60 degrees of flexion and subsequent extension. Since the foot is no longer in contact with the ground, compressive loading during this phase is at a minimum [58,113]. The complete motion between two segments comprises a total of six degrees of freedom: three rotations and three translations.

The testing apparatus should be capable of reproducing the external loading environment at the knee without constraining or altering any of the resultant kinematic motion of the knee (ie. six degrees of freedom). For this work, the test apparatus had to be designed to limit any motion constraints, while providing control of the remaining degrees of freedom of the knee joint, as best as possible, and to satisfy the following specifications. Consequently, the following design specifications were identified.

1. Permit reconstruction of different alignment conditions: varus/valgus offset, neutral alignment and post-osteotomy alignment. This will enable the recreation of the imbalanced loading state between the medial and lateral compartments.

2. Provision and control of a flexion/extension knee pattern representative of the stance phase of walking.

3. Permit constrained or unconstrained axial rotation of either the femur or tibia.

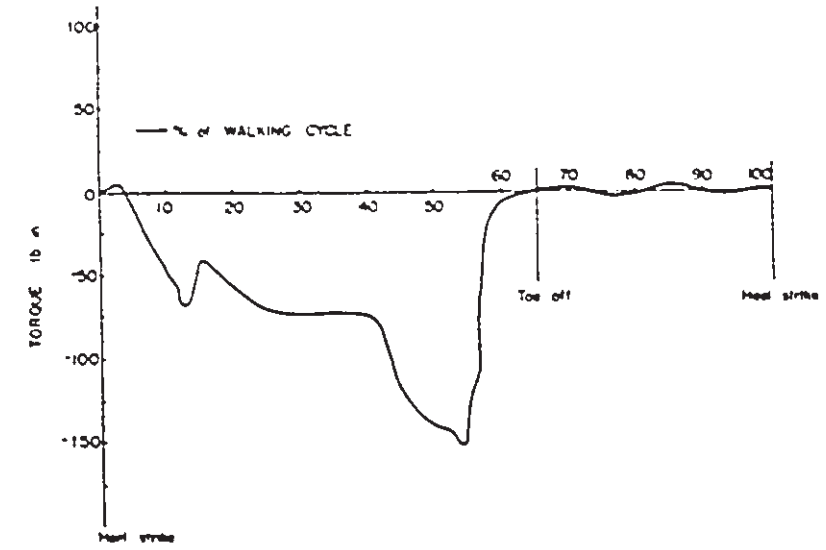

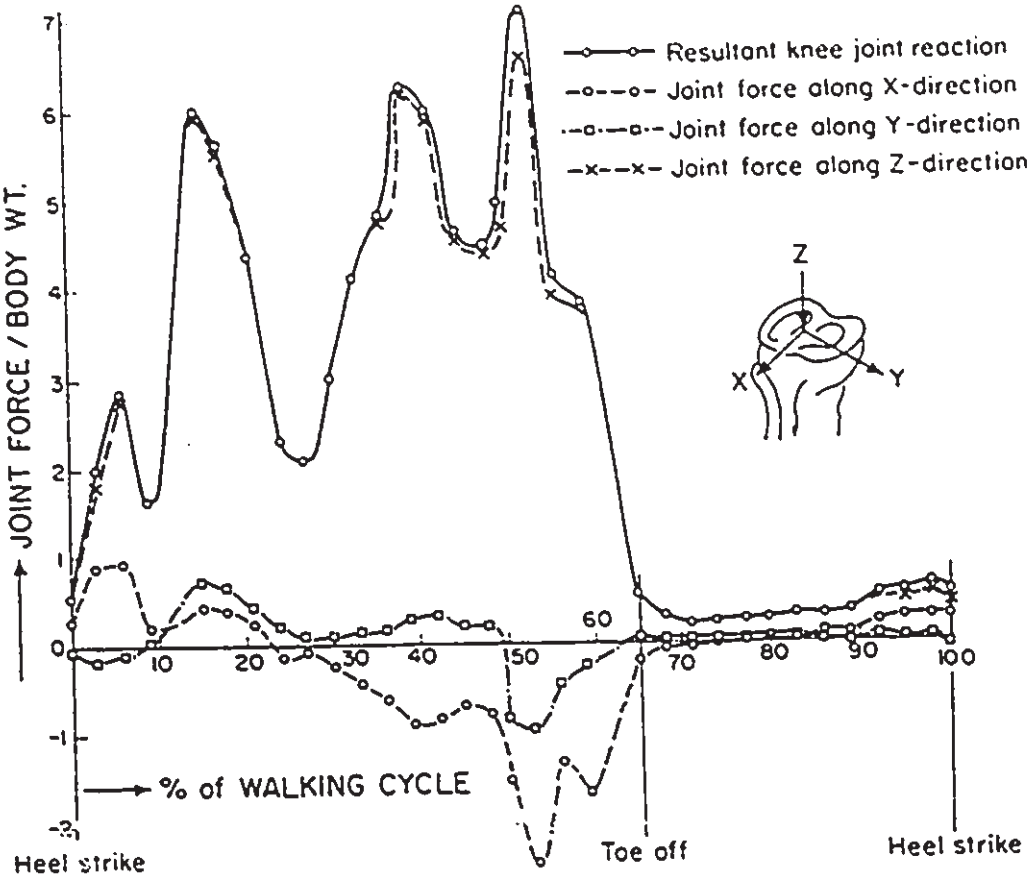

Knee joint reaction and components.

Figure 5.17: Rotation torque and reaction loads encountered at the knee joint during walking [113,145].

4. Allow the knee to follow, as closely as possible, its normal path of rotation between the tibia and femur in the sagittal plane. This not only consisted of the flexion/extension rotation, but included the relative displacements that occurred in the A - P and superior-inferior (S - I) directions.

5. Provision and control of an externally applied forcing function directed along the length of the tibial shaft that simulates the physiological loading environment at the knee joint present during walking activities.

Before setting out to design a completely new testing apparatus, a review of the currently available test equipment was carried out. Research on knee joint pathomechanics has resulted in the design of specialized jigs and fixtures that enable a knee specimen to be mounted in the load train of an Instron or Materials Testing System (MTS) machine.

In parallel with the experimental work on joint pathomechanics, wear screening tests of joint replacement materials have been undertaken. This work has often evolved into the design and fabrication of hybrid testing equipment, referred to as joint simulators. These mechancial devices are designed to provide controlled motion of a joint for cyclical wear testing of implant components [146,154]. Development of a knee joint simulator had been undertaken by Dr. I. Harrington of the Toronto East General Hospital (TEGH) and ORTECH (formerly the Ontario Research Foundation), and its use for the proposed research was granted by Dr. Harrington. Thus, two alternatives were available for a testing system. The first would be to design the necessary jigs to

mount a knee specimen in an MTS machine, and the second involved retrofitting the existing knee simulator.

The use of an MTS machine would limit the study to a quasi-static analysis at best, as only force control or position control is possible, but not both, as is desired. Furthermore, the joint oreintation would be held constant. Since the MTS machine utilizes a function generator to regulate the motion control, the resultant profiles are limited to either sine, square or haversine waves. However, the external load and movement patterns of the knee can not be reproduced with these waves; hence reproduction of the physiological mechanics of the joint are prohibited. Due to these limitations and the potential flexibility of using a simulator, greater consideration was given to incorporate the TEGH simulator in this research.

5.3.1 Toronto East General Hospital (TEGH) Simulator

The TEGH simulator was originally designed to permit in vitro wear testing of joint replacement materials, and through personal communication with the designers, it was determined that, once in an operational state, it should satisfy most of the specifications previously delineated. The equipment was in storage, and supposively in a functional state. Therefore, it was decided to develop the necessary jigs to hold a cadaveric knee specimen in the simulator and that all the effort should be placed on making it work instead of considering an alternative design approach.

5.3.2 Basic Construction of the TEGH Simulator

The simulator is shown in figure 5.18 and consists of a main frame housing a moving carriage, three stepper motors with dedicated microprocessors and translators, a minicomputer with external floppy disk drive, and a load cell. The motion of the carriage was dictated by two slotted plates located on either side of the simulator that traced out a specific arc representative of an averaged knee flexion angle curve. Stepper motors located on either side of the main structure were driven by the displacement microprocessor and regulated the position of the carriage using a gear and rack drive system. The gear mounted onto the end of the motor shaft and mated with the rack. A pillow block, housing a linear bearing, was mounted at each end of the rack and was guided by horizontal bearing rods fixed to the side of the simulator. Each block, in turn, was connected to the carriage through a slider linkage mechanism. As a result, the angular displacement of the carriage was governed by the horizontal translation of the rack.

A third motor, suspended from the underside of the moving carriage, was controlled by the force microprocessor and regulated the axial load transmitted through the tibial shaft. The load cell was located below the tibial support cup on the trolley, and was part of a closed-feedback control system for the force motor. The front panel of the simulator has been removed in figure 5.19 to illustrate the location of the force motor.

5.3.3 Operation and Control Strategy

Real-time microprocessor control was employed to operate the

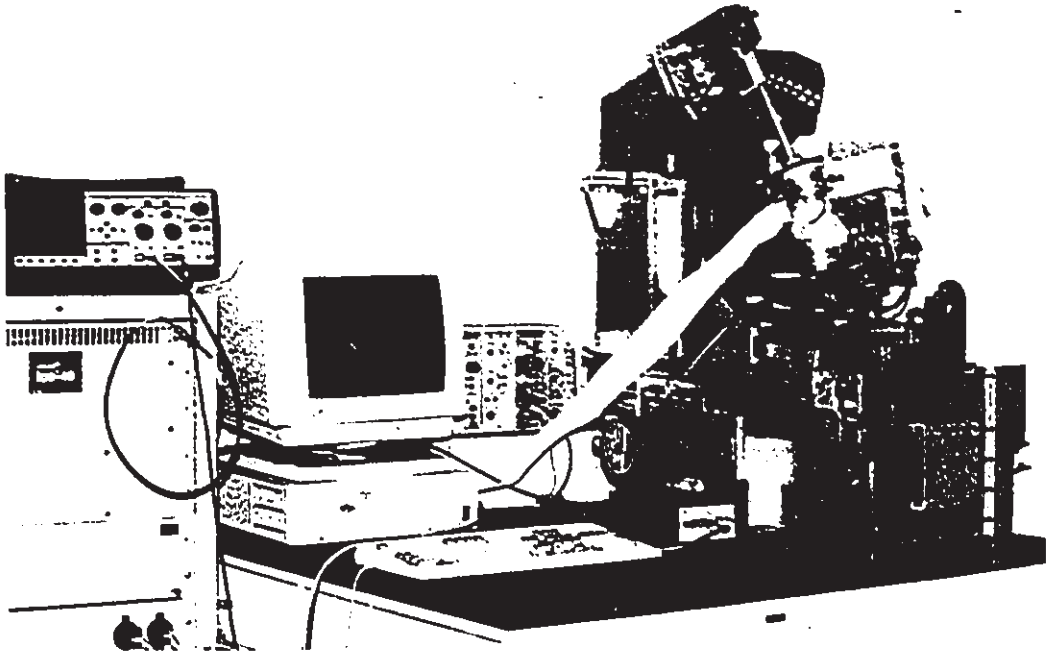

Figure 5.18: The Toronto East General Hospital (TEGH) joint simulator.

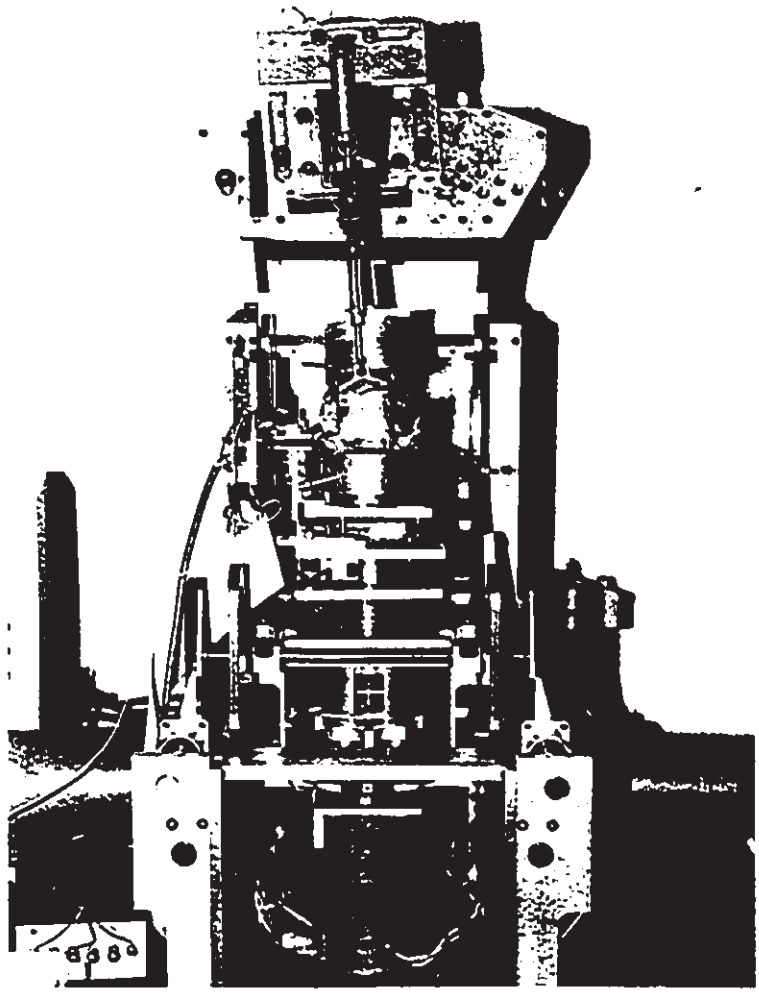

Figure 5.19:
Frontal view of the TEGH joint simulator. Force motor is suspended from the base plate of the moveable carriage.

stepper motors and produce independent control of two variables: (i) the joint flexion angle and (ii) joint compressive load. The microprocessors were programmed with specific control algorithms that output a prescribed pulse-train signal to the motor translators, which in turn, established the step pattern, as well as the step rate and rotational direction of the motor. Access to the control algorithms was accomplished via a minicomputer.

The existing control strategy had the operator generate a desired knee angle curve or external force profile on the monitor using a light pen. Once the profile was created on the screen, a linear differentiation approach was implemented to generate the time derivatives of the displacement and force profiles, and hence the step rate pattern of each motor. The resultant curves were reduced to a series of incremental data values readable by the microprocessors, and stored on a floppy disk for later retrieval. A second computer routine allowed the operator to program the microprocessors with these profiles, as well as turn the motors off or on, using a keyboard entry.

Operation of the force motor was synchronized with the displacement motor using a limit switch that was secured to the side of the simulator, and was triggered by the carriage position. A keyboard entry was used to execute the motion profiles stored on the microprocessors. At start-up, the carriage was first brought to a designated home or start position, which was chosen to be complete extension of the knee. Once the switch was tripped, the force microprocessor was activated and both joint load and knee flexion angle were synchronized. By altering the location of the switch relative to

the carriage position, the onset of the motion cycle could be varied to give a variety of different knee orientations at start-up. That is, the test cycle can start with the knee set to any amount of flexion.

5.3.3.1 Angular Displacement Control.

The displacement motors operated under open loop control and were programmed to follow the prescribed displacement profile. Here, each data value translated to a motor step. The frequency and number of motor steps established the angular speed and total angular displacement of the carriage. Since the motors could be sped up or slowed down, simulation of a range of walking speeds was possible. The angular travel of the carriage was measured manually with a goniometer and permitted between 5° degrees hyperextension to 60° knee flexion. This was sufficient to reproduce the flexion angle pattern of the knee during level walking.

5.3.3.2 Force Control.

A closed feedback control algorithm programmed on the microprocessor was used to operate the force motor and worked in conjunction with the drive translator and motor, load cell and signal conditioning hardware, data acquisition interface and digital I/O, and an AT personal computer. Each component contributed to the overall feedback circuit. The signal conditioning electronics on the load cell served to amplify and low pass filter the output signal. Once conditioned, signals were digitized by a dedicated 12 bit analog to digital converter and then delivered to the microprocessor.

The control algorithm computed the difference in the measured and programmed loads. This difference could be reduced by adjusting the motor speed and/or direction until the measured load was within a specified error tolerance. The new speed was established from the torque-speed curve of the stepper motor, as well as the mechanics of the lead screw mechanism on the force motor drive system. A change in the axial force output was converted to a relative motor torque, from which the corresponding motor speed was estimated from the performance curve.

To help simplify the control strategy, a look up table was produced that represented the speed - torque curve; the speed range was divided into six equal parts that covered the entire speed range of the motor. This served to reduce the overall run time, as the numerical calculations to convert the speed-torque values into an axial force were minimized.

The ORTECH design specification on the force drive system of the simulator was listed as having a maximum output capacity of 2500 N. However, validation of the maximal output load was not confirmed until after the experiments with the actual cadaveric specimens were performed. This resulted in further complications with the existing force drive system and is discussed in the next section.

5.3.4 Limitations and Modifications to the TEGH Simulator

As with most experimental endeavours, unforeseen problems can arise that delay progress and completion time of the work; this research is not without exception. Due to early equipment malfunctions and a shortage of funds, no previous tests with the simulator were ever

completed, and thus, its development was not complete. A summary of the problems encountered with the TEGH simulator are outlined below and include a brief description of the steps taken to overcome them.

1. Problems occurred during the operation of the existing computer system, including the external floppy drive, keyboard keys and computer terminal. Malfunctions were also noted with the existing software used to generate the displacement profiles. An AT personal computer was installed to run the microprocessor boards, which eliminated the requirement for the operator to use an external floppy drive system used to generate the motion profiles and program the controllers. The existing computer had only 16 k of RAM. It should be noted that the existing software had to be rewritten to be compatible with the AT PC, and by doing this, the accuracy of controlling the stepper motors was improved. The replacement computer was also used for the data acquisition phase.

2. The existing control strategy had the user create the desired knee flexion/extension pattern and force profiles on the video terminal of the computer; an internal software program automatically produced the necessary control parameters for the microprocessors. The information was then programmed onto the microprocessor boards and enabled the user to run the equipment. However, during the initial start-up and running of the displacement motors, excessive mechanical vibrations had occurred with movement of the carriage. It is believed that the acceleration limits of the motors had been exceeded, and created the jerky carriage motion.

The control strategy should account for any inertial problems

that can occur when attempting to control a swinging mass, such as the moving carriage itself. This was most likely due to the fact that during creation of the desired displacement profiles, the existing software did not perform sufficient checks to ensure that the kinematic expressions of the motors did not contain any discontinuities that would cause abrupt motion changes to the carriage. Furthermore, the accuracy of the control system was dependent on the resolution of the video terminal and light pen.

To overcome these limitations, the existing computer program, used to generate the pulse train patterns from the screen image, was replaced with a QuickBasic program that employed the kinematic equations of cycloidal motion to create the step profiles of the motors. The cycloidal motion curves are shown in figure 5.20. This was advantageous, as the displacement, velocity and acceleration curves do not contain any discontinuities (Wilson [167]). In addition, the program also permits easier adjustment to the final selection of the motor speed and direction. As a result, control of the carriage motion could now compensate for minor changes to the combined weight of the specimen and carriage. The program is completely interactive and enables the user to set the time of the flexion/extension phase and the total degree of knee travel.

3. Prior to establishing the control parameters for the displacement motors, the kinematic relationship between the gear rack drive system on the displacement motors and the slider linkage mechanism were required. This involved measuring the relative angular position of the carriage for each incremental step of the motor. As stated previously, the

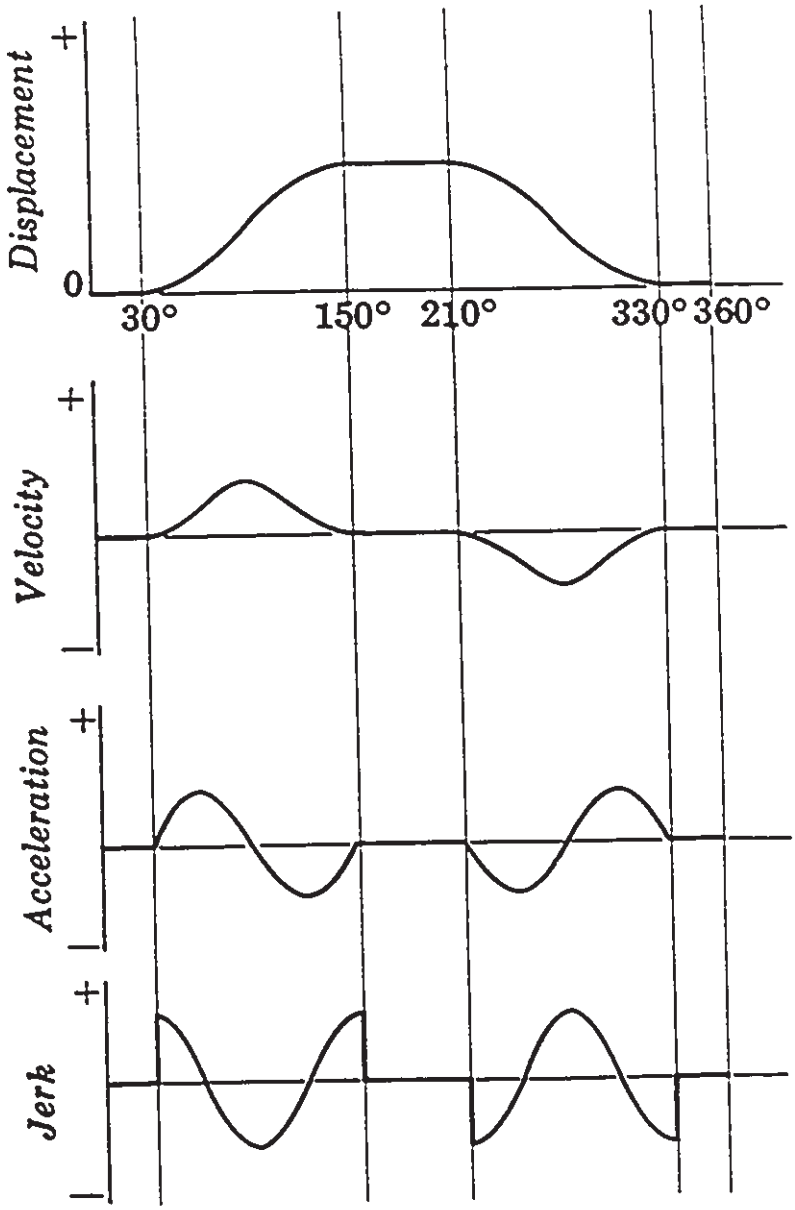

Figure 5.20: Typical kinematic diagrams of cycloidal motion [167].

motion of the trolley was dictated by two slotted plates located on the sides of the simulator that trace out a particular polycentric arc.

Calibration of the trolley position with rotation of the displacement motor involved seating two straight rods into the support cups on the simulator, representing the attachment of the proximal end of the femur and distal end of the tibia. The orientation between the two rods was measured with a goniometer for every five steps of the displacement motors. The measured relationship is shown in figure 5.21, and was estimated to be 4.537 motor steps per degree of knee flexion. The ratio was incorporated into the kinematic expressions used to generate the pulse train patterns, and improved the overall system performance of the stepper motors by eliminating the mechanical vibrations. The error tolerance on the carriage position was measured with a goniometer and could be controlled to within +/- 1/2 degree over the entire 65 degrees of angular travel.

4. Problems were noted with the feedback loop of the force motor control, and included overshooting the peak target value, and an inability to sustain a static load. The control circuit employed a look up table method to help reduce the execution time. However, one drawback with this approach was that the speed adjust values in the table became the limiting factor. Small incremental changes in the force required minor adjustments to the motor speed and/or direction, but at times, the smallest value from the table could only produce a speed change with a magnitude greater than that estimated by the program. Fortunately, the need for a static load was not necessary for this study. However, the limitation of overshooting the peak target

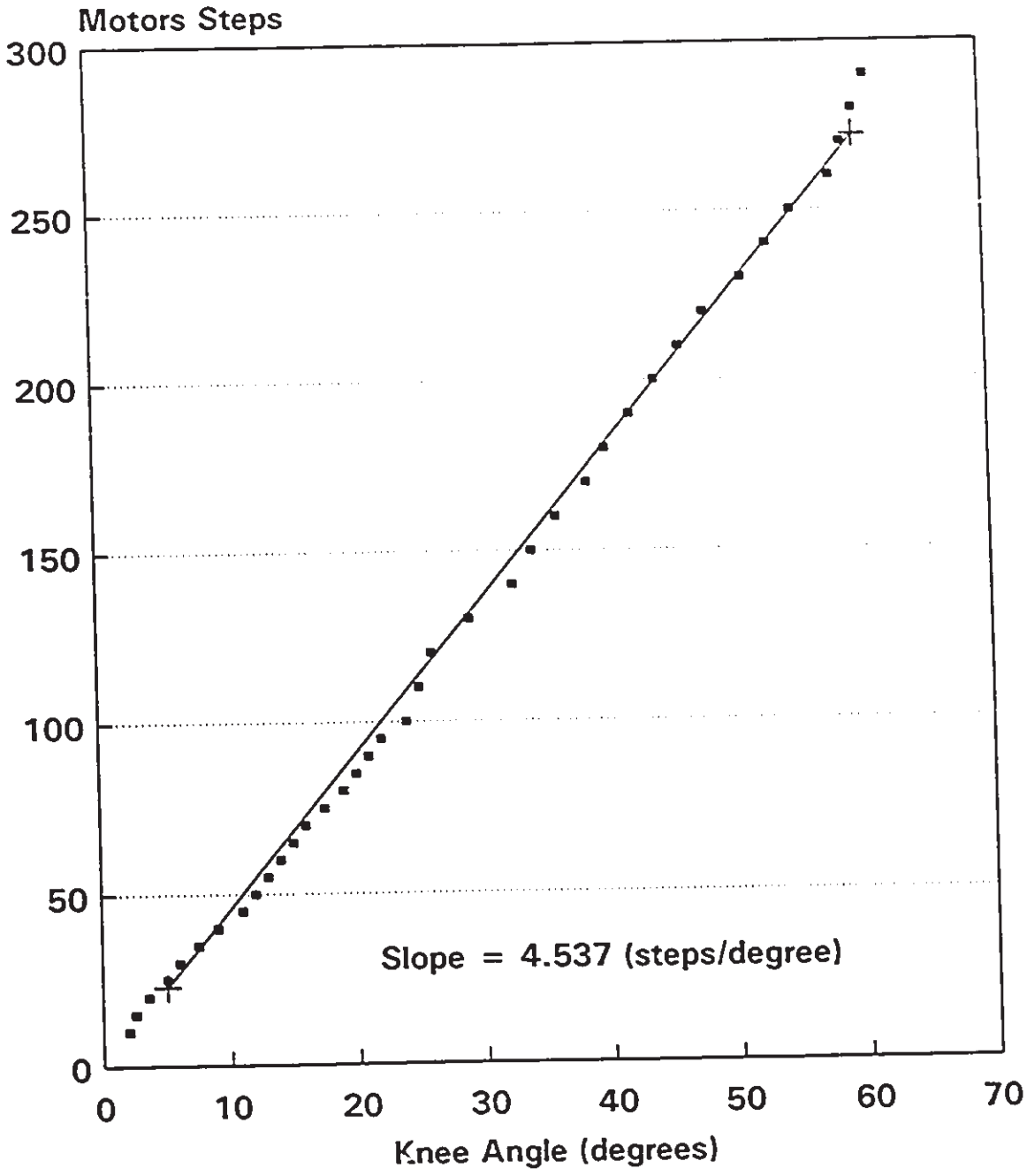

Figure 5.21: Calibration curve of displacement motor output versus carriage location.

could not be resolved.

5. Preliminary testing of the force motor control loop was delayed due to problems with the existing circuit hardware; replacement of an amplifier module rectified the problem. Verification of the load cell involved recalibrating the signal response from the replacement amplifier. The original circuit was set at 9.8 N per a/d value, with a full scale of 255 a/d values available. A peak target load of 2225 N had been selected and required a gain of 100 for the amplifier module.

6. Plastic replicas of the tibia and femur, with a total knee replacement joint, were mounted in the simulator and used to check the control loop. To avoid fracturing the plastic bones, peak loads of 450 N were used during the prelimnary testing of the force motor drive system and control circuit. Unfortunately, the maximum capacity of 2500 N had not been confirmed and proved to be a serious error that was not realized until the tests were carried out on the cadaveric specimens. The maximum possible ouput from the force motor drive system turned out to be only 550 N. It was initially thought that the force constraint was due to either the limitations with the control software or the lead screw mechanism on the force motor drive system. Since the control loop on the force motor functioned properly during the preliminary tests up to 450 N, it was believed that the problem was a mechanical one.

The existing force drive mechanism used a power screw mechanism, fixed to the output shaft of the motor, to convert the rotational output of the motor shaft into a linear ouput. The original engineering design calculations had the motor rated at 5.65 N-m (50 lbf-in), and a lead

thread of 16 threads per inch on a 2.54 cm (1 inch) collar diameter, giving a maximum 445 N (100 lbf) at the screw radius. Using the theory of power screws, the ratio of the rotational force at the screw radius to axial force output was increased to 1:5. Thus the maximum possible axial force is 5 * 445 N or 2225 N. Note that any increase in output force caused a reduction in nut axial speed. The mechanics of power screws are illustrated in figure 5.22, and have the following torque-force relationship.

$$T = \frac{F * dm}{2} \left\{ \frac{l + \mu * dm * \sec(\alpha)}{\pi * dm - \mu * l * \sec(\alpha)} \right\} \qquad (5.1)$$

where T = motor shaft torque

F = axial force output

l = lead of screw thread

dm = screw diameter

μ = friction factor

α = one - half of thread angle

In these calculations the friction factor of the acme threads was estimated as 15%, but could have been much higher if proper lubrication was not used. A very light machine oil was added to the threads to determine if thread friction was the problem; however, this did not result in an increase in the force output from the motor.

At that time, it was still unknown why the peak loads were only 550 N. Thus, a design change to the present force drive system on the

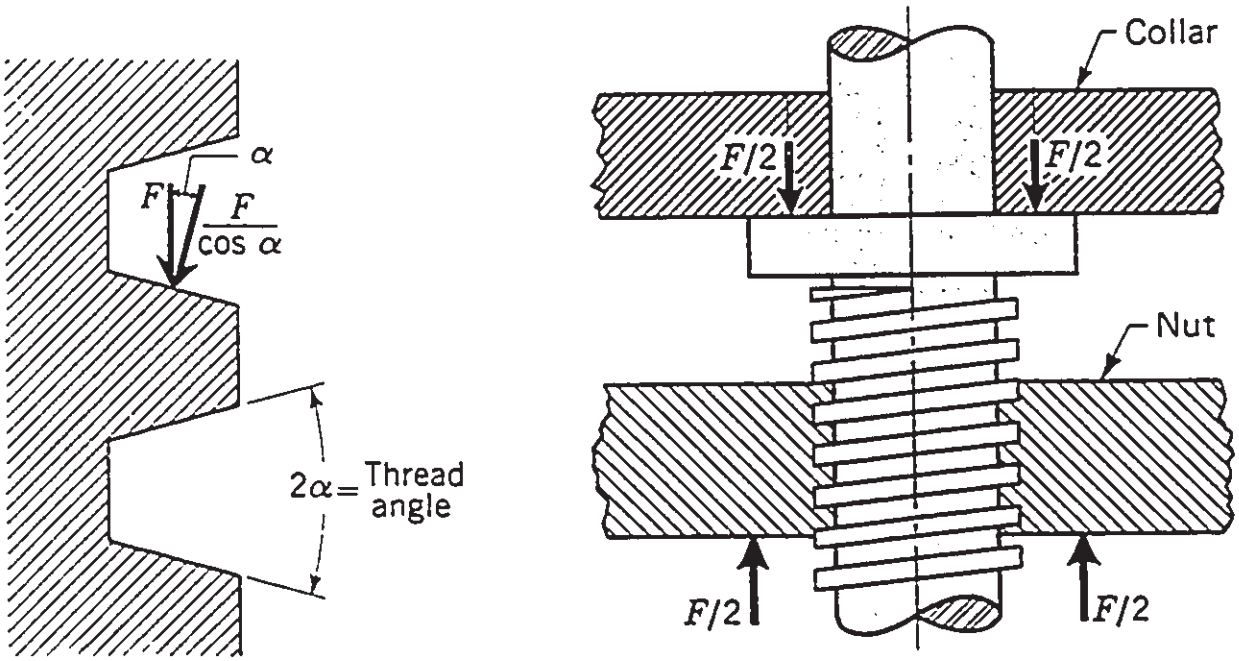

Figure 5.22: Mechanics of power screws when nut is held stationary. Rotation of nut causes translation of collar [148].

simulator was indicated. Two immediate options were to replace the motor and translator, or to redesign the ball screw mechanism. The latter option was considered to be the more feasible of the two, and thus pursued further.

Upon dismantling the equipment it was discovered that the force motor on the trolley had a torque rating of only 2.15 N-m (19 lbf-in), and not the 5.65 N-m as stated in the design calculations. As a result, the existing control software and force motor had been operating near their maximum rated capacity. It should be noted that the original design reports made no mention of a replacement motor. One possible explanation for this change is that the original, larger motor added too much weight to the trolley and created acceleration problems for the displacement motors. To overcome the acceleration problems, the mass of the moving carriage was reduced by suspending a lighter, smaller motor from it. Consequently, the resultant peak loads were much lower.

One option was to use a more powerful motor, but this would be more expensive, and there was a limitation on the clearance available between the bottom of the motor and the bottom plate of the simulator. Furthermore, a larger motor could create the acceleration problems mentioned above. No smaller and lighter motor was available with a rated output greater than 5.65 N-m. Thus, this option of a motor change was not feasible.

5.3.4.1 Design of a Speed Reducer Drive System.

Realizing these limitations, the alternate option of redesigning the lead screw mechanism on the existing force drive system was pursued.

A speed reducer and ball screw drive mechanism was designed and fabricated that could produce the necessary force output. A ball screw system was selected over a conventional taper threaded screw system because of its superior reduction in friction and increased torque efficiency. Recall that the original motor had a torque rating of 2.15 N-m, and used a 1 inch diameter lead nut screw, while the required torque output was 5.65 N-m. Thus, a force mulitplier of 2.7 times or greater was required. The motor torque output was increased through a gear and pinion system, and the axial force was produced through a ball screw mechanism. One should also realize that the increased torque from such a mechanism comes at the expense of a reduced nut speed. Two gears having 1.5 and 5 inch diameters were selected, thus increasing the torque by a factor of 3.33 times, or to 7.17 N-m.

The design of the ball screw mechanism is given below by equation (5.2), and the efficiency was estimated at 90% for both the gears and ball screw. The ball screw selected for this design had a lead of 8 mm.

$$F = \frac{T * 2 * \pi * \mu}{l} \qquad (5.2)$$

$$= \frac{(.9 * 7.17) * 2 * 3.14 * .9}{.008} = 4.56 \text{ kN}$$

Thus, the maximum axial force output satisfies the design criteria of 2500 N. A schematic of the ball screw - speed reducer is shown in figure 5.23, with the completed mechanism pictured in figure 5.24.

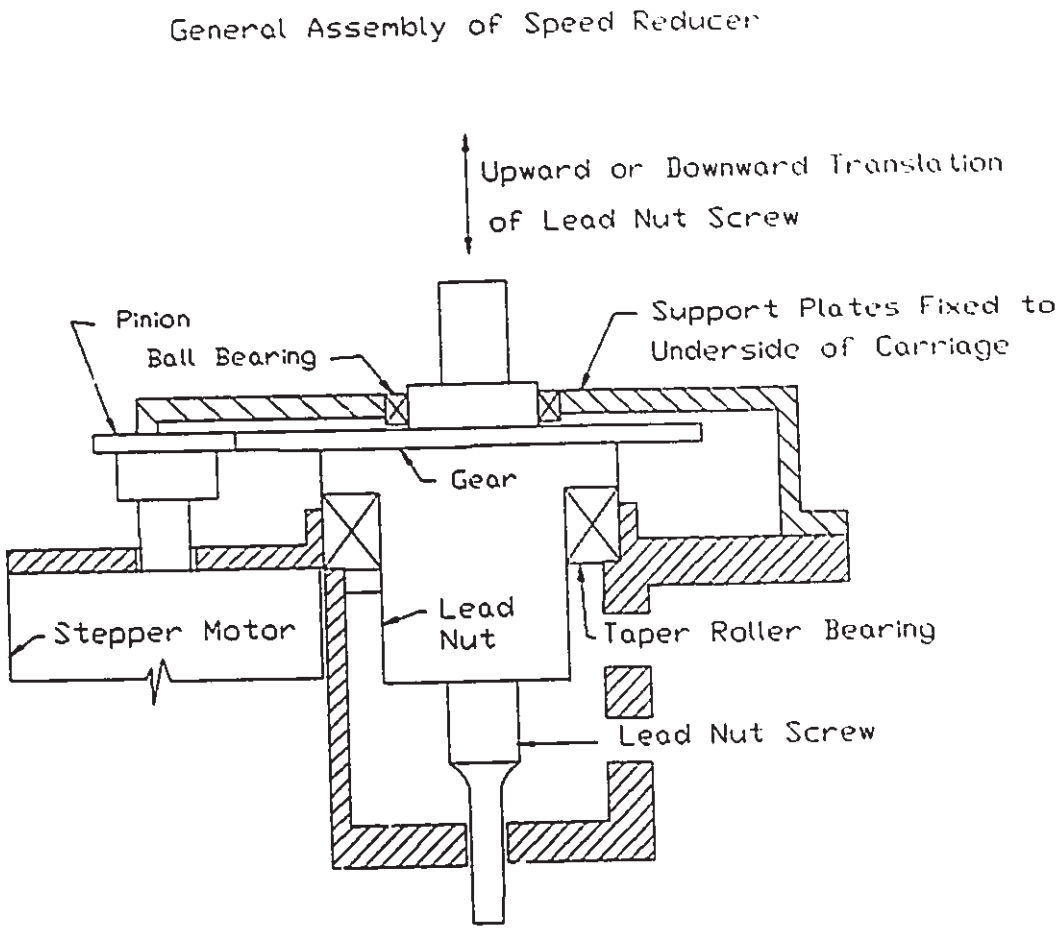

Figure 5.23: Schematic diagram of the speed reducer drive system.

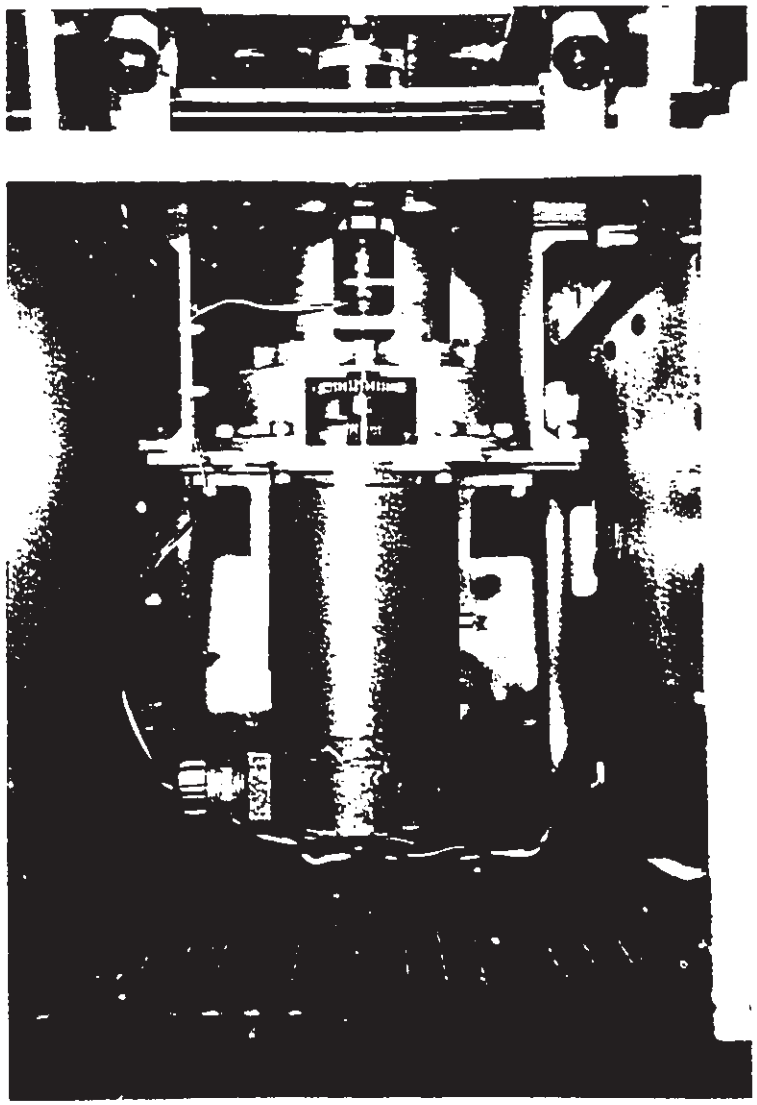

Figure 5.24: Speed reducer mechanism suspended from the underside of the moveable carriage.

7. The original hardware arrangement used a single ribbon cable to connect the computer to both microprocessor boards. It was uncertain as what potential problems existed with this set-up, as a feedback control loop had been implemented on the force control board only, and not on the displacement board. Separate RS-232 cables were installed between each board and the computer. This required installation of a second serial port.

8. Loose wires and poor solder connections were detected on the existing hardware. New cables and connectors were installed and most solder connections redone, in an attempt to eliminate the recurrence of hardware problems. The arrangement of the power supply connections on the microprocessor boards were also modified to prevent failure of the clock chips which had occurred throughout previous trial runs with the simulator.

After completing the above modifications to the equipment, the simulator satisfied the original specifications, and operated in a consistent and reliable fashion.

5.4 Design of Mounting Fixtures for Simulator

The TEGH simulator was originally designed to perform wear studies on artificial knee implants, whereas this research was an investigation into the biomechanics of high tibial osteotomy surgery, and was to employ cadaveric specimens. Thus, additional fixtures were required, not only to mount a cadaver knee, but to permit alterations to the resultant knee alignment.

A knee deformity can cause increased compartment loading and

enhance the progression of osteoarthritis in the joint. To properly evaluate the effects of the osteotomy on the joint mechanics, a procedure was necessary that altered the knee alignment in incremental steps. A knee specimen with an existing deformity was corrected with an osteotomy. However, if a specimen with a normal alignment were used, a deformity had to be simulated. This was achieved by either altering the varus/valgus angle or by performing a series of osteotomies. Engin [46] built a mechanical device that altered the mechanical axis of the knee joint by displacing the distal ends of the tibia and femur to produce a deformity, and studied the resultant effects on load tansmission. However, the applied load was completely static and malaligned conditions of 2.5 and 5 degrees were analyzed. For this study, changes to the alignment were simulated by repositioning the femur and tibia, rather than attempting a series of osteotomies.

To recreate the different alignment configurations with a cadaveric knee mounted in the joint simulator, special adapter components were designed and built that attached to the existing structure of the simulator. A brief description of the additional parts added to the simulator is provided next, and these are catagorized as femoral components and tibial components.

5.4.1 Femoral Components

The overall arrangement of the knee joint mounting apparatus is illustrated in figure 5.25. The femoral components included a 1 inch diameter shaft that resembled the anatomical axis of the femur. Rotation about the long axis of the shaft (ie. in the transverse plane)

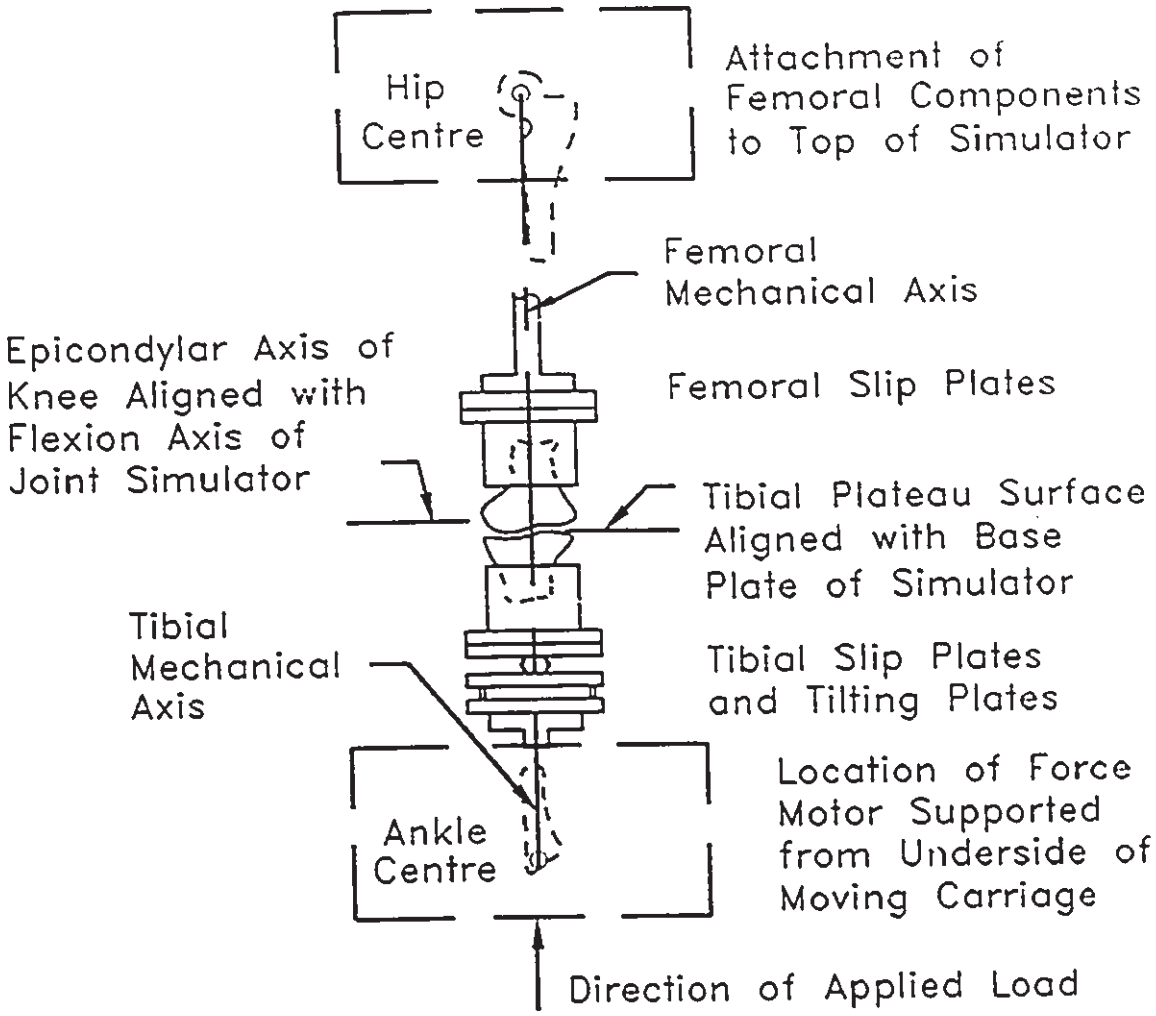

Figure 5.25: Neutral alignment configuration of knee specimen in simulator.

was permitted, or could be set to a preferred orientation and held constant. The proximal end of the shaft attached to a coupler plate that was modified to mate with an existing hole pattern in the top structure of the simulator. The upper attachment also permited adjustment of the vertical height of the femur, and the varus/valgus orientation. In the sagittal plane, the knee was positioned such that the centre of rotation of the joint (epicondylar axis) aligned with the centre of rotation of the carriage.

The opposite end of the shaft attached to a set of slip plates, which were fastened to an aluminum pot. The proximal end of the femur is anchored in the pot with a low melting point alloy (Cerrobond). The slip plates permited adjustments to the A-P and M-L alignments of the knee joint relative to the simulator structure.

5.4.2 Tibial Components

The tibial components included two sets of slip plates, a set of tilting plates separated by a ball bearing, a tibial cup, and a special adapter component that mated with the existing coupler on the carriage. All these parts are illustrated in figure 5.25. The slip plates allowed adjustments to the position of the tibia in the A-P and M-L directions. The tilting plates were used to obtain the angular offset of the tibial plateau relative to the base plate of the carriage; the procedure for simulating the post-osteotomy and malaligned configurations is discussed in Chapter 6. The force motor load vector was aligned perpendicular to the tibial plateau surface in both the A-P and M-L views, passing through the mid-distance of the joint in the A-P plane and between the

centre of the femoral condyles in the M-L plane. The varus-valgus angulation was adjusted by offsetting each segment as much as 15 degrees from the vertical plane to compensate for excessive alignment deformities.

5.5 Design of Alignment Jig

Mounting a knee joint directly in the simulator and achieving a desired alignment configuration became a rather cumbersome and difficult task to perform with any consistancy and accuracy; thus an alignment jig was specially designed for the initial alignment phase. The jig consisted of two aluminum bars bolted together with support cups fastened to the outer ends, and was used to establish neutral alignment of the cadaveric knee specimen. The distances between the bolt centre and end cup holders were identical to that between the centre of rotation of the simulator and the accompanying cup holders on the support fixtures on the simulator. This provided a more reliable method of potting and aligning each specimen. The attachment fixtures were removed from the simulator and seated in the alignment jig. The distal part of the tibia was placed in the lower cup and held in place with Cerrobond. Bone screws were fixed to the distal tibia to provide additional anchorage.

Neutral alignment of the tibia was established with the plateau surface parallel to the base plate of the jig, and the patella facing forward. The posterior aspect of the femoral condyles was aligned parallel to the back side of the jig. This approximates a vertical orientation of the knee as occurs in the human during walking. Once the

alloy solidified, the jig was turned upside down, leaving the proximal femur hanging down into the upper support cup. Bone screws were also added to the proximal femur to provide additional anchorage. The alignment jig with a mounted knee specimen is shown in figure 5.26. The potted knee joint and fixtures could be unseated from the support cups on the jig and transferred to the simulator. Any minor adjustments to the final alignment of the knee joint in the simulator were carried out using the slip plates and tilting plates.

5.6 Retrieval and Preparation of Knee Specimens

A total of twelve cadaveric knee specimens were acquired for testing. Two knees were discarded because of severe arthritis throughout the joints, while a second pair of knees was sacrificed during the developmental stages of the measurement pad. The remaining eight cadaveric knee joints were included in the study and assessed on an individual basis.

The knee specimens were obtained from elderly cadavers and frozen at -20° C. After thawing in water, all soft tissue and muscle were removed, leaving the joint capsule and surrounding ligaments intact. The specimens were cut 8 cm proximal and 10 cm distal to the tibial plateau surface. The patellar tendon was cut at its proximal origin and remained attached distally. Access to the anterior region of the medial compartment was provided by a horizontal cut through the joint capsule extending from the base of the patella to the medial edge of the knee, just anterior to the medial collateral ligament. A horizontal cut through the joint capsule at the posterior aspect of the

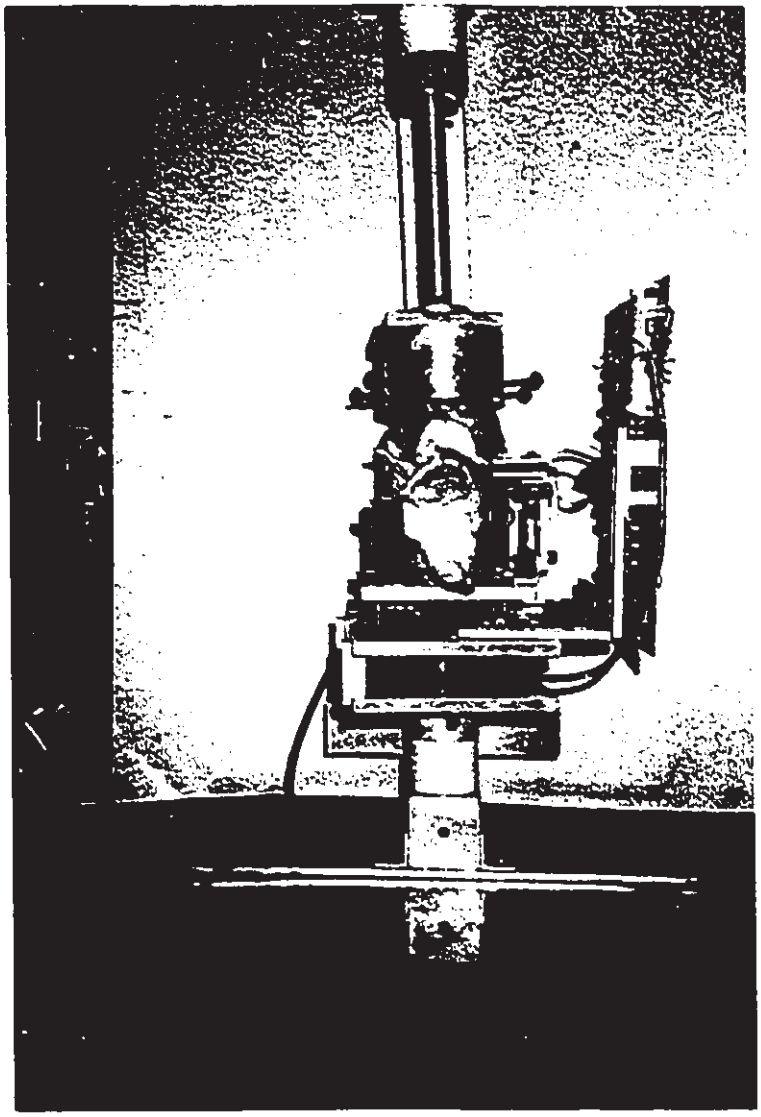

Figure 5.26: Alignment jig with mounted knee specimen.

medial compartment provided access to the top surface of the medial meniscus. The available widths of the incisions were identified previously in figure 5.4.

These incisions also provided inspection of the gross pathology of the articular surface. One pair of knee joints had extensive joint pathology (degradation of the meniscus and articular cartilage) and was not suitable for the study. The incisions were also necessary to enable insertion of the pressure measurement pad. Following testing, all joints were radiographed to confirm the level of joint pathology. Only one joint was found to have a mild grade of arthritis on the articular surface , as ranked by an orthopaedic resident. To carry out the analysis on the test data, a full size image of the tibial plateau surface was required to determine the exact location of each sensor element on the medial compartment. This involved unpotting and disarticulating the joint to expose the articular surfaces. Photographs of the tibial plateau surface of the specimens and a cross-sectional view of the medial femoral condyle were produced after the completion of the tests, and are pictured in figures 5.27 to 5.34.

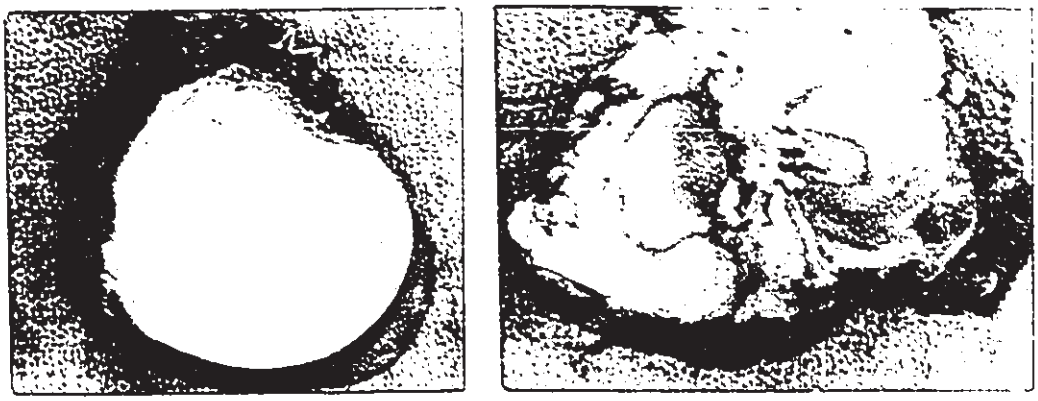

a) b)

Figure 5.27: Specimen one: a) medial-lateral cross-sectional view of the medial femoral condyle, and b) tibial plateau surface.

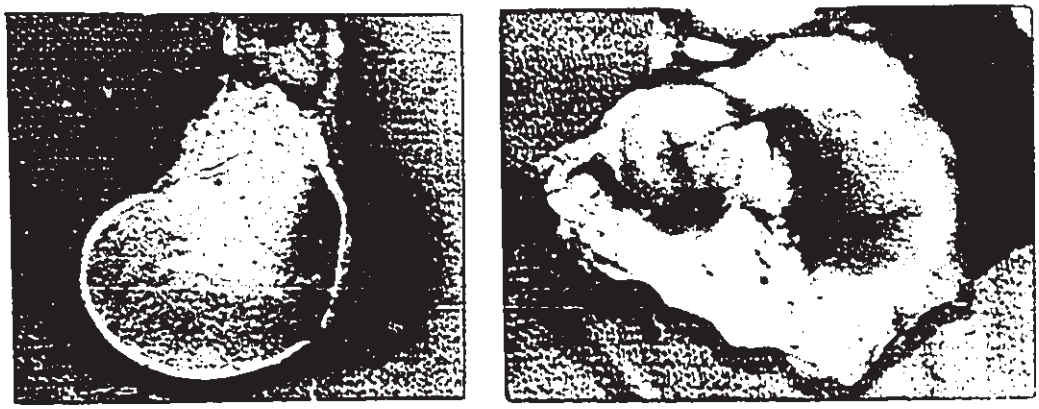

a) b)

Figure 5.28: Specimen two: a) medial-lateral cross-sectional view of the medial femoral condyle, and b) tibial plateau surface.

a) b)

Figure 5.29: Specimen three: a) medial-lateral cross-sectional view of the medial femoral condyle, and b) tibial plateau surface.

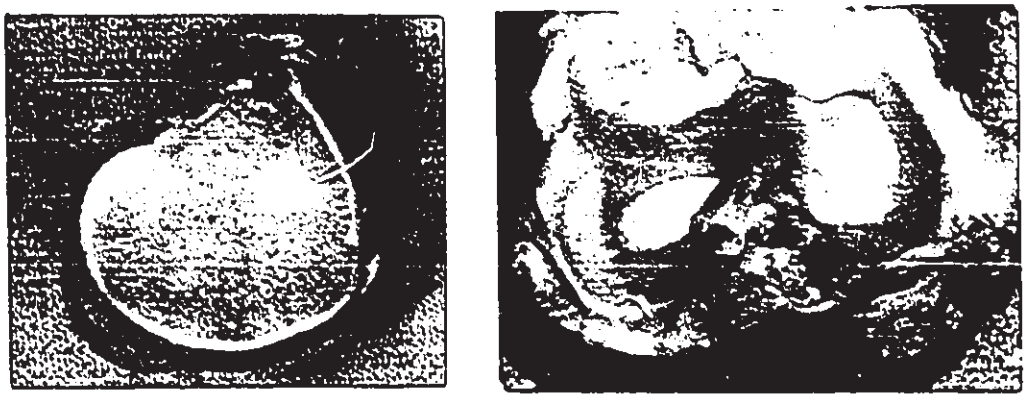

a) b)

Figure 5.30: Specimen four: a) medial-lateral cross-sectional view of the medial femoral condyle, and b) tibial plateau surface.

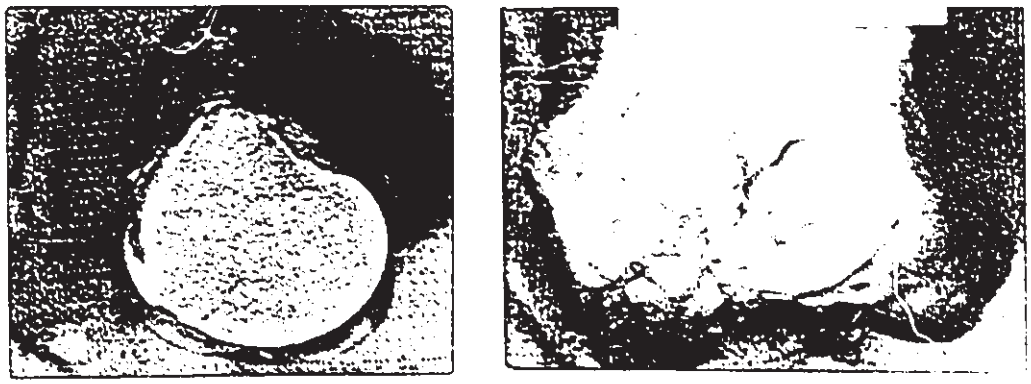

a) b)

Figure 5.31: Specimen five: a) medial-lateral cross-sectional view of the medial femoral condyle, and b) tibial plateau surface.

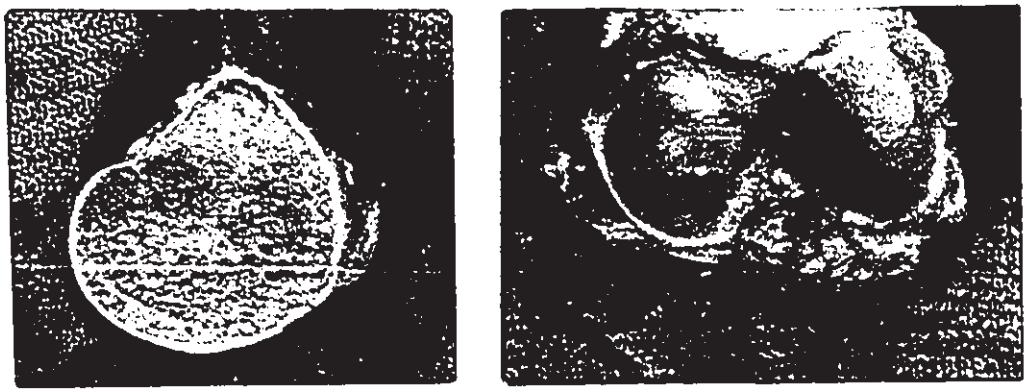

a) b)

Figure 5.32: Specimen six: a) medial-lateral cross-sectional view of the medial femoral condyle, and b) tibial plateau surface.

a) b)

Figure 5.33: Specimen seven: a) medial-lateral cross-sectional view of the medial femoral condyle, and b) tibial plateau surface.

a) b)

Figure 5.34: Specimen eight: a) medial-lateral cross-sectional view of the medial femoral condyle, and b) tibial plateau surface.

CHAPTER 6.0

METHODS

6.1 Procedure of Mounting Specimen in Simulator

The sequence of steps used to achieve neutral alignment of the knee specimen in the joint simulator is summarized below.

1. The joint was first potted and aligned in a neutral position using the alignment jig, as described in section 5.5. The joint was then transferred to the simulator.

2. The measurement pad was inserted into the knee joint between the medial meniscus and medial femoral condyle.

3. Alignment of the joint in the M-L and A-P directions, was accomplished using the femoral and tibial slip plates. The epicondylar axis of the joint was aligned with the rotational axis of the moveable carriage. Final alignment was secured by locking the upper attachment plate to the top plate of the simulator.

Recall that three alignment configurations were studied, beginning with the neutral orientation, and followed by the malaligned and post-osteotomy arrangements. A detailed outline of the steps implemented to achieve the different alignment configurations is provided in section 6.3.

4. The signal conditioning board and measurement pad clamp were aligned with the final position of the measurement pad and locked into place. The ends of the pad were inserted into the connectors on the circuit board.

5. At the completion of testing all three alignment cases, calibration of each active sensor element was performed, as described in section 5.2.4.

The remaining phase of the experimental set-up was to develop an operating system capable of performing data collection, as well as, simultaneously programming and running the simulator.

6.2 Operating and Data Acquisition System

The measurement pad required a real-time data acquisition system to monitor the dynamic behaviour, whereas the simulator was accessed through the control parameters of the microprocessors. The basic features of the operating system are illustrated in the flowchart shown in figure 6.1, and described next.

An existing Quick Basic data acquistion package was selected as the operating program, as the software was compatible with the microprocessor boards and the existing A/D hardware. A series of routines were added to the existing acquisition package in order to program and run the simulator. The operator began by defining the displacement and force profiles for the stepper motors; the profiles were automatically downloaded to the microprocessor boards. The ability to generate a different motion profile was also possible by specifying different control paramaters for the stepper motors.

The final motion curves of the displacement and force motors employed in this study are illustrated in figure 6.2. The test cycle simulated the early part of the stance cycle where the joint compressive load increased with an increase in knee flexion. The knee motion was

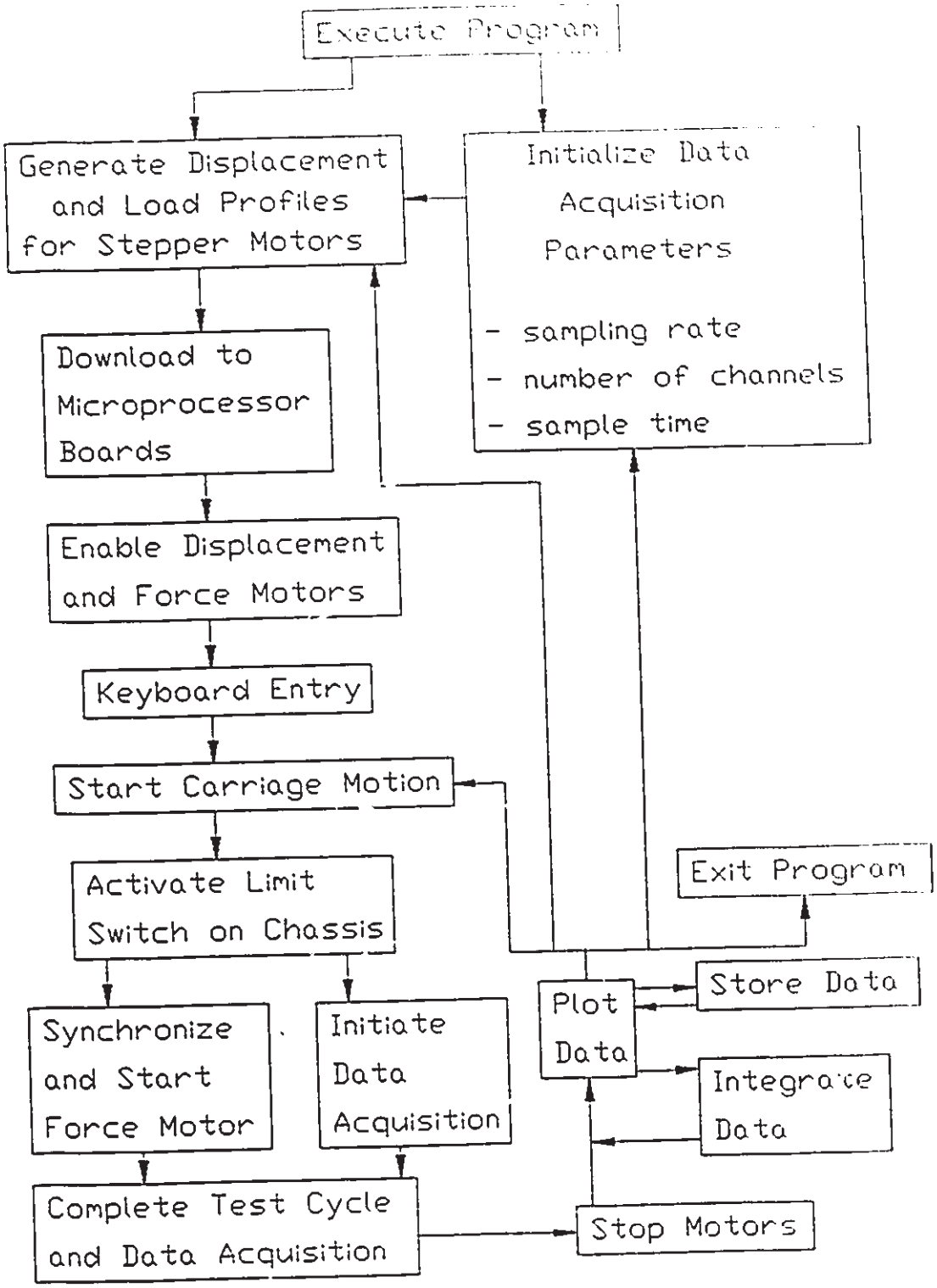

Figure 6.1: Flowchart of control strategy of data acquisition system and operation of simulator.

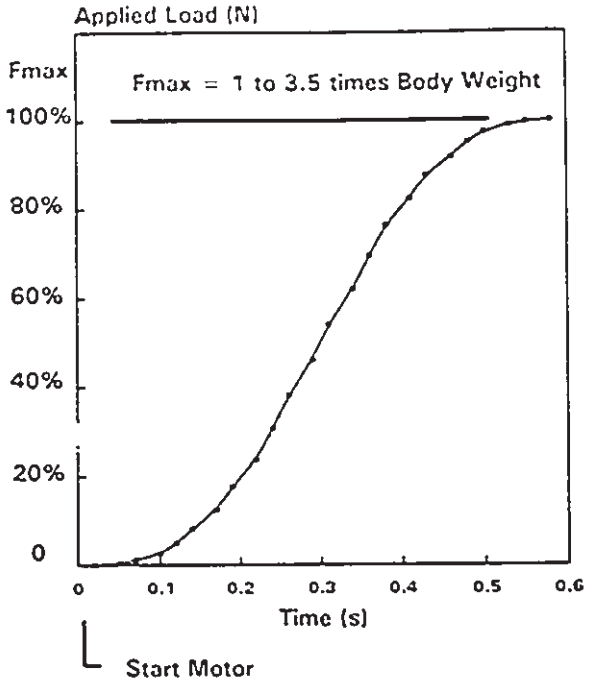

a) Joint compressive force curve.

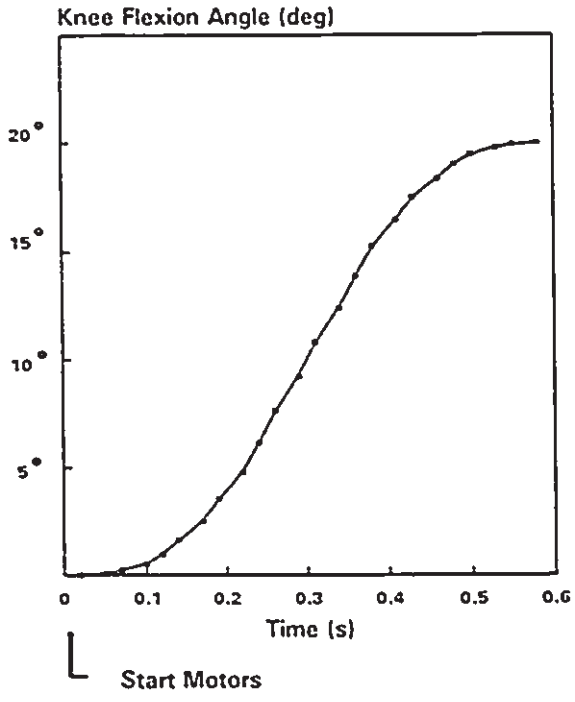

b) Carriage motion - knee angle curve.

Figure 6.2: Motion curves of stepper motors.

selected to flex from a completely extended orientation to 20 degrees in 0.6 seconds. During that time, compressive loads, ranging between 1 to 3.5 times body weight, were applied across the joint.

Options to initialize the A/D board were then carried out, and included setting the sampling rate per channel, number of channels to sample and total sampling time for each channel. The user then activated the displacement and force motors from the keyboard. Although the force motor was in a ready mode, it did not start until after a limit switch on the chassis was tripped by the carriage. This occurred when the knee began to flex from the completely extended position, corresponding to the beginning of the stance phase of gait.

Initialization of the data collection phase was done through a keyboard entry command. This step allowed the operator to run the simulator and confirm the stepper motor patterns; a few cycles were recommended to ensure that the profiles were correct. This also served to precondition the cadaver specimen prior to data collection. Experiments with repeated loading - unloading cycles on the same specimen exhibit stress relation and creep phenomena characterized by a hysterysis loop in the stress - strain curve. The shape of the curve is a function of the viscoelastic properties of the bone, cartilage and meniscus. For this experimental work, the specimens were cycled a minimum of five times before the first set of data was collected.

Upon inputing the go ahead command, the limit switch signal connected directly to the external trigger on the A/D board and synchronized data collection with the running of the force and displacement motors. At the completion of the motion cycle, the stepper

motors could be stopped.

The output signals from the measurement pad could be plotted on the computer screen in graph form, and stored on the hard drive, if preferred. Integration of the data was also available, with an option to replot or store on the hard drive, as well. The final option was to repeat the test cycle, reprogram the force or displacement motors, change the A/D parameters or exit from the program.

6.3 Knee Alignment Configurations used in the Simulations

The procedure for mounting the knee in the simulator was described in Chapter 5, and included the preliminary steps of potting the joint in the alignment jig. A brief description of the method used to produce the different knee alignment configurations with the simulator is provided below. All knees were first tested in a neutral orientation, followed by the malaligned and post-osteotomy configurations. Furthermore, the latter two cases were always established relative to the neutral alignment.

6.3.1 Neutral Alignment Configuration

Neutral alignment of the knee was first established using the alignment jig. The potted knee joint, including support fixtures, was transferred from the jig to the simulator and mounted with the joint completely extended. The centre of rotation of the knee was taken to lie along the epicondylar axis, traveling in a M - L direction through both femoral epicondyles. The location of this axis was aligned with the centre of rotation as defined by the slotted path on the side plates

of the simulator. The centre line of the joint in the A-P plane was aligned with the centre line of the simulator to ensure that the line of action of the force motor was directed through the centre of the joint and perpendicular to the tibial surface. Neutral alignment of the joint was similar to that depicted in figure 5.25.

The carriage and distal components were then manually moved with both force and displacement motors turned off to check that the joint did not bind or separate as flexion progressed. By leaving the bolt connections on the proximal slip plates loose at the start, the knee would tend to seek out a natural normal position. Once optimal alignment was achieved, the remaining bolt connections were tightened, thus establishing the neutral alignment position for the joint. As mentioned previously, the remaining two alignment configurations were established relative to this neutral position.

6.3.2 Varus Alignment Configuration

A 15° varus offset at the knee was selected for the malaligned configuration and comprised of an 8° outward tilt of the tibia about the ankle joint and a 7° outward tilt of the femur about the hip joint. The summation of the angles was measured between the mechanical axes of each bone and a vertical reference frame on the simulator and equaled 15°. The procedure involved detaching the femoral slip plates at the top of the simulator and loosening the tilting plates on the tibial components. The knee joint could then be moved to any new position. Aluminum spacers were inserted between the tilting plates and automatically set the tibia to the 8° offset. To have the force vector pass medial to the

knee centre, as occurs in a malaligned knee, the entire tibial pot was translated laterally by approximately 5 cm. This value was representative of an average distance between the knee centre and a line joining the hip and ankle joint centres. The height of the knee centre relative to the base of the trolley was also reset such that the centre of rotation of the knee remained aligned with that of the simulator. The final alignment configuration is illustrated in figure 6.3.

6.3.3 Post-Osteotomy Alignment Configuration

The goal of high tibial osteotomy surgery was to restore the alignment of the lower limbs. This in turn was believed to reduce the contact pressure on the affected compartment and retard the advancement of osteoarthritis. Two of the more common surgical procedures selected for investigation in this study were the dome osteotomy, advocated by Maquet et al. [98,99], and the standard close-wedge osteotomy, recommended by Coventry [32,33,34,35]. The outcome of both surgical methods resulted in a similar realignment of the knee, with the femoral and tibial mechanical axes aligned with each other. As well, both surgical procedures reposition the tibial plateau in a downward slope, going from a medial to lateral direction, and was often referred to as over-correction in the literature. Therefore, simulation of only one knee alignment condition was required to investigate the post-osteotomy configuration in this study. To achieve the re-oriented position, two special aluminum spacers were inserted between the tilting plates of the tibial components. The femoral components automatically adjusted to the new realigned configuration. Note that the amount of rotational offset

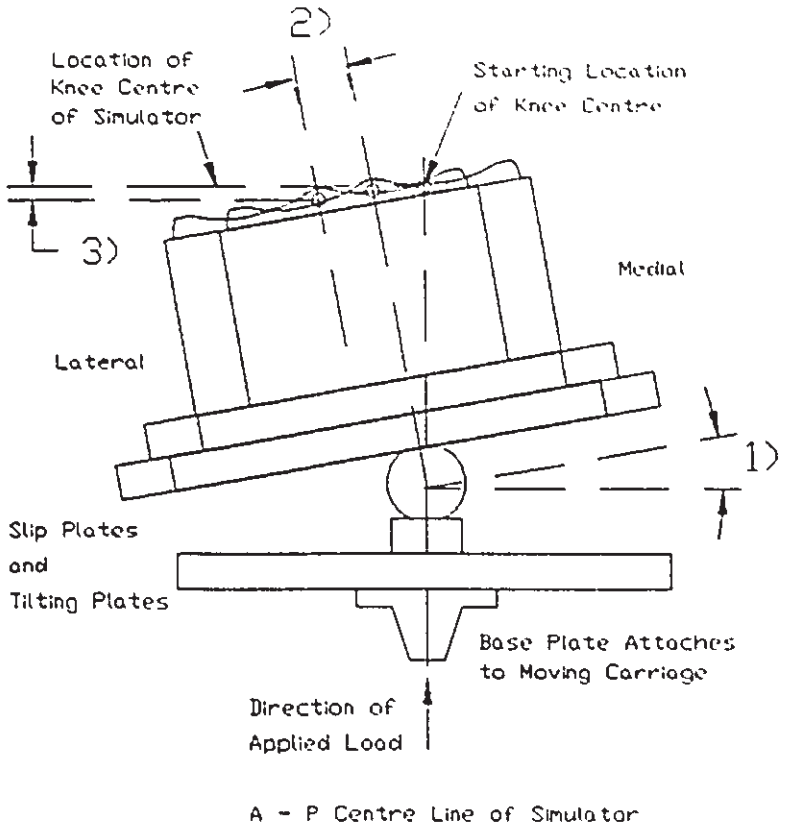

Steps to create
varus malalignment:

1) Rotate - - - - -

2) Translate — - - —

3) Raise ————

Figure 6.3: Procedure to simulate a varus malalignment of a cadaveric knee mounted in the joint simulator.

of the tibial plateaus was always relative to the neutral orientation.

Final alignment of the post-osteotomy configuration is illustrated in figure 6.4. In the A-P plane, the load line of the simulator passed through the centre of the femoral condyles, and was accomplished by translating the tibial pot in the medial to lateral direction. In the sagittal plane, the load line of the simulator remained aligned with the mid-distance of the tibial plateau.

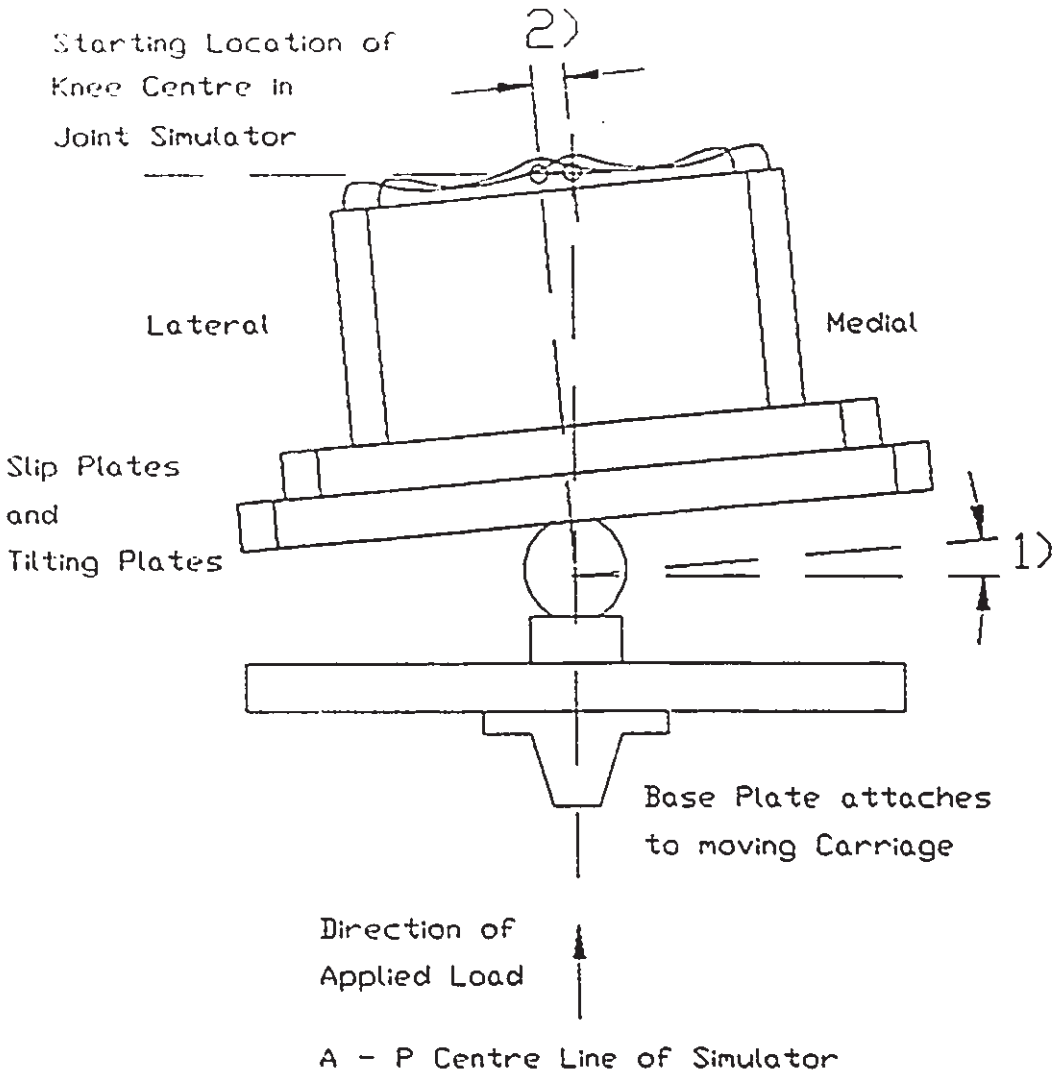

Steps to create post - osteotomy malalgnment:

1) Rotate - - - - -

2) M-L Translate — - - —

3) Raise ————
(minimal adjustment was required)

Figure 6.4: Procedure to simulate a post-osteotomy alignment of a cadaveric knee mounted in the joint simulator.

CHAPTER 7.0

RESULTS

7.1 Introduction

The first pair of knees tested employed one of the original prototype measurement pads, which became prone to mechanical breakdowns. Rather than omitting the results from the study, those elements remaining active throughout the experiments were included in the analysis. This was still beneficial as each sensor element provided information on local contact behaviour.

The effects of knee alignment on the contact response characteristics at the articular surface will be analyzed in two parts: 1) the active contact area zones and 2) the contact pressure patterns.

7.2 Identification of the Active Contact Zone

Before dismounting the joint from the simulator, the position of the measurement pad on the tibial plateau was recorded relative to specific anatomical structures: medial collateral ligament, intercondylar eminence and outer perimeter of the knee capsule. The location of the underlining meniscus was also noted. Photographs of the articular surface were obtained at this time, and were presented in figures 5.27 to 5.34.

To further help with the analysis, the medial compartment was divided into five quadrants, each covering a specific region of the

articular surface. The arrangement and relative location of each quadrant is shown in figure 7.1. The first two quadrants represent the central portion of the exposed articular cartilage surface not covered by the meniscus, and were divided into anterior and posterior regions. The third and fourth quadrants contained the remaining posterior surface area, and were divided into medial and lateral zones. The last quadrant included the remaining anterior surface area. Most of the surface area contained by the last three quadrants included that surface in direct contact with the meniscus.

A transparent sheet with the sensor array pattern traced onto it was placed over top of an actual size photograph of the medial tibial compartment and properly positioned using the referenced anatomical landmarks. This enabled identification of the sensor elements contained within each quadrant. Recalling that element numbering was established during the design phase of the signal processing hardware; a total of four groups (0,1,2,3), with nine channels (1 though 9) in each, was selected. Each sensor element was referenced by its occurrence in the sampling order and consisted of the group number and sampling channel; ie. element 15 represents the fifth channel to be collected in group one.

Some of the peripheral elements did not register any signal response, as they came to lie outside the immediate contact area. Only those elements responding to the load were used to estimate the active contact zone. This was accomplished by tracing the outer perimeter of the area enclosed by these elements. The boundary line followed a path along the mid-distance of the active and nonactive elements. The test

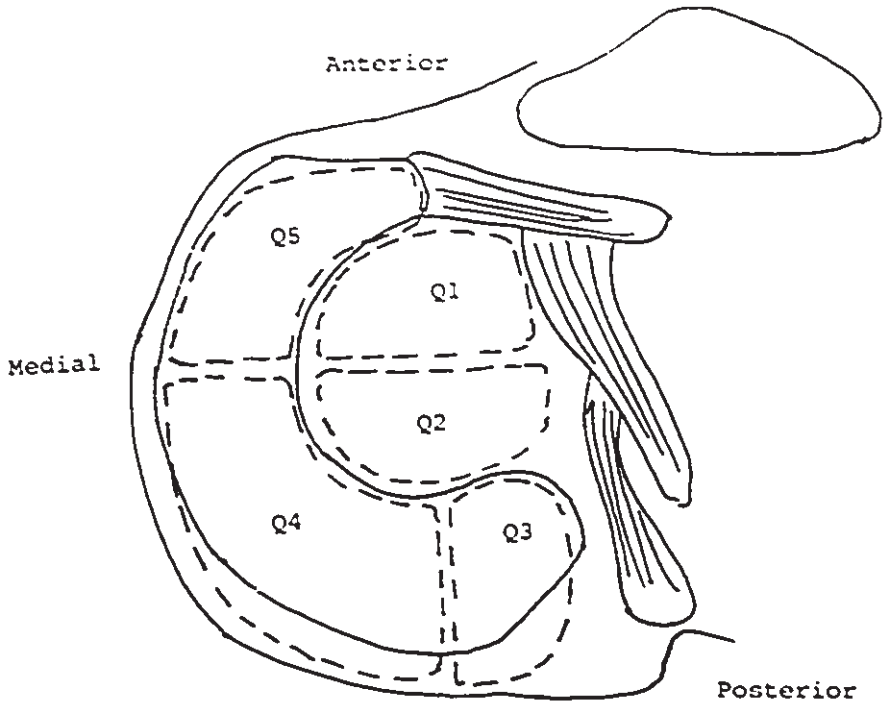

Figure 7.1: Division of medial tibial compartment into specific quadrants.

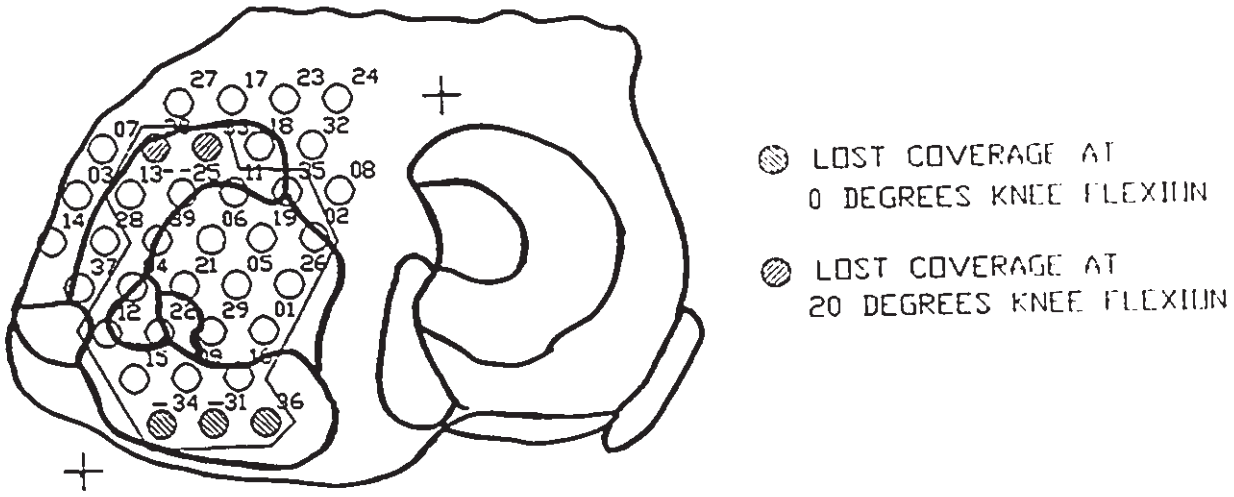

Figure 7.2: Relative coverage of medial compartment: Contact area coverage for specimen one.

results for specimen one are used to demonstrate the technique. Referring to figure 7.2, the solid line encloses the total contact area of all of the active elements. Calculation of the area was reduced to a planar projection of the tibial surface, and performed using a utility feature in the AUTOCAD drafting program. The same program was used to design the layout of the measurement pad. These calculations represent an average of the total surface area that came under contact during the entire test cycle, ie. knee flexion from 0 to 20 degrees.

Most investigators calculated the contact area under static load conditions for knee orientations of either complete extension or 15° flexion. Therefore, two additional area calculations were performed and represented an average of the active area under contact at complete knee extension and at 20° flexion. Area measurements were made at the completion of the data collection phase. The load cycle was reapplied with the knee fixed at the two different orientations. Signal responses of the active elements were monitored again to identify which elements, if any, were no longer responding, and thus indicating loss of contact. Those elements across the anterior periphery were more likely to lose contact when the knee was flexed, while the posterior elements were more likely to lose contact when the knee was completely extended.

7.3 Contact Pressure Patterns

7.3.1 Estimation of the Normal Contact Pressure

Because of the large loads placed across the joint and the variations in the mating articular surfaces, physical bending of an

element was unavoidable. As a result, elements were analyzed by comparing the relative differences in signal magnitude for the three different alignment cases. Furthermore, the occurrence of bending of the sensor element prevented the output from being converted to an actual force value, as no calibration factors pertaining to bending of the sensor elements were determined. This is largely due to the inability to place each element on the measurement pad under a bending load in a consistent and repeatable manner, while inserted in the knee joint. This does not restrict the use of this data, however, as the performance characteristics of the piezofilm display a linear output response to a bending load, similar to that for direct compressive loading. The only notable difference between the two modes of loading was that the magnitude of the signal output for bending was much greater than for pure compression. It should also be remembered that the measurement pad was designed to reduce and limit the occurrence of bending by the addition of the copper shims in the final prototype design of the measurement pad.

Averaged values of the integrated signal responses from each element were computed from five successive loading cycles. Each value was subsequently normalized to the corresponding applied load. Means and standard deviations of the normalized signal responses (NSR) were calculated and categorized by alignment set-up and quadrant number. Plots of the normalized output from all active elements were also generated for each specimen and grouped by their appropriate quadrant. Any element experiencing a bending mode was appropriately identified along the top of the chart, and was classified as having either a

concave upward shape or a convex downward shape.

The results of the NSR values from each sensor element represented the percentage of applied load acting over the entire surface area of one sensor element, ie. AS = 11.4 mm^2. However, the surface area of an element covered only a portion of the articular surface area. This is illustrated in figure 7.3, where a series of grids were formed by drawing lines along the midpoints of two adjacent elements. Each grid area (AG) included one sensor element and covered 43.8 mm^2 of the articular surface. Thus, each sensor element covered approximately 26% of the available articular surface. If contact normally occurred over the entire area of the articular surface enclosed by a grid, then the output from the average contact pressure on the element was higher; by a factor of (AG/AS) = 1/.26 = 3.84. That is, more load was borne by the reduced area of the element and increased the contact pressure readings. As a result, the average contact pressure values from the elements were expected to be higher than those estimated by other measurement devices. The differences in the two area zones and corresponding contact pressure values are described below.

$$\text{Contact Pressure per element} = \frac{\text{Force on Sensor}}{\text{Area of Sensor Element}} \qquad (7.1)$$

and

$$\text{Contact Pressure per grid} = \frac{\text{Force on Sensor}}{\text{Area of One Grid}} \qquad (7.2)$$

$$\text{NSR} = \frac{\text{Contact Pressure}}{\text{Applied Force}} = \left(\frac{\text{Force on Sensor}}{\text{Applied Force}}\right) / \left(\text{Area of Sensor Element}\right)$$

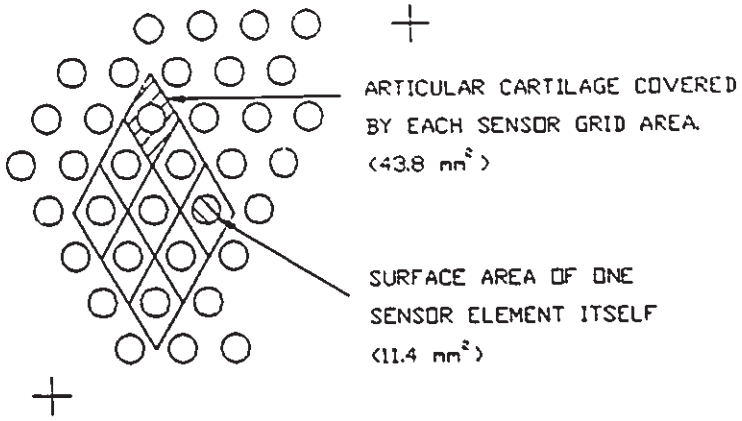

Figure 7.3: Percentage of articular surface covered by a single sensor element.

or NSR = (% of Applied Force) / Area (7.3)

If the sensor element area (AS) was used, then the normalized average pressure values corresponded to (% of applied load / 11.4 mm^2). Likewise, if the contact was across the entire articular surface area of each grid, the normalized average contact pressure was (% of applied load / 43.8 mm^2).

Recall that the peak external loads applied to the joint ranged between 1 and 3.5 times body weight. For an assumed body weight of 700 N, this translated to a load range between 700 and 2500 N. For the neutral and post-osteotomy alignment configurations, the external applied load was shared between the two tibial compartments, whereas for the malaligned case, all of the load was directed to the medial compartment.

If all of the applied load acts on only one element, then the maximum average contact pressure for the neutral or post-osteotomy configuration varied between :

Minimum Contact Pressure = 350 / 11.4 Mpa = 30.7 MPa

Maximum Contact Pressure = 1250 / 11.4 MPa = 61.4 MPa

Likewise, if the total surface of one grid was under contact, then the contact pressure varied between

Minimum Contact Pressure = 350 / 43.8 Mpa = 8.0 MPa

Maximum Contact Pressure = 1250 / 43.8 MPa = 16.0 MPa

Similarly, if all of the applied load acted on only one element for the malaligned knee configuration , then the maximum average contact pressure varied between :

Minimum Contact Pressure = 700 / 11.4 Mpa = 61.4 MPa

Maximum Contact Pressure = 2500 / 11.4 MPa = 215 MPa

and if the total surface of one grid was under contact, then the contact pressure varied between

Minimum Contact Pressure = 700 / 43.8 Mpa = 16.0 MPa

Maximum Contact Pressure = 2500 / 43.8 MPa = 57.1 MPa

However, it is impossible for one element to carry all of the applied load. For the neutral and osteotomy alignment cases, if up to 10% of the applied load acted on any one element, the pressures ranged between 3 to 10 MPa when the sensor element area is used, and 1 to 6 MPa when the area per grid was used. These ranges were similar to those recorded by other investigators when tested under similar conditions, and are listed in Table 7.1. Note that these values are simply doubled for the malaligned case.

As a result, if the normalized peak values exceeded 15% for the neutral and postosteotomy configurations and greater than 25% for the malaligned configuration, then a condition of element bending was considered present. To accommodate this, the plots of the tabulated values of the normalized contact pressures are shown up to a peak limit

of 25%. Surprisingly, there was a consistant trend in the data to lay within these ranges when the element was placed under a purely compressive load. Elements experiencing a bending load had signal peaks which greatly exceeded the upper limit of 25% of the applied load.

Table 7.1: Estimations of Contact Pressure on One Sensor Element

Percentage of Applied Load	Contact Pressure = ‡ (% of BW / Area) MPa							
	Neutral and Post-Osteotomy				Varus Malalignment			
	(1/2 BW)		(1.75 BW)		(1 BW)		(3.5 BW)	
	AS	AG	AS	AG	AS	AG	AS	AG
100%*	30.7	8.0	109.6	28.5	61.4	16.0	219.2	57.0
5%	1.5	0.4	5.5	1.4	3.1	0.8	12.0	2.9
10%	3.0	0.8	11.0	2.8	6.1	1.6	6.0	5.8
25%	7.7	2.0	27.4	7.1	15.3	4.0	54.8	14.2

* Contact pressure calculated as if all or a percentage of the applied load acted on either the element area or grid area.

‡ AS: sensor element area (11.4 cm^2)

AG: grid area (43.8 cm^2)

BW: Body weight estimated to be 700 N

7.4 Test Results for Specimen One

As previously mentioned, the original prototype pressure sensor pad was used with this specimen and only partial measurements were obtained. However, the data still provided useful information on local contact behaviour and was therefore included. A large tear was present in the posterior - lateral region of the medial meniscus. The tibial plateau surface of specimen one was shown in figure 5.27. No other gross pathology was observed on the remaining articular surface of the tibia or femur. It was not known as to how the meniscal tear affected the resultant motion and joint contact. Bylski-Austrow [21] observed an outward translation of the medial meniscus in a direction posterior and away from the joint centre, when placed under direct compression and knee flexion between $0^{\circ}$to 30°. However, no meniscal tears were present in the knee specimens included in their study. Similar movement of the meniscus with this specimen may not have occurred because of the possibilites of the tear producing an unnatural loading condition. Added to the uncertainties of the actual meniscal movement, were the mechanical malfunctions present with the original prototype measurement pad.

7.4.1 Active Contact Area Zones

The total surface area under contact comprised twenty - four sensor elements. Nine were determined to be non - functional at some interval during the test period, but these laid within the boundary of the contact zone and were therefore included in the area calculations. The arrangement and position of the active elements on the medial

compartment of specimen one are illustrated in figure 7.4. Using this figure, each element was assigned to one of the five quadrants, as detailed in table 7.2.

The average contact area zones are shown in figure 7.5, and were estimated to be 10.72 cm^2, 9.38 cm^2, and 9.87 cm^2, corresponding to the total active area, the area under contact at complete extension and the contact area for 20° knee flexion, respectively.

Table 7.2: Assignment of Active Elements by Quadrant Location for Specimen One

Quadrant Number	Channel Identification *
Q1	06 35 (11 19)
Q2	01 05 26 29 (21)
Q3	16 36 (31)
Q4.	12 15 22 34 (04 09)
Q5	25 28 38 (13 33 39)

* Elements encountering a malfunction are enclosed in brackets.

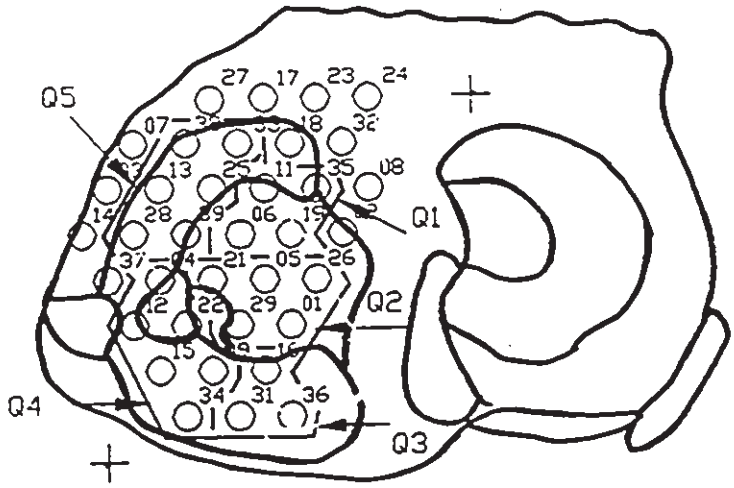

Figure 7.4: Location of measurement pad on medial compartment of specimen one. Quadrants separated by dashed lines.

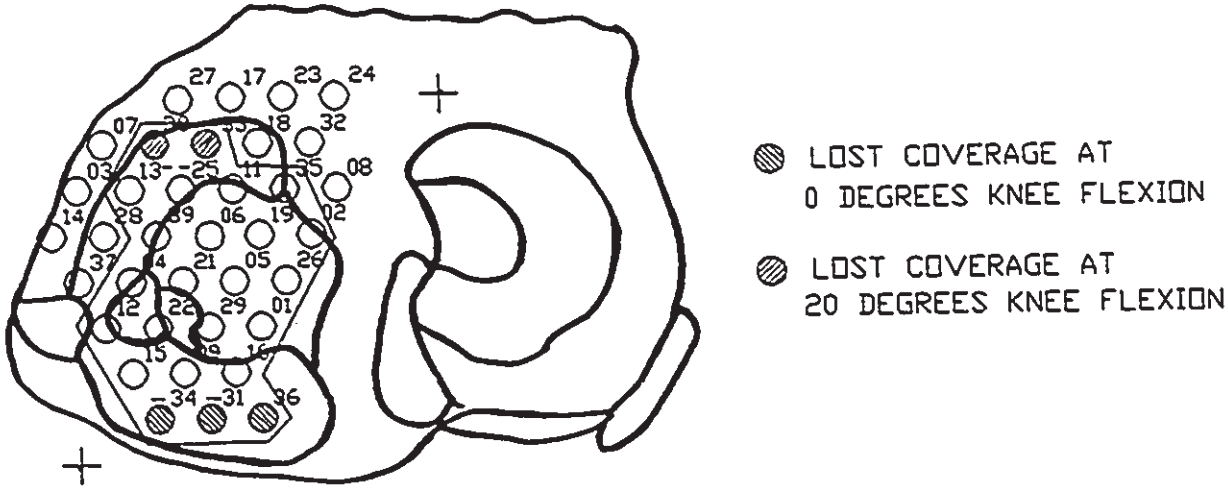

Figure 7.5: Area coverage of medial compartment of specimen one.

7.4.2 Normalized Contact Pressure Patterns

The mean and standard deviation values of the normalized signal responses (NSR) and applied loads are shown in table 7.3. The normalized data are also charted in figure 7.6, illustrating variations within each quadrant. The effect of the alignment changes on load transmission at local points of contact will be discussed next, beginning with quadrant one.

7.4.2.1 Quadrant One: Anterior Central Region

Two of the four elements laying within the boundaries of quadrant one malfunctioned, leaving only elements 06 and 35 active. Element 06 was located on a relatively flat section of the articular cartilage surface not in contact with the meniscus. Signal responses typical of compressive loading were registered for all three knee alignment conditions. The malaligned case generated the greatest output while the normal case had the lowest. This indicated an inward shift in the contact load towards the joint centre with the post-osteotomy alignment compared to the neutral situation.

Element 35 was positioned along inner region of the medial compartment, close to the anterior attachment site of the medial meniscus. A convex bending response was observed for all of the alignment cases, and was greatest following the post-osteotomy alignment tests. The increased curvature of the plateau surface in this region and the inward translation of the femoral condyle against the intercondyar tubercle was most likely responsible for bending of the element. The output from both elements indicated that the medial

compartment experienced an increased loading state when the knee was malaligned, and that the contact load translated toward the joint centre following the post-osteotomy realignment, when compared to the neutrally aligned knee.

7.2.4.2 Quadrant Two: Posterior Central Region

A total of five elements were contained by quadrant two: 01, 05, 21, 26 and 29; element 21 was not analyzed because of mechanical problems. Elements 01 and 05 were located along a flatter region of the articular surface, with 05 anterior and medial to 01. A similar output pattern occurred at both elements for the neutral and malaligned cases, and gave a weaker response for the post-osteotomy alignment case. Element 26 laid along the extreme inner surface of the compartment, directly posterior to element 35 in quadrant one. Similar signal patterns to those of element 35 were also observed, where all peak values were of a convex bending nature. The greatest output from 26 occurred during the malalignment tests, followed by the post-osteotomy and neutral cases. The low magnitude of the bending - type signals for the latter two alignment cases indicated minimal load transfer occurred.

Figure 5.26 shows where a section of the torn meniscus was unconstrained and free to drift inward. It is doubtful that the motion of the meniscus was similar to that observed by Bylski-Austrow [21], (ie. in an outward - posterior direction). Element 29 was situated in the vicinity of the tear and was nearly inactive when the knee was aligned neutrally. However, a notable increase in the contact behaviour occurred when the alignment was altered, being greatest for the

malaligned condition.

The overall responses for elements in quadrant two indicated that contact was maintained across the central portion of the articular surface, regardless of the alignment, and that it was greatest for the malaligned case and least following the post-osteotomy alignment.

7.4.2.3 Quadrant Three: Inner Posterior Region

Element 31 was non-operable during the tests and removed from the study, leaving elements 16 and 36 to be analyzed. Element 16 laid directly anterior to the inner edge of the meniscus close to the proximal attachment site, and element 36 was positioned posterior to 16 in contact with the meniscus. Contact in this region occurred during the latter phase of the loading cycle near peak flexion (limited to 20° for all tests). As a result, relatively low compressive-type peak signal responses were observed. It was also observed that during the tests the backward translation of the femoral condyle on the tibial plateau also pushed the meniscus backwards. However, because of its outer constraints, the meniscus would bulge outward and sometimes upward. It is thought that this bulging might promote a bending response at those elements immediately on top of the meniscus.

Signal output patterns were compressive for element 36 and bending for 16. Bending of element 16 was likely due to the difference in height between the articular surface and top of the meniscus. Regardless, the largest response occurred for the realigned osteotomy alignment and supported the concept of joint stabilization along the intercondylar tubercle.

7.4.2.4 Quadrant Four: Outer Posterior Region

Two of the six elements in this quadrant were not used (04 and 09); elements remaining active were 12, 15, 22 and 34. Two of the elements were anterior to the tear in the meniscus (12 and 22), and two posterior (15 and 34). All elements laid on the top surface of the meniscus and responded with large signals, indicative of bending. The high occurrence of bending at the outer two elements (12 and 15) demonstrated the limitation of the measurement pad, as it functions optimally when placed between two level and conforming surfaces. However, the increased signal peaks indicated more load transfer, especially for the malaligned case compared to the neutral test results. A similar trend occurred at the inner two elements, (22 and 34) in that the malaligned case had the greatest peak responses.

7.4.2.5 Quadrant Five: Anterior Outer Peripheral Region

Elements 25, 28 and 38 remained active, while 13 and 39 were lost to mechanical breakdowns. Figure 7.4 shows element 25 resting on top of the anterior part of the cartilage near the meniscus - cartilage junction, with elements 28 and 38 located lateral and anterior to 25, furthest from the joint centre. All output responses were of a concave upward bending nature for elements 28 and 38. Element 28 had a substantially larger peak value when the joint was malaligned. Of interest was the lower output signal peaks with the post-osteotomy realignment. This again supported the concept of an unloading along the outer periphery of the medial compartment following a high tibial osteotomy.

Element 25 was located more central on the anterior part of the meniscus and generated output patterns similar to those observed for elements included in quadrant one. Results for the malaligned and osteotomy cases exceeded those for the neutral case; all responses remained within the limits of a purely compressive mode of loading.

Table 7.3: Normalized Average Pressure Measurements for Specimen One

Alignment Configuration		Quadrant One: Active Elements	
		06	35
Normal	NSR	.003/.003	.264/.109‡
	Load	1464/156	2571/85
Mal.	NSR	.065/.037	.970/.133‡
	Load	1272/35	1824/58
Ost.	NSR	.026/.017	2.03/.200‡
	Load	650/45	945/45

		Quadrant Two: Active Elements			
		01	05	26	29
Normal	NSR	.127/.043	.060/.015	.205/.058‡	.007/.008
	Load	1517/111	1463/46	1734/35	1699/55
Mal.	NSR	.121/.026	.050/.030	2.40/.608‡	.150/.060
	Load	1254/27	1308/89	1281/18	1290/20
Ost.	NSR	.043/.023	.005/.006	.428/.258‡	.017/.035
	Load	663/55	653/49	640/70	660/63

All responses are for a compressive load, unless otherwise specified.
†: Concave Bending Response and ‡: Convex Bending Response.

NSR: Normalized Signal Response
Load: Externally Applied Load (N)

Table 7.3: Normalized Average Pressure Measurements for Specimen One

Alignment Configuration		Quadrant Three: Active Elements	
		16	36
Normal	NSR	.193/.037‡	.036/.017
	Load	1748/27	1775/53
Mal.	NSR	.335/.117‡	.011/.005
	Load	1357/58	1254/44
Ost.	NSR	1.41/.362‡	.028/.016
	Load	636/36	645/20

		Quadrant Four: Active Elements			
		12	15	22	34
Normal	NSR	1.72/.566†	.077/.021	.010/.006	.125/.030
	Load	1739/31	2531/53	1690/51	1770/53
Mal.	NSR	2.56/.534†	5.26/.409†	.076/.032	.148/.035
	Load	1294/31	1299/31	1272/15	750/75
Ost.	NSR	2.67/.978†	4.19/1.53†	.003/.001	.008/.004
	Load	630/40	876/45	670/12	715/60

		Quadrant Five: Active Elements		
		25	28	38
Normal	NSR	.061/.030	4.86/2.85†	.290/.038†
	Load	2482/85	2433/58	1813/60
Mal.	NSR	.164/.043	31.7/4.90†	.407/.100†
	Load	1855/27	1890/76	1278/50
Ost.	NSR	.103/.033	.241/.325†	.438/.174†
	load	636/65	907/89	657/38

All responses are for a compressive load, unless otherwise specified.
†: Concave Bending Response and ‡: Convex Bending Response.

NSR: Normalized Signal Response
Load: Externally Applied Load (N)

Figure 7.6 a): Normalized signal output patterns: Specimen one - Quadrants one and two.

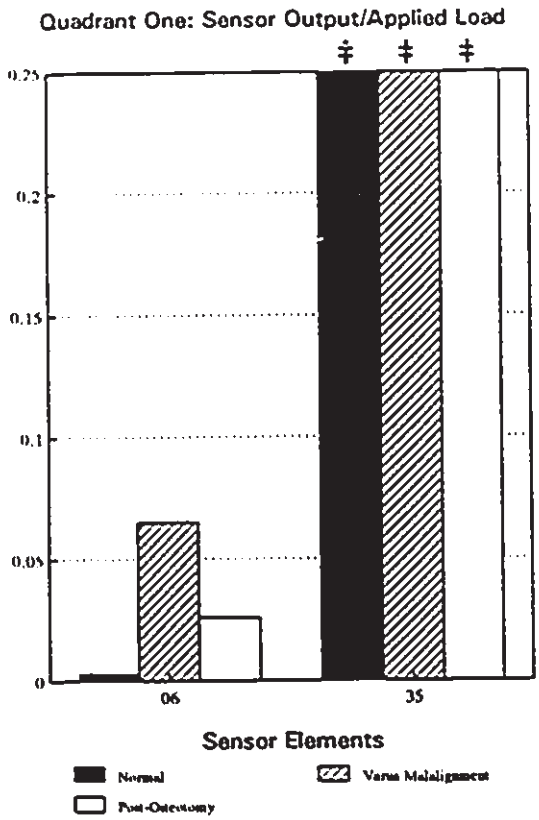

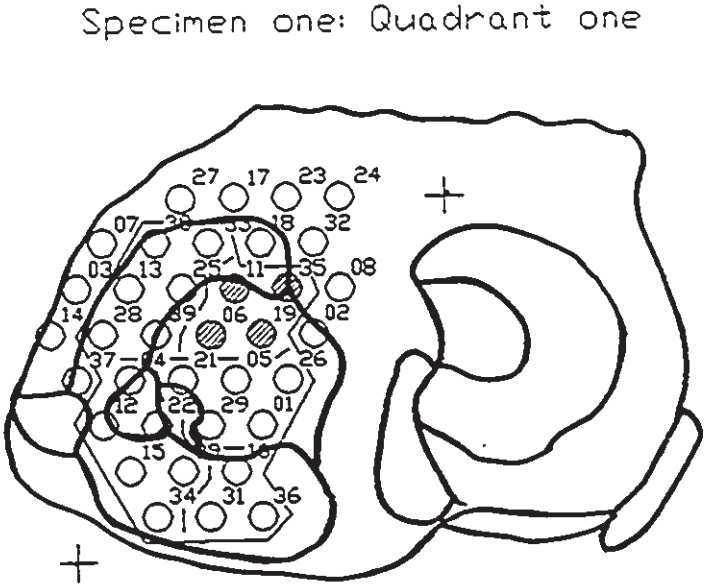

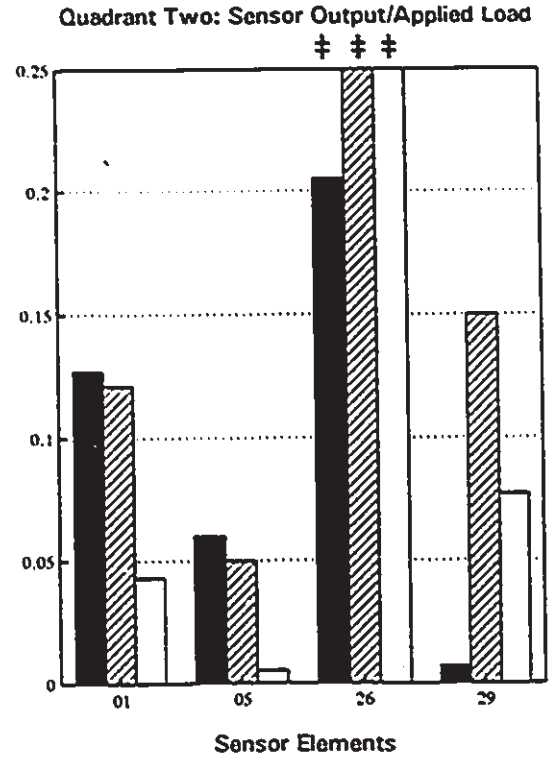

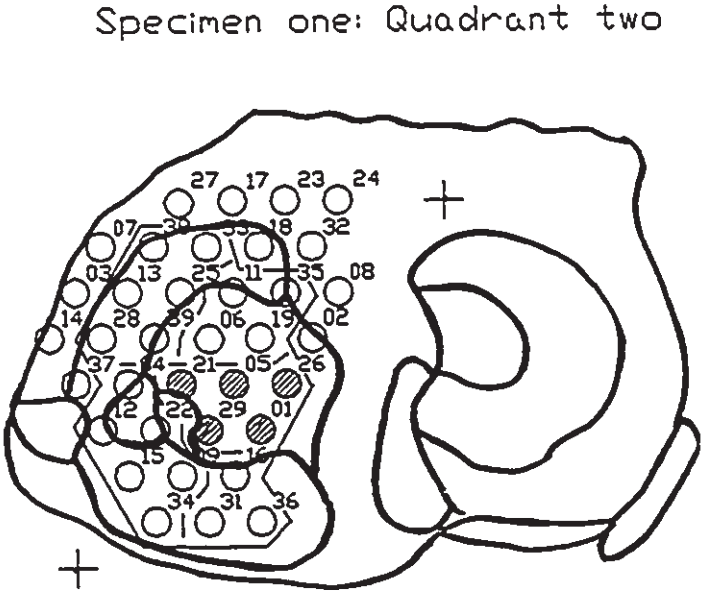

Figure 7.6 b): Normalized signal output patterns: Specimen one - Quadrants three and four.

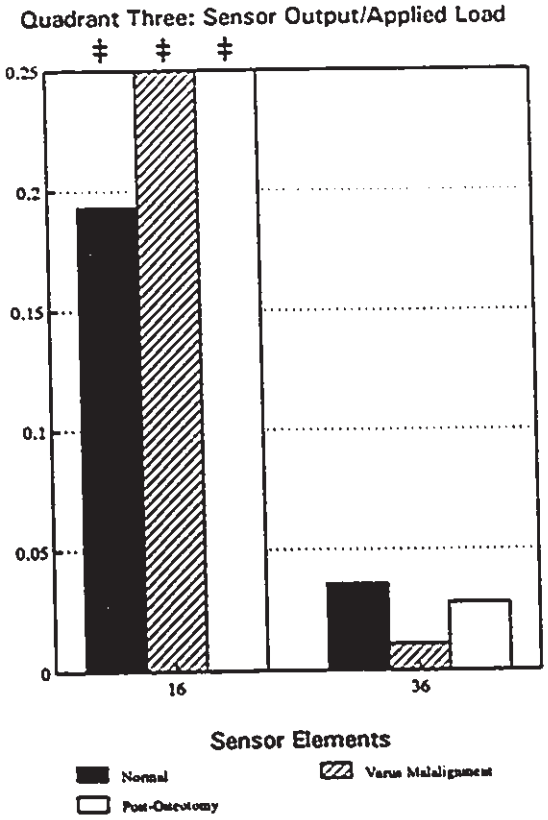

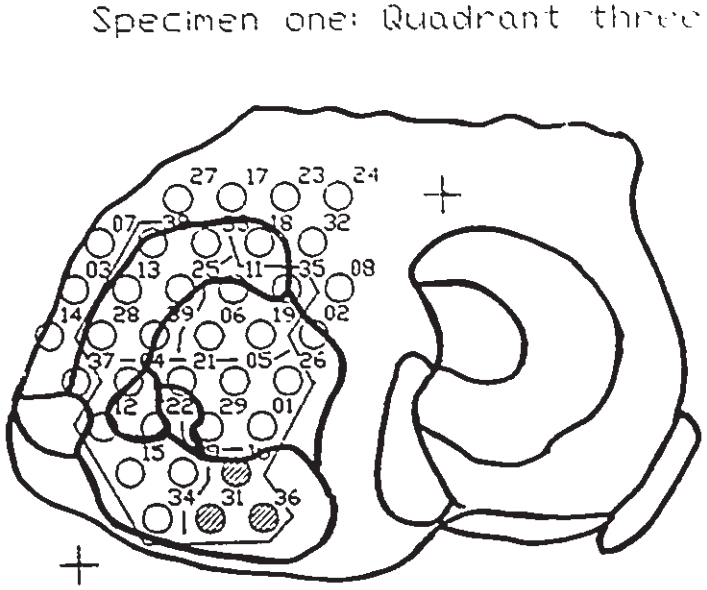

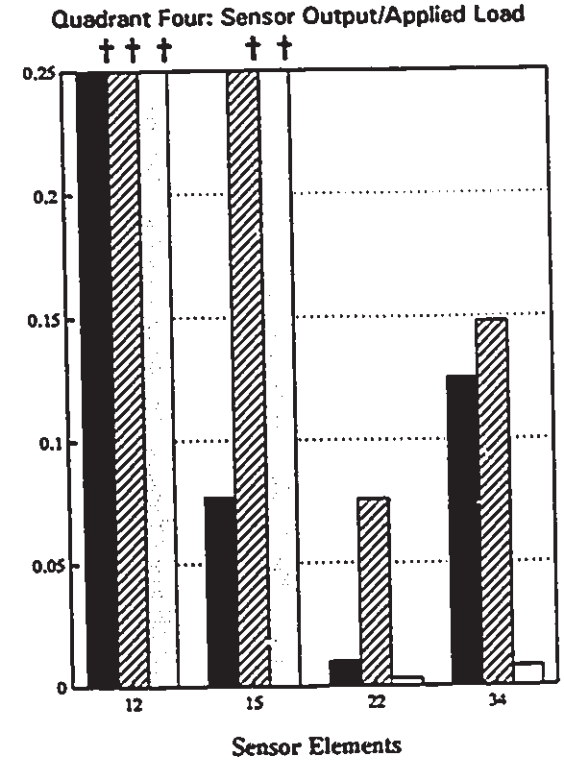

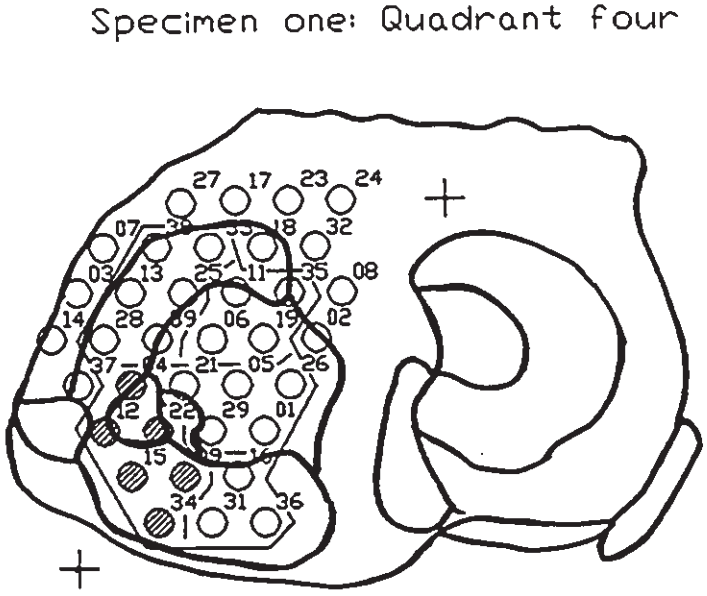

Figure 7.6 c): Normalized signal output patterns: Specimen one - Quadrant five.

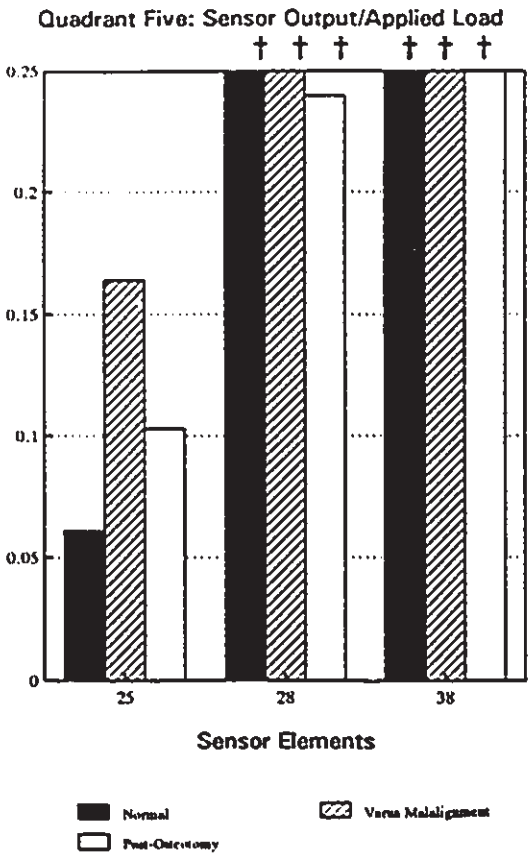

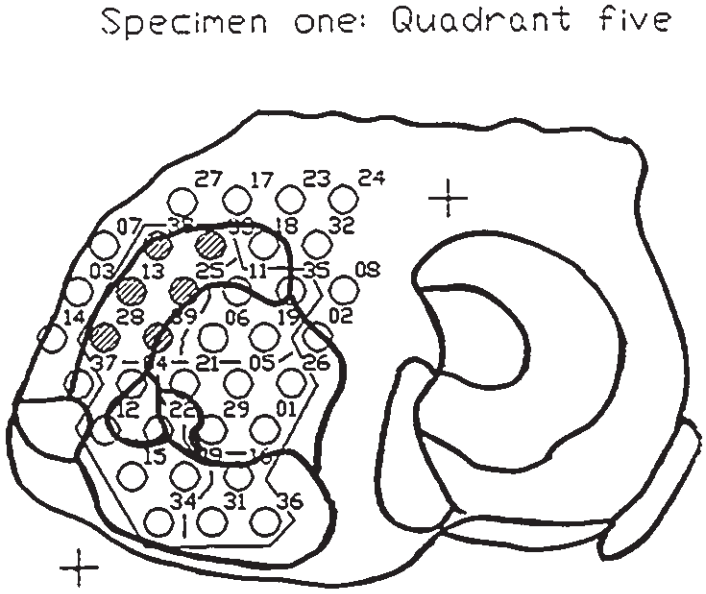

7.5 Tests Results for Specimen Two

Specimen two was the left mate to specimen one, the articular surface of the tibial plateau of the joint was shown in figure 5.28, and had no visible signs of gross pathology. A grade two level of osteoarthritis was present at the lateral part of the medial femoral condyle in the weight bearing area, measuring 2 cm by 1/2 cm, and was under contact during slight flexion (0° to 30°).

7.5.1 Active Contact Area Zones

The location of the measurement pad on the medial compartment is illustrated in figure 7.7. Twenty-one active elements were identified and assigned to specific quadrants, as detailed in table 7.4. No elements were lost due to malfunction problems.

Estimations of the average contact area zones for specimen two are demonstrated in figure 7.8. The total active area was 9.15 cm^2, and reduced to 7.86 cm^2 and 8.72 cm^2 for 0° and 20° knee flexion, respectively.

Table 7.4: Assignment of Active Elements by Quadrant Location for Specimen Two

Quadrant Number	Channel Identification
Q1	06 11 19 25 39
Q2	05 21
Q3	01 16 29 31 36
Q4	09 12 15 22 34
Q5	04 13 28 33

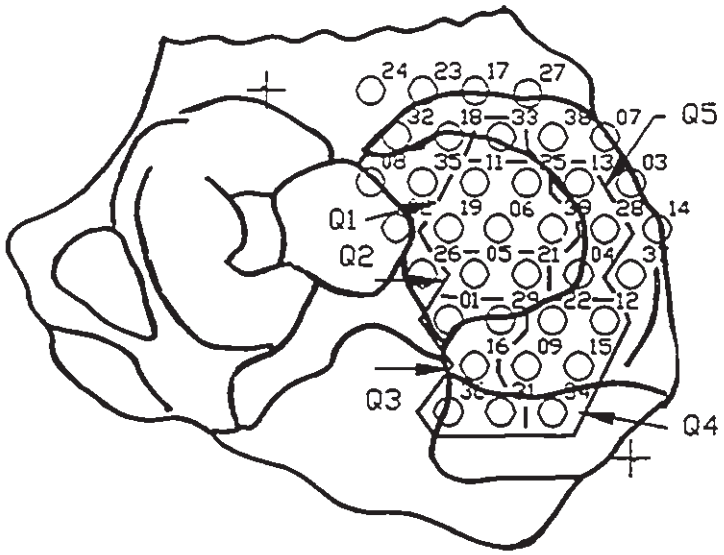

Figure 7.7: Location of measurement pad on medial compartment of specimen two. Quadrants separated by dashed lines.

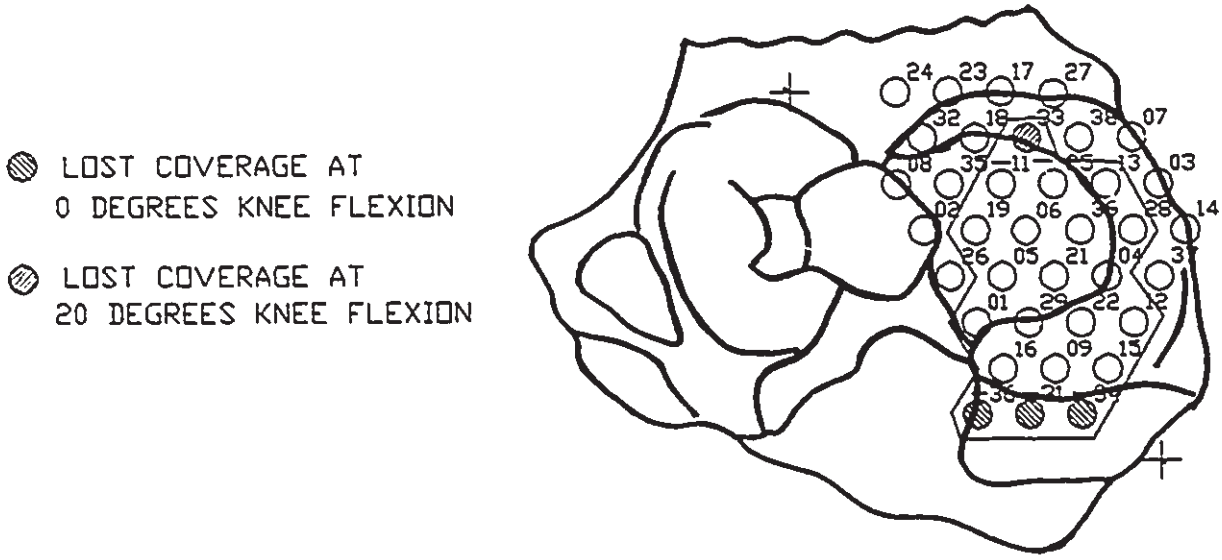

Figure 7.8: Area coverage of medial compartment of specimen two.

7.5.2 Normalized Contact Pressure Patterns

The averaged peak values of the signal responses from each element were calculated for five successive loading cycles and normalized with respect to the applied load. Means and standard deviations of the normalized peak outputs and applied load are provided in table 7.5, and have been grouped by alignment set-up and quadrant location. Plots of the normalized outputs for the three alignment methods are shown in figure 7.9. Elements undergoing bending during the tests are identified at the top of the charts. Trends in the dynamic contact response patterns at local points across the medial compartment are provided next for the different alignment conditions, and are presented on a quadrant by quadrant basis.

7.5.2.1 Quadrant One : Anterior Central Region

Quadrant one included five elements; 06, 11, 19, 25, 39. Elements 19 and 25 laid closer to the knee centre, whereas 06 and 25 were central, and 39 was along the outer limits of the quadrant. All responses were of a compressive nature, except for the results for the realigned osteotomy case at element 11. No plausible reason can be given for this occurrence.

The relative differences in the three peak outputs for elements 06, 19 and 25 were minimal. This indicated a consistant level of load transmission across the anterior aspect of articular cartilage surface, regardless of the knee alignment. It is worth noting that element 39, situated along the outer boundary of quadrant one, had a larger peak value for the neutral alignment compared to the other two alignment

configurations.

7.5.2.2 Quadrant Two: Posterior Central Region

Quadrant two covered a small area of the posterior cartilage surface that was relatively flat and included only two elements, 05 and 21. Element 05 was located nearer to the joint centre than 21 and had minimum and maximum peaks for the neutral and osteotomy cases, respectively. Element 21, located directly lateral to 05 closer to the outer perimeter of joint, had maximal and minimal peak responses for the neutral and post-osteotomy alignment configurations. The only difference between these two test set-ups was that the overcorrection caused a slight alteration to the actual load applied normal to the articular surface. Other factors need to be considered which would bring about the differences observed in the output patterns. Although an osteotomy realignment generated a shearing component across the articular surface, it may also aid in redistributing the loads across the central region of the compartment. The shearing component was resisted by the ligament and muscular structure surrounding the knee and the surface morphology of the two mating surfaces. The overcorrection helped to shift the load pattern towards the joint centre, which indirectly reduces any overturning moment about the knee centre, thereby improving the joint stability.

7.5.2.3 Quadrant Three: Inner Posterior Region

Quadrant three included those elements under contact during the latter phase of the loading cycle, situated on top of the meniscus near

the posterior attachment site (01, 16, 29, 31, 36). Element 01, located closest to the knee centre, had higher responses for the malaligned case than the neutral set-up; direct compression was present for both alignment conditions. The post-osteotomy realignment generated signal peaks substantially greater than the other two configurations, indicating some bending of the element. Since output voltages from the piezomaterial are much greater when the material is being bent as opposed to being compressed, it is probable that the highest load transfer occurred following the osteotomy tests. Unfortunately, a quantitative comparison was not possible, as no calibration factors pertaining to bending of the elements were obtainable.

Adjacent to 01 was element 29, which recorded compressive peaks throughout the testing, and remained greatest for the neutral case. The large concave bending signals at 16 indicates that adequate contact was present in this region during the three alignment cases. The final two elements (31 and 36) lay along the posterior ridge of the medial compartment and required knee flexion to create contact. Minimal activity occurred across this region and was highest when the osteotomy alignment was simulated.

7.5.2.4 Quadrant Four: Outer Posterior Region

Five elements were contained in quadrant four, 09, 12, 15, 22 and 34. The neutral alignment produced the lowest outputs for all elements, except 09; here the osteotomy configuration had the lowest output response. The two outer most elements, 15 and 34, had similar output patterns but had the greatest responses for the realigned

osteotomy set-up.

If the meniscus translated in a posterior and lateral direction with continuing knee flexion and load, as noted by Bylski-Austrow [21], then the two adjacent surfaces to element 22 no longer remained flat and continuous during the course of the test cycle. This affected the manner in which the element was being placed under load and accounted for the exccessive bending responses recorded during the malaligned tests. Element 12 registered minimal activity, as it came to lay just outside the lateral edge of the contact zone, yet the largest peaks were recorded for the malaligned case.

7.5.2.5 Quadrant Five: Anterior and Outer Peripheral Region

Of the four elements found in the last quadrant, the three elements nearer to the centre of the medial compartment (04, 13, 33) displayed a consistant response pattern of compressive loading, being lowest for the neutral alignment. The low activity level of element 33 illustrated in figure 7.9 was partly due to the short duration over which the element was placed under load, as direct contact was lost with increased knee flexion. The fourth element, 28, was the most extreme outer element of all of the active sensors and registered some form of bending-type responses for the three alignment tests. Elements in this region were often susceptible to bending because of the change in the surface profile of the two mating surfaces, ie. the outer edge of the femoral condyle and the upper, outer ridge of the meniscus.

Table 7.5: Normalized Average Pressure Measurements for Specimen Two

Alignment Configuration		Quadrant One: Active Elements				
		06	11	19	25	39
Normal	NSR	.005/.002	.004/.002	.001/.001	.100/.015	.091/.022
	Load	2024/81	2108/42	2099/42	2019/138	2046/115
Mal.	NSR	.007/.004	.027/.004	.004/.004	.061/.018	.012/.010
	Load	1718/107	1757/59	1761/59	1797/68	1831/72
Ost.	NSR	.004/.003	.251/.046‡	.002/.003	.089/.009	.019/.010
	Load	2241/48	2171/114	2172/116	2090/126	2040/55

		Quadrant Two: Active Elements	
		05	21
Normal	NSR	.002/.001	.023/.018
	Load	2028/79	1998/135
Mal.	NSR	.006/.004	.009/.002
	Load	1562/68	1798/68
Ost.	NSR	.011/.022	.002/.001
	Load	2259/39	2082/117

All responses are for a compressive load, unless otherwise specified.
†: Concave Bending Response and ‡: Convex Bending Response.

NSR: Normalized Signal Response
Load: Externally Applied Load (N)

Table 7.5: Normalized Average Pressure Measurements for Specimen Two

Alignment Configuration		Quadrant Three: Active Elements				
		01	16	29	31	36
Normal	NSR	.029/ .001	4.23/.644†	.090/.014	.005/.004	.004/.002
	Load	1992/39	2098/42	1998/135	2046/102	2013/15
Mal.	NSR	.045/.033	2.29/.620†	.051/.020	.011/.006	.011/.014
	Load	1668/174	1760/59	1808/73	1806/86	1809/78
Ost.	NSR	8.59/1.55‡	2.51/.492†	.023/.016	.053/.028	.024/.016
	Load	2235/52	2172/114	2082/129	2040/55	2046/12
		Quadrant Four: Active Elements				
		09	12	15	22	34
Normal	NSR	.026/.009	.002/.002	.010/.008	.034/016	.059/.015
	Load	1997/44	2099/42	2098/42	1970/136	2033/110
Mal.	NSR	.034/.029	.018/.013	.321/.002‡	.648/.234†	.078/.007
	Load	1672/131	1761/59	1788/60	1827/41	1831/72
Ost.	NSR	.007/.005	.004/.004	.434/.101‡	.072/.025	.083/.009
	Load	2242/49	2170/114	2166/127	2091/127	2073/12
		Quadrant Five: Active Elements				
		04	13	28	33	
Normal	NSR	.048/.003	.037/.005	1.15/.372†	.005/.006	
	Load	2021/37	2098/42	1998/135	2046/101	
Mal.	NSR	.087/.020	.076/.013	.152/.073†	.016/.008	
	Load	1690/140	1761/59	1798/68	1810/78	
Ost.	NSR	.096/.017	.051/031	1.54/.423‡	.019/.011	
	Load	2242/48	2157/123	2081/118	2046/58	

All responses are for a compressive load, unless otherwise specified.
†: Concave Bending Response and ‡: Convex Bending Response.

NSR: Normalized Signal Response
Load: Externally Applied Load (N)

Figure 7.9 a): Normalized signal output patterns: Specimen two - Quadrants one and two.

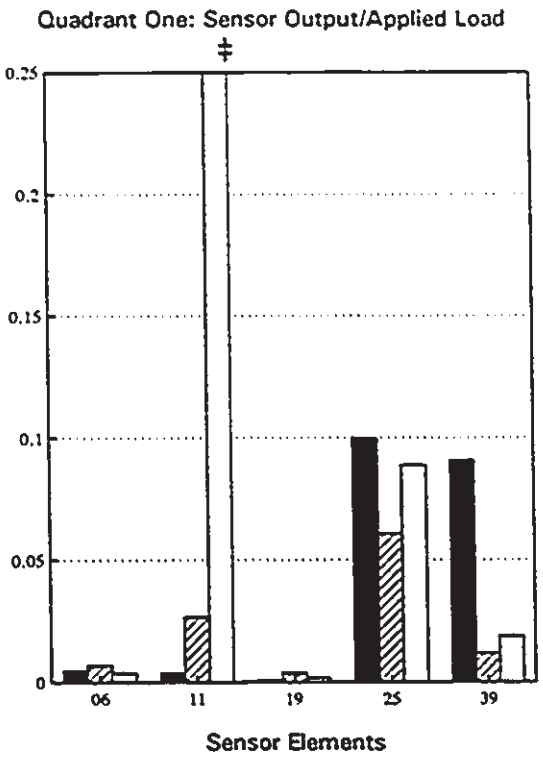

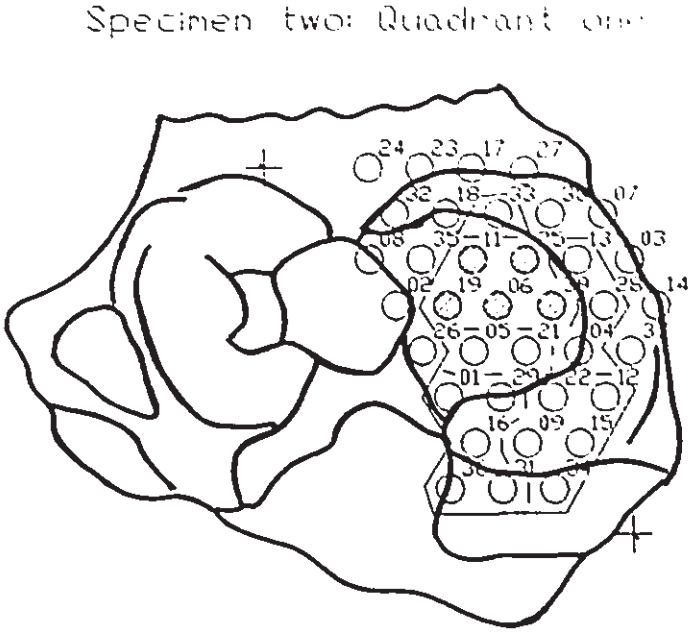

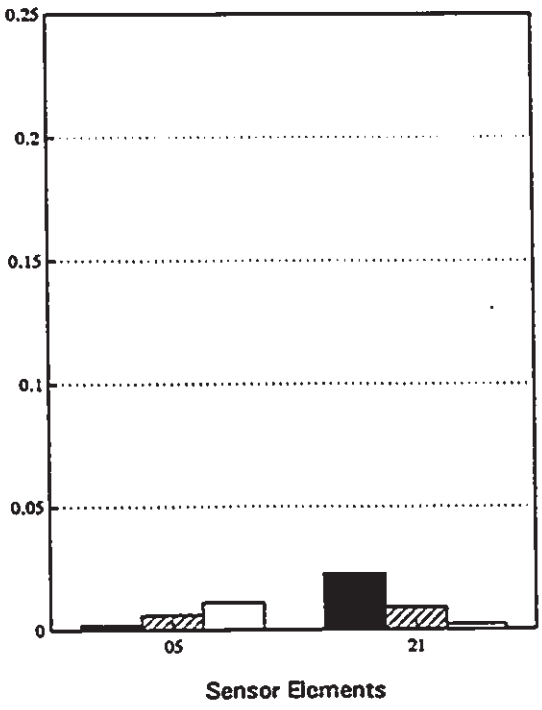

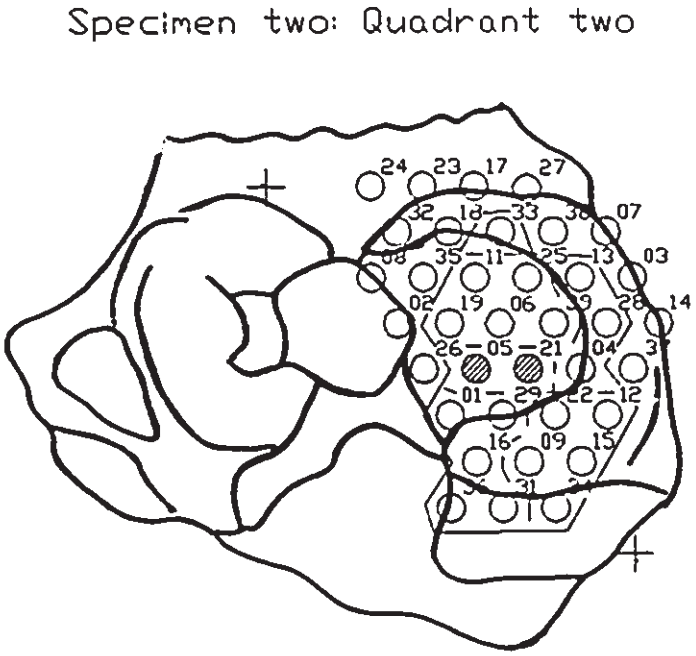

Figure 7.9 b): Normalized signal output patterns: Specimen two - Quadrants three and four.

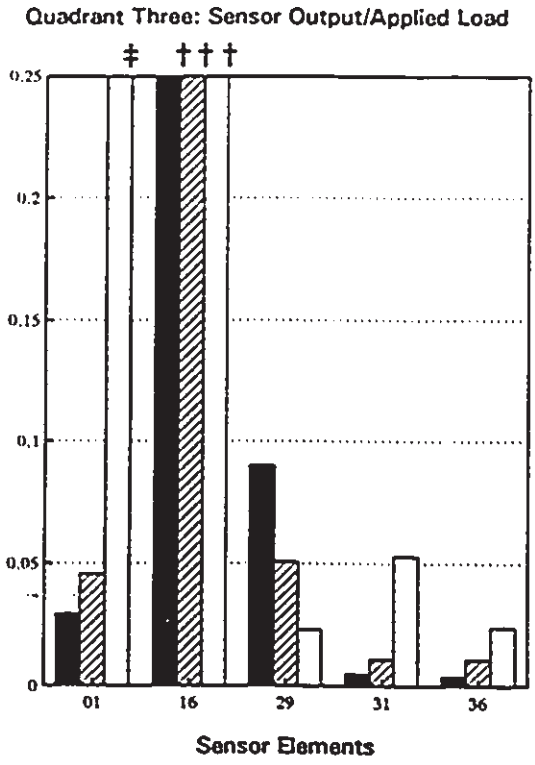

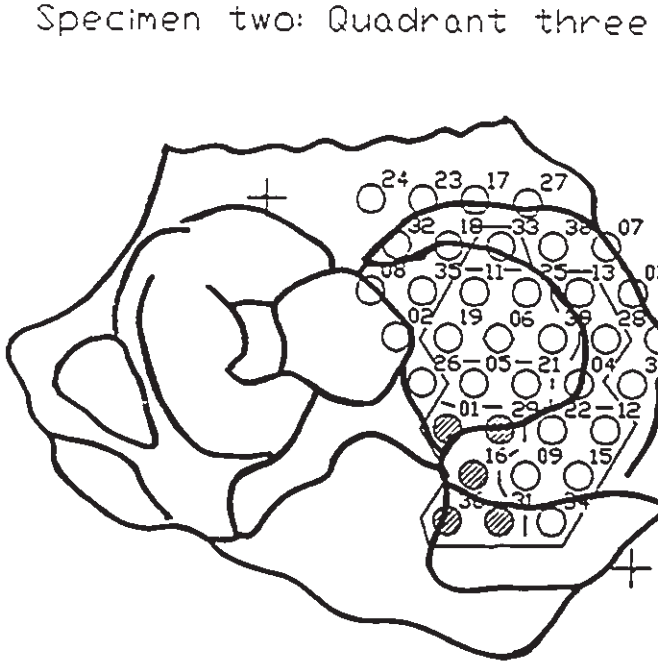

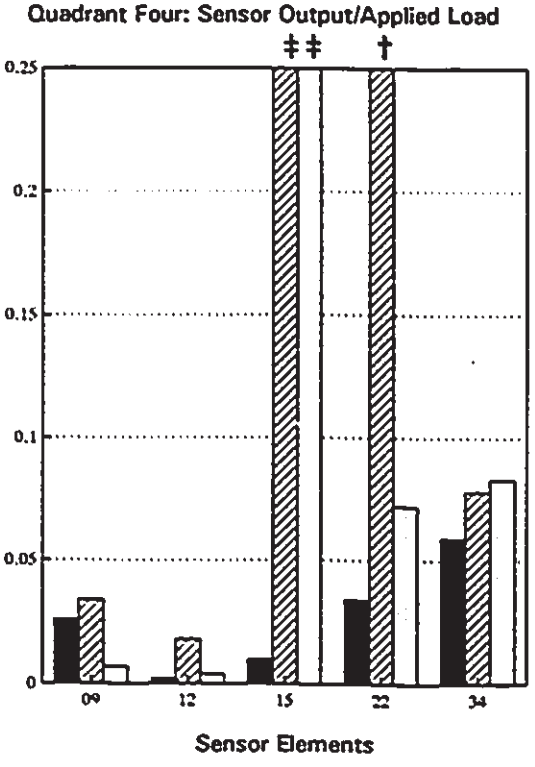

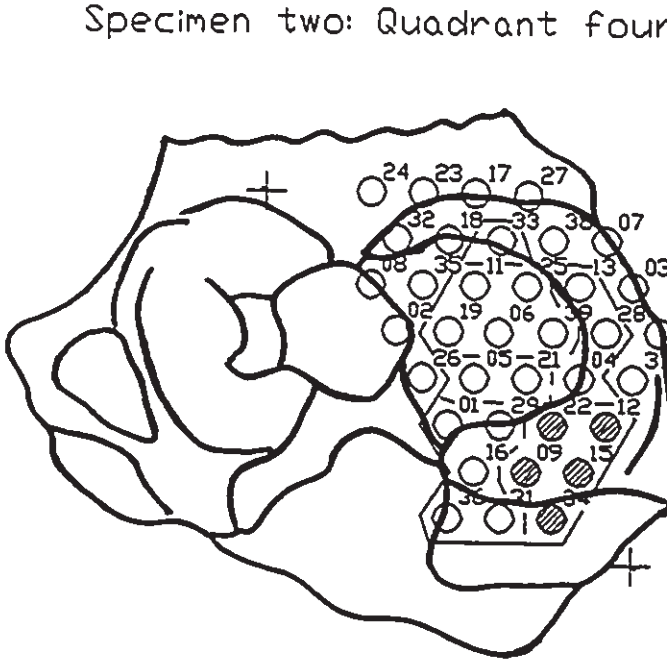

Figure 7.9 c): Normalized signal output patterns: Specimen two - Quadrant five.

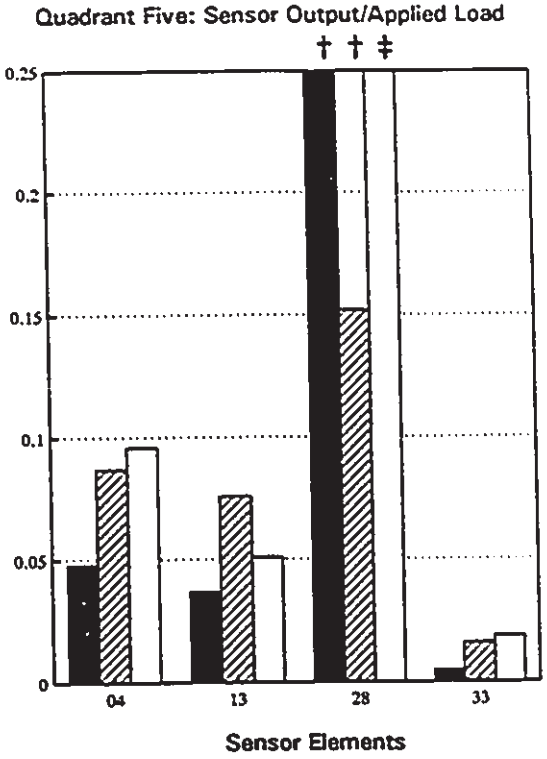

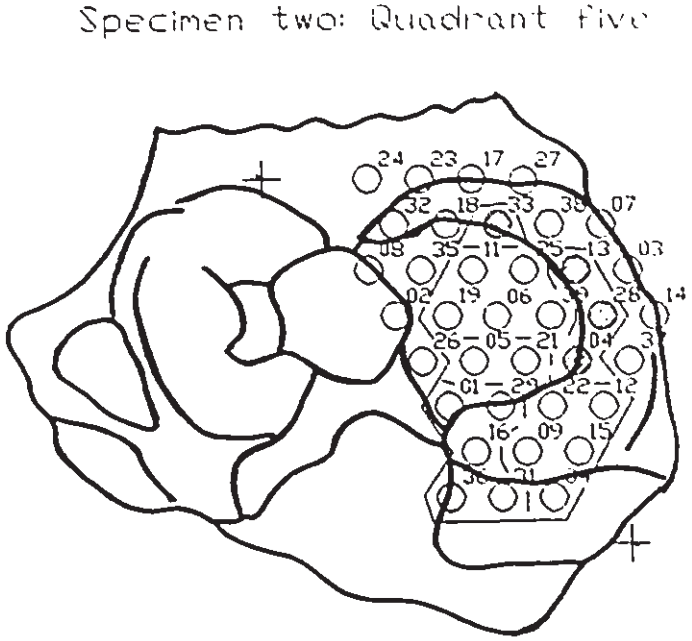

7.6 Test Results for Specimen Three

Specimen three was a right knee joint having a healthy articular cartilage surface. A top view of the proximal tibia was shown in figure 5.29. During the malaligned and post-osteotomy test runs, it was noted that element 19 became inoperable and was thus removed from the analysis. Upon completion of the tests, the malfunction was determined to be due to a break in the lead wire tracings. No other mechanical problems were encountered with the measurement pad during the remaining tests on specimen three.

7.6.1 Active Contact Area Zones

The final placement of the measurement pad on the medial compartment is illustrated in figure 7.10. Twenty - two elements were processed; the assignment of elements to a specific quadrant is provided in table 7.6. The three zones of contact area are illustrated in figure 7.11, corresponding to the total active area, as well as the area under contact at 0° and 20° knee flexion. The total active area measured 10.32 cm^2 and reduced to 9.09 cm^2 at complete extension. Knee flexion resulted in a notable reduction, as the contact area measured only 6.73 cm^2. The loss of contact across the anterior region was believed to be due to a loose anterior attachment of the medial meniscus. This allowed the meniscus to be displaced forward relative to the tibial plateau surface, which in turn, exposed more articular cartilage sooner, as knee flexion progressed.

Table 7.6: Assignment of Active Elements by Quadrant Location for Specimen Three

Quadrant Number	Channel Identification*
Q1	06 11 35 (19)
Q2	01 05 21 26 29
Q3	16 31 36
Q4	04 09 15 22 34
Q5	13 18 25 33 38 39

* Elements encountering a malfunction are enclosed in brackets.

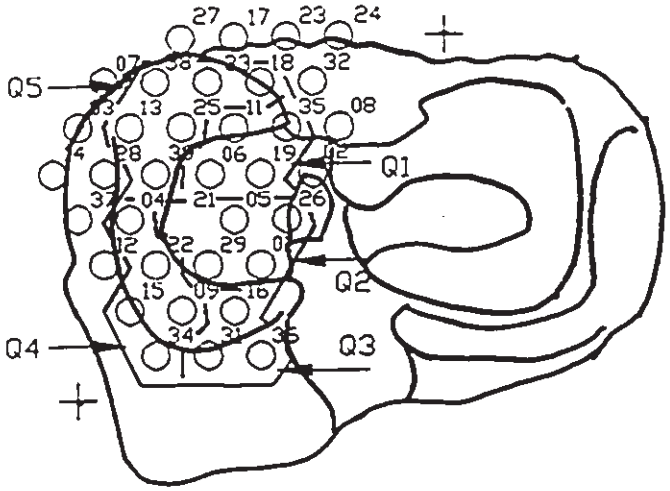

Figure 7.10: Location of measurement pad on medial compartment of specimen three. Quadrants separated by dashed lines.

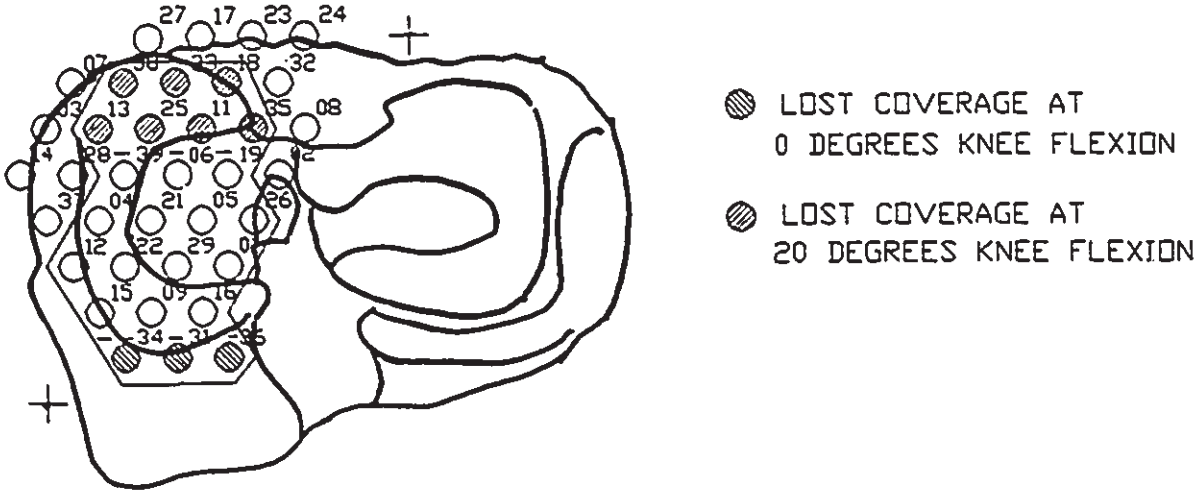

Figure 7.11: Area coverage of medial compartment of specimen three.

7.6.2 Normalized Contact Pressure Patterns

The normalized peak values of each active element are shown in table 7.7 and include the means and standard deviations averaged over five successive trial runs. Peak responses are also charted in figure 7.12, illustrating variations within each quadrant. The effect of the alignment changes on load transmission at local points of contact will be discussed next, beginning with elements in the central region.

7.6.2.1 Quadrant One: Anterior Central Region

Four elements (06, 11, 19 and 35) were positioned across the anterior region of the cartilage surface. As mentioned previously, element 19 was removed due to mechanical problems. Figure 7.10 shows elements 11 and 35 were positioned in the vicinity of the cartilage-meniscus interface. Element 35 was also located along the inner edge of the intercondylar eminence.

A consistant level of compressive contact was present at all three elements. Minimal differences were noted in the output patterns of elements 06 and 35. However, a notable increase in the output peaks of element 11 resulted for the two realigned tests. Regarding the malaligned test set - up, the increased load at 11 corresponded to reduced loads at the elements directly anterior to it (18 and 33 in quadrant five). It is possible that the malalignment delayed the load application across the anterior region. Similar findings were observed amongst the other knee specimens.

7.6.2.2 Quadrant Two: Posterior Central Region

All elements in quadrant two were active and under direct compression during the neutral knee alignment tests, except element 26. It was positioned high up along the tibial spine near the attachment site of the anterior cruciate ligament. The larger peak values for 26 depict element bending representative of a convex downward profile. The post-osteotomy tests produced the greatest signal peaks, slightly larger than that for the malaligned case, but notably larger than the normal alignment situation. The trend of larger bending signals from elements located along the base of the intercondylar tubercle was present with all of the knee specimens. Overall, this supported the concept of an inward shift in load transfer towards the joint centre following osteomtomy surgery.

Contact pressure levels at elements 01 and 05 were consistant for all three alignments, except for an increase in the peak output at 05 for the neutral orientation. Elements 21 and 29 came to rest near the cartilage - meniscus interface, which probably contributed to the occurrence of element bending during the realigned tests. This was considered a limitation of the measurement pad, as it was unable to accommodate any relative translation of the meniscus.

7.6.2.3 Quadrant Three : Inner Posterior Region

All three elements in quadrant three laid along the top surface of the meniscus. Elements 31 and 36 required knee flexion before contact was established. In addition, the extreme posterior positioning of the elements contributed to the bending responses at elements 31 and

36. This would be enhanced if the meniscus bulged outward and upward when placed under load.

The third and final element in quadrant three was 16, and was shown in figure 7.10 to lay just inside the posterior fringe of the meniscus. All output signals were of a concave bending nature, indicative of the action of the femoral condyle rolling over the element and pushing it into the meniscus.

7.6.2.4 Quadrant Four: Outer Posterior Region

Quadrant four includes those elements located along the posterior peripheral region of the medial compartment: 04, 09, 15, 22 and 34. Elements along the outer lateral posterior edge (04, 15, 34) encountered slight bending. However, the low magnitudes support minimal contact across this zone. Only element 15 generated a significant bending response for the malaligned case. The two remaining elements (09 and 22) laid directly on top of the meniscus. Load transmission was consistant at 09 for all alignment set-ups, while minimal pressure levels were registered at element 22 following the knee realignments.

7.6.2.5 Quadrant Five : Outer Anterior Region

The increased surface area of specimen three contributed to more active elements across the anterior region. The increased surface area was lost, however, as soon as knee flexion began. Here, a total of six elements were monitored and include 13, 18, 25, 33, 38 and 39. Elements 18, 33 and 38 laid across the anterior edge of the meniscus, while the remaining three elements laid adjacent to them but more posterior. All

of these outer elements had a reduction in the contact pressure for the 15° varus malalignment, while the two inner elements registered an increased in pressure.

The post-osteotomy alignment resulted in either minimal change or a reduction in the loading across this region, except at elements 18 and 39. The increase at 18 was partly due to the shift in the applied load towards the joint centre.

Table 7.7: Normalized Average Pressure Measurements for Specimen Three

Alignment Configuration		Quadrant One: Active Elements		
		06	11	35
Normal	NSR	.006/.001	.023/.001	.020/.020
	Load	1419/98	1445/133	1401/133
Mal.	NSR	.002/.002	.128/.017	.013/.002
	Load	1535/418	1328/27	1339/45
Ost.	NSR	.006/.007	.134/.043	.006/.002
	Load	876/55	894/71	997/35

		Quadrant Two: Active Elements				
		01	05	21	26	29
Normal	NSR	.047/.007	.096/.011	.032/.010	.763/.040‡	.051/.016
	Load	1423/98	1419/98	1343/53	1328/62	1343/53
Mal.	NSR	.051/.023	.024/.016	.197/.051	3.14/.519‡	.467/.117†
	Load	1663/463	1539/418	1272/27	1245/50	1245/49
Ost.	NSR	.055/.010	.023/.016	.540/.091†	4.42/.778‡	.709/.108†
	Load	872/62	845/53	1054/36	1054/3	1054/35

		Quadrant Three: Active Elements		
		16	31	36
Normal	NSR	.531/.097†	.581/.159‡	.014/.016
	Load	1497/127	1361/147	1361/147
Mal.	NSR	.351/.075†	2.16/.251‡	.465/.024‡
	Load	1303/13	1339/45	1339/45
Ost.	NSR	.168/.031†	5.54/.933‡	.065/.038
	Load	862/89	996/36	987/31

All responses are for a compressive load, unless otherwise specified.
†: Concave Bending Response and ‡: Convex Bending Response.

NSR: Normalized Signal Response
Load: Externally Applied Load (N)

Table 7.7: Normalized Average Pressure Measurements for Specimen Three

Alignment Configuration		Quadrant Four: Active Elements				
		04	09	15	22	34
Normal	NSR	.024/.008‡	.042/.003	.310/.152‡	.061/.016	.005/.002‡
	Load	1454/88	1423/98	1540/119	1357/53	1360/145
Mal.	NSR	.194/.020‡	.049/.019	6.40/1.63†	.004/.005	.452/.066‡
	Load	1337/54	1663/462	1315/29	1272/63	1339/43
Ost.	NSR	.059/.027‡	.052/.026	.018/.003‡	.002/.002	1.20/.147‡
	Load	923/28	872/62	873/83	2144/71	991/37
		Quadrant Five: Active Elements				
		13	18	25	33	38
Normal	NSR	.009/.007	.217/.029	.090/.018	.038/.011	.147/.008
	Load	1485/131	1437/124	1334/53	1361/147	1210/24
Mal.	NSR	.001/.000	.188/.050	2.11/.308‡	.002/.003	.033/.006
	Load	1317/28	1317/31	1272/64	1339/45	1339/45
Ost.	NSR	.004/.003	.827/.073†	.004/.003	.065/.014	.028/.010
	Load	849/90	850/89	1054/34	996/35	983/27
		Quadrant Five: Active Elements				
		39				
Normal	NSR	.008/.003				
	Load	1361/147				
Mal.	NSR	.139/.025				
	Load	1339/45				
Ost.	NSR	.353/.039†				
	Load	996/35				

All responses are for a compressive load, unless otherwise specified.
†: Concave Bending Response and ‡: Convex Bending Response.

NSR: Normalized Signal Response
Load: Externally Applied Load (N)

Figure 7.12 a): Normalized signal output patterns: Specimen three - Quadrants one and two.

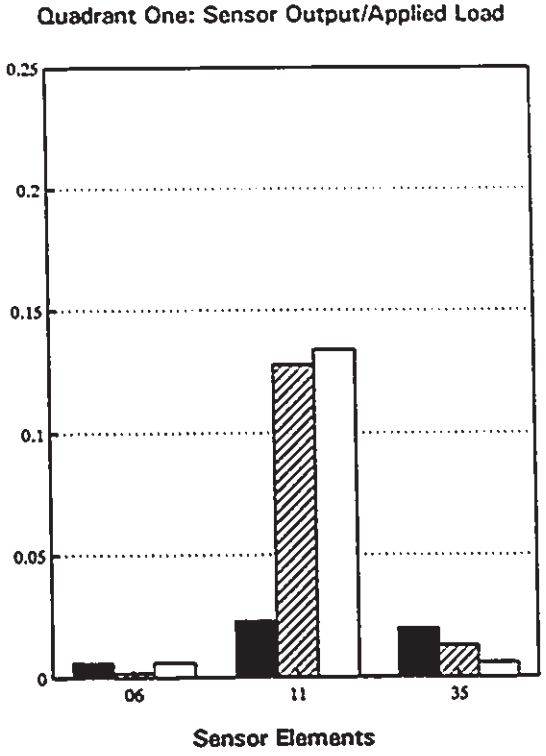

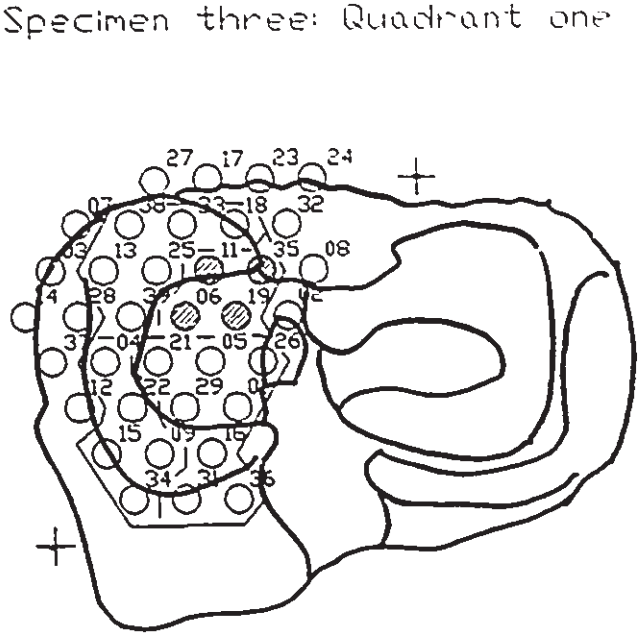

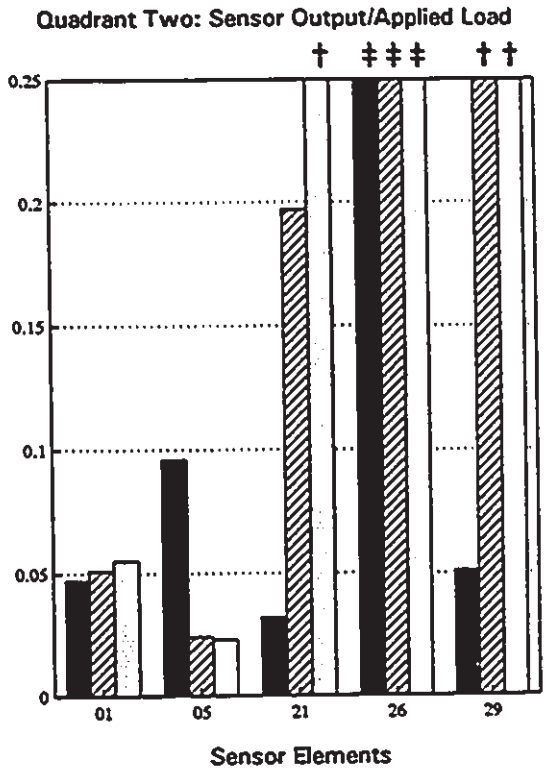

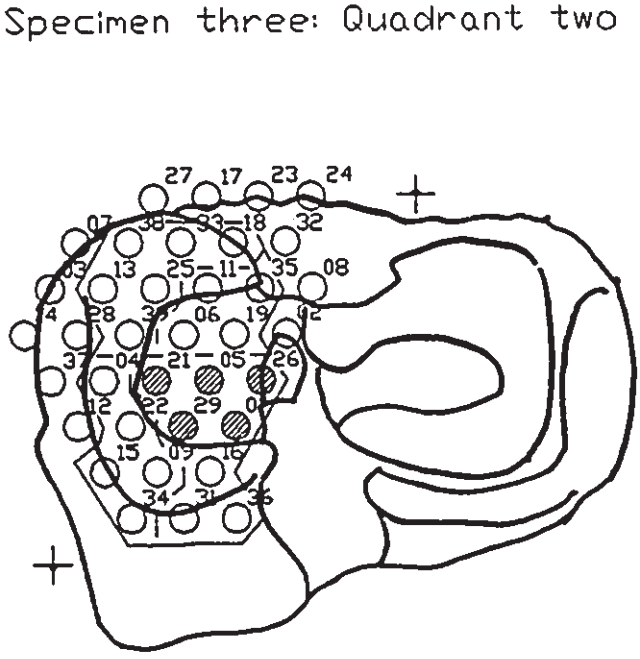

Figure 7.12 b): Normalized signal output patterns: Specimen three - Quadrants three and four.

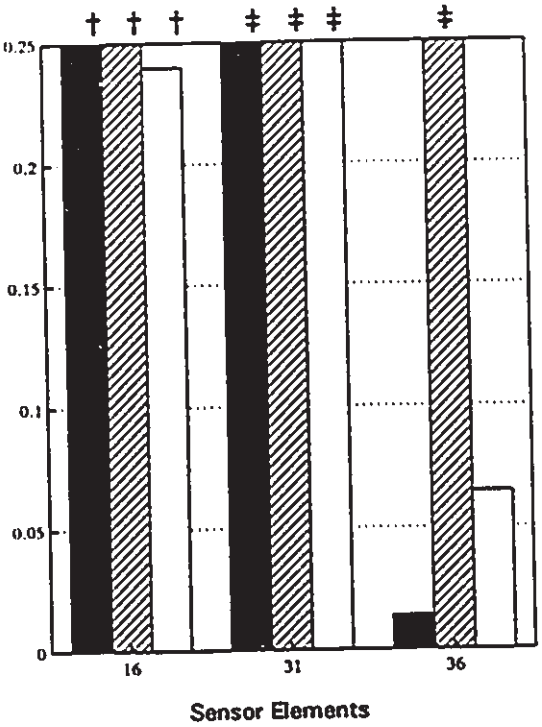

Specimen three: Quadrant three

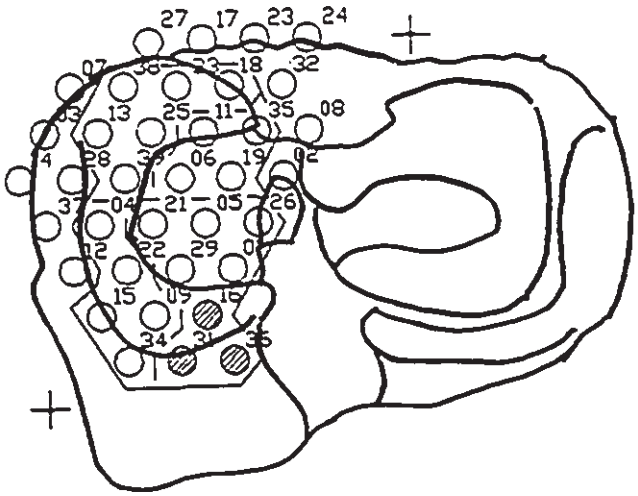

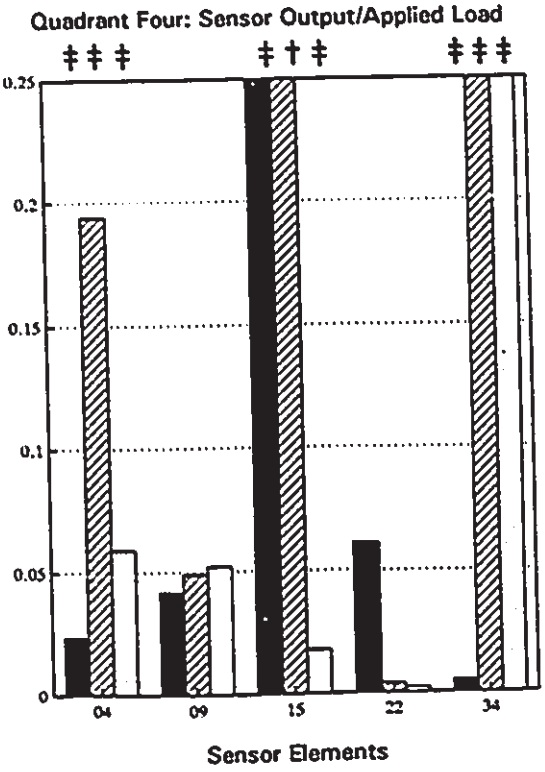

Specimen three: Quadrant four

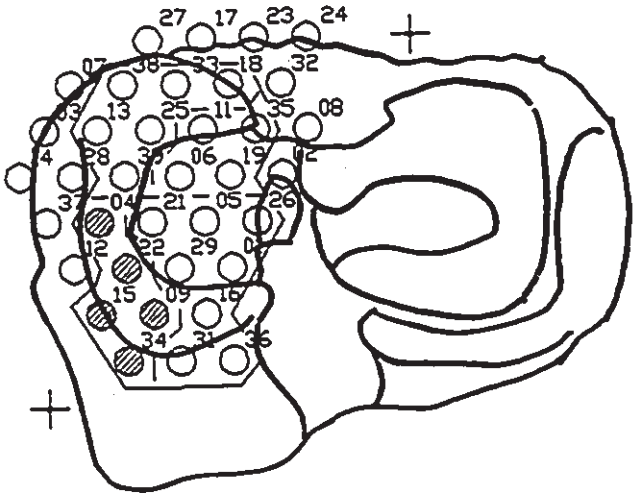

Figure 7.12 c): Normalized signal output patterns: Specimen three - Quadrant five.

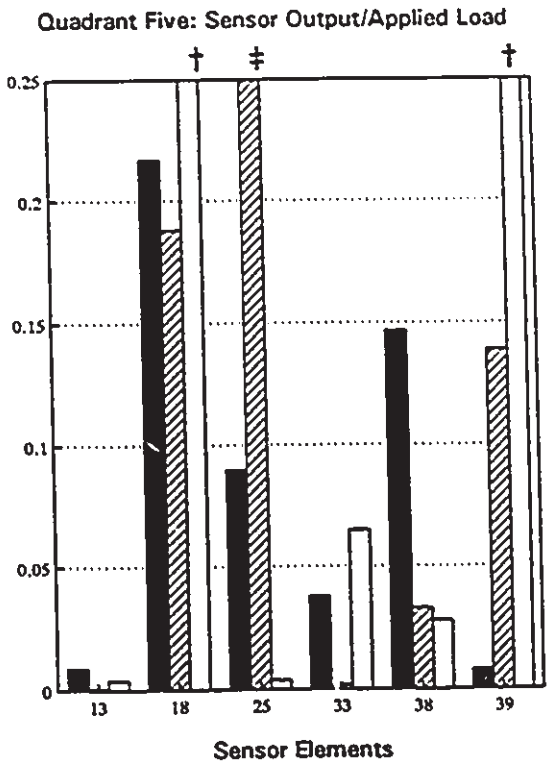

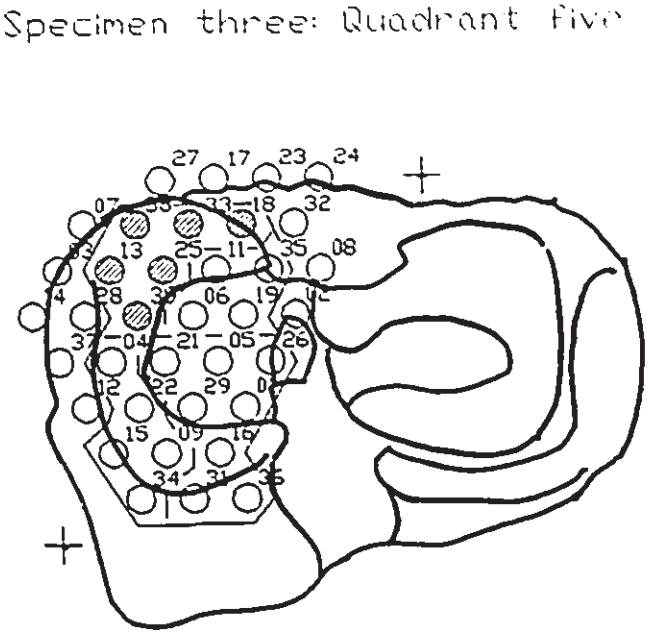

7.7 Tests Results for Specimen Four

Specimen four was the mate to specimen three, and was one of the larger knee joints included in this study. No visible signs of joint pathology were observed across the articular surface of the tibial and femoral condyles. A view of the tibial plateau surface was shown in figure 5.30. A loose attachment of the anterior portion of the meniscus was present, and permitted greater displacement of the meniscus relative to the tibial surface. No mechanical malfunctions were encountered with the measurement pad during the testing of specimen four.

7.7.1 Active Contact Area Zones

The larger plateau surface area generated more active elements; figure 7.13 shows the final arrangement of the measurement pad on the medial compartment. The assignment of elements to specific quadrants is listed out in table 7.8. All twenty - one elements remained active over the test cycle. The total contact area enclosed by the elements measured 9.0 cm^2. No change was recorded between the total area and that measured at complete knee extension. However, knee flexion reduced the contact area to 7.28 cm^2. This can partially be attributed to the loose anterior meniscal attachment. The affected zone is illustrated in figure 7.14. This limited the amount of radial tension produced across the anterior meniscus. As a result, the reduced tension no longer maintained contact between the meniscus and the femoral condyle during knee flexion.

Table 7.8: Assignment of Active Elements by Quadrant Location for Specimen Four

Quadrant Number	Channel Identification
Q1	11 18 25 33 35
Q2	05 06 19 21 26
Q3	01 16 29
Q4	04 09 15 22 28
Q5	13 38 39

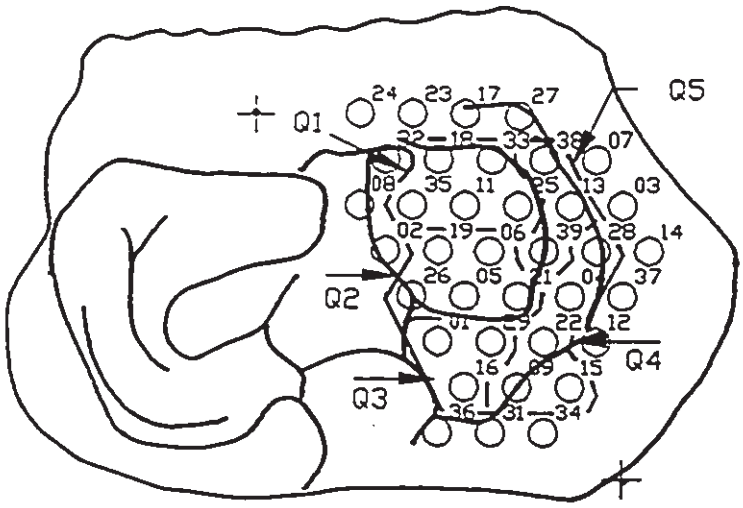

Figure 7.13: Location of measurement pad on medial compartment of specimen four. Quadrants separated by dashed lines.

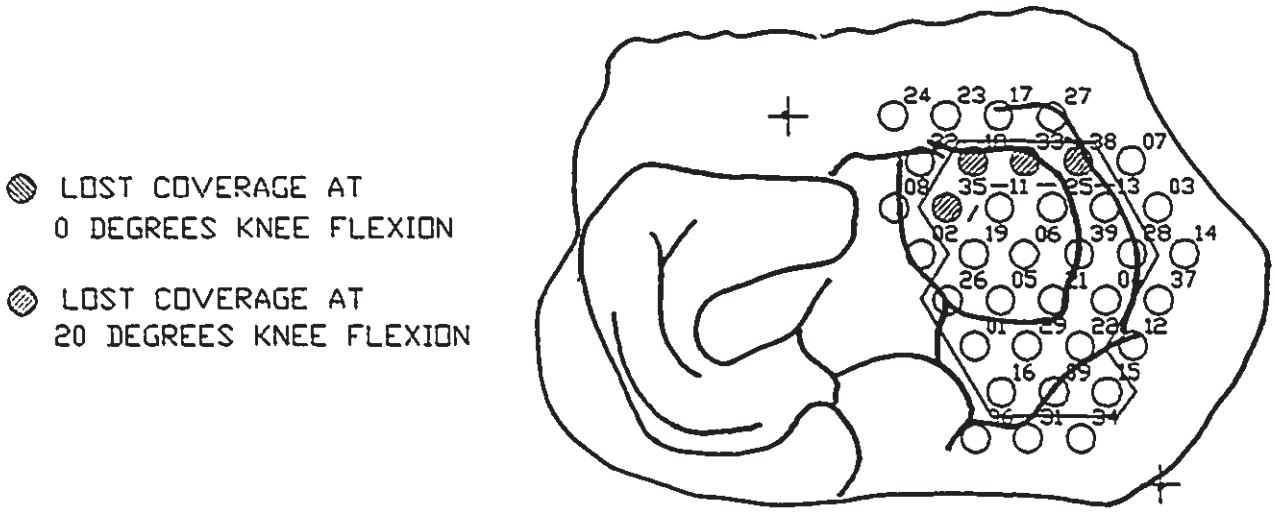

Figure 7.14: Area coverage of medial compartment of specimen four.

7.7.2 Normalized Contact Pressure Patterns

The normalized pressure measurements recorded at local points across the medial plateau are listed in table 7.9 for the three different alignment configurations. The relative differences in the signal peaks are presented in chart form in figure 7.15. As with all knees tested, five successive test runs were recorded to determine average signal responses of all active elements, and are discussed by quadrant allocation.

7.7.2.1 Quadrant One: Anterior Central Region

The loose anterior attachment of the meniscus allowed more articular cartilage to be exposed. As a result, elements 18 and 33 were assigned to quadrant one rather than five. They are shown in figure 7.13 to lay along the anterior section of the cartilage surface near the meniscus. The proximity of the elements to the cartilage - meniscus junction contributed to the bending of the elements. Elements 11, 25 and 35, directly posterior to elements 18 and 33, aligned with each other in the medial - lateral direction.

Signal peaks characteristic of compressive loading were recorded at four of the five elements in quadrant one; only 35 registered bending signals. The increased curvature of the articular surface at the base of intercondylar eminence promoted the bending response, yet the low magnitudes of the normalized pressure readings suggest that contact was present, but was minimal.

On average, the varus malalignment increased the load transmission, whereas the post-osteotomy realignment reduced the peak

pressures. Figure 7.15 shows the relative differences in the local pressure measurements for the two realignment cases compared to a neutrally aligned knee joint.

7.7.2.2 Quadrant Two: Posterior Central Region

A consistant pattern of direct compression occurred at elements 05, 06, 19, 21 and 26, dispersed across the posterior half of the cartilage surface. All elements were active with the knee aligned neutrally, while realigning the knee to 15° varus caused minimal changes to the central elements. An increase in the peak response occurred at the inner most element, 26, while a decrease in the load transfer occurred at the postlateral element, 21.

Having the knee realigned to an overcorrected orientation resulted in noticeable increases at the inner elements (05, 19, 26) and slight variations at the remaining two elements. These findings support the concept of an inward shift in the contact load following a high tibial osteotomy.

7.7.2.3 Quadrant Three: Inner Posterior Region

Quadrant three includes those elements located along the most inner posterior region of the medial compartment, (01, 16, 36). Compressive loading was prevalent for the neutral alignment tests, except at 16, where the element was placed under a bending mode having a concave profile. Surprisingly, the peak values decreased at elements 01 and 29 for the malaligned case, while remaining constant at 16. The loss of load transmission in the posterior region was believed to have

been compensated for by the increase in loading on the central elements in quadrant two. Also, the realigned post-osteotomy brought about a notable decrease in the degree of load transmission in this region.

7.7.2.4 Quadrant Four: Outer Posterior Region

A total of five elements (04, 09, 15, 22, 28) were assigned to quadrant four, all of which were placed under direct compression for the three tested alignment configurations. Having the knee offset by 15° varus increased loading along the inner ridge of the meniscus, ie. elements 09, 22 and 28. At elements 04 and 15 the force reduced. As observed at element 16 in quadrant three, the post-osteotomy alignment reduced the loading at the more posterior and lateral elements ,15 and 28. The remaining elements either had an increase in the contact pressure, or remained unchanged.

7.7.2.5 Quadrant Five: Outer Anterior Region

Three elements were located along the outer periphery of the medial compartment on top of the meniscus (13, 38 and 39), and aligned with each other in the A-P direction. Figure 7.15 shows that compressive loading was present throughout the region, regardless of the knee alignment. Contact was essentially lost at element 38 as knee flexion progressed, yet some amount of activity was registered.

Having the knee set to 15° varus resulted in a decrease in load transfer at the anterior elements (13, 38), and increased at 39, compared to the neutral alignment results. A similar unloading had occurred at elements 13 and 38 following the osteotomy realignment.

Reduced loading across the anterior elements, with a posterior shift in the contact zone, was also observed in the other knee specimens.

Table 7.9: Normalized Average Pressure Measurements for Specimen Four

Alignment Configuration		Quadrant One: Active Elements				
		11	18	25	33	35
Normal	NSR	.016/.001	.113/.014	.033/.091	.037/.014	.319/.022†
	Load	1788/138	1752/129	1583/72	1655/55	1646/45
Mal.	NSR	.101/.014	.150/.051	.206/.054	.088/.010	.172/.029†
	Load	1690/62	1679/56	1792/90	1779/50	1731/71
Dome	NSR	.011/.001	.058/.020	.073/.007	.011/.003	.101/.022†
	Load	1268/147	1345/45	1210/129	1285/93	1331/95

		Quadrant Two: Active Elements				
	05	06	19	21	26	
Normal	NSR	.022/.003	.023/.007	.054/.019	.090/./018	.056/.005
	Load	1727/94	1727/94	1815/142	1690/49	1651/49
Mal.	NSR	.013/.001	.009/.001	.060/.019	.007/.002	.08[illegible]/.027
	Load	1783/42	1770/45	1766/84	1752/107	1752/107
Dome	NSR	.087/.015	.020/.003	.183/.049	.100/.028	.130/.018
	Load	1254/187	1232/205	1267/142	1174/120	1210/129

All responses are for a compressive load, unless otherwise specified.
†: Concave Bending Response and ‡: Convex Bending Response.

NSR: Normalized Signal Response
Load: Externally Applied Load (N)

Table 7.9: Normalized Average Pressure Measurements for Specimen Four

Alignment Configuration		Quadrant Three: Active Elements		
		01	16	29
Normal	NSR	.120/.070	1.02/.129†	.180/.011
	Load	1787/22	1824/133	1650/49
Mal.	NSR	.009/.004	1.10/.280†	.026/.001
	Load	1770/45	1734/90	1770/102
Dome	NSR	.005/.003	.063/.046†	.044/.006
	load	1290/138	1267/130	1210/129

		Quadrant Four: Active Elements				
		04	09	15	22	28
Normal	NSR	.022/.006	.048/.002	.079/.027	.001/.001	.124/.020
	Load	1726/93	1766/49	1779/142	1650/49	1650/49
Mal.	NSR	.002/.001	.096/.007	.021/.003	.019/.008	.138/.043
	Load	1770/45	1770/45	1688/62	1757/98	1792/89
Dome	NSR	.030/.004	.068/.011	.043/.006	.034/.014	.062/.019
	Load	1254/187	1255/187	1263/160	1170/116	1210.129

		Quadrant Five: Active Elements		
		13	38	39
Normal	NSR	.066/.018	.031/.002	.024/.006
	Load	1788/133	1649/45	1650/49
Mal.	NSR	.021/.007	.004/.003	.056/.008
	Load	1732/85	1726/67	1757/31
Dome	NSR	.016/.003	.017/.004	.027/.003
	Load	1259/142	1312/84	1281/93

All responses are for a compressive load, unless otherwise specified.
†: Concave Bending Response and ‡: Convex Bending Response.

NSR: Normalized Signal Response
Load: Externally Applied Load (N)

Figure 7.15 a): Normalized signal output patterns: Specimen four - Quadrants one and two.

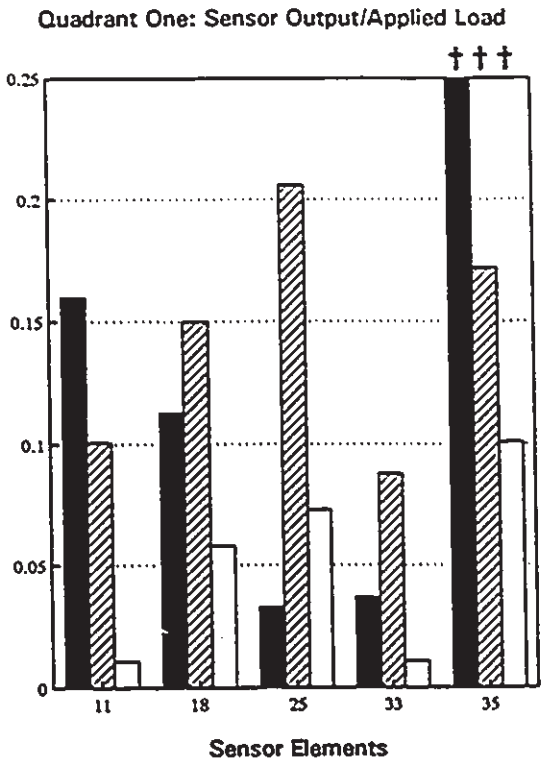

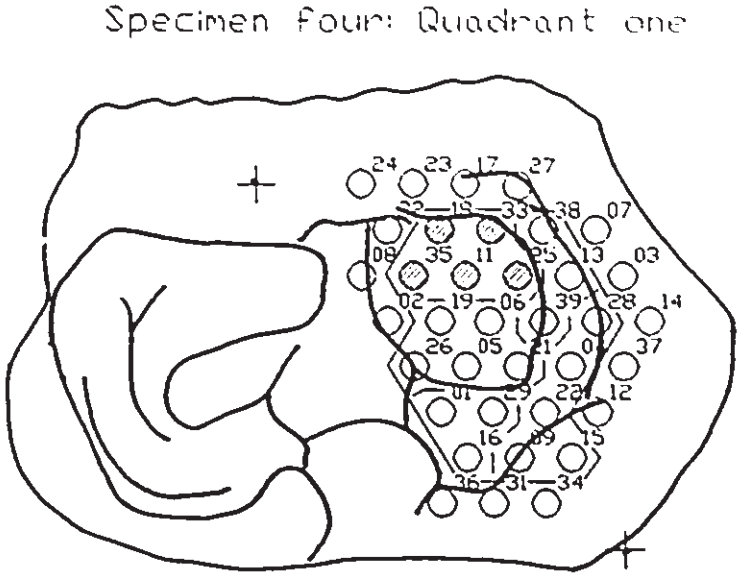

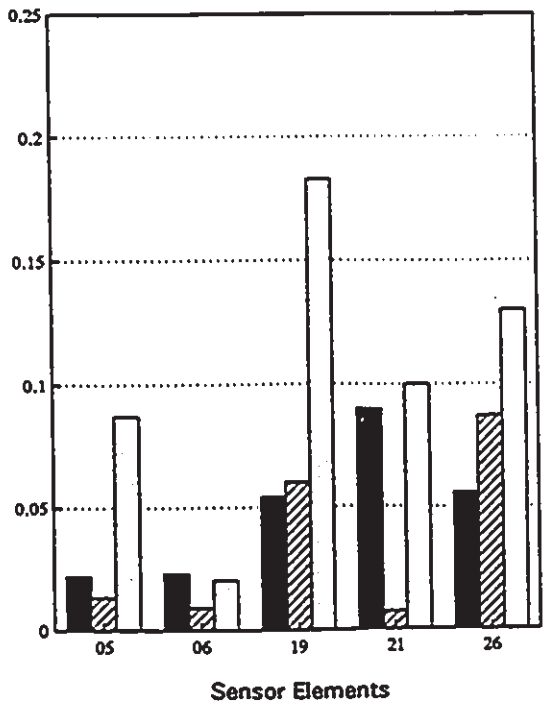

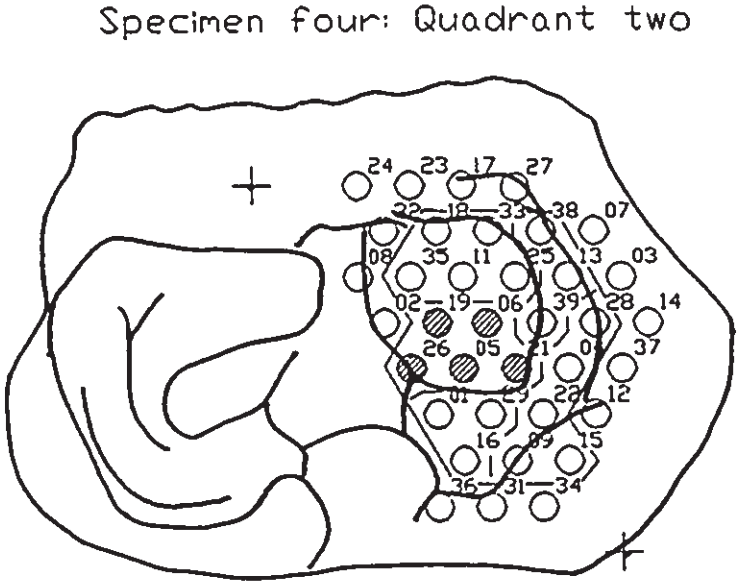

Figure 7.15 b): Normalized signal output patterns: Specimen four - Quadrants three and four.

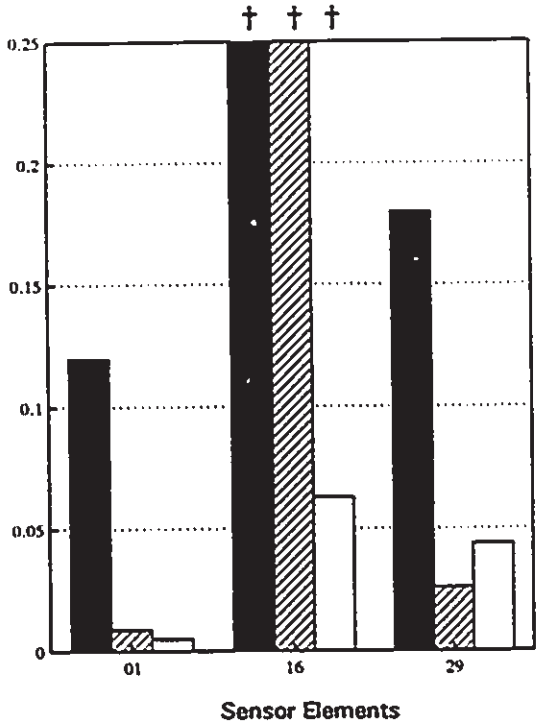

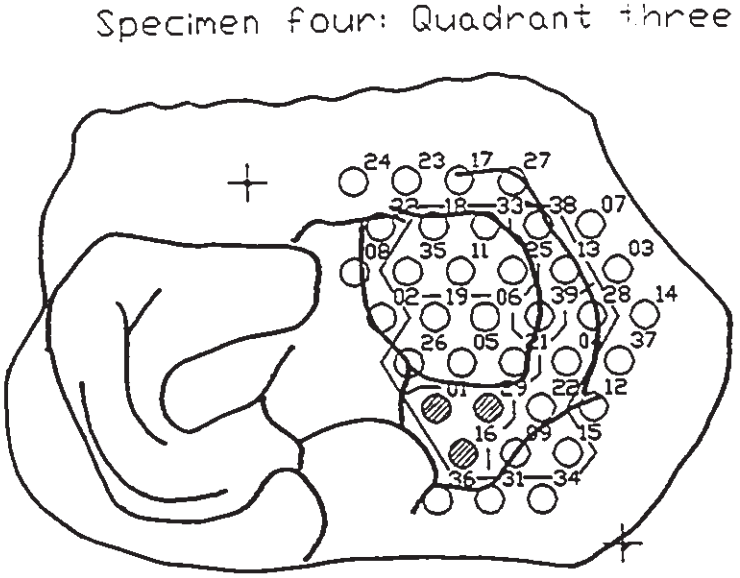

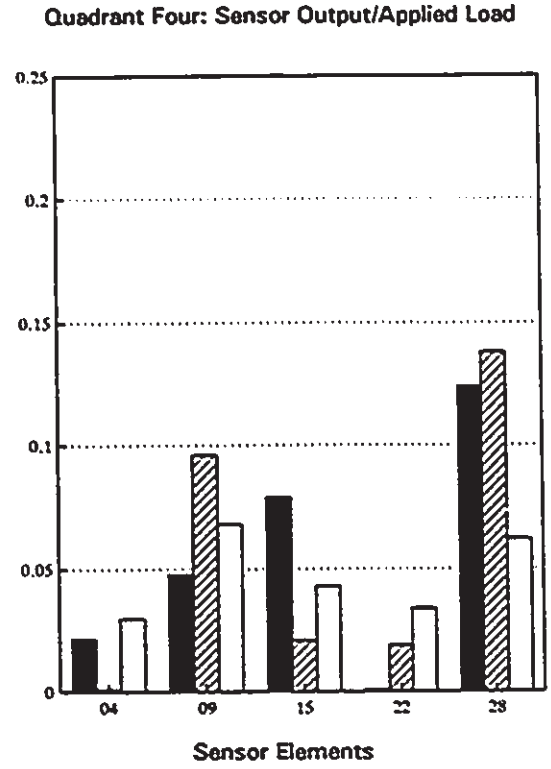

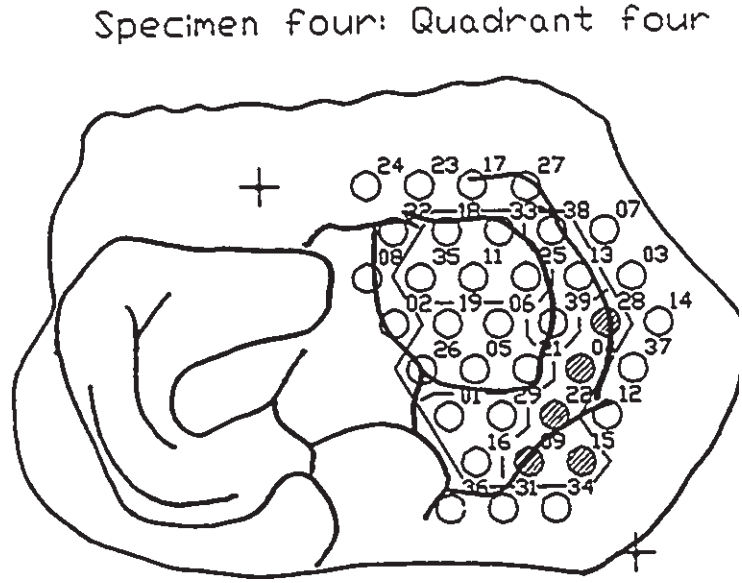

Figure 7.15 c): Normalized signal output patterns: Specimen four - Quadrant five.

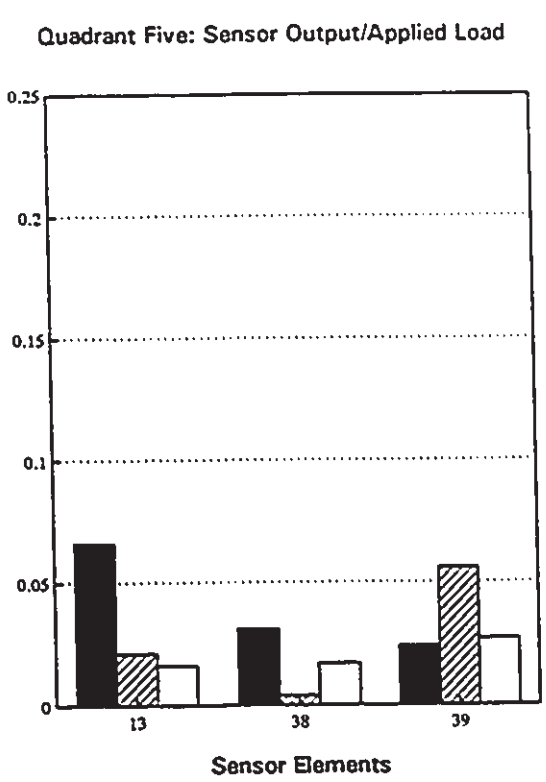

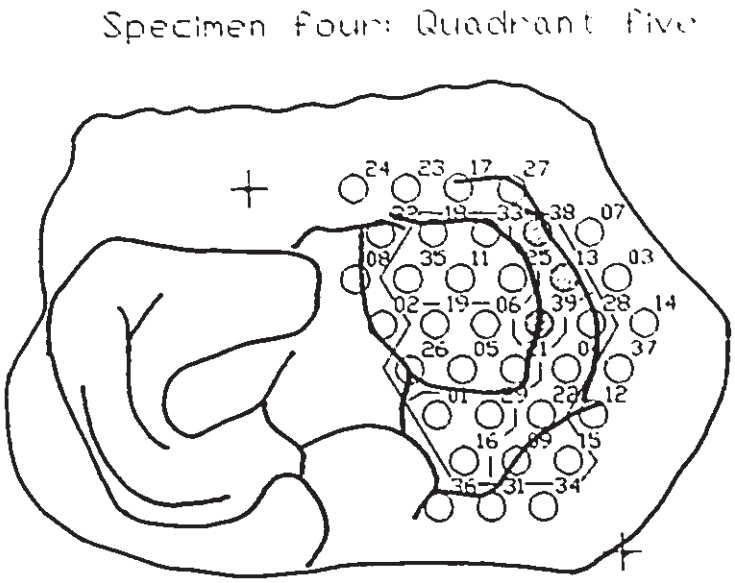

7.8 Test Results for Specimen Five

Specimen five showed no visible signs of cartilage degeneration on the tibial surface, but the medial femoral condyle had a grade II level of arthritis on the lateral aspect measuring 2 cm by 0.5 cm. Slight contact occurred over the affected region during weight bearing but was lost with increased knee flexion.

7.8.1 Active Contact Area Zones

A loose anterior attachment of the mensicus caused more of the tibial cartilage surface to make direct contact with femoral condyle. Specimen five was one of the smallest knees included in this study and had fewer active elements than any other knee specimen, except for its left mate. The articular surface of the joint was shown in figure 5.31; the final arrangement and location of the measurement pad traced on the tibial plateau surface is displayed in figure 7.16. Only nineteen elements were active for the three alignment tests and were designated to specific quadrants, as detailed in table 7.10. All elements remained active and under contact during the realigned tests. The total active contact zone is outlined in figure 7.17 and measured 8.23 cm^2. This was the smallest area measured amongst the knee specimens tested.

Table 7.10: Assignment of Active Elements by Quadrant Location for Specimen Five

Quadrant Number	Channel Identification
Q1	05 06 19 21 26
Q2	01 29
Q3	16 31 36
Q4	09 12 15 22 34
Q5	04 11 25 39

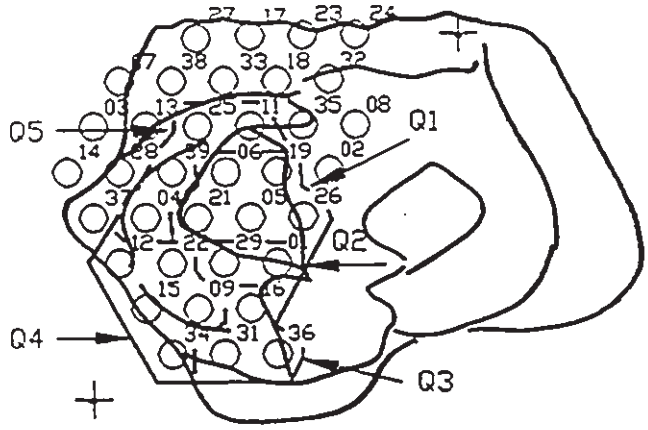

Figure 7.16: Location of measurement pad on medial compartment of specimen five. Quadrants separated by dashed lines.

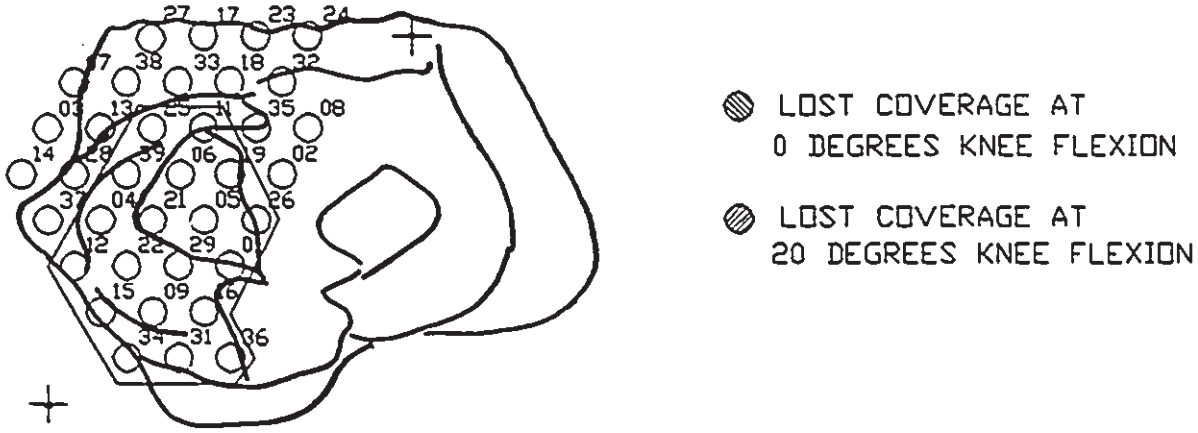

Figure 7.17: Area coverage of medial compartment of specimen five.

7.8.2 Normalized Contact Pressure Patterns

The normalized peak values for each element are tabulated in table 7.11 and plotted in figure 7.18 A higher incidence of element bending was observed at the peripheral elements and was due to the reduced surface area and the narrow width of the medial femoral condyle. As a result, more elements came to lay near or on the meniscal - cartilage interface, with less on the central cartilage region.

7.8.2.1 Quadrant One: Anterior Central Region

The loose anterior attachment of the medial meniscus lead to elements 06 and 19 being assigned to quadrant one rather than five. The next three immediately posterior elements on the measurement pad (05, 21 and 26) covered the mid-portion of the central cartilage surface, and were aligned with each other in the medial - lateral direction. Element 26, positioned at the extreme interior aspect of the compartment, was affected by the increased curvature of the tibial surface, as it folded against the anterior cruciate ligament.

Neutral alignment of the knee resulted in minimal load transfer at the central elements 05 and 06, while elements 19 and 21 were under direct compression. Altering the alignment of the joint caused minimal variations at elements 05, 06 and 19, while the most laterally located element, 21, registered increased peak values for both the malaligned and post-osteotomy alignment cases. The data reveals that contact was maintained throughout this region, regardless of the knee alignment.

7.8.2.2 Quadrant Two: Posterior Central Region

The posterior portion of the medial meniscus covered slighty more articular cartilage than had been observed with the other knee specimens, leaving only two elements assigned to quadrant two; 01 and 29. Element 01, located posterior to 26, was also affected by the increased curvature along the base of the intercondylar eminence. Realignment of the knee increased loading on the medial compartment and caused the element to be affected by the increased curvature of the articular surface. Element 01 registered a bending response for the two realigned tests, while element 29 remained under compression. A reduction in the load transfer at element 29 occurred for the post-osteotomy case. This confirmed the concept of a inward shift in loading created by the tilting of the tibial plateau surface, and the idea that a severe varus deformity increased the load on the articular cartilage near the inner edge of the meniscus.

7.8.2.3 Quadrant Three: Inner Posterior Region

Elements enclosed by the posterior region of the medial compartment of specimen five included 16, 31 and 36. Figure 7.16 shows element 16 laid by the interface of the meniscus and articular cartilage, while the remaining two elements were positioned directly posterior to 16. Consistant compressive loads occurred at 16, but not at elements 31 and 36. It was believed that both elements were positioned too far posteriorly on the medial compartment to be under direct compression and thus recorded bending signals. The low magnitude of the reverse bending peak values for 36 indicated minimal load

transfer throughout the region; similarly the peak values at 31 were notably larger in magnitude but had also remained relatively constant.

7.8.2.4 Quadrant Four: Outer Posterior Region

Elements located across the outer posterior area of specimen five included 09, 12, 15, 22 and 34. The low peak values for element 12 were expected, as the element laid along the extreme outer region of the medial compartment close to the medial collateral ligament, and did not appear to be under complete contact. All elements remained active during the alignment tests, but responded differently to the loads. The two inner most elements (09 and 22) registered direct compressive peaks, whereas elements 15 and 34, positioned more laterally and posteriorly, experienced concave bending. The more anterior of these two elements was 15, and registered larger but consistant peak values, whereas 34 had low level repsonses, indicating minimal load transfer.

When the knee was aligned to a neutral orientation load transfer was more prominent at the posterior elements than the anterior ones. Realignment of the joint brought about slight variations in the contact behaviour. Element 09 recorded lower peaks for the malaligned and post-osteotomy configurations, while element 22 had an increased response for the malaligned case only.

7.8.2.5 Quadrant Five: Outer Anterior Region

All four elements identified in quadrant five laid on top of the medial meniscus. Element 04 was positioned between the outer mating edge of the femoral condyle and tibial plateau. Although signal peaks

were of a concave bending nature, the magnitudes were low, indicating minimal contact pressure.

Neutral alignment resulted in partial loading across the anterior region but was affected by the loss of contact brought on by knee flexion. Having the knee reoriented caused a posterior shift in joint loading, as all three remaining elements had lower peak values for the osteotomy and malaligned cases. Similar findings were observed with the other knee specimens, suggesting that for this particular experimental setup, more load was transferred to the anterior region with a neutrally aligned knee, and moved posteriorly when the joint alignment was altered.

Table 7.11: Normalized Average Pressure Measurements for Specimen Five

Alignment Configuration		Quadrant One: Active Elements				
		05	06	19	21	26
Normal	NSR	.001/.001	.002/.002	.093/.038	.031/.003	2.22/.175‡
	Load	2026/126	2028/125	2286/45	1561/258	1597/208
Mal.	NSR	.003/.001	.012/.002	.069/.003	.058/.011	2.14/.159‡
	Load	2294/64	2295/62	2171/71	2126/120	2124/120
Ost.	NSR	.002/.001	.002/.004	.088/.009	.066/.007	2.51/.426‡
	Load	2049/107	2046/107	1984/76	1921/62	1926/58

		Quadrant Two: Active Elements	
		01	29
Normal	NSR	.009/.004	.093/.023
	Load	1979/73	1632/218
Mal.	NSR	22.1/10.8†	.158/.056
	Load	2295/62	2126/120
Ost.	NSR	.502/.151†	.022/.005
	Load	2066/114	1926/58

All responses are for a compressive load, unless otherwise specified.
†: Concave Bending Response and ‡: Convex Bending Response.

NSR: Normalized Signal Response
Load: Externally Applied Load (N)

Table 6.11: Normalized Average Contact Force Measurements for Specimen Five

Alignment Configuration		Quadrant Three: Active Elements		
		16	31	36
Normal	NSR	.076/.012	2.28/.539†	.132/.036‡
	Load	1864/53	1779/93	1777/93
Mal.	NSR	.054/.013	1.93/.576†	.415/.061‡
	Load	2210/76	2104/80	2102/79
Ost.	NSR	.087/.011	2.48/.767†	.129/.016‡
	Load	1984/76	1904/62	1903/62

		Quadrant Four: Active Elements				
		09	12	15	22	34
Normal	NSR	.110/.035	.002/.003	2.41/.572‡	.002/.0	.290/.054‡
	Load	2015/133	1872/55	1866/56	1597/209	1777/93
Mal.	NSR	.062/.017	.013/.010	1.95/.420‡	.022/.005	.276/.029‡
	Load	2299/22	2211/80	2210/78	2126/120	2102/79
Ost.	NSR	.061/017	.002/.002	2.62/.345‡	.001/.0	.132/.031‡
	Load	2064/115	1982/76	1979/87	1926/58	1903/62

		Quadrant Five: Active Elements			
		04	11	25	39
Normal	NSR	.109/.031‡	.136/.028	.352/.075†	.071/.020
	Load	2026/126	1864/53	1597/209	1779/93
Mal.	NSR	.072/.012‡	.009/.005	.079/.050	.037/.011
	Load	2295/64	2211/80	2095/115	2104/80
Ost.	NSR	.248/.079‡	.045/.022	.324/.182‡	.047/.006
	Load	2066/114	2028/71	1907/48	1904/62

All responses are for a compressive load, unless otherwise specified.
†: Concave Bending Response and ‡: Convex Bending Response.

NSR: Normalized Signal Response
Load: Externally Applied Load (N)

Figure 7.18 a): Normalized signal output patterns: Specimen five - Quadrants one and two.

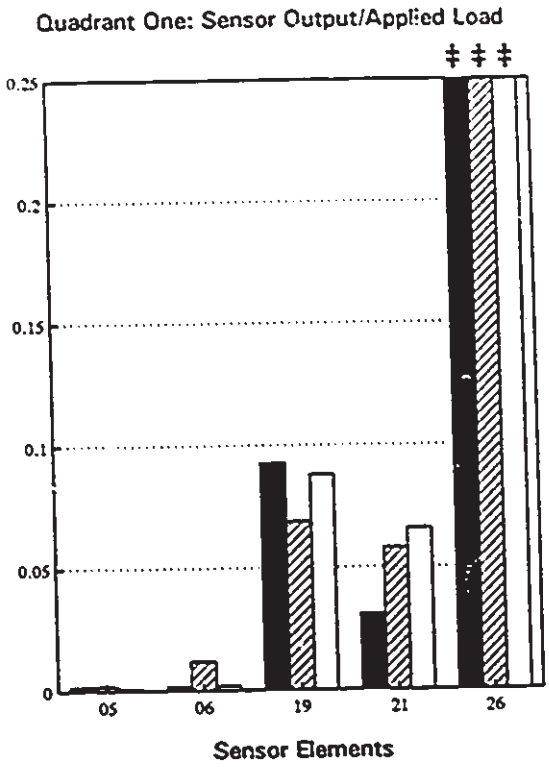

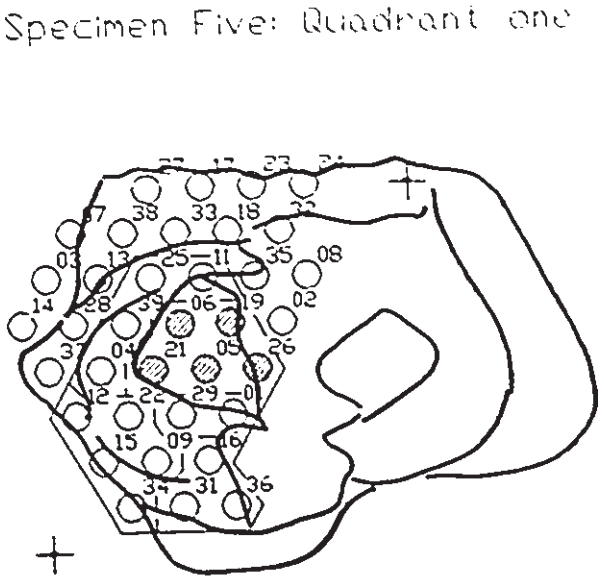

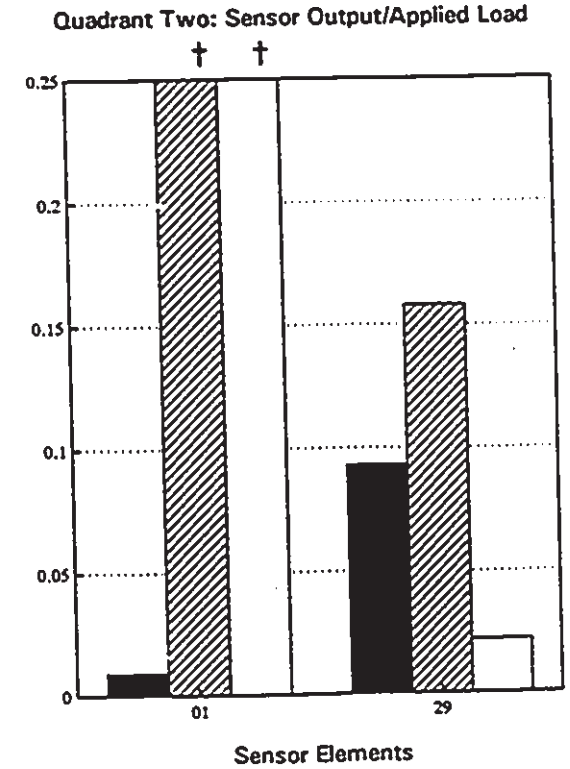

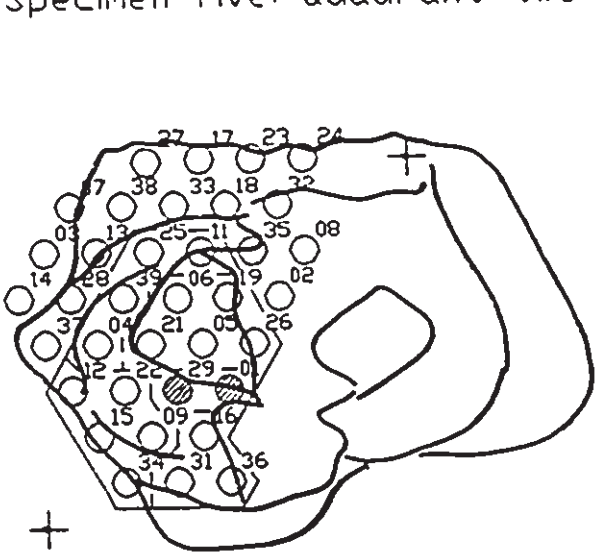

Figure 7.18 b): Normalized signal output patterns: Specimen five - Quadrants three and four.

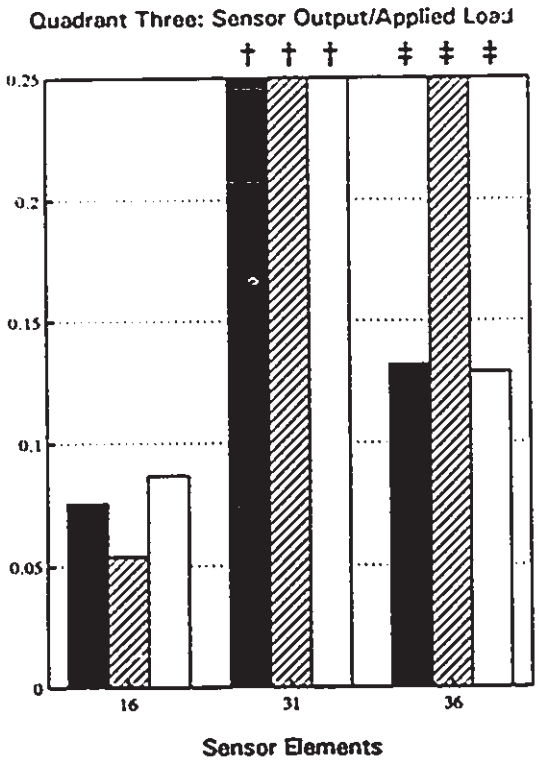

Specimen five: Quadrant three

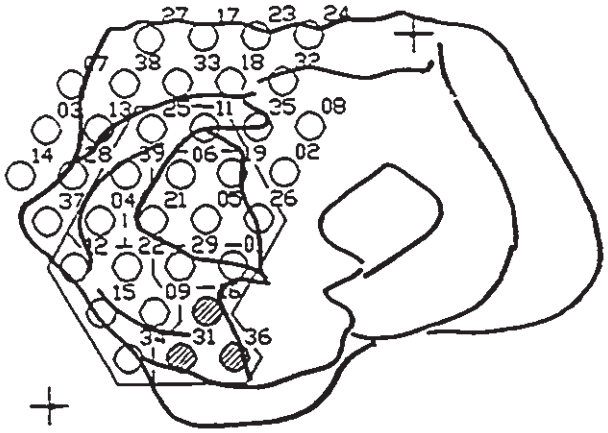

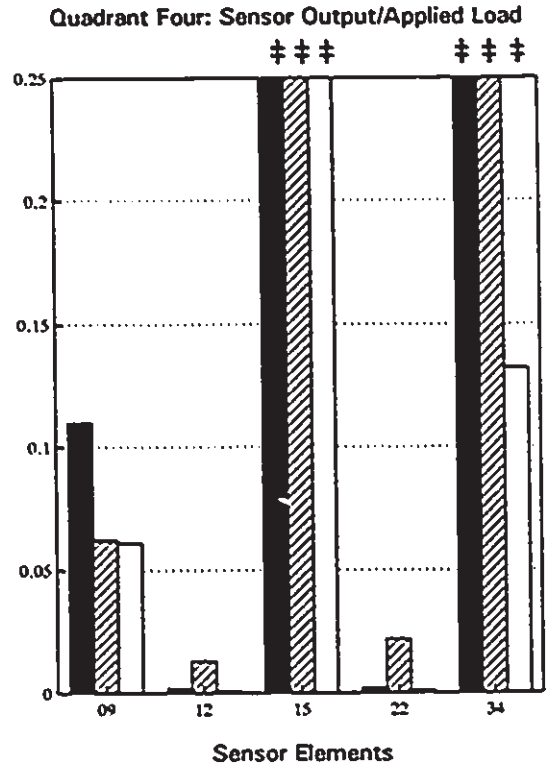

Specimen five: Quadrant four

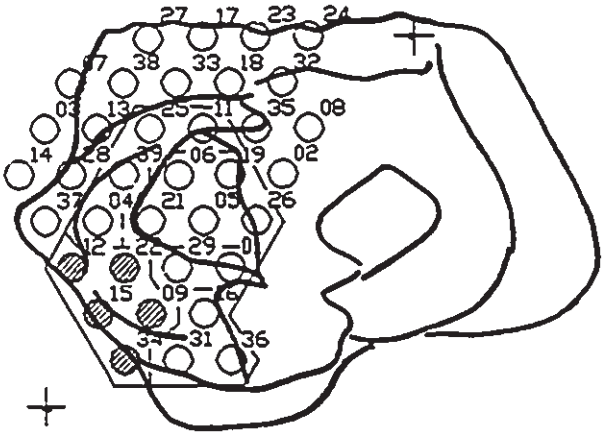

Figure 7.18 c): Normalized signal output patterns: Specimen five - Quadrant five.

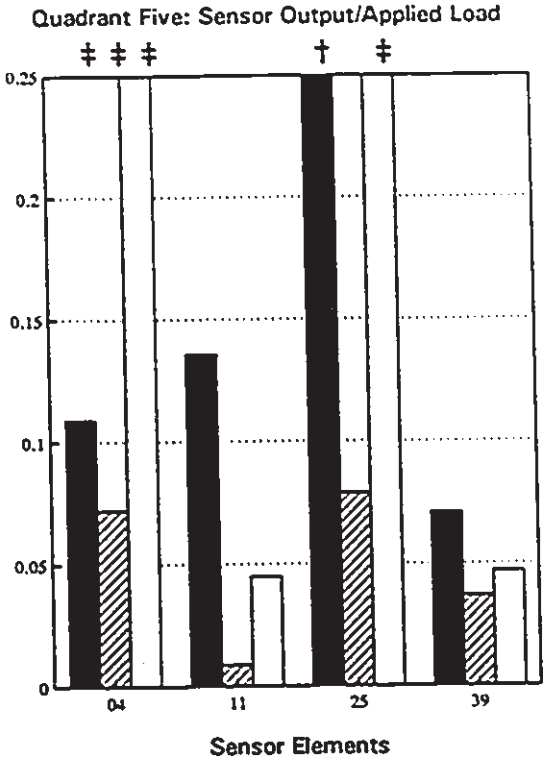

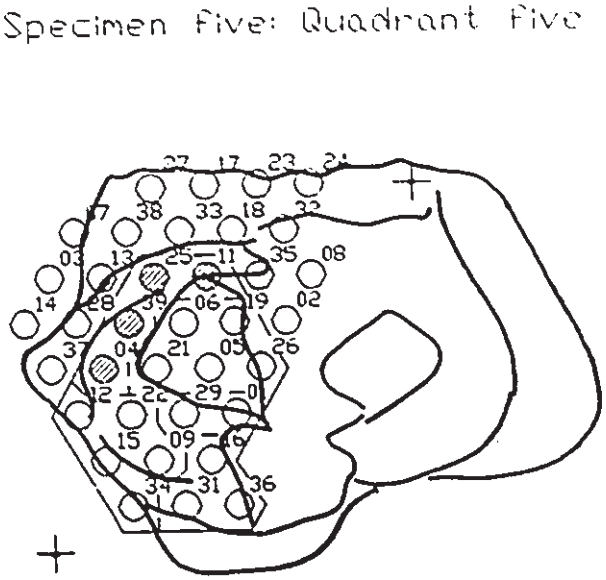

7.9 Test Results for Specimen Six

Specimen six was the left mate to specimen five and measured the smallest in width of all knees included in this study. The tibial plateau surface was shown in figure 5.32, and had a loose anterior attachment of the medial meniscus. However, no visible signs of degenerative joint pathology were observed.

7.9.1 Active Contact Area Zones

The final location of the measurement pad on the medial compartment is illustrated in figure 7.19. Only seventeen elements were active, which was due to the reduced surface area of the specimen. The allocation of elements to specific quadrants is identified in table 7.12. The total active contact area measured 9.38 cm^2, and is outlined in figure 7.20. All elements remained active at complete knee extension; knee flexion brought about a loss of contact at elements 11 and 25, and reduced the contact area to 6.50 cm^2. This was the smallest measured area at 20 degrees flexion of the knee specimens included in this study.

Table 7.12: Assignment of Active Elements by Quadrant Location for Specimen Six

Quadrant Number	Channel Identification
Q1	06 19
Q2	01 05 21 22 29
Q3	16 31 36
Q4	04 09 15 34
Q5	11 25 39

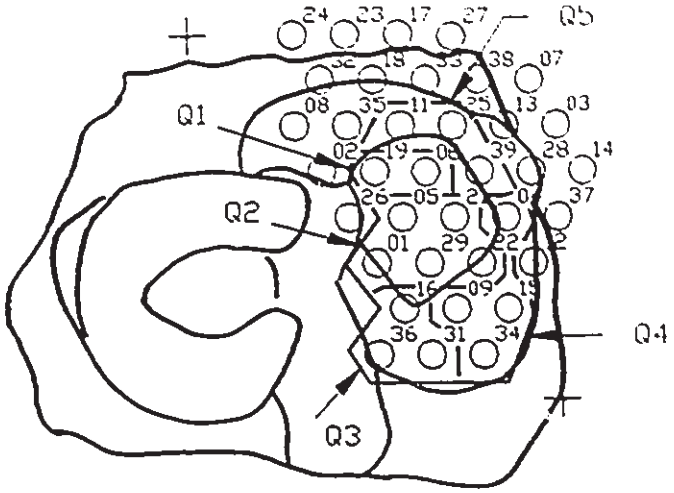

Figure 7.19: Location of measurement pad on medial compartment of specimen six. Quadrants separated by dashed lines.

LOST COVERAGE AT
0 DEGREES KNEE FLEXION

LOST COVERAGE AT
20 DEGREES KNEE FLEXION

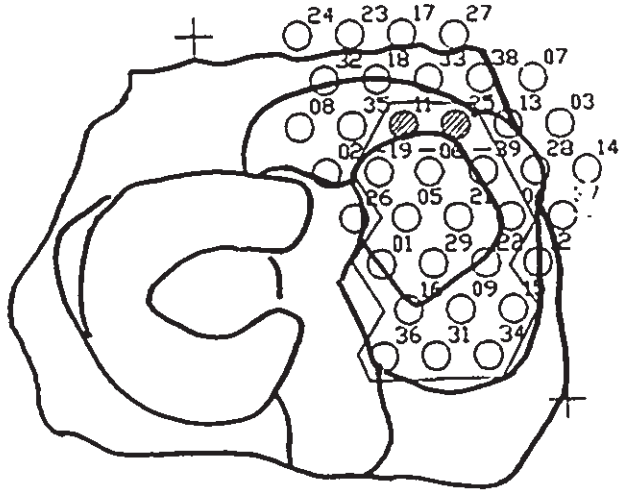

Figure 7.20: Area coverage of medial compartment of specimen six.

7.9.2 Normalized Contact Pressure Patterns

Means and standard deviations of the normalized peak outputs are provided in table 7.13, and have been grouped by alignment set-up and quadrant location. Plots of the normalized outputs for the three alignment methods are provided in figure 7.21.

7.9.2.1 Quadrant One: Anterior Central Region

The anterior region of the articular cartilage included elements 06 and 19. Element 19 was located at the inner edge of the medial compartment close to the anterior attachment site of the meniscus, while element 06 was immediately lateral. Both elements were active during the neutral tests and experienced a notable increase in load transmission when the joint was reoriented to 15° varus. However, the realigned osteotomy case brought about a load increase at 06, while 19 had actually dropped off, but still remained under compression. This behaviour was consistant with the results from the other specimens, in that some level of contact was always maintained across the articular surface and that deviations from the neutral orientation resulted in increased loading in the central portion. This was often accompanied with a decrease in load transmission across the anterior region, as confirmed by the responses from elements in quadrant five.

7.9.2.2 Quadrant Two: Posterior Central Region

Quadrant two included elements 01, 05, 21, 22 and 29 dispersed across the posterior cartilage surface. Element 01 sat tightly against the intercondylar eminence. The concave bending responses were caused

by the increased curvature of the mating surfaces in this region. All other elements remained active during the neutral tests, however the outer two most elements (21, 22) responded with minimal peaks.

Minimal changes were noted at elements 21 and 22 for both realigned cases. The two remaining elements (05 and 29) laid closer to the joint centre, as shown in figure 7.19, and had lower values for the malaligned case. A further reduction was recorded at 05 following the osteotomy alignment, whereas element 29 doubled in magnitude. The increased external load borne by the medial compartment did not bring about the increased loading at these elements, as had been expected and observed with the other knee specimens.

7.9.2.3 Quadrant Three: Inner Posterior Region

Quadrant three included elements 16, 31 and 36 located along the inner posterior region of the medial compartment. Element 31 generated consistant bending peaks for all tested alignment cases, suggesting that contact was maintained but was not affected by an alignment deviation or correction. The similar bending responses for element 16 were marginal but also did not exhibit large variations with changes in the knee alignment. The third element (36) was also under minimal compression during the neutral tests, and changed to slight bending when the knee orientation was altered.

7.9.2.4 Quadrant Four: Outer Posterior Region

Elements included in quadrant four were 04, 09, 15 and 34, and are shown in figure 7.19 to lay along the outer periphery of the medial

compartment adjacent to the meniscal surface. The curvature of the lateral edge of the medial femoral condyle caused the elements to mimic the surface profile. This occurred at elements 04 and 15, located between the outer lateral edge of the medial femoral condyle and the meniscus. This was previously identified as a region of the medial compartment where the operation of the measurement pad was limited by the surface profile.

Element 34, the most posterior - lateral positioned element, registered minimal peak contact pressure readings for the different alignment orientations. Similar results occurred at element 09, positioned just inward from 34.

7.9.2.5 Quadrant Five: Outer Anterior Region

Three sensor elements came to lay within the boundary of the anterior region of the medial compartment (11, 25 and 39), of which, two lost contact due to knee flexion (11 and 25). Minimal activity occurred at element 11 for all tested alignment conditions, whereas element 25 was under excess bending loads. The contact pressure at 25 was reduced when the knee alignment was changed. This was partly the result of the loss of contact during knee flexion and the loose anterior attachment of the medial meniscus.

Having the knee offset by 15° varus delayed loading at the remaining element (11); similar results occurred following the simulation of the high tibial osteotomy.

Table 7.13: Normalized Average Pressure Measurements for Specimen Six

Alignment Configuration		Quadrant One: Active Elements	
		06	19
Normal	NSR	.006/.003	.049/.023
	Load	1726/471	1891/104
Mal.	NSR	.132/.026	.157/.021
	Load	1761/62	1882/28
Ost.	NSR	.034/.005	.018/.013
	Load	2162/111	2065/76

		Quadrant Two: Active Elements				
		01	05	21	22	29
Normal	NSR	8.33/1.49‡	.110/.024	.018/.002	.004/.002	.057/.017
	Load	1637/476	1699/471	1917/138	1921/120	1886/124
Mal.	NSR	6.26/4.29‡	.073/.012	.002/.002	.004/.002	.009/.003
	Load	1730/49	1272/45	1801/102	1801/102	1873/45
Ost.	NSR	.876/.192‡	.017/.007	.007/.007	.002/.001	.110/.020
	Load	2206/67	2162/111	1996/38	1966/35	1966/35

All responses are for a compressive load, unless otherwise specified.
†: Concave Bending Response and ‡: Convex Bending Response.

NSR: Normalized Signal Response
Load: Externally Applied Load (N)

Table 7.13: Normalized Average Pressure Measurements for Specimen Six

Alignment Configuration		Quadrant Three: Active Elements		
		16	31	36
Normal	NSR	.364/.059‡	.893/.207‡	.006/.001
	Load	1885/107	1988/49	1988/45
Mal.	NSR	.260/.078‡	.874/.236‡	.184/.042‡
	Load	1881/31	1816/60	1837/67
Ost.	NSR	.509/.135‡	.849/.306‡	.219/.034‡
	Load	2064/76	2077/31	2001/98

		Quadrant Four: Active Elements			
		04	09	15	34
Normal	NSR	.562/.165†	.002/.002	2.19/1.07†	.010/.001
	Load	1726/483	1726/485	1887/108	1988/45
Mal.	NSR	.744/.072‡	.001/.001	.893/.100†	.035/.011
	Load	1775/18	1766/62	1867/54	1837/67
Ost.	NSR	.606/.144‡	.003/.001	1.20/.502†	.047/.011
	Load	2162/111	2162/111	2096/84	2001/98

		Quadrant Five: Active Elements		
		11	25	39
Normal	NSR	.003/002	6.88/1.42‡	.190/.0
	Load	1886/107	1988/45	2002/50
Mal.	NSR	.003/.004	1.10/.087‡	.002/.003
	Load	1881/27	1815/107	1819/64
Ost.	NSR	.004/.001	.911/.126‡	.004/.002
	Load	2064/76	1970/40	2046/59

All responses are for a compressive load, unless otherwise specified.
†: Concave Bending Response and ‡: Convex Bending Response.

NSR: Normalized Signal Response
Load: Externally Applied Load (N)

Figure 7.21 a): Normalized signal output patterns: Specimen six - Quadrants one and two.

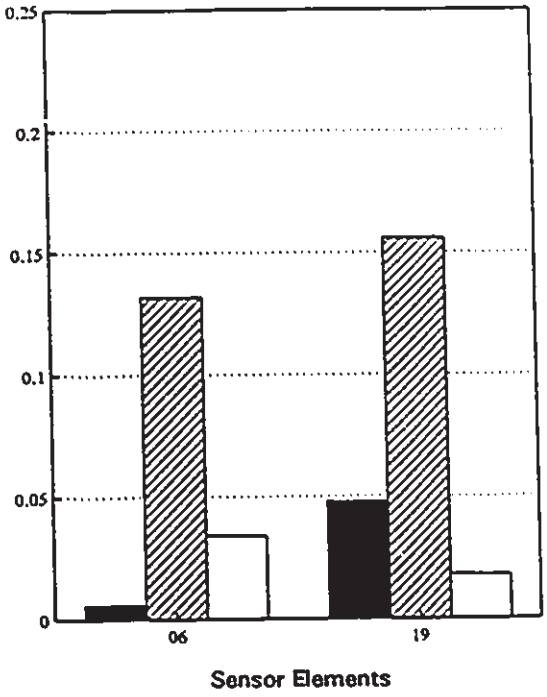

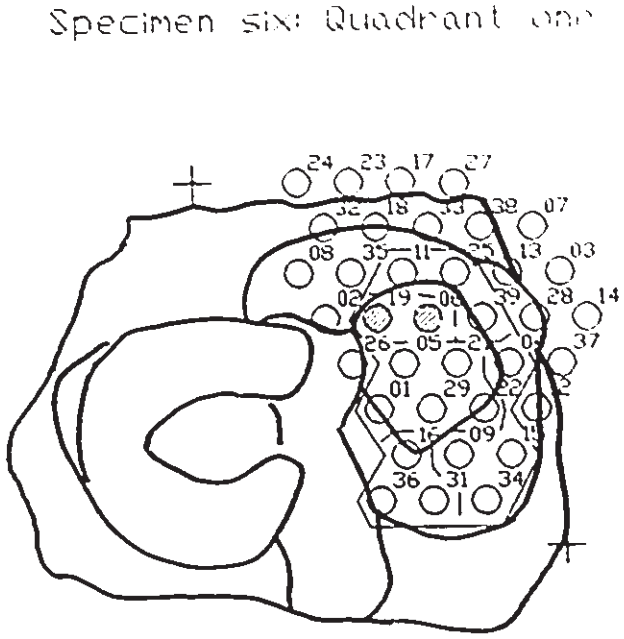

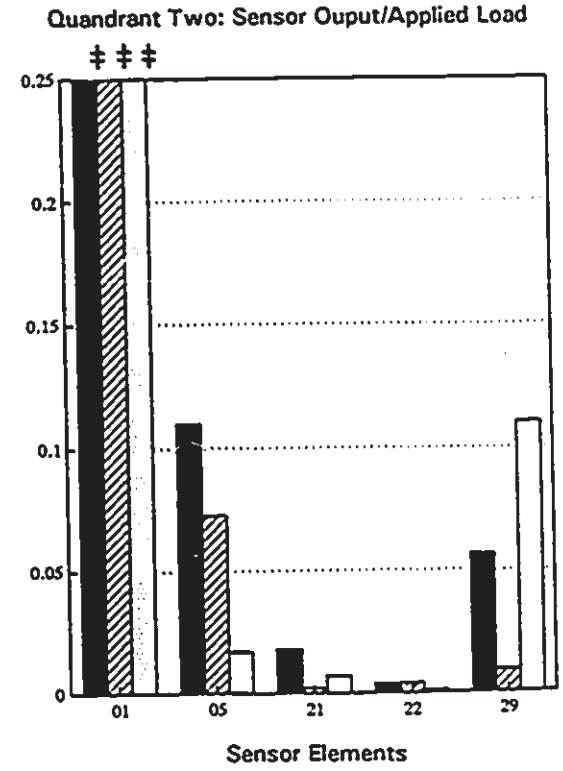

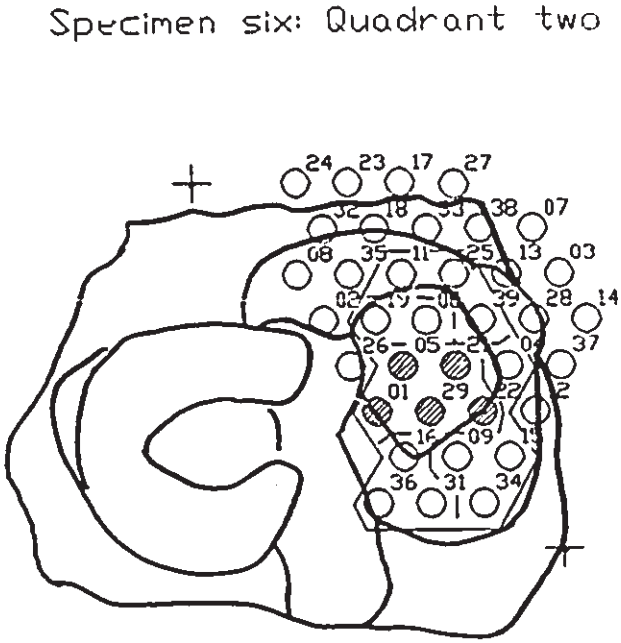

Figure 7.21 b): Normalized signal output patterns: Specimen six - Quadrants three and four.

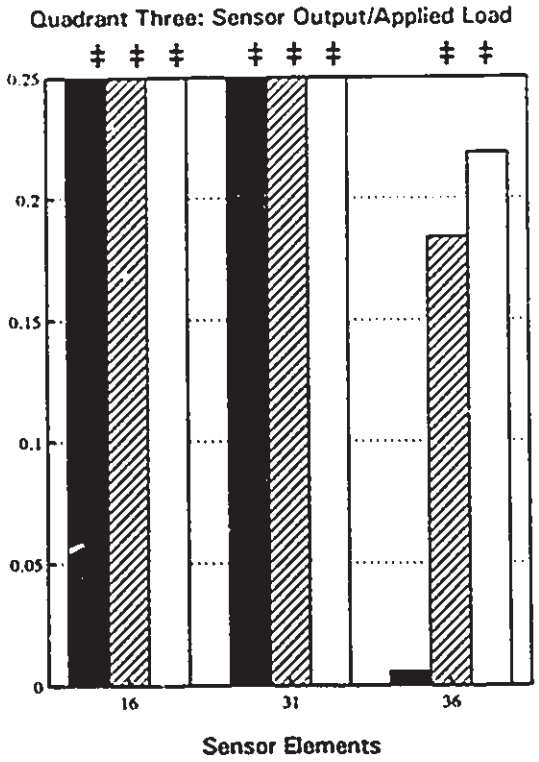

Specimen six: Quadrant three

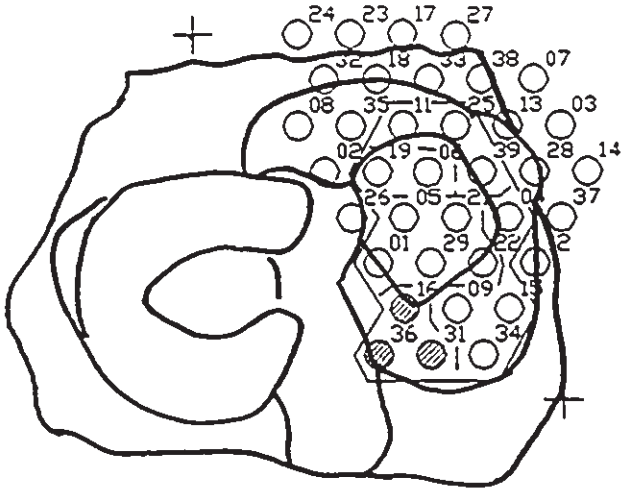

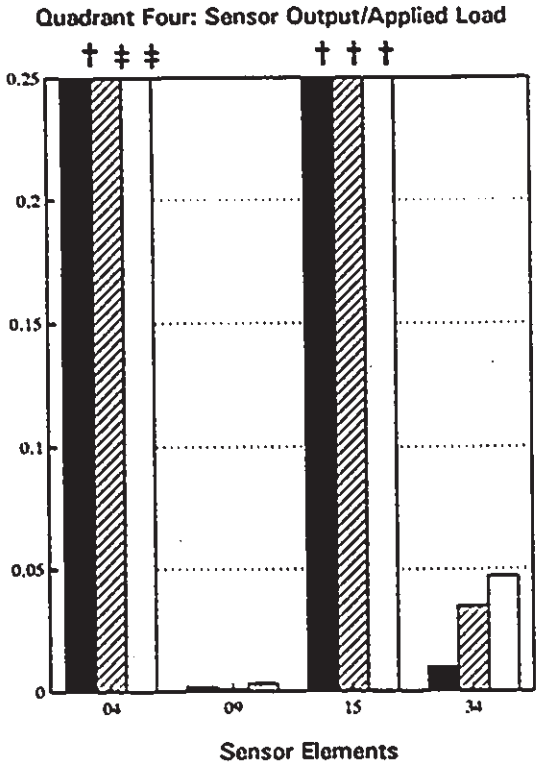

Specimen six: Quadrant four

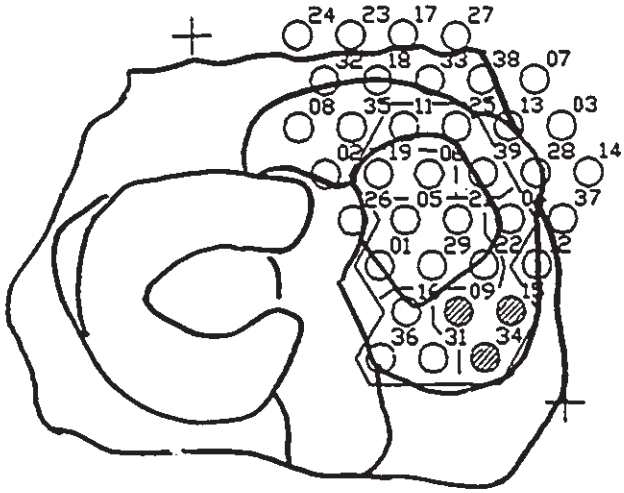

Figure 7.21 c): Normalized signal output patterns: Specimen six - Quadrant five.

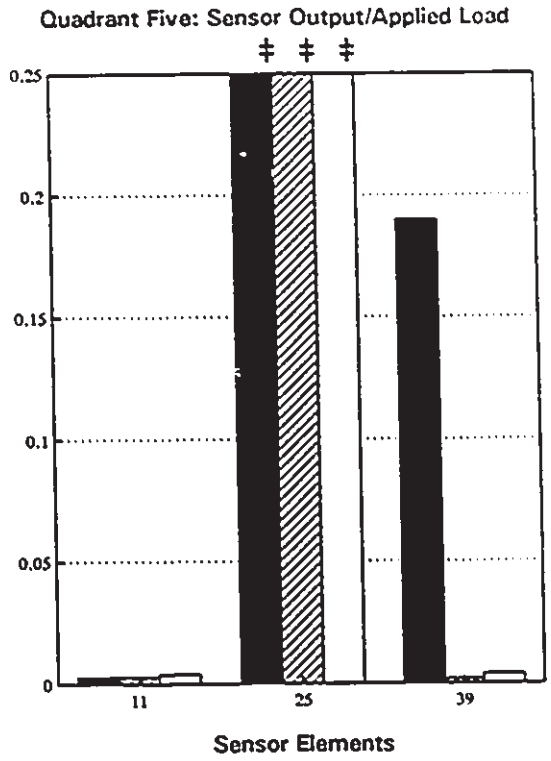

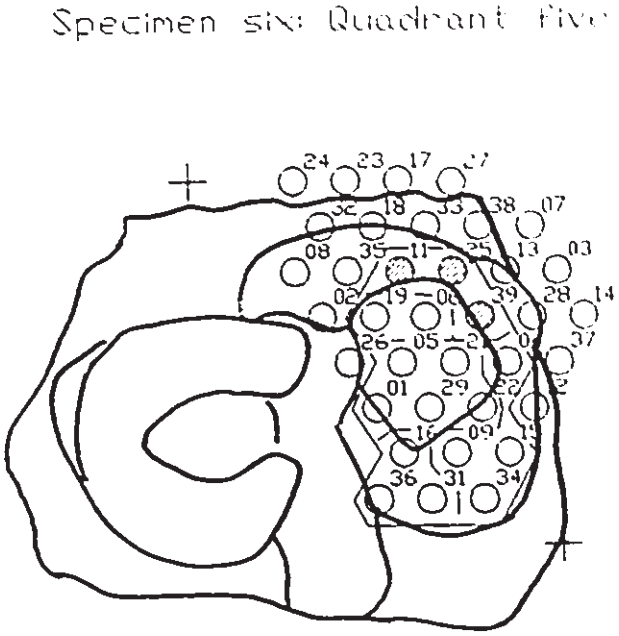

7.10 Test Results for Specimen Seven

Specimen seven had a small tear at the outer posterior corner of the medial meniscus; the extent of the tear is illustrated in figure 5.33. No other visible signs of joint pathology were noted. It remained unknown as to how the tear affected the relative motion between the two mating surfaces or its affect on the resultant transfer of force in the immediate region.

A modified version of the measurement pad was used to test the last pair of knee specimens. The pad had a total of twenty-eight sensor elements; eight less than the previous design. It was hoped that this modification allowed the pad to sit snugger in the joint capsule and reduce bending of the peripheral elements.

7.10.1 Active Contact Area Zones

The final location and arrangement of the measurement pad is shown in figure 7.22. Nineteen active elements were identified and assigned to specific quadrants, as indicated in table 7.14. No malfunctions were encountered with the measurement pad during the tests; however, the location of elements 12, 15 and 22 near the meniscal tear, affected their performance. The outline of the total active surface area is illustrated in figure 7.23 and covered 10.12 cm^2. Element 31 was not under contact at complete knee extension, while elements 33 and 38 lost contact with knee flexion. The corresponding area measurements were 7.75 cm^2 and 7.32 cm^2 for 0° and 20° knee flexion, respectively.

Table 7.14: Assignment of Active Elements by Quadrant Location for Specimen Seven

Quadrant Number	Channel Identification
Q1	06 19 39
Q2	01 05 21 22 26 29
Q3	09 16 31
Q4	04 15
Q5	11 13 25 33 38

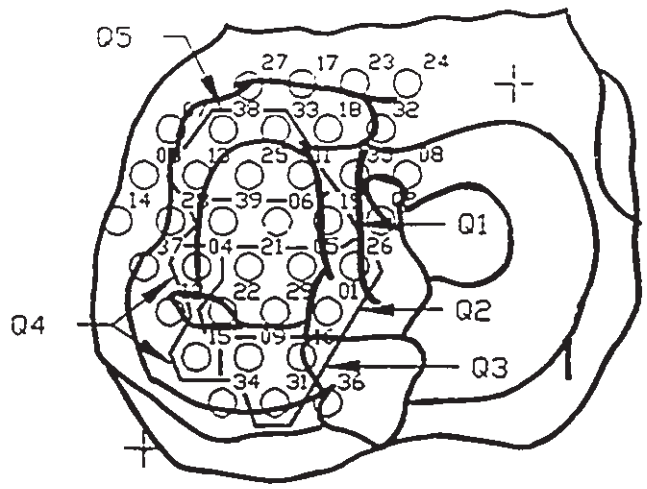

Figure 7.22: Location of measurement pad on medial compartment of specimen seven. Quadrants separated by dashed lines.

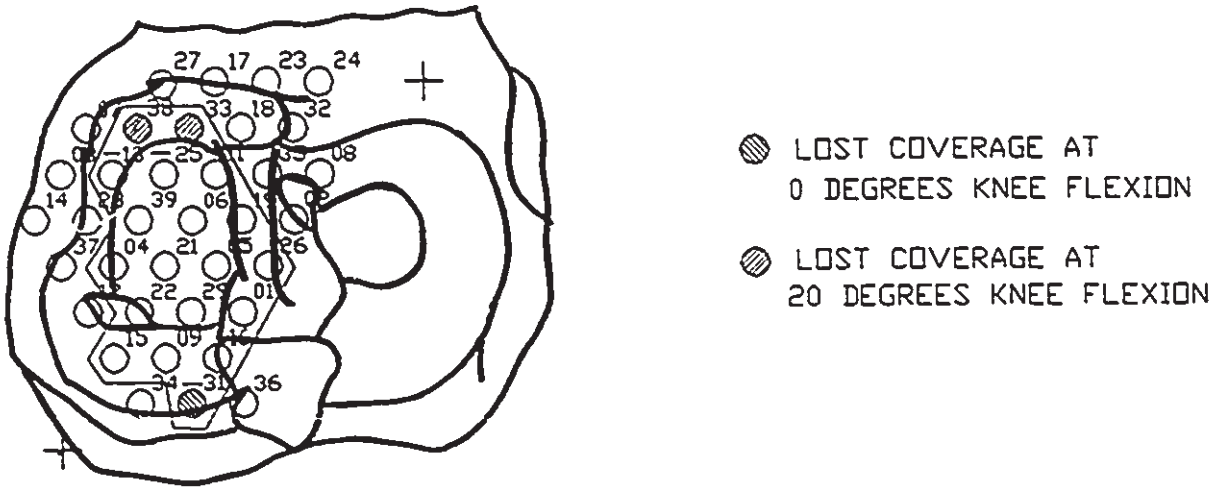

Figure 7.23: Area coverage of medial compartment of specimen seven.

7.10.2 Normalized Average Pressure Patterns

Peak pressure values were normalized with respect to the applied load and tabulated in table 7.15. The average mean and standard deviations of the normalized values are also plotted in figure 7.24 for the five different quadrants. The effects of knee alignment on local contact pressure variations are discussed next.

7.10.2.1 Quadrant One: Anterior Central Region

Quadrant one included elements 06, 19 and 39, aligned with each other across the width of the medial compartment and in contact with articular cartilage. Compressive signal responses were registered at each element for the three different alignment conditions. Minimal pressure variations occurred at 06 for the malaligned and post-osteotomy cases, whereas 19 registered a reduction in the local contact pressure. Similar responses occured at 39 for the simulated osteotomy alignment, having a notable increase when the joint was set to 15° varus.

7.10.2.2 Quadrant Two: Posterior Central Region

Five of the six elements in quadrant two laid directly on the cartilage surface (01, 05, 21, 22, 29); the remaining element was located at the base of the intercondylar eminence (26). The increased curvature in this region caused element 26 to respond with bending signals. This was consistent with the results from the other knee specimens, as the final mode of loading on elements in this region was often dictated by the surface curvature.

Figure 7.24 shows that the five central elements were active

during the neutral case and experienced an increase in load transmission when the joint was malaligned. This supports the concept of increased loading over the posterior central region with the deformed joint. The last alignment condition included the simulation of the osteotomy. Here the inner medial elements (21, 22) increased peak outputs, while 05 decreased and 01 remained minimal. The output response from element 29 was representative of convex bending of the element. However, it is unknown as to why the element responded in this manner. A similar trend of compressive load responses across the central cartilage surface was also observed with the other knee specimens.

7.10.2.3 Quadrant Three: Inner Posterior Region

Of the three elements located along the inner posterior aspect of the medial compartment (09, 16, 31), element 31 required some knee flexion before contact was made. Minimal variations in the peak pressures occurred at 09, whereas 16 was prone to be bending during the neutral and malaligned tests, and under compression for the osteotomy set-up. Because element 16 laid near the posterior attachment site of the medial meniscus, this enhanced bending of the element.

7.10.2.4 Quadrant Four: Outer Posterior Region

Elements 04 and 15 were identified within the bounds of quadrant four along the lateral posterior ridge, with 04 lying well anterior of 15 on the cartilage - meniscus junction, and 15 within the region of the meniscal tear. Large fluctuations in the signal outputs from element 15 were due to its proximity to the tear. As for element 04, the contact

pressure decreased as the knee orientation changed.

7.10.2.5 Quadrant Five: Outer Anterior Region

The remaining active elements were dispersed across the anterior region of the medial compartment, and included elements 11, 13, 25, 33 and 38. As knee flexion progressed, contact was lost at the anterior elements (33, 38); however, this did not appear to affect the operation of the sensors. Output patterns at all of the elements were representative of a true compressive load. Referring to the photograph of the tibial plateau in figure 5.33, the anterior aspect of the mensicus was drawn forward because of its loose anterior attachment. This resulted in elements 11 and 25 making contact with the articular cartilage rather than the meniscus.

With the knee in a neutral position, contact was maximal at elements 11, 13 and least at 33. The low magnitude of the normalized values for element 25 suggested that load transmission was minimal but that contact was maintained regardless of the knee orientation.

The varus malalignment brought about a decrease at all locations, except at element 33. The reduced pressure values across the anterior region for the malaligned case were consistant with the results from the other knee specimens. With regards to the post-osteotomy results, less load was transferred across the anterior region than for the neutrally aligned knee, as only element 38 registered an unchanged peak response. This finding was also noted with the other knee specimens.

Table 7.15: Normalized Average Contact Pressure Measurements for Specimen Seven

Alignment Configuration		Quadrant One: Active Elements		
		06	19	39
Normal	NSR	.078/.023	.134/.106	.029/.002
	Load	1815/156	1663/80	1761/58
Mal.	NSR	.115/.026	.031/.006	.123/.033
	Load	1806/98	1712/18	1801/111
Ost.	NSR	.085/.023	.026/.013	.027/.007
	Load	1703/53	1659/84	1601/84

		Quadrant Two: Active Elements				
		01	05	21	22	26
Normal	NSR	.003/.003	.036/.017	.005/.005	.022/.004	.958/.109‡
	Load	1899/62	1899/62	1717/89	1726/40	1659/67
Mal.	NSR	.001/.001	.122/.013	.041/.040	.100/.045	.394/.076‡
	Load	1806/98	1806/98	1784/98	1717/102	1784/115
Ost.	NSR	.005/.005	.003/.002	.066/.036	.066/.018	.500/.103‡
	Load	1704/53	1695/58	1708/76	1663/35	1735/62

		Quadrant Two: Active Elements
		29
Normal	NSR	.042/.027
	Load	1752/58
Mal.	NSR	.230/.006†
	Load	1784/58
Ost.	NSR	1.64/.185†
	Load	1699/18

All responses are for a compressive load, unless otherwise specified.
†: Concave Bending Response and ‡: Convex Bending Response.

NSR: Normalized Signal Response
Load: Externally Applied Load (N)

Table 7.15: Normalized Average Contact Pressure Measurements for Specimen Seven

Alignment Configuration		Quadrant Three: Active Elements		
		09	16	31
Noraml	NSR	.017/.014	.719/.283†	.032/.002
	Load	1899/62	1735/142	1761/58
Mal.	NSR	.020/.006	.505/.094†	.004/.001
	Load	1788/102	1681/49	1801/102
Ost.	NSR	.016/.003	.060/.007	.030/.008
	Load	1726/36	1676/93	1601/84

		Quadrant Four: Active Elements	
		04	15
Normal	NSR	.134/.021	.244/.183†
	Load	1899/62	1784/133
Mal.	NSR	.042/.036	2.79/.568†
	Load	1846/107	1695/45
Ost.	NSR	.040/.240	.132/.092‡
	Load	1726/35	1686/84

		Quadrant Five: Active Elements				
		11	13	25	33	38
Normal	NSR	.077/.038	.143/.067	.015/.010‡	.004/.008	.038/.010
	Load	1766/125	1708/93	1490/45	1761/57	1748/58
Mal.	NSR	.024/.007	.010/.002	.034/.011‡	.050/.018	.031/.005
	Load	1690/45	1681/45	1836/98	1801/98	1801/98
Ost.	NSR	.030/.006	.080/.035	.077/.028‡	.010/.008	.043/.012
	Load	1601/22	1704/89	1732/80	1606/93	1606/93

All responses are for a compressive load, unless otherwise specified.
†: Concave Bending Response and ‡: Convex Bending Response.

NSR: Normalized Signal Response
Load: Externally Applied Load (N)

Figure 7.24 a): Normalized signal output patterns: Specimen seven - Quadrants one and two.

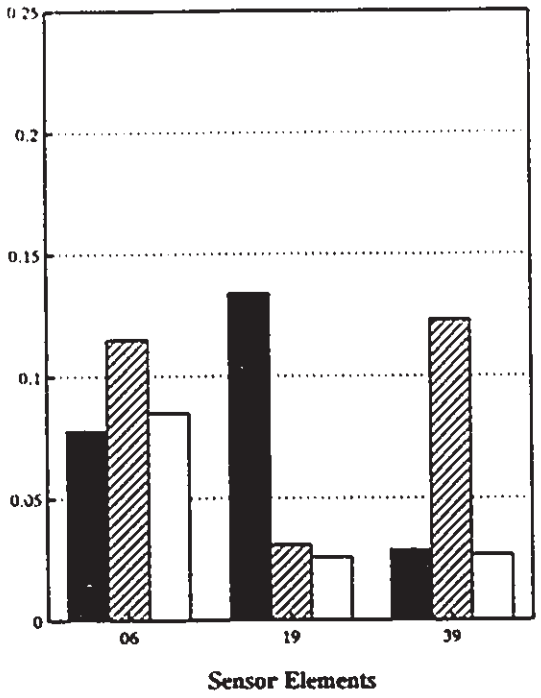

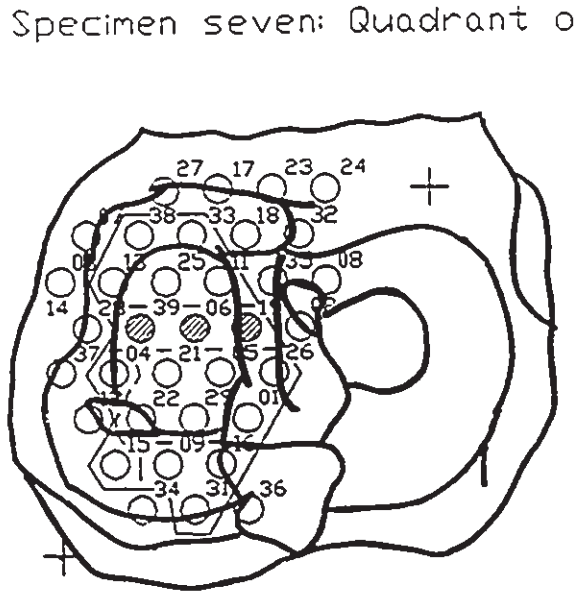

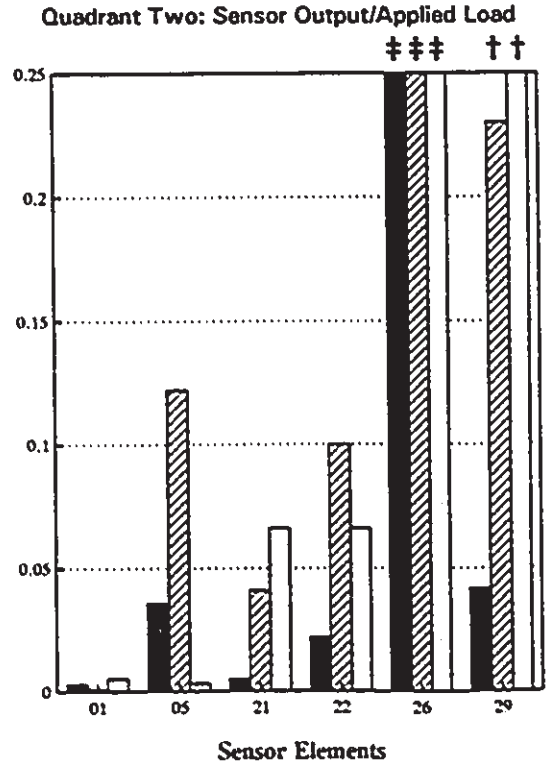

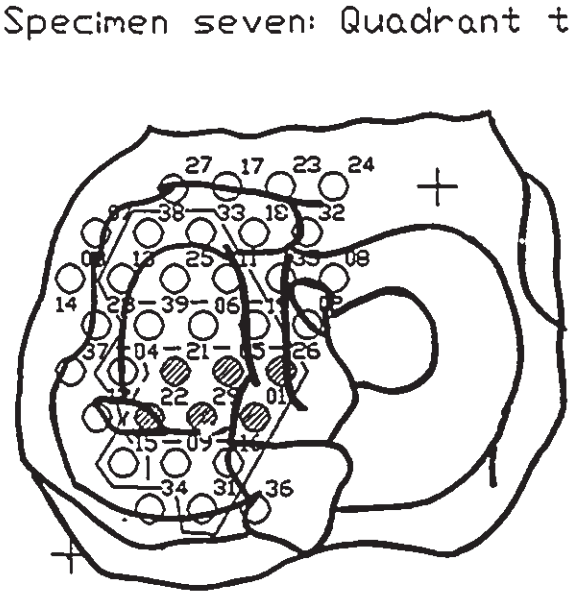

Figure 7.24 b): Normalized signal output patterns: Specimen sever - Quadrants three and four.

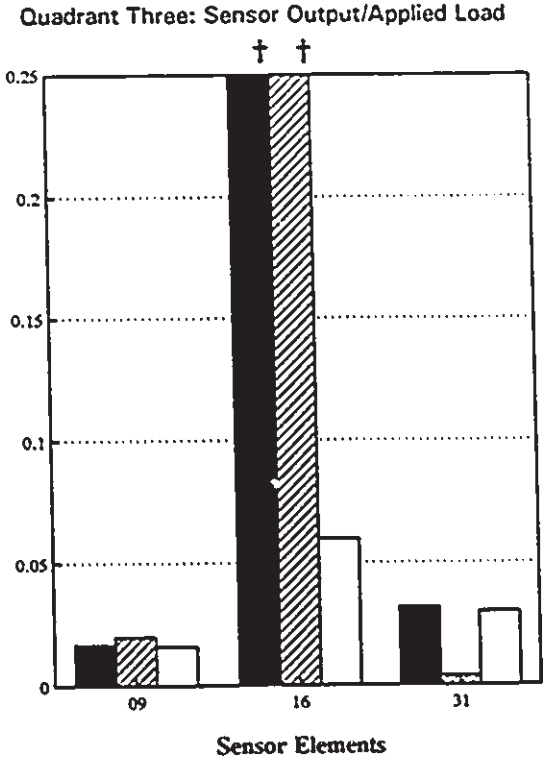

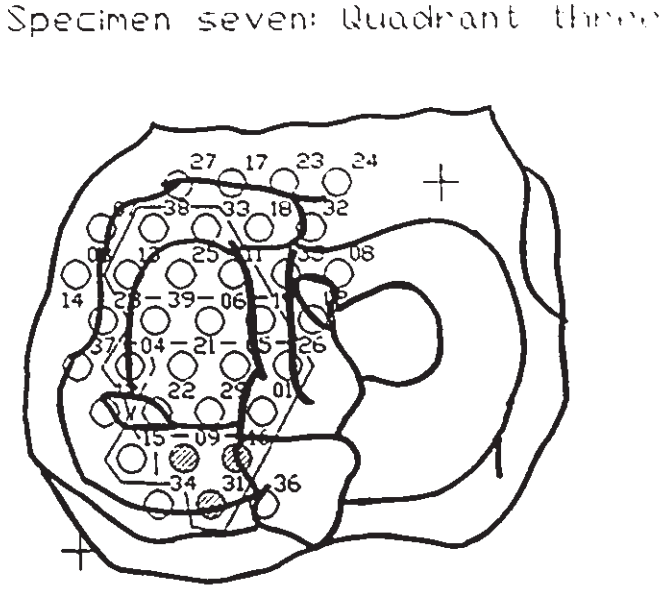

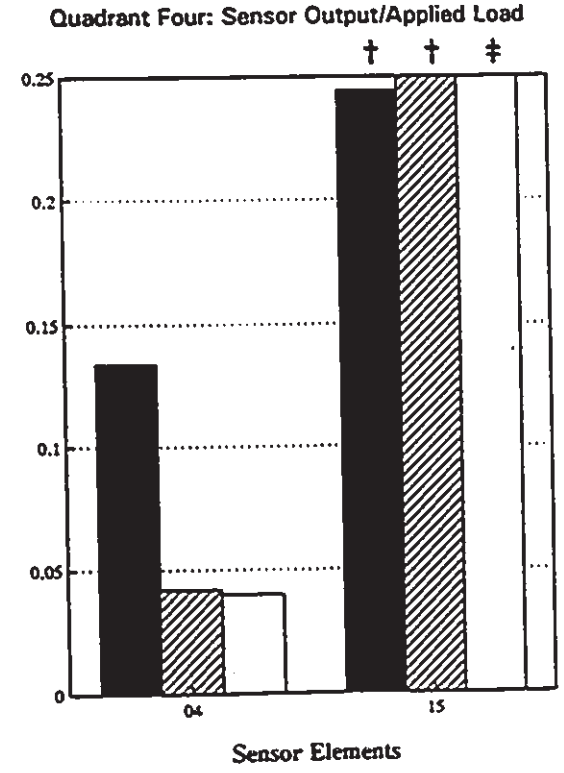

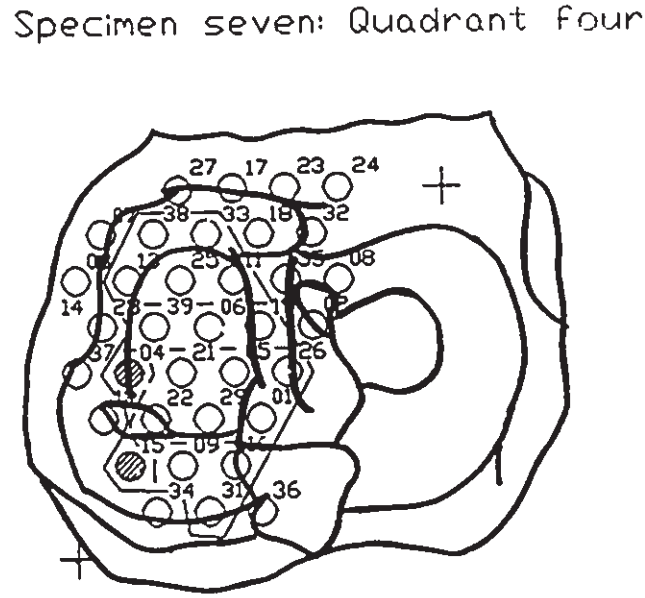

Figure 7.24 c): Normalized signal output patterns: Specimen seven - Quadrant five.

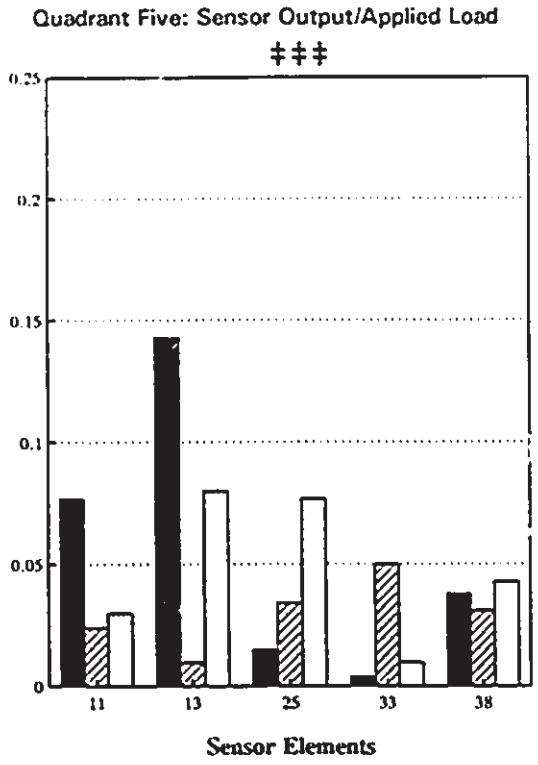

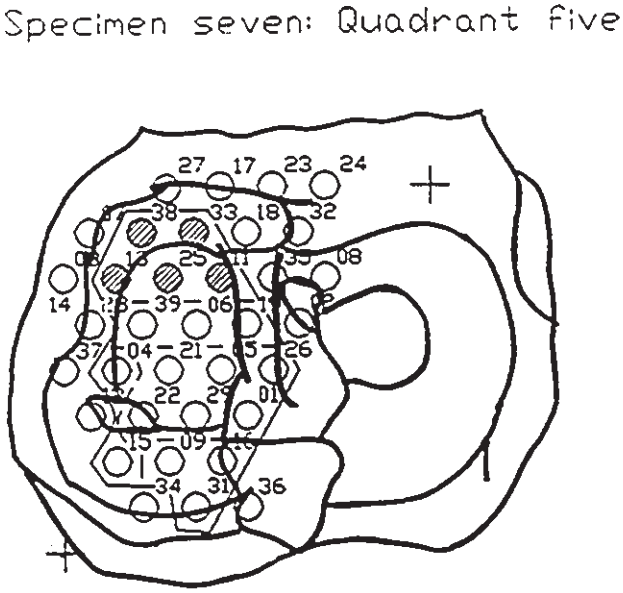

7.11 Test Results for Specimen Eight

The eighth knee specimen was the left mate to specimen seven. It had a similar loose anterior attachment of the medial meniscus, but did not have any tears within the meniscus. The articular surface of the medial plateau was illustrated in figure 5.34; no visible signs of joint pathology were observed.

7.11.1 Active Contact Area Zones

The final location of the measurement pad on the medial compartment is shown in figure 7.25, and the assignment of elements to specific quadrants is listed in table 7.16. The modified measurement pad, similar to that used with specimen seven, was also employed during the testing of specimen eight; a total of twenty-two elements were active. The total area enclosed by the elements is outlined in figure 7.26, and measured 8.65 cm^2. Only knee flexion brought about a reduction in the contact area zone; the smaller area measured 7.78 cm^2.

Table 7.16: Assignment of Active Elements by Quadrant Location for Specimen Eight

Quadrant Number	Channel Identification
Q1	06 11 19 25 39
Q2	05 21 26
Q3	01 09 16 29
Q4	04 12 15 22
Q5	13 28 33 38

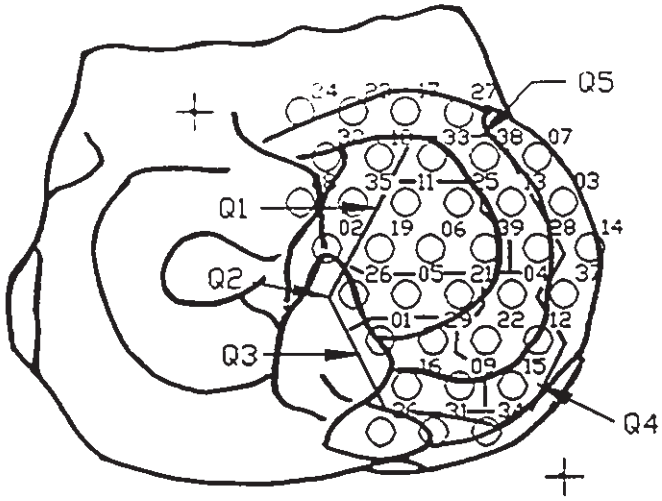

Figure 7.25: Location of measurement pad on medial compartment of specimen eight. Quadrants separated by dashed lines.

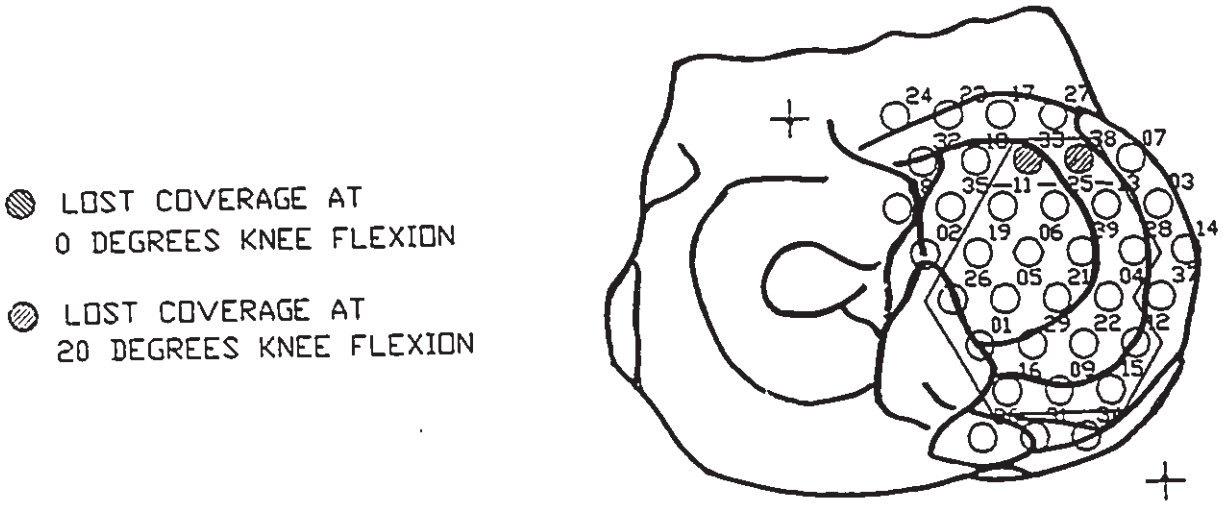

Figure 7.26: Area coverage of medial compartment of specimen eight.

7.11.2 Normalized Contact Pressure Patterns

As with all tests, data from five successive runs were averaged to determine a mean peak pressure at each sensor element. The peak values were normalized with respect to the applied load and are listed in table 7.17 and plotted in figure 7.27.

7.11.2.1 Quadrant One: Anterior Central Region

Five elements were included in quadrant one (06, 11, 19, 25 and 39); all of which came to lay on top of the articular cartilage. Signals representative of compressive loading were registered across the central elements, except at element 25. Results for the neutral knee alignment set-up showed that all elements shared in transmitting the load.

Having the knee offset by 15° varus, created an inward and posterior shift in loading of the medial compartment, as local pressure readings increased at elements 06 and 19, and decreased slightly at element 39. Only element 11, located anterior to these three, had a significant reduction. It was possible that reorientation caused a delay in the application of the load, thereby delivering more load to the central portion and less to the anterior section. It should also be realized that any quadriceps activity would undoubtedly affect the way in which the anterior elements were loaded. When the post-osteotomy alignment was simulated, all elements registered an increase in the normalized contact pressure, compared to the neutrally aligned knee.

7.11.2.2 Quadrant Two: Posterior Central Region

With the knee in the neutral orientation, compressive loading occurred at the three central elements included in quadrant two (05, 21, 26). An increase in the pressure readings at elements 05 and 26 were recorded for the malaligned case, while element 21 registered a slight decrease. Simulation of the osteotomy alignment resulted in minimal changes to the loading behaviour at element 21, whereas elements 05 and 26, located closer to the joint centre, both recorded increased pressure levels. The increased loading along the base of the intercondylar eminence during the osteotomy test supports the concept of redistributing the applied load across the joint surface and possibly shifting the loading vector closer to the joint centre. This also has the overall benefit of reducing the external varus moment produced about the knee centre.

7.11.2.3 Quadrant Three: Inner Posterior Region

The inner posterior region of the medial compartment of specimen eight contained four elements (01, 09, 16, 29). Element 16 laid along the extreme backside of the meniscus, which contributed to bending of the element and account for the increased signal peaks. The two more centrally located elements (09 and 29) had a consistant level of loading regardless of the knee alignment. The last element in quadrant three, 01, also remained under load during the neutral alignment tests, but registered decreased readings of the contact pressure when the joint was realigned to a varus or post-osteotomy configuration.

7.11.2.4 Quadrant Four: Outer Posterior Region

The four elements contained in quadrant four helped to identify the outer, lateral aspect of the contact zone (04, 12, 15, 22). Elements 04 and 15 aligned with each other in the A-P direction, while elements 22 and 12 laid between them and aligned with each other in the M-L direction. The relative locations are shown in figure 7.25.

Elements 12 and 22 registered minimal activity, suggesting contact was present but was not significant, whereas elements 04 and 15 appeared to be placed in a bending mode. Elements within this region were typically influenced by the curvature of the lateral femoral condyle, as the measurement pad no longer came to lay between two smooth level surfaces. As a result, element bending was unavoidable. The concave profile of the signal peaks from elements 04 and 15 mimiced the curvature of the femoral condyle. The two remaining elements , 12 and 22, registered minimal pressure levels.

7.11.2.5 Quadrant Five: Outer Anterior Region

Elements identified in quadrant five laid along the lateral ridge of the medial meniscus (13, 28, 33, 38). Low but consistant levels of pressure were registered at elements 13, 33 and 38, as shown in figure 7.25; only element 28 recorded bending signals. Elements 33 and 38 were the most anterior of all active elements and had increased pressure readings for the malaligned case, but minimal changes following the osteotomy simulation. Element 13, positioned further outward and posterior to elements 33 and 38, generated slightly lower pressure levels when the knee alignment deviated from the neutral position.

Overall, the osteotomy alignment did not affect the contact pressure levels relative to a neutrally aligned knee joint, whereas the malaligned joint encountered an increase in the contact pressure levels at the central anterior sites.

Table 7.17: Normalized Average Contact Pressure Measurements for Specimen Eight

Alignment Configuration		Quadrant One: Active Elements				
		06	11	19	25	39
Normal	NSR	.002/.001	.076/.023	.055/.020	.684/.192†	.082/.014
	Load	2139/173	2486/71	2518/76	2104/85	2308/67
Mal.	NSR	.026/.009	.019/.010	.110/.013	1.44/.321†	.040/.024
	Load	1468/365	1810/67	1810/67	1530/36	1575/67
Ost.	NSR	.007/.001	.125/.041	.073/.015	.295/.091†	.102/.016
	Load	1561/84	1592/142	1592/1421	1503/120	1592/49

		Quadrant Two: Active Elements		
		05	21	26
Normal	NSR	.002/.002	.009/.001	.095/.037
	Load	2144/173	2215/136	2135/98
Mal.	NSR	.077/.021	.006/.007	.119/.034
	Load	1468/365	1579/45	1526/40
Ost.	NSR	.007/.008	.010/.017	.196/.072
	Load	1615/80	1468/104	1539/67

All responses are for a compressive load, unless otherwise specified.
†: Concave Bending Response and ‡: Convex Bending Response.

NSR: Normalized Signal Response
Load: Externally Applied Load (N)

Table 7.17: Normalized Average Contact Pressure Measurements for Specimen Eight

Alignment Configuration		Quadrant Three: Active Elements			
		01	09	16	29
Normal	NSR	.075/.016	.048/.005	2.16/1.07†	.105/.018
	Load	2050/84	2139/173	2580/18	2180/120
Mal.	NSR	.004/.002	.040/.007	1.51/.148†	.130/.023
	Load	1579/365	1748/329	1810/67	1530/36
Ost.	NSR	.040/.021	.048/.012	1.34/.365†	.157/.034
	Load	1579/67	1597/84	1592/142	1495/120

		Quadrant Four: Active Elements			
		04	12	15	22
Normal	NSR	1.30/.106†	.029/.005	4.66/.805†	.002/.001
	Load	2140/173	2504/71	2580/18	2224/98
Mal.	NSR	1.66/.811†	.015/.007	.166/.089†	.023/.005
	Load	1886/67	1810/67	1806/67	1570/40
Ost.	NSR	4.91/2.31†	.003/.002	5.72/.782‡	.010/.005
	Load	1561/85	1632/129	1592/142	1468/102

		Quadrant Five: Active Elements			
		13	28	33	38
Normal	NSR	.029/.007	1.20/.316‡	.007/.003	.005/.001
	Load	2518/76	2179/120	2309/67	2309/67
Mal.	NSR	.012/.007	.927/.169‡	.036/.006	.062/.002
	Load	1810/67	1548/67	1574/67	1575/67
Ost.	NSR	.013/.015	.392/.072‡	.012/.005	.009/.007
	Load	1592/142	1468/116	1592/49	1592/62

All responses are for a compressive load, unless otherwise specified.
†: Concave Bending Response and ‡: Convex Bending Response.

NSR: Normalized Signal Response
Load: Externally Applied Load (N)

Figure 7.27 a): Normalized signal output patterns: Specimen eight - Quadrants one and two.

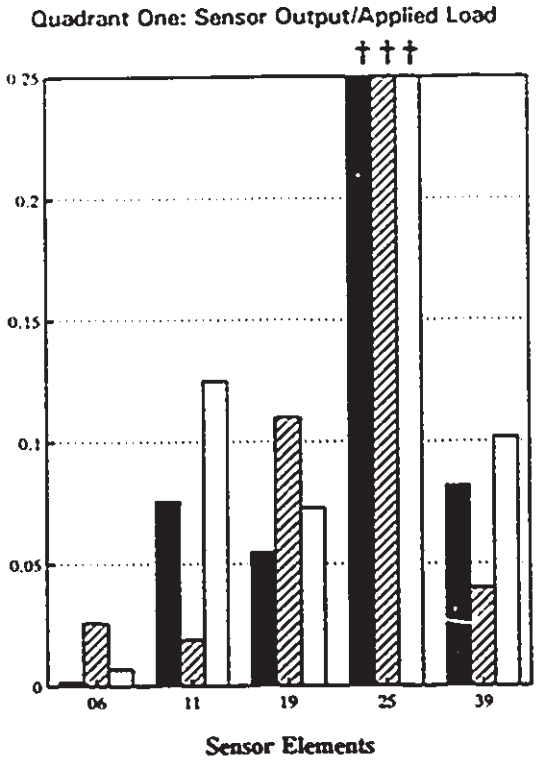

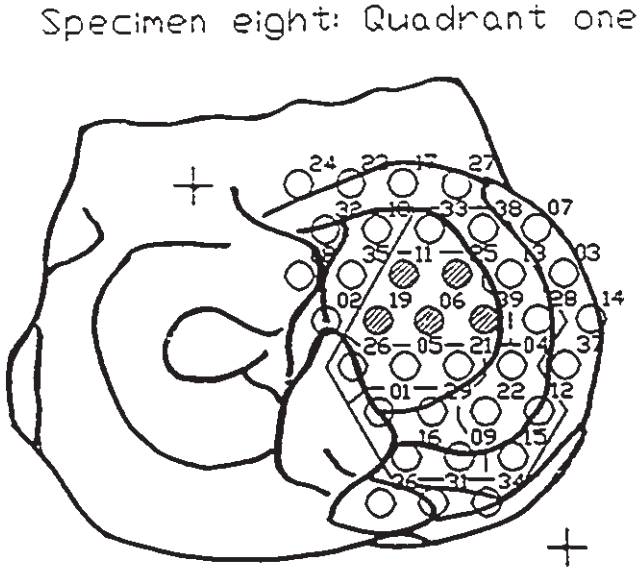

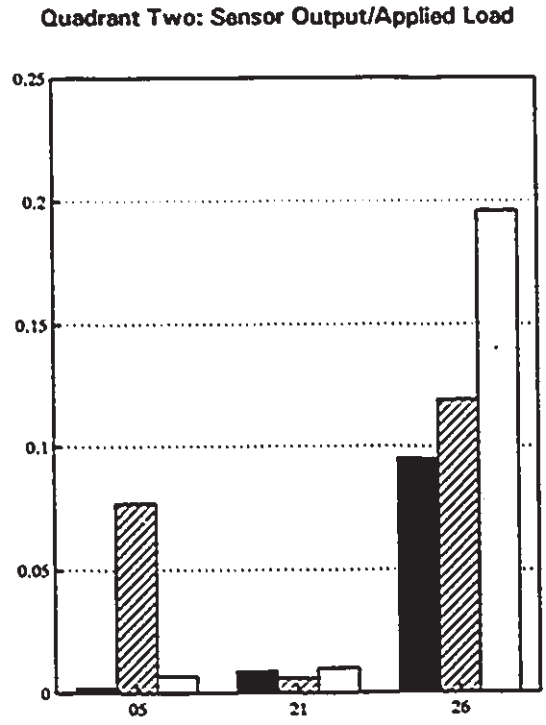

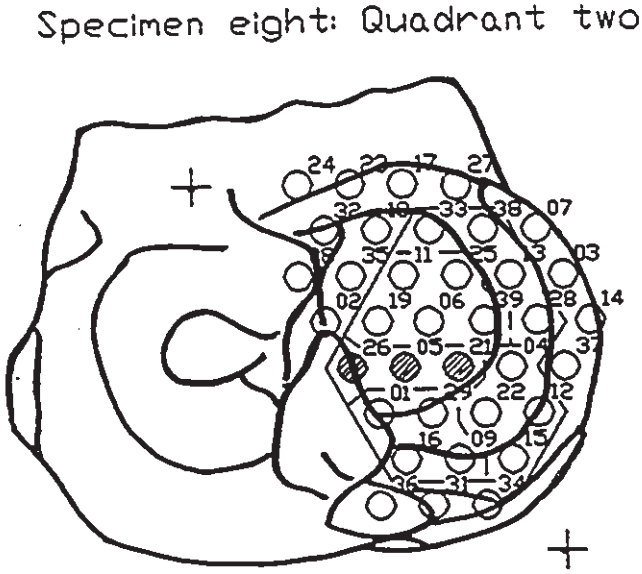

Figure 7.27 b): Normalized signal output patterns: Specimen eight - Quadrants three and four.

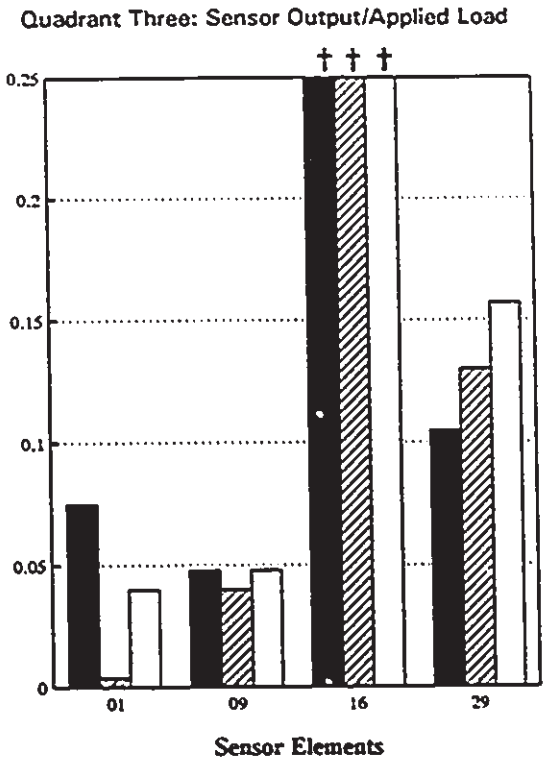

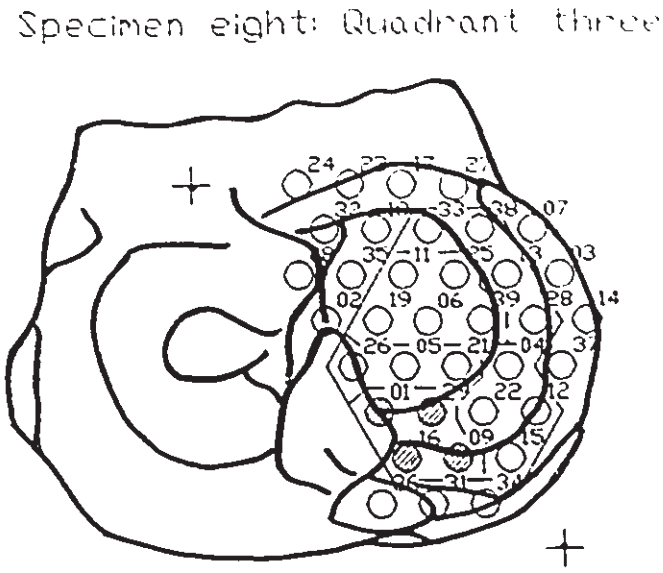

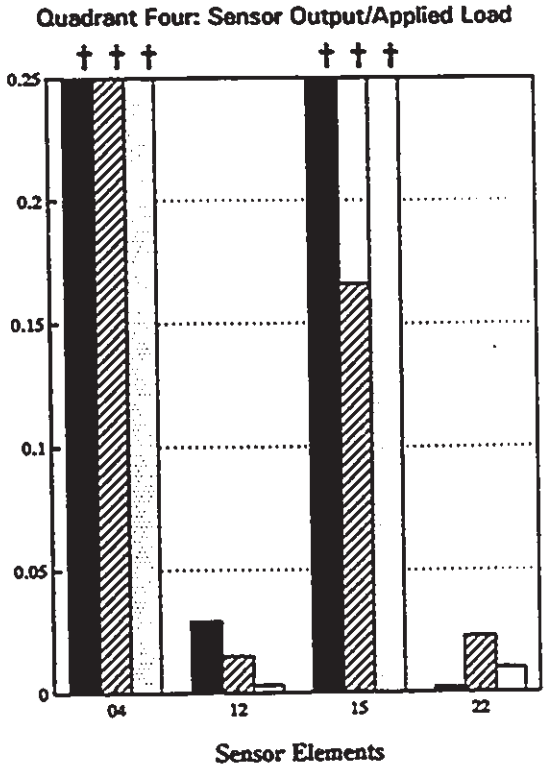

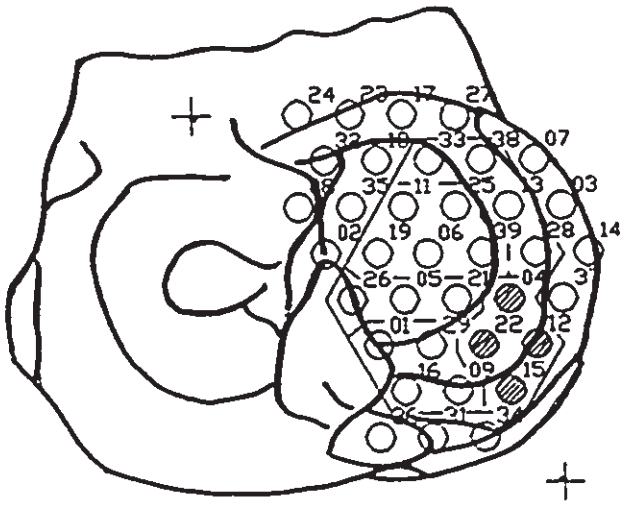

Figure 7.27 c): Normalized signal output patterns: Specimen eight - Quadrant five.

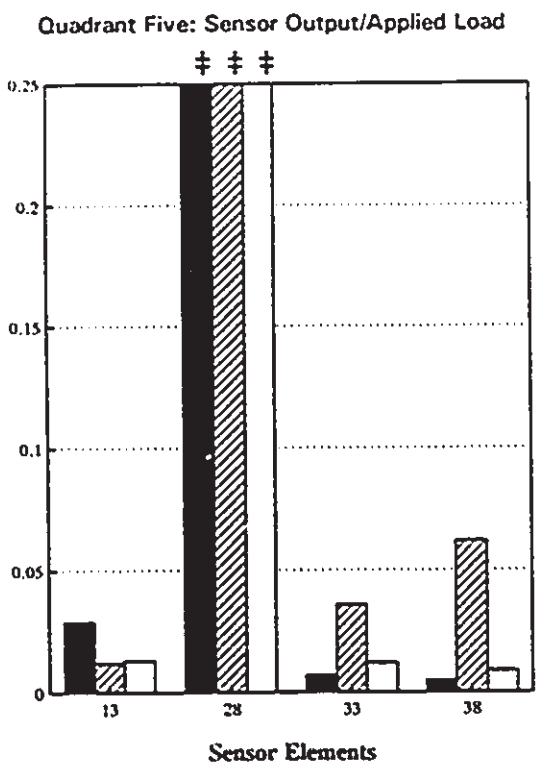

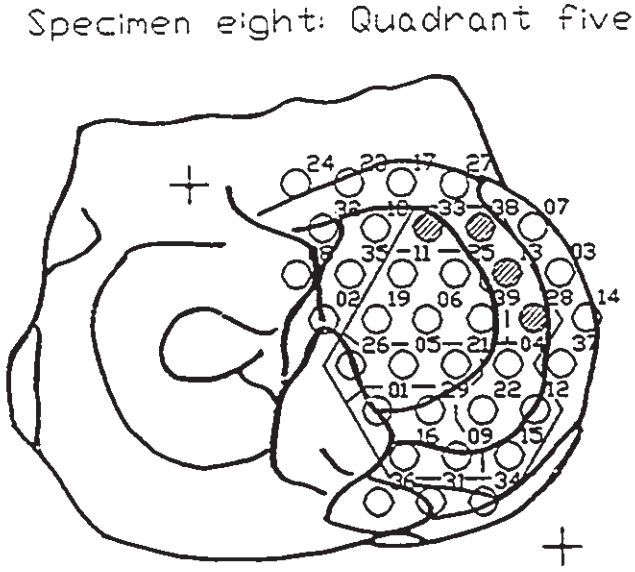

CHAPTER 8.0

DISCUSSION

8.1 Contact Area Patterns

8.1.1 Validity of Results

In order to assess the validity of the experimental results, the estimations of the contact area zones were compared to those obtained by other investigators [8,49,80,97,104,134,144] for similar testing conditions and a neutral tibiofemoral alignment. The contact area measurements at 0 and 20 degrees knee flexion are listed in table 8.1. Included in table 8.1 are contact area measurements given by other investigators for similar test conditions (Maquet [97]).

It should be restated that the measurement pad was designed to monitor the pressure variations across the tibial surface. Calculations of the contact area zones were, at best, estimations only, as the measurement pad was unable to determine the amount of surface area of each sensor element actually under contact. However, the technique still provided some insight into what regions of the medial compartment were mating with the medial femoral condyle.

The technique of quantifying the coverage of the contact zones, as outlined in Chapter 7, was structured to slightly over - estimate the contact area. That is, the contact area was considered to extend beyond the boundaries of all of the peripheral elements, rather than across a portion of them. However, if the contact zone was recalculated as that

Table 8.1: Measurements of the Coverage of the Medial Tibial Compartment

Specimen Number	Original Area Coverage (cm^2)			Modified Area Coverage (cm^2)			External Load (N)
	0°	20°	Total	0°	20°	Total	
one	9.38	9.87	10.72	6.19	6.30	6.57	1900
two	7.86	8.72	9.15	5.09	5.41	5.48	2039
three	9.09	6.73	10.32	6.20	4.84	6.57	1394
four	9.00	7.28	9.00	5.70	5.20	5.70	1707
five	8.23	8.23	8.23	5.04	5.04	5.04	1838
six	9.38	6.50	9.38	4.16	3.86	4.16	1867
seven	7.75	7.32	10.12	4.75	4.53	4.82	1771
eight	8.65	7.75	8.65	5.48	5.19	5.48	2288
Average	8.67	7.80	9.45	5.33	5.05	5.48	1850

Other Studies	Medial Coverage (cm^2) 0°	15°	Load (N)
Baratz [8]	7.6		1800
Fukubayashi et al. [49]	6.4		1000 - 1500
Riegger et al. [134]	7.5		1958
Seedhom et al. [144]	6.1		668
Kettalkamp et al. [80]		3.9	78
Maquet [97]		9.4	2200
McKellop et al. [104]		7.9	2400

area enclosed by joining the centre points of all of the peripheral active elements, then the remeasured areas fell within the original estimations and those reported by other investigators. The modified contact area zone of specimen one is demonstrated in figure 8.1. The recalculated values of the contact area zones of the remaining specimens are also listed in table 8.1.

8.1.2 Coverage of Medial Compartment

When a compressive load is applied across the knee joint, the femoral condyles contact the cartilage surface of the tibia and the meniscus. When and where contact occurs has not been consistantly agreed upon in the literature. Fairbank [48] stated that the cartilage surface deformed first before the meniscus contacted the femur, whereas Takei [155] suggested the femur and tibia possibly never come into contact. Seedhom [143,144] indicated that a thicker meniscus may prevent or limit contact between the femur and tibia.

Results from previous experimental investigations directly measuring the contact pressure at the tibial plateau surface have shown that both the central cartilage region and the meniscus share in transmitting load through the knee joint (Maquet [98], Ahmed et al.[3]). Bylski-Austrow et al. [21] assessed the meniscal movements under simulated physiological applied loads and conluded that the knee joint could not assume a position in which the menisci were not sharing in the transmission of stress between the tibia and femur.

The resulting area patterns from the current study also demonstrated that contact occurred across both the central articular

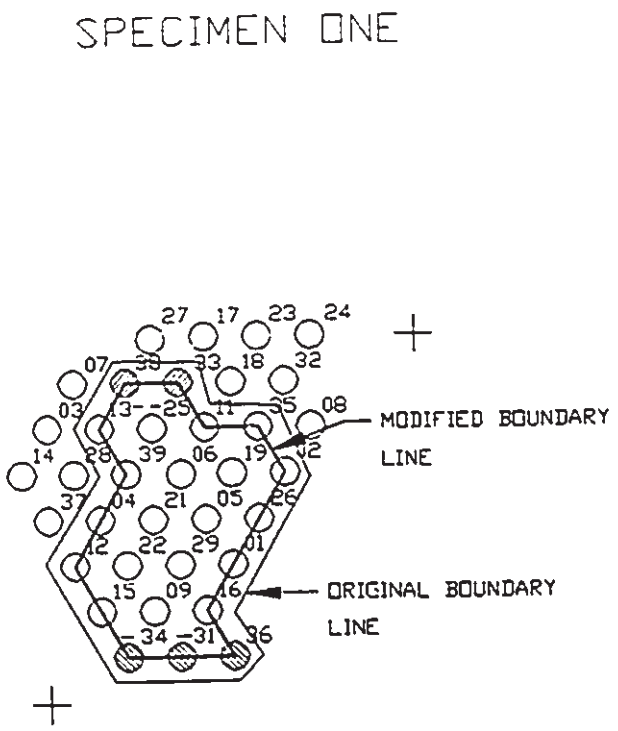

Figure 8.1: Modified contact area zone of medial compartment of specimen one.

cartilage surface and surrounding meniscus. In addition, all regions of the mensicus were under contact during some phase of test cycle; ie. elements located at the anterior, lateral and posterior sections of the meniscus registered some level of activity. Although elements located at the edges of the mensicus registered activity, many of these elements were affected by the increased surface curvature, and responded with bending - type signal outputs. As a result, the level of load transmitted over this area was not quantifiable. Nevertheless, activity at these elements confirmed the belief that they shared in the load transmission, and that the mensicus served to widen the overall tibiofemoral contact area.

8.1.3 Effects of Knee Alignment

Although a 20° varus malalignment caused a shift in the knee centre relative to the load bearing axis, no changes in the size of the contact area zone were observed. Those sensor elements confirmed to be active during the neutral alignment tests remained active for both the malaligned and realigned post-osteotomy alignment tests. However, as indicated previously, although it was possible to identify the contact area of the medial compartment, contact pressure could only be looked at in relative terms, but not absolute ones. No changes were noted in the size of the contact coverage on the medial tibial compartment for the different tibiofemoral alignment conditions, nor did any apparent systematic shift in the location of the contact area zone occur.

8.1.4 Effects of Knee Flexion

Knee flexion brought about a reduction in the measured contact area zones in six of the eight knee specimens. The averaged contact areas at complete knee extension measured 8.67 cm^2 and decreased to 7.8 cm^2 by 20° knee flexion. These observations were similar to those found by other researchers [99,114]. As well as becoming progressively smaller, the contact zones were also noted to move in a posterior direction on the tibial plateau. Recall that maximal loading occurs at approximately 20° of flexion during the stance phase of the walking cycle. Thus, having a reduction in the contact zone at a time of maximal loading has a net effect of increasing the load per unit area of the medial compartment, ie. the average contact pressure increases.

8.2 Contact Pressure

8.2.1 Limitations and Validity of the Measurement Readings

Although the measurement pad was designed and calibrated for compressive loads, the increased surface curvature of the medial compartment and femoral condyle, and the viscoelastic nature of the meniscus, promoted conditions of element bending. As such, no bending-mode calibration factors could be obtained. This limited part of the analysis to a qualitative discussion on the relative changes in the contact pressure. Those elements most often affected were located either along the base of the intercondylar eminence, on the meniscus itself, or at the cartilage - meniscus junction. As well, any tears or relative movement of the meniscus enhanced the occurrence of element

bending. Therefore, rather than quantifying the actual change in the contact pressure at each active element, a relative comparison of the normalized signal responses was carried out for the three different alignment configurations.

The format of presenting the signal data involved normalizing the signals with respect to the applied load. This step compensated for any minor differences in the final load applied during each successive test cycle. Conversion to a normalized pressure value required dividing the normalized data by the amount of area coverage of each element. When the grid area was used and the external load was assumed to be shared between tibial compartments, as in the neutral and post-osteotomy cases, a value of 10% equated to an average pressure ranging between 0.8 and 2.8 MPa. Similarly, values of 25% equated to pressure ranges between 2 and 7 MPa. As stated previously in Chapter 7, these values were similar to previous measurement results given by other investigators (see table 7.1). However, in this study, less emphasis was placed on the actual pressure value, but rather, a relative comparison was carried out between the normalized readings of the neutral case and those of the realigned cases. In this way, both the compressive and bending - type responses could be included in the analysis.

8.2.2 Effects of Surface Coverage

Fukubayashi and Kurosawa [49] and Inaba and Arai [68] both observed initial increases in the contact area on the medial compartment when the applied load increased up to a finite load (less than body

weight), afterwhich the rate of enlargement of the contact area reduced. As a result, they concluded that the average contact pressure increased as the applied load increased. In this study, the magnitude of the applied loads exceeded those employed by Fukubayashi and Kurosawa [49] and Inaba and Arai [68], while the measured contact area zones on the medial compartment were of a similar size. Thus, a similar trend was observed here as well, where the contact pressure increased as the applied load increased.

8.2.3 Effects of Knee Flexion

As knee flexion progressed, an overall reduction in size of the contact zone occurred, and the location of the contact zone moved posteriorly, regardless of the knee alignment configuration. Consequently, the contact pressure across the posterior region increased. This was observed in six of the eight specimens.

However, for the first pair of knees tested, a relative increase in the contact coverage occurred between 0° and 20° knee flexion. This was attributed to less area being in contact at complete knee extension rather than more area coming under contact as the knee flexed. Some of the elements in the anterior region of these speciemens that were typically active in the other specimens, but inactive here, were element 18 in specimen 1, and elements 18 and 33 in specimen two. The loose attachment of the anterior horn of the meniscus contributed to the loss of contact at these elements, and the subsequent reduced surface coverage.

The increased contact pressure across the posterior region of

the medial compartment is probably caused by the fact that the medial meniscus can not undergo as much displacement as the lateral one, due to its stronger peripheral attachments. Thus, the increased contact pressure and restricted meniscal movement may help to explain the predominance of meniscal tears in the posterior aspect of the medial mensicus [3,21].

8.3 Varus Malalignment Configuration

Having the knee centre displaced laterally from the weight bearing axis, while rotating the adjacent limb segments to create the 15° varus deformity, resulted in minimal changes to the contact area patterns. However, the percentage of the external load directed to the medial compartment, theoretically, increased. This is demonstrated in figure 8.2 using a simple 2-D model of the knee. The increased malalignment created a condition of unicompartmental loading, where tension in the lateral collateral ligament and quadriceps muscle was required to counterbalance the over - turning external moment and stabilize the joint.

Kettalkamp and Chao [81], and Minns [109] developed simple two dimensional analytical models of the knee to assess the force behaviour at each compartment for different alignment conditions. They showed that as the varus alignment increased, a condition of single point contact occurred on the medial compartment where the load increased proportionally to the external moment. What remained unknown was the relative change that occurred in the contact pressures at different locations on the articular surface of the joint.

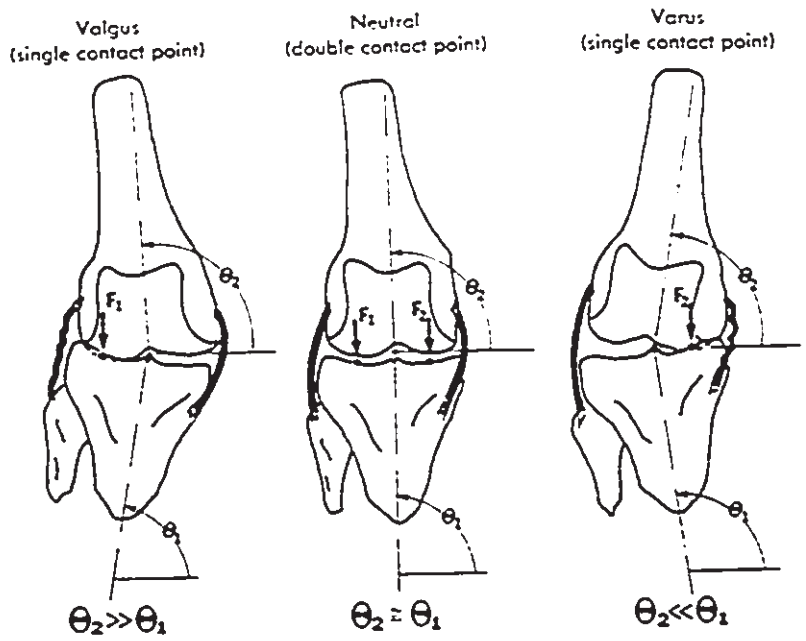

Figure 8.2: Effects of varus/valgus alignment on knee joint compartment loading in anteroposterior plane. Mechanical axes of the femur and tibia are used for measurement of angles θ_1 and θ_2 [25].

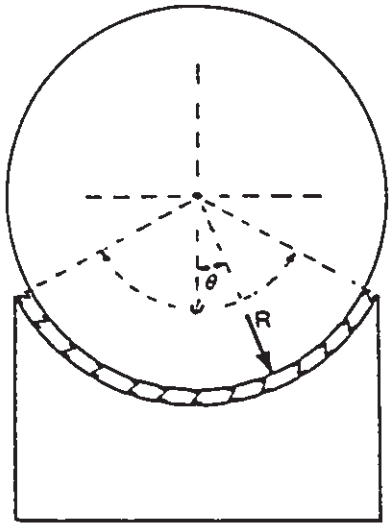

Figure 8.3: Two dimensional hinged joint model proposed by An et al. [4]. The available articular surfaces are expressed by the subtended angle of ψ. The externally applied load, R, is located at the angle, θ, from the centre of the arc.

An et al. [4] developed a generalized method, based on the rigid spring model, to determine the two dimensional joint contact pressure of any shape of articular surface. The derivation of the model was based on the minimum strain energy principle, as used in most of the formulation of finite element codes [4]. The model was applied to a hinge joint having two ideal congruent circular arc surfaces, and is shown in figure 8.3. The model calculated the magnitude of the peak pressure (Pm) at any given point on the articular surface, as well as, the direction and amount of the relative (or attempted) displacement between the two surfaces. The results of the hinged joint case are shown in figure 8.4. The location of the resultant joint force (R) on the articular surface is given by θ, and the angle ϕ represents the direction of the virtual displacement (U); both are measured from the centre of the circular arc.

Their results for off - centre loading of the pressure distribution indicated that the peak pressure increased as the point of application of the load approached the edge of the supporting arc, and the relative direction of the rigid body coincided with the direction of the external load, when the applied load was located centrally. However, as the load was applied eccentrically, the direction of the virtual displacement deviated from that of the applied load, and approached the edge of the arc. From these results, they hypothesized that three types of motion conditions existed between the two rigid bodies, all of which were functions of the directions of the resultant joint force and virtual displacement vector. Referring to figure 8.5, the three conditions are: 1) a stable joint with minimal displacement,

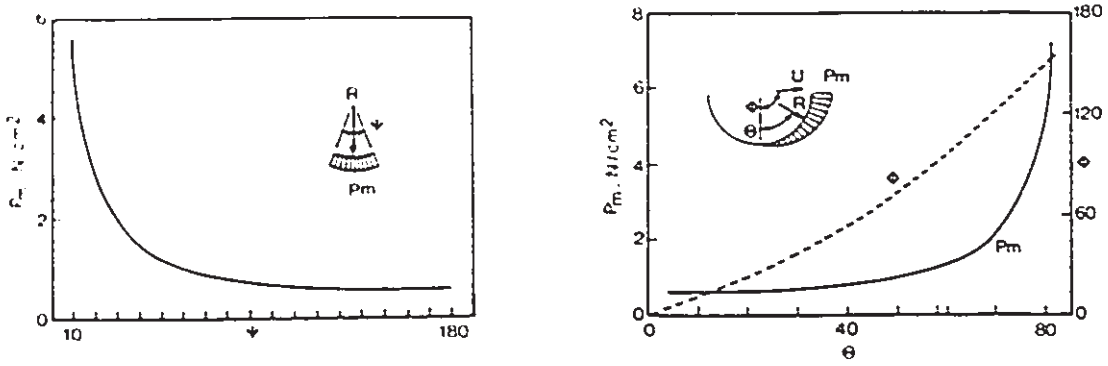

Figure 8.4: Results of hinged joint model [4]. The peak pressure, Pm, on the articular surface and the direction of the virtual displacement of the articulating bodies, U, are related to the available contact surface enclosed by angle ψ, and location θ, of the resultant joint force. The effect of $\theta = 0^{\circ}$ is shown on the left, and the effect of $\theta = 180^{\circ}$ is shown on the right.

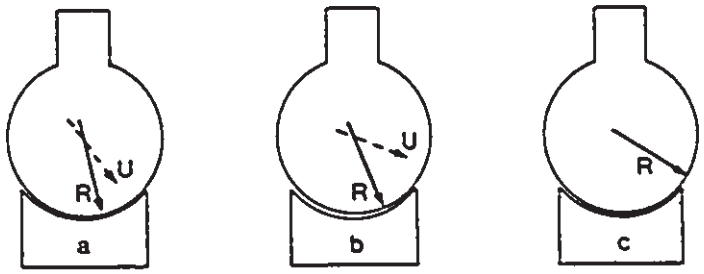

Figure 8.5: Three types of motion conditions hypothesized by An et al. [4], based on the relationship of the directions of the resultant joint force, R, and the virtual displacement, U, of the articulating body: a) stable, b) subluxation, c) dislocation.

having both the joint force and relative displacement vectors pass within the bounds of the articular surface, 2) subluxation of the joint caused by the resultant force passing within the arc of the surfaces but the virtual displacement passing outside, or 3) complete dislocation of the joint, when both the resultant force and virtual displacement vectors pass outside the articular surface.

If their hypotheses were correct, the case of the malaligned knee would direct the reaction force vector across the medial compartment away from the joint centre. As a result, the contact pressure on the central and outer - lateral regions of the medial compartment should increase, while the inner region of the compartment should experience a reduction in contact pressure. Final assessment of the experimental data involved a local, element by element, analysis of the normalized pressure responses.

8.3.1 Central Region

Elements identified within the central region of the medial compartment, not covered by the meniscus, were assigned to quadrants one and two. The normalized response data indicated a consistant level of compressive loading occurred between the medial femoral condyle and the articular surface of the tibia. The flatter, more congruent mating surfaces permitted the measurement pad to function as designed, and respond to the compressive loads.

Elements located along the inner aspect of these quadrants typically experienced a reduction in the normalized pressure values, whereas those in the central and outer aspects either increased or

remained unchanged from the neutral alignment results. These findings indicate an outward shift in the load vector, and confirm the previous observations of An et al. [4], Kettalkamp and Chao [81], and Minns [109].

8.3.2 Peripheral Region

The remaining active elements, laid across the periphery of the compartment, and were typically in contact with the meniscus. Overall, a greater incidence of element bending was observed, and attributed to both the viscoelastic properties of the meniscus and the increased surface curvature.

Elements in the inner posterior region (quadrants three) responded with lower normalized pressure values, similar to that observed at elements in the central region. Since a greater portion of the external load was borne by the medial compartment, the reduction in contact pressure across quadrant three must have been accompanied by an increase in contact pressures at elements in the adjacent quadrants. This was confirmed by the responses of elements in quadrant four. Some of the elements were positioned along the outer region on the meniscus or along the cartilage - meniscus interface, and were thus affected by the increased surface curvature of the mating surfaces and the height differences at the interface junction. Consequently, bending of the elements occurred. Nevertheless, a similar response to that already observed across the central region reoccurred here, as the signal magnitudes were typically greater for the maligned knee case than for the neutrally aligned one.

A different trend was present in the signal patterns of the extreme anterior elements, where a reduction in the signal peaks was detected. As well, many of these elements no longer maintained contact when the knee was flexed 20°. The realignment delayed the onset of loading to this region, thereby reducing the time during which the elements were compressed. This may not have occurred if the quadriceps muscle had been used to load the joint (Riegger et al. [134]).

8.4 Post-Osteotomy Alignment Configuration

The simulated osteotomy alignment had no affect on the resultant contact area patterns, and the percentage of external load directed to the medial side was equivalent to that used for the neutral alignment tests. The only factor differing between the two alignments was the tilt of the plateau surface relative to the horizontal reference frame, sloping downward in the medial to lateral direction. The final arrangement is shown in figure 8.6, and introduced a slight shearing component across the plateau surface. This was mostly resisted by the geometrical conformity of the condylar surfaces and the ligamentous structure (Hsieh and Walker [62], Morrsion [113]).

Riegger et al. [134] measured the contact pressure on the tibial plateau for simulated knee alignments of neutral and a 5° close wedge osteotomy. They found that the osteotomy was unable to reliably reduce the average and maximum pressures on the medial compartment. However, their analysis was completely static, and did not include any multi - site assessment. As a result, they were unable detect any shifts in the direction of the contact force across the compartment, as well as,

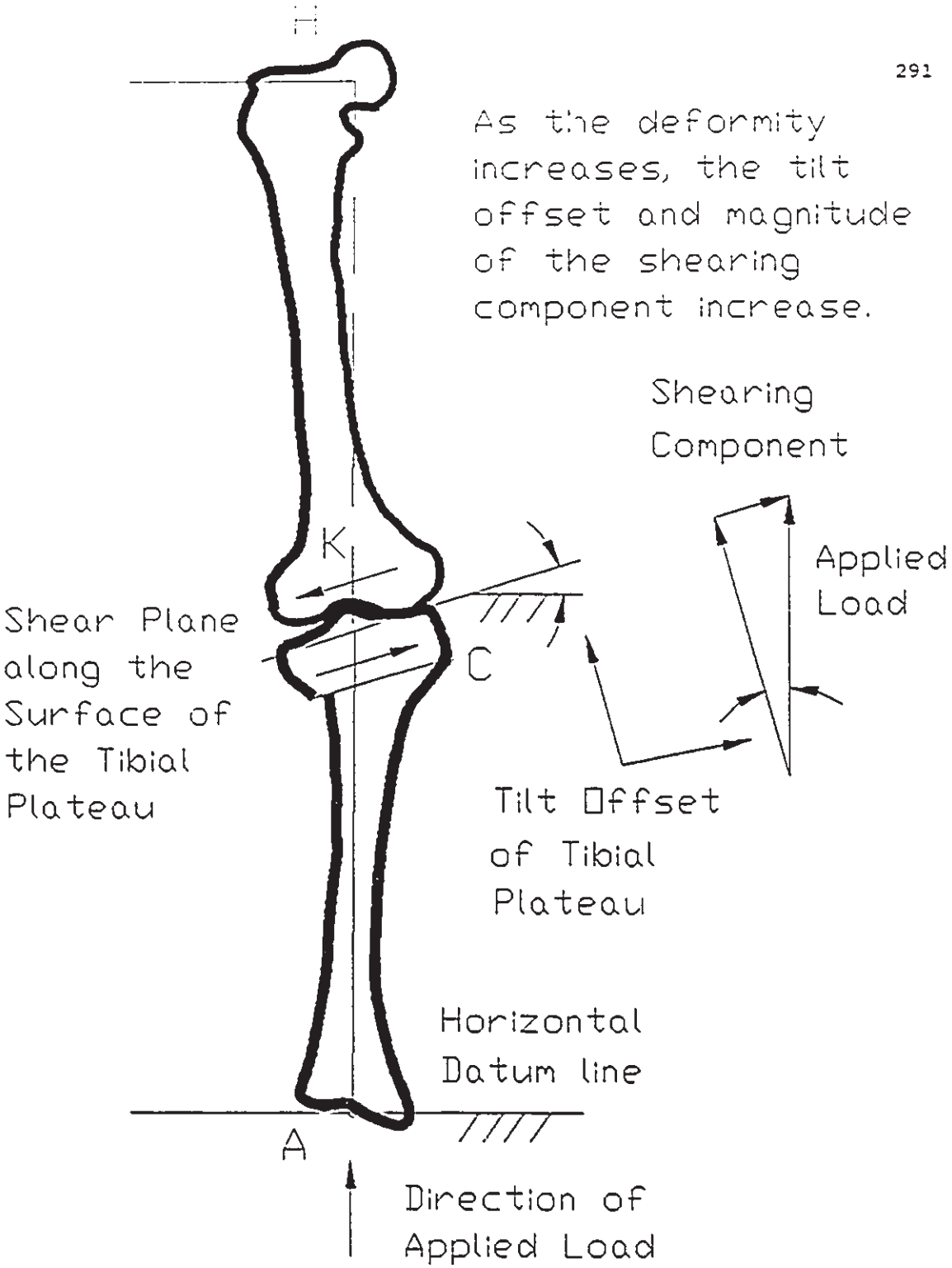

Figure 8.6: Introduction of a shearing component across the tibial plateau surface with increased alignment deformity.

whether or not the intercondylar eminence contributed to resisting the shearing load.

Application of An's model [4] to the post-osteotomy condition indicated a type 1 condition existed, where both the force and displacement vectors passed through the bounds of the articular surface. The realignment altered the level of loading amongst the active elements in the region. As well, if the shearing load tending to sublux the joint was partially resisted by the conforming surfaces of the intercondylar eminence, an increase in the pressure readings would occur at those elements located in this region.

8.4.1 Central Region

Those elements in direct contact with the articular surface of the tibia were assigned to quadrants one and two. A response pattern similar to that of the neutral alignment case reoccurred during the post-osteotomy alignment tests, where compressive signal responses prevailed. However, the degree of loading at each element varied, as most signal peaks either increased or decreased, while few remained at the same level. This indicated a minor redistribution of the external load. Unfortunately, no consistant pattern was detected between specimens regarding which elements increased or decreased, except at those elements located along the extreme inner edge.

8.4.2 Peripheral Region

The peripheral region included elements in quadrants three, four and five, and typically included half of all active elements. Response

patterns along the inner posterior surface (quadrant three) either increased or remained unchanged relative to the neutral arrangement. This confirmed the concept of the contact force translating inward towards the joint centre.

Contact pressure readings along the outer posterior region (quadrant four) and central - lateral edge (parts of quadrant five) either reduced or remained unchanged. Of those specimens having a pressure reduction, an increase in pressure was detected along the inner edge. This also supports the notion of the contact stress moving towards the joint centre following an osteotomy.

Finally, contact pressure readings throughout the extreme anterior region either reduced or remained unchanged. A similar trend was present when the knee was malaligned. Of those specimens having a reduction, pressure levels were increased in the posterior central region. The realignment altered the surface conformity, thereby changing the contact behaviour and delaying the onset of loading.

CHAPTER 9.0

CONCLUSIONS

9.1 Original Contributions

Three unique and original contributions were generated through this research work, and included: 1) the design of a direct measurement system for local dynamic contact pressures in a knee joint, 2) the retrofitting of an existing (non - operative) joint simulator capable of controlling the joint flexion angle and joint compressive load, and 3) development of an analytical model of the lower extremity that analyzed the conventional methodology of high tibial osteotomy surgery. A brief discussion of each is provided next.

9.1.1 Pressure Measurement System

The objective of this research was to monitor, in vitro, the local dynamic contact pressure behaviour between the articular surfaces of the knee for different lower extremity alignment conditions. Previous studies of contact pressure measurement between articular surfaces have mostly been limited to static techniques. A novel measurement system was designed and developed that permitted local measurement of the dynamic pressure patterns across the tibial plateau surface. A custom designed measurement pad was fabricated that could be inserted between the knee joint surfaces, and provided complete coverage of the medial tibial compartment.

A dedicated signal conditioning hardware and data acquisition

system were also produced to process the signal responses. Currently there are no measurement systems available, specifically designed for the knee joint, that satisfy the above delineated objectives. The data acquisition system was also customized to be compatible with the operating control software of the joint simulator.

The proposed measurement system provided a reliable and reproducible method for direct measurement of local dynamic contact pressures in cadaveric knee joints. Furthermore, the technology incorporated in the design of the measurement pad could also be employed to design other dedicated measurement systems for different articular joints, which are currently unavailable.

9.1.2 Joint Simulator

This research required the use of a mechanical testing apparatus capable of simulating the dynamic motion of the knee during normal level walking. Use of an MTS or Instron machine would have resulted in the application of a cyclic dynamic load to the articular surface of a fixed, motionless cadaveric joint. This, however, would not have simulated the dynamics of load involved in a physiological situation, where there is motion of the two articulating surfaces.

An existing joint simulator, originally stated to be functional, was made available for this work. However, due to equipment malfunctions and shortage of funding, the apparatus was later determined to have never been operational. Numerous design modifications were completed before the simulator was functional, and operating in a reliable and consistant manner. As a result of these contributions, the

joint simulator has evolved into a valuable testing apparatus which can be used for future research endeavours in orthopaedic joint biomechanics.

In summary, these contributions (ie. pressure measurement system, joint simulator and data acquisition system) permitted direct measurement of local contact pressures in a cadaveric knee joint in which physiological load and movement conditions were simulated.

9.1.3 Analytical Model of High Tibial Osteotomy Surgery

A two dimensional trigonometric model of the lower extremity was formulated which provided a more precise method of analyzing and forecasting the changes to the knee joint and lower limb orientations following high tibial osteotomy surgery. The model also provided information on the changes required at the adjacent hip and ankle joints to achieve the realigned orientation, as well as, changes to the overall standing leg length and the final orientation of the tibial plateau surface relative to a horizontal reference frame.

An interactive computer program of the trigonometric model was developed to be used by the orthopeadic surgeon during the preoperative stages of a high tibial osteotomy. The model identified the limitations and errors associated with the conventional methodology of the close wedge and dome osteotomies. The most common technical error limiting the outcome of high tibial osteotomy surgery has been under-correction of the deformity. However, there is a general lack of objective criteria that supports the thoeretical justification of the different procedures. A modified approach to each surgical method was thus

formulated that resolved these limitations and errors, with the intent to improve the post-operative success rate of the osteotomy.

Lastly, the model was used to redefine the terminology of over-correction or under-correction of the tibiofemoral angle, so as to relate to a neutral limb alignment. This enabled one to more accurately describe the resultant lower limb alignment and permitted comparison of this alignment between the different surgical methods.

9.2 Concluding Remarks

9.2.1 Limitations of the Experimental Model

The experimental work included a number of assumptions inherent with testing of cadaveric specimens in which physiological load and movement conditions were simulated.

1. The model permitted four degrees of freedom. The varus/valgus offset could be set but remained fixed for the duration of the test cycle, and medial-lateral translation between the tibia and femur was restricted.
2. A multitude of different alignment configurations (neutral, varus or valgus malalignment, and realigned post-osteotomy) can occur at the knee. However, the test results are valid for the conditions under which the joint was positioned and loaded; ie. 0° to 20° knee flexion and loads ranging between 1 to 3.5 times body weight.
3. Neutral alignment of each specimen (to within a few degrees) could be achieved using the proposed alignment jig. It should be noted that the remaining two alignment conditions were relative to the neutral configuration and were consistantly reproducible.

4. All knees were tested under a purely axial compressive load that was directed up through the centre of the femoral condyles in the neutral case. This, however, allowed the measurement of the contact pressures and areas associated with a neutrally alignment knee to be compared with those from previous studies.

5. The effects of alignment variations on the medial tibial compartment only were analyszed; no analysis was performed on the lateral tibial compartment.

6. A simulated osteotomy can not account for the biological repair that occurs at the surface of the osteotomy cut, and at any degenerative articular cartilage.

7. Continually bathing the specimen and articular surface between test cycles reduced the side effects of testing the specimen over a six to eight hour period.

8. Reproducibility is a typical problem in tests with biological tissue. An inherent hysterysis loop occurs in the force - displacement curve, as the tissue relaxes under load. Other investigators have cyclically loaded the specimens prior to data collection to enable the tissue to reach a steady state mode. In this study, the specimens were preconditioned prior to data collection, and average values of the output data were calculated from five successive test cycles.

9. The contact area patterns were estimated as planar projections of the tibial surface, and did not include the changing curvature of the surface. This, however, allowed for comparison and validation of the area results to those given by other investigators employing similar measurement techniques.

10. The thickness of the measurement pad was assumed not to have altered the contact behaviour between the mating surfaces, but may have generated higher pressure readings overall, compared with other measurement devices. A similar limitation was encountered with the measurement technique employed by Walker and Erkman [160].

11. The scatter of the normalized peak pressure readings for the different alignment configurations and knee specimens, as reflected by the large standard deviations, may have been caused by the variations in the sizes and shapes of the knee specimens, and the quality of the articular cartilage and meniscus. Thus, only a comparative analysis of the local pressure variations within each specimen was carried out between the different alignment configurations.

12. Eight knee specimens were tested; testing more knee specimens under similar conditions may help to confirm that the observed trends in the pressure patterns for the three alignment configurations were significantly different.

9.2.2 Findings of the Analytical Model

A two dimensional trigonometric model of the lower extremity was developed and formulated into a computer program that was used to review the methodology of the close wedge and dome osteotomies. The model clearly demonstrated the limitations of each method when the conventional procedure was implemented. In the case of correction of a varus tibiofemoral malalignment, the final rotational correction of the tibia was always less than the original alignment deformity, hence producing an under-corrected tibiofemoral alignment. Furthermore, the

amount of additional correction beyond that predicted by the conventional procedure, increased as the original malalignment deformity increased. That is, more additional rotation was necessary for a 20° varus deformity than for a 10° one.

The computer program was also modified to determine the actual wedge correction or rotational correction necessary to restore the tibiofemoral angle to a neutral orientation (or any other preferred alignment, ie. an over-corrected valgus tibiofemoral angle).

Lastly, consideration to the final placement of the osteotomy on the proximal tibia relative to the length and width of the tibia could be included in the preoperative planning stages. It was determined that the degree of additional correction always increased as the ratio of the depth of cut to tibia length increased, as well as with an increase in the ratio of the depth of cut to tibial width.

9.2.3 Findings of the Experimental Model

The results of the contact area patterns of the medial compartment were in good agreement with those from previous investigators. However, previous studies were often limited to static loading conditions and were seldom able to consider the effects of joint rotation on the contact area. In this research, joint flexion reduced the surface coverage of the medial compartment. However, when the joint alignment was altered (ie. varus or post-osteotomy), no differences were noted in the contact area patterns.

When a varus tibiofemoral alignment was simulated, a decrease in local contact pressures were observed across the anterior region of the

medial compartment. This was compensated by an increase in the local contact pressures throughout the central region of the medial compartment, uncovered by the meniscus. In the peripheral region of the compartment, decreases in local pressures were registered along the inner posterior region, while the outer lateral region typically remained unchanged or increased slightly.

The experimental results for the simulated post-osteotomy alignment case indicated an increase in local pressure readings along the base of the intercondylar eminence. This was often accompanied by a reduction along the lateral edge of the compartment near the cartilage - meniscus junction, as well as on the meniscus itself. This supported the concept of an inward shift in the contact force on the medial compartment following a high tibial osteotomy, which relied on surface conformity and ligamentous structures to maintain joint stability and prevent joint subluxation.

Contact was maintained across the central region of the medial compartment, uncovered by the meniscus. A trade off of increasing and decreasing pressures was present throughtout the central region. However, no consistant trend was present between specimens regarding which elements increased or decreased, except along the extreme inner edge.

9.4 Future Work

In addition to the work already undertaken to quantify the biomechanics of high tibial osteotomy surgery, future research work may include: 1) identification of the threshold knee joint alignment, where

the joint force dramatically shifts to the medial compartment, for an increased varus malalignment, ie. an acceptable/critical amount of varus deformity, 2) the amount of overcorrection of the tibiofemoral angle required before the load borne by the lateral compartment reaches a steady state and no longer increases, 3) upgrading of the analytical model to include the effects of an internal/external rotational deformity of the femur or tibia. This would expand the model into three dimensions.

The proposed pressure measurement system and redesigned joint simulator could also be employed to investigate other orthopaedic biomechanic research projects, not directly related to osteotomy surgery. The technology incorporated in the design of the pressure measurement pad for the knee joint could also be employed to design dedicated measurement systems for other articular joints. Such a system would permit a direct method of measuring, in vitro, the local dynamic contact pressure patterns at the articular surface of the joint.

The joint simulator could also be used in other research projects, including 1) wear testing of total replacement joint materials, 2) performance evaluation of the initial fixation of different knee implant designs, and 3) evaluation and comparison of internal fixation methods employed in lower extremity surgery.

REFERENCES

1. Aglietti, P., Rinonapoli, E., Stringa, G., and Taviani, A. Tibial Osteotomy for the Varus Osteoarthritic Knee, Clin. Orthop. Rel. Res., 176, 1983.

2. Ahmed, A.M., A Pressure Distribution Transducer for In Vitro Static Measurements in Synovial Joints, J. of Biomech. Eng., 105, 1983.

3. Ahmed, A.M. and Burke, D.L., In Vitro Measurement of Static Pressure Distribution in Synovial Joints - Part 1: Tibial Surface of the Knee, J. of Biomech. Eng., 105, 1983.

4. An, K.N. and Chao, E.Y.S., Kinematic Analysis of Human Movement, Annals of Biomed. Eng., 12, 1984.

5. An, K.N., Himeno, H., Tsumura, H., Kawai, T., and Chao, E.Y.S., Pressure Distribution on Articular Surfaces: Application to Joint Stability Evaluation, J. Biomech., 23, (10), 1990.

6. Andriacchi, T.P., Galante, J.O., and Fermier, R.W., The Influence of Total Knee Replacement Design on Walking and Stair Climbing, J.B.J.S., 64-A, (9), 1982.

7. Ateshian, G.A., Soslowsky, L.J., and Mow, V.C., Quantification of Articular Surface Topography and Cartilage Thickness in Knee Joints using Stereophotogrammetry, J. Biomech., 24, (8), 1991.

8. Baratz, M.E., Fu, F.H., and Mengato, R., Meniscal Tears: The Effect of Menisectomy and Repair on Intraarticular Contact Areas and Stress in the Human Knee. A Preliminary Report, Am. J. Sports Med., 14, 1986.

9. Bärr, H.F. and Breitfuss, H., Analysis of Angular Deformities on

Radiographs, J.B.J.S., 71-B, (4), 1989.

10. Bean, J.C., Chaffin, D.B., and Schultz, A.B., Biomechanical Model Calculation of Muscle Contraction Forces : A Double Linear Programming Method, J. Biomech., 21, (1), 1988.

11. Berman, L., Mitchell, R., and Katz, D., Ultrasound Assessment of Femoral Anteversion - A Comparison with Computerized Tomography, J.B.J.S., 1987.

12. Berman, A.T., Zarro, V.J., Bosacco, S.J., and Israelite, C., Quantitative Gait Analysis after Unilateral or Bilateral Total Knee Replacement, J.B.J.S., 69-A, (9), Dec. 1987.

13. Berns, G.S., Hull, M.L., and Patterson, H.A, Implementation of a Five Degree of Freedom Automated System to Determine Knee Flexibility In Vitro, J. Biomech. Eng., 112, 1990.

14. Blankevoort, L., Huiskes, R., and de Lange, A., Helical Axes of Passive Knee Joint Motions, J. Biomech., 23, (12), 1990.

15. Bohannon, R.W., Tiberio, D., and Zito, M., Selected Measures of Ankle Dorsiflexion Range of Motion: Differences and Incorrections, Foot and Ankle, 10, (2), 1989.

16. Brinckmann, P., Frobin, W., and Hierholzer, E., Stress on the Articular Surface of the Hip Joint in Healthy Adults and Persons with Idiopathic Osteoarthrosis of the Hip Joint, J. Biomech., 14, (3), 1981.

17. Brown, T.D., Anderson, D.D., Nepola, J.V., Singerman, R.J., Pedersen, D.R., and Brand, R.A., Contact Stress Aberrations following Imprecise Reduction of Simple Tibial Plateau Fractures, J. Orthop. Res., 6, 1988.

18. Brown, T.D. and Shaw, D.T., In Vitro Contact Stress Distributions in

the Natural Human Hip, J. Biomech., 16, (6), 1983.

19. Bryant, J.T. and Cooke, T.D.V., Standardized Biomechanical Measurement for Varus-Valgus Stiffness and Rotation in Normal Knees, J. Orthop. Res., 6, 1988.

20. Pullough, P. and Goodfellow, J., The Significance of the Fine Structure of Articular Cartilage, J.B.J.S., 50-B, 1968.

21. Bylski-Austrow, D.I., Goldstein, M.J., Ciarelli, and Mathews, L.S., Correlation of Meniscal Failure Patterns with Meniscal Displacements and Surface Strains Measured In Situ, ASME DE - Vol. 6, 1987.

22. Cass, J.R. and Bryan, R.S., High Tibial Osteotomy, Clin. Orthop. Rel. Res., 230, 1988.

23. Chand, R., Haug, E., and Rim, K., Stresses in the Human Knee Joint, J. Biomech., 9, 1976.

24. Chao, E.Y.S., Rim, K., Smidt, G.L., and Johnston, R.C., The Application of 4x4 Matrix Method to the Correction of the Measurements of Hip Rotations, J. Biomech., 3, 1970.

25. Chao, E.Y.S., Biomechanics of High Tibial Osteotomy, in American Academy of Orthopaedic Surgeons : Symposium on Reconstructive Surgery of the Knee. St. Louis, C.V. Mosby, 1978.

26. Chow, C.K. and Jacobson, D.H., Studies in Human Locomotion via Optimal Programming, Math. Biosci., 10, 1971.

27. Cooke, T.D.V., Saunders, G., Siu, D., Yushioka, Y., and Weavers, H., Universal Bone Cutting Device for Precision Knee Replacement Arthroplasty and Osteotomy, J. Biomed. Eng., 7, Jan. 1985.

28. Cooke, T.D.V., Pichora, D., Siu, D., Scudamore, R.A., and Bryant, J.T., Surgical Implications of Varus Deformity of the Knee with

Obliquity of Joint Surfaces, J.B.J.S., 71-B, (4), 1989.

29. Cooke, T.D.V., Scudamore, R.A., Bryant, J.T., Sorbie, C., Siu, D., and Fisher, B., A Quantitative Approach to Radiography of the Lower Limb: Principles and Applications, J.B.J.S., 73-B, (5), 1991.

30. Crowninshield, R., Pope, M.H., and Johnson, R.J., An Analytical Model of the Knee, J. Biomech., 9, 1976.

31. Coventry, M.B. and Bowman, P.W., Long Term Results of Upper Tibial Osteotomy for Degenerative Arthritis of the Knee, Acta Orthop. Belg., 48, (1), 1982.

32. Coventry, M.B., Upper Tibial Osteotomy, Clin. Orthop. Rel. Res., 182, 1984.

33. Coventry, M.B., Current Concepts Review - Upper Tibial Osteotomy for Osteoarthritis, J.B.J.S., 67-A, (7), 1985.

34. Conventry, M.B., Proximal Tibial Varus Osteotomy for Osteoarthritis of the Lateral Compartment of the Knee, J.B.J.S., 69-A, (1), 1987.

35. Coventry, M.B., The Classic Osteotomy of the Upper Portion of the Tibia for Degenerative Arthritis of the Knee: A Preliminary Report, Clin. Orthop. Rel. Res., 248, 1989.

36. Day, W.H., Swanson, S.A.V., and Freeman, M.A.R., Contact Pressures in the Loaded Human Cadaver Hip, J.B.J.S., 57-B, (3), 1975.

37. Dias, J.J., Stirling, A.J., Finlay, D.B.L., and Gregg, P.J., Computerized Axial Tomography for Tibial Plateau Fractures, J.B.J.S., 69-B, (1), 1987.

38. Eftekhar, N.S., Total Knee Replacement Arthroplasty, J.B.J.S., 65-A, (3), March 1983.

39. Edholm, P., Lindahl, O., Lindholm, B., Myrnerts, R., Olsson, K., and

Wennberg, E., Knee Instability and Tibial Osteotomy - A Clinical Study, Acta Orthop. Scand., 48, 1977.

40. Elias, S.G., Freeman, M.A.R., and Gokcay, E.I., A Correlative Study of the Geometry and Anatomy of the Distal Femur, Clin. Orthop. Rel. Res., 260, 1990.

41. Engel, G.M. and Lippert, F.G., Valgus Tibial Osteotomy : Avoiding the Pitfalls, Clin. Orthop. Rel. Res., 160, 1981.

42. Engelbrecht, E., Bucholz, H.W., and Siegel, A., Characteristics of the Knee Joint Prosthesis Model "ST. Georg" and Clinical Experiences, I. Mech. Engr. CP-16, 1974.

43. Engin, A.E. and Korde, M.S., Biomechanics of Normal and Abnormal Knee Joint, J. Biomech., 7, 1974.

44. Engin, A.E., Passive and Active Resistive Force Characteristics in Major Human Joints, in Biomechanics of Normal and Pathological Human Articulating Joints, Ed. by N. Berme, A.E. Engin and K.M. Correira da Silva, Martinus Nijhoff Publ. NATO ASI Series, 1985.

45. Engin, A.E., Berme, N. and Akkas, N., Dynamic Modelling of Human Articulating Joints, in Biomechanics of Normal and Pathological Human Articulating Joints, Ed. by N. Berme, A.E. Engin and K.M. Correira da Silva, Martinus Nijhoff Publ., NATO ASI Series, 1985.

46. Engin, A.E., Mechanics of the Knee Joint Guidelines for Osteotomy in Osteoarthritis, in Orthopaedic Mechanics, Procedures and Devices, Ed. by D.N. Ghista and R. Roaf, Academic Press Inc., London, 1978.

47. Erkman, M.J., and Walker, P.S., A Study of Knee Geometry applied to the Design of Condylar Prostheses, Biomed. Eng., 1974.

48. Fairbank, T.J., Knee Joint changes after Menisectomy, J.B.J.S.,

30-B, 1948.

49. Fukubayashi, T. and Kurosawa, H., The Contact Area and Pressure Ditribution Pattern of the Knee, Acta Orthop. Scan., 51, 1980.

50. Gely, P., Drouin, G., Thiry, P.S., and Tremblay, G.R., Torsion and Bending Imposed on a New Anterior Cruciate Prosthesis During Knee Flexion: An Evaluation Method, J. of Biomech. Eng., 106, 1984.

51. Goldflies, M.L., Andriacchi, T.P., and Galante, J.O., The Relationship Between Varus Deformity and Moments at the Knee During Gait and Changes at the Knee after High Tibial Osteotomy, Orthop. Trans., 6, 1981.

52. Greenwald, A.S., and O'Connor, J.J., The Transmission of Load Through the Human Hip Joint, J. Biomech., 4, 1971.

53. Grood, E.S. and Hefzy, M.S., An Analytical Technique for Modelling Knee Joint Stiffness - Part 1: Ligamentous Forces, J. of Biomech. Eng., 104, 1982.

54. Grood, E.S. and Suntray, W.J., A Joint Coordinate System for the Clinical Description of Three Dimensional Motions: Application to the Knee, J. of Biomech. Eng., 105, 1983.

55. Guilak, F., Hou, J.S., Ratcliffe, A., and Mow, V.C., A. ticular Cartilage under Hydrostatic Loading, AMSE Publ.,New York, BED - Vol. 8, 1988.

56. Harding, M.L., Harding, L., and Goodfellow, J.W., Technical Note: A Preliminary Report of a Simple Rig to aid Study of the Functional Anatomy of the Human Knee Joint, J. Biomech., 10, 1977.

57. Harper, M.C. and Canale, S.T., Angulation Osteotomy : A Triangular Analysis, Clin. Orthop. Rel. Res., 166, 1982.

58. Harrington, I.J., Static and Dynamic Loading Patterns in Knee Joints with Deformities, J.B.J.S., 65-A, (2), 1983.

59. Hart, R.A., Mote, C.D., and Skinner, H.B., A Finite Helical Axis as a Landmark for Kinematic Reference of the Knee, J. Biomech. Eng., (113), 1991.

60. Hernigou, P.H., Medevielle, D., Debeyne, J., and Goutallier, D., Proximal Tibial Osteotomy for Osteoarthritis with Varus Deformity: A Ten to Thirteen Year Follow-up Study, J.B.J.S., 69-A, (3), 1987.

61. Hille, E., Schulitz, K.P., and Schneider, T., Pressure and Contact-Surface Measurements Within the Femoropatellar Joint and Their Variations Following Lateral Release, Acta. Orthop. Trauma. Surg., 104, 1985.

62. Hsieh, H.H., and Walker, P.S., Stabilizing Mechanisms of the Loaded and Unloaded Joint, J.B.J.S., 58-A, (1), 1976.

63. Hsu, R.W., Himeno, S., Conventry, M., and Chao, E.Y.S., Normal Axis Alignment of the Lower Extremity and Load Bearing Distribution at the Knee, Clin. Orthop. Rel. Res., (255), 1990.

64. Huiskes, R., Kremers, J., DeLange, A., Woltring, H.J., Selvik, G., and Van Rens, Th. J.G., Analytical Stereophotogrammetric Determination of Three Dimensional Knee Joint Geometry, J. Biomech., 18, (8), 1985.

65. Huiskes, R., Van Dijk, R., de Lange, A., Woltring, H.J., and Van Rens, Th. J.G., Kinematics of the Human Knee Joint, in Biomechanics of Normal and Pathological Human Articulating Joints, Ed. by N. Berme, A.E. Engin and K.M. Correia da Silva, Martinus Nijhoff Publ., NATO ASI Series, Dordrecht, 1985.

66. Hsu, H.P., Garg, A., Walker, P.S., Spector, M., and Ewald, F.C.,

Effect of Knee Compartment Alignment on Tibial Load Distribution with Clinical Correlation, Clin. Orthop. Rel. Res., 248, 1989.

67. Inaba, H., and Arai, M., A Method for Measuring Contact Pressures Instantaneously in Articular Joints, J. Biomech., 22, (11/12), 1989.

68. Inaba, H., and Arai, M., Direct Measurement of Dynamic Contact Pressure on the Tibial Plateau of the Knee, in Biomechanics: Basic and Applied Research. Ed. by G. Bergmann, Kölbel, R. and A. Rohlmann, Martinus Nijhoff Publ., Dordrecht, 1987.

69. Insall, J.N., Joseph, D.M., and Msika, C., High Tibial Osteotomy for Varus Gonarthrosis, J.B.J.S., 66-A, (7), 1984.

70. Jiang, C.C., Hang, Y.S., and Liu, T.K., A New Jig for Proximal Tibial Osteotomy, Clin. Orthop. Rel. Res., 226, 1988.

71. Jiang, C.C. and Insall, J.N., Effect of Rotation on the Axial Alignment of the Femur: Pitfalls in the use of Intermedullary Guides in Total Knee Arthoplasty, Clin. Orthop. Rel. Res., 248, 1989.

72. Johnson, E.E., Multiplane Correctional Osteotomy of the Tibial for Diaphyseal Malunion, Clin. Orthop. Rel. Res., 215, 1987.

73. Johnson, F., Leitl, S., and Waugh, W., The Distribution of Load Across the Knee, A Comparison of Static and Dynamic Measurements, J.B.J.S., 62-B, 3, 1980.

74. Johnson, F., Scarrow, P., and Waugh, W., Assessments of Loads on the Knee Joint, Med. and Biol. Eng. and Comput., 19, 1981.

75. Johnson, F. and Waugh, W., Method for Routine Clinical Assessment of Knee Joint Forces, Med. Biol. Eng. and Comput., 17, 1979.

76. Jokio, P.J., Lindholm, T.S., and Vankka, E., Comparison Between Radiologic Lower Extremity Angles of Femur and Tibia and Articular

Surface Pressure Measurements in Gonarthrosis Treated by High Tibial Osteotomy, Acta Orthop. Belgica., 50, 1984.

77. Kanaujia, R.R., Yoshioka, K., and Murakami, T., A Fixation Device for Corrective Osteotomy : Brief Report, J.B.J.S., 70-B, 2, 1988.

78. Kärrholm, J., Selvik, G., Elmqvist, L., and Hansson, L.I., Active Knee Motion after Cruciate Ligment Rupture : Stereoradiography, Acta Orthop. Scand., 59, (2), 1988.

79. Kennedy, J.C. and Fowler, P.J., Medial and Anterior Instability of the Knee, J.B.J.S., 53-A, (7), 1971.

80. Kettalkamp, D.B. and Jacobs, A.W., Tibiofemoral Contact Area - Determination and Implications, J.B.J.S., 54-A, (2), 1972.

81. Kettalkamp D.B. and Chao, E.Y.S., A Method for Quantitative Analysis of the Medial and Lateral Compression Forces at the Knee During Standing, Clin. Orthop. Rel. Res., 83, , 1972.

82. Kettalkamp, D.B., Leach, R.E., and Nasca, R., Pitfalls of Proximal Tibial Osteotomy, Clin. Orthop. Rel. Res., 106, 1975.

83. Kettalkamp, D.B., Wenger, D.R., Chao, E.Y.S., and Thompson, C., Results of Proximal Osteotomy, The Effects of Tibiofemoral Angle, Stance-Phase Flexion-Extension and Medial Plateau Force, J.B.J.S., 58-A, (7), 1976.

84. Kettalkamp, D.B. and Nasca, R., Biomechanics and Knee Replacement Arthroplasty, 7th Applied Mechanisms Conference, Oklahoma State University, 1981.

85. Kettalkamp, D.B., and Colyer, R.A., Osteoarthritis of the Knee, in Osteoarthritis, Diagnosis and Management, Ed. by R.W. Moskowitz, D.S. Howell, V.M. Goldberg and H.J. Mankin, W.B. Saunders Company,

Philadelphia, London, Toronto, 1984.

86. King, A.I., A Review of Biomechanical Models, J. of Biomech. Eng., 106, 1984.

87. Kinzel, G.L. and Gutkowski, L.J., Joint Models, Degrees of Freedom and Anatomical Motion Measurement, J. of Biomech. Eng., 105, 1983.

88. Krackow, K.A., Pepe, C.L., and Galloway, E.J., Basic Science: A Mathematical Analysis of trhe Effect of Flexion and Rotation on Apparent Varus/Valgus Alignment at the Knee, Orthop., 13, (8), 1990.

89. Krackow, K.A., Techniques of Knee Arthoplasty, C.V. Mosby Co., St. Louis, 1990.

90. Krackow, K.A., Review: Approaches to Planning lower Extremity Alignment of Total Knee Arthoplasty and Osteotomy about the Knee, Adv. in Orthop. Surg., 1983.

91. Kreighbaum, E. and Barthels, K.M., Biomechanics: A Qualitative Approach for Studying Human Movement, Burgess Publ. Co., Minn., 1981.

92. Kurosawa, H., Walker, P.S., Abe, S., Garg, A., and Hunter, T., Geometry and Motion of the Knee for Implant and Orthotic Design, J. Biomech., 18, 1985.

93. Kwan, M.K., Lai, W.M., and Mow, V.C., Fundamentals of Fluid Transport through Cartilage in Compression, Annals Biomed. Eng., 12, 1984.

94. Lewis, J.L., Lew, W.D., and Schmidt, J., Description and Error Evaluation of an In Vitro Knee Joint Testing System, J. Biomech. Eng., 110, 1988.

95. Manouel, M., Pearlman, H.S., Belakhlef, A., and Brown, T.D., Technical Note: A Miniature Piezoelectric Polymer Transducer for In

Vitro Measurement of the Dynamic Contact Stress Distribution, J. Biomech., 25, (6), 1992.

96. Mansour, J.M. and Pereira, J.M., Quantitative Functional Anatomy of the Lower Limb with Application to Human Gait, J. Biomech., 20, (1), 1987.

97. Maquet, P.G., Van Der Berg, A.J., and Simonet, J.C., Femorotibial Weight-Bearing Areas, J.B.J.S., 57-A, (6), 1975.

98. Maquet, P., Biomechanics of the Knee Joint. 2nd Ed., Springer-Verlag, Berlin, Heidelberg, New York, 1984.

99. Maquet, P., The Treatment of Choice in Osteoarthritis of the Knee, Clin. Orthop. Rel. Res., 192, 1985.

100. Markolf, K.L., and Amstutz, H.C., The Clinical Relevance of Instrumented Testing for ACL Insufficiency: Experience with the UCLA Clinical Knee Testing Apparatus, Clin. Orthop. Rel. Res., 223, 1987.

101. Markolf, K.L., Bargar, W.L., Shoemaker, S.C., and Amstotz, H.C., The Role of Joint Load in Knee Stability. J.B.J.S., 63-A, (4), 1981.

102. Martin, J.W., and Whiteside, L.A., The Influence of Joint Line Position on Knee Stability After Condylar Knee Arthroplasty, Clin. Orthop. Rel. Res., 259, 1990.

103. Matthews, L.S., Goldstein, S.A., Malvitz, T.A., Katz, B.P., and Kaufer, H., Proximal Tibial Osteotomy, Clin. Orthop. Rel. Res., 229, 1988.

104. McKellop, H.A., Sigholm, G., Redfern, F.C., Dolye, B., Sarmiento, A., and Luck, J.V., The Effect of Simulated Fracture-Angulations of the Tibia on Cartilage Pressures in the Knee Joint, J.B.J.S., 73-A, (9), 1991.

105. Meachim, G. and Brooke, G., The Pathology of Osteoarthritis, in Osteoarthritis - Diagnosis and Management. Ed. by R.W. Moskowitz, D.S. Howell, V.M. Goldberg and H.J. Mankin, W.B. Saunders Co., 1984.

106. Messieh, S.S., Fowler, P.J., and Munro, T., Anterior Radiographs of the Osteoarthritic Knee, J.B.J.S., 72-B, 4, 1990.

107. Moore, T.M. and Harvey, J.P., Roentgenographic Measurement of Tibial Plateau Depression Due to Fracture, J.B.J.S., 56-A, (1), 1974.

108. Mikosz, R.P., Andriacchi, T.P., and Anderson, G.B., Model Analysis of Factors Influency the Predictions of Muscle Forces at the Knee, J. Orthop. Res., 6, 1988.

109. Minns, R.J., Forces at the Knee Joint : Anatomical Considerations, J. Biomech., 14, (9), 1981.

110. Miyanaga, Y., Fukubayashi, T., and Kurosawa, H., Contact Study of the Hip Joint Load Deformation Pattern, Contact Area and Contact Pressure, Acta. Orthop. Trauma Surg., 103, 1984.

111. Moreland, J.R., Mechanisms of Failure in Total Knee Arthroplasty, Clin. Orthop. Rel. Res., 226, 1988.

112. Morrey, B.F., Upper Tibial Osteotomy for Secondary Osteotarthritis of the Knee, J.B.J.S., 71-B, (4), 1989.

113. Morrison, J.B., The Mechanics of the Knee Joint in Relation to Normal Walking, J. Biomech., 3, 1970.

114. Muller, W., The Knee, Form, Function and Ligament Reconstruction. Springer-Verlag, Berlin, Heidelberg, New York, 1983.

115. Murray, M.P., Gait as a Total Pattern of Movement, Am. J. Phys. Med., 46, 1967.

116. Myrnerts, R., The SAAB Jig : An Aid in High Tibial Osteotomy, Acta

Orthop. Scand., 49, 1978.

117. Nisell, R., Mechanics of the Knee, A Study of Joint Muscle Load with Applications, Acta Orthop. Scand. Suppl., 216, (56), 1985.

118. Nissan, M., Review of Some Basic Assumptions in Knee Biomechanics, J. Biomech., 13, 1980.

119. Noyes, F.R., Levels of Knee Joint Research, How to Bridge the Gap, J. of Biomech. Eng., 108, 1986.

120. Odenbring, S., Egund, N., Hagstedt, B., Larsson, J., Lindstrand, A., and Toksvig-Larsen, S., Ten Year Results of Tibial Osteotomy for Medial Gonarthrosis: The Influence of Overcorrection, Arch. Orthop. Trauma Surg., 110, 1991.

121. Ogata, K., Interlocking Wedge Osteotomy of the Proximal Tibia for Gonarthrosis, Clin. Orthop. Rel. Res., 186, 1984.

122. Ogata, K., Yoshii, I., Miura, H., Arizono, T., and Sugioka, Y., Standing Radiographs can not determine the correction in High Tibial Osteotomy, J.B.J.S., 73-B, 6, 1991.

123. Paley, D., Chaudray, M., Pirone, A.M., Lentze, P., and Kantz, D., Treatment of Mal - Nonunions of the Femur and Tibia by Detailed Preoperative Planning and The Ilizarov Techniques, Orthop. Clin. of North Amer., 21, (4), 1990.

124. Paul, J.J., Force Actions Transmitted in the Knee of Normal Subjects and by Prosthetic Joint Replacements, I. Mech. Engr., CP16, 1974.

125. Pauwels, F., Atlas zur Biomechanik der gesunden und kranken Hüfte. Prinzipien, Techik und Resultate einer Kausalen Therapie. Springer, Berlin, Heidelberg, New York, 1973a.

126. Pennock, G.R. and Clark, K.J., An Anatomy Based Coordinate System for the Description of the Kinematic Displacements in the Human Knee, J. Biomech., 23, (12), 1990.

127. Pennwalt Corp., Kynar Piezo Film: Technical Manual, 1987.

128. Petersen, T.D. and Rohr, W. Improved Assessment of Lower Extremity Alignment Using New Roentgenographic Techniques, Clin. Orthop. Rel. Res., 219, 1987.

129. Prodromos, C.C., Andriacchi, T.P., and Galante, J.O., A Relationship between Gait and Clinical changes following High Tibial Osteotomy, J.B.J.S., 67-A, (8), 1985.

130. Puno, R.M., Vaughan, J.J., Von Fraunhofer, J.A., Stetten, M.L., and Johnson, J.R., A Method of Determining the Angular Malalignments of the Knee and Ankle Joints Resulting from a Tibial Malunion, Clin. Orthop. Rel. Res., 223, 1987.

131. Radin. E.L., Yang, K.H., Riegger, C., Kish, V.L., and O'Conner, J.J., Relationship between Lower Limb Dynamics and Knee Joint Pain, J. Orthop. Res., 9, 1991.

132. Radin, E.L., Biomechanical Considerations, in Osteoarthritis, Diagnosis and Management, Ed. by R.W. Moskowitz, D.S. Howell, V.M. Goldberg and H.J. Mankin, W.B. Saunders Company, Philadelphia, London, Toronto, 1984.

133. Rehder, U., Technical Note - Morphometrical Studies on Symmetry of the Human Knee Joint : Femoral Condyles, J. Biomech., 16, (5), 1983.

134. Riegger, C.L., Hayes, W.C., and Gerhart, T.N., Tibiofemoral Contact Pressure and Area in Neutral, Varus, and Post-osteotomy Loading Conditions, 33rd Mtg. Orthop. Res. Soc., San Fransico, Calif., 1987.

135. Reuleaux, E., Theortische Kinematic: Grundzüge einer Theorie des Maschinewesen, F. Kieveg und Sohn, Brauschweig, 1900. (also translated by A.B.W. Kennedy: The Kinematics of Machinery, reprinted by Dover Publication, New York, 1963.

136. Röhrle, H., Scholten, R., Sigolotto, C., Sollbach, W. and Kellner, H., Joint Forces in the Human Pelvis Leg Skeleton During Walking, J. Biomech., 17, (6), 1984.

137. Rudan, J.F., and Simurda, M.A., Valgus High Tibial Osteotomy: A Long Term Follow-up Study, Clin. Orthop. Rel. Res., 268, 1991.

138. Sangeorzan, B.P., Judd, R.P., and Sangeorzan, B.J., Technical Note: Mathematical Analysis of Single Cut Osteotomy for Complex Long Bone Deformity, J. Biomech., 22, (11/12), 1989.

139. Sasaki, T., Yagi, T., Monji, J., Yasuda, K., and Tsuge, H., High Tibial Osteotomy combined with Lateral Displacement of the Tibial Tubercle for Osteoarthritis of the Knee, Int. Orthop., 10, 1986.

140. Scherrer, P.K. and Hillberry, B.M., Piecewise Mathematical Representation of Articular Surfaces, J. Biomech., 12, 1979.

141. Schipplein, O.D. and Andriacchi, T.P., Interaction between Active and Passive Knee Stabilizers during Level Walking, J. of Orthop. Res., (9), 1991.

142. Schomtzer, H., Learmonth, I.D., and Vaughan, C.L., The effect of Selected Muscle Groups on Knee Pressure Distribution, 7th Meeting of European Soc. of Biomech., Denmark, 1990.

143. Seedhom, B.B., Transmission of the Load in the Knee Joint with Special Reference to the Role of the Menisci. Part I: Anatomy, Analysis and Apparatus, Eng. in Med., 8, 1979.

144. Seedhom, B.B. and Hargreaves, D.J., Transmission of the Load in the Knee Joint with Special Reference to the Role of the Menisci. Part II: Experimental Results, Discussion and Conclusion, Eng. in Med., 8, 1979.

145. Seireg, A. and Arvikar, R.J., The Prediction of Muscular Load Sharing And Joint Forces in the Lower Extremities During Walking, J. Biomech., 8, 1975.

146. Shaw, J.A. and Murray, D.G., Knee Joint Simulator, Clin. Orthop. Rel. Res., 194, 1973.

147. Shiavi, R., Limbird, T., Frazer, M., Stivers, K., Strauss, A., and Abromovitz, J., Helical Motion Analysis of the Knee - 1. Methodology for Studying Kinematics During Locomotion, J. Biomech., 20, (5), 1987.

148. Shigley, J.E., Mechanical Engineering Design, 3rd Ed., McGraw-Hill, Inc., New York, 1977.

149. Siu, D., Bryant, J.T., and Wevers, H.W. Three Dimensional Reconstruction of Joint Surface using a Microcomputer, Med. Biol. Eng. Comp., 1986.

150. Sommer, H.J. and Miller, N.R., A Technique for the Calibration of Instrumented Spatial Linkages used for Biomechanical Kinematic Measurements, J. Biomech., 14, 1981.

151. Soudan, K., Van Audekercke, R., and Martens, M., Methods, Difficulties, and Inaccuracies in the Study of Human Joint Kinematics and Pathokinematics by the Instant Axis Concept. Example: The Knee Joint, J. Biomech., 12, 1979.

152. Sundaram, N.A., Hallett, J.P., and Sullivan, M.F., Dome Osteotomy of the Tibia for Osteoarthritis of the Knee, J.B.J.S., 68-B, (5), 1986.

153. Suntay, W.J., Grood, E.S., Hefzy, M.S., Bulter, D.C., and Noyes,

F.R., Error Analysis of a System for Measuring Three Dimensional Joint Motion, J. Biomech. Eng., 105, 1983.

154. Szklar, O. and Ahmed, A.M., A Simple Unconstrained Dynamic Knee Simulator, J. of Biomech. Eng., 109., 1987.

155. Takei, T., Deformation of the Articular Cartilage and Joint Space under Static Load, J. Jap. Orthop. Ass., 53, 1979.

156. Townley, C.O., Total Knee Arthoplasty: A Personal Retrospective and Prospective Review, Clin. Orthop. Rel. Res., 236, 1988.

157. Townsend, M.A., Tzak, M., and Jackson, R.W., Total Motion Knee Goniometry, J. Biomech., 10, 1977.

158. Veldpaus, F.E., Woltring, H.J., and Dortmans, L.J., A Least Square Algorithm for the Equiform Transformation from Spatial Marker Coordinates, J. Biomech., 21, (1), 1988.

159. Walker, P.S. and Hajek, J.V., The Load Bearing Area in the Knee Joint, J. Biomech., 5, 1972.

160. Walker, P.S. and Erkman, M.J., The Role of the Menisci in Force Transmission Across the Knee, Clin. Orthop. Rel. Res., 109, 1975. (114)

161. Walker, P.S., Shoji, H., and Erkman, M.J., The Rotational Axis of the Knee and its Significance to Prosthesis Design, Clin. Orthop. Rel. Res., 89, 1972.

162. Waugh, W., Tibial Osteotomy in the Management of Osteoarthritis of the Knee, Clin. Orthop. Rel. Res., 210, 1986.

163. Whiteside, L.A., Kasselt, M.R., and Haynes, D.W., Varus-Valgus and Rotational Stability in Rotationally Unconstrained Total Knee Arthroplasty, Clin. Orthop. Rel. Res., 219, 1987.

164. Whiteside, L.A. and Amador, D.D., Rotational Stability of a

Posterior Stabilized Total Knee Arthroplasty, Clin. Orthop. Rel. Res., 242, 1989.

165. Wilder, M., Peters, A., Hellich, J., and Reichelt, A., Complications of High Tibial Osteotomy and Internal Fixations with Staples, Arch. Orthop. Trauma Surg., 111, 1992.

166. Williams, A.E., Rand, J.A., An, K.N., Chao, E.Y.S., and Kelly, P.J., The Early Healing of Tibial Osteotomies Stabilized by One Plane or Two Plane External Fixation, J.B.J.S., 69-A, (3), 1987.

167. Wilson, C.E., Salder, J.P., and Michels, W.J., Kinematics and Dynamics of Machinery, Harper and Row, Publ., New York, 1983.

168. Winter, D.A., Biomechanics of Human Movement, John Wiley & Sons, Inc., New York, 1979.

169. Wismans, J., Veldpaus, F. Janssen, J., Huson, A., and Struben, P., A Three Dimensional Mathematical Model of the Knee Joint, J. Biomech., 13, 1980.

170. Wolff, A.M. and Krackow, K.A., The Treatment of Nonunion Proximal Tibial Osteotomy with Internal Fixation, Clin. Orthop. Rel. Res., 250, 1990.

171. Wongchaisuwat, C., Hemami, H., and Buchner, H.J., Control of Sliding and Rolling at Natural Joints, J. of Biomech. Eng., 106, 1984.

172. Wright, J.G., Treble, N., and Feinstein, A.R., Measurement of Lower Limb Alignment using Long Radiographs, J.B.J.S., 73-B, 5, 1991.

173. Yasuda, K., and Sasaki, T., The Mechanics of Treatment of the Osteoarthritic Knee with a Wedged Insole, Clin. Orthop. Rel. Res., 215, 1987.

174. Yoshioka, Y., Siu, D., and Cooke, D.V., The Anatomy and Functional

Axes of the Femur, J.B.J.S., 69-A, (6), 1987.

```
C
C       PROGRAM TO SIMULATE THE CLOSE WEDGE OSTEOTOMY METHOD:
C       CONVENTIONAL AND MODIFIED APPROACHES
C       LABELS AND NOTATION CORRESPOND TO TEXT IN CHAPTER 4.0
C
      COMMON A1, CVN, TF, XL1, XL2, ATL, AW, DELTAH, DELTAA
      COMMON FMAO, TMAO, PI, TP, FL, TL, WP, PO
 100  WRITE(*,*) 'ENTER TIBIOFEMORAL ANGLE'
      READ(*,*) TF
      TF = TF * (-1.)
      WRITE(*,*) 'ENTER DEPTH OF OSTEOTOMY CUT FROM TIBIAL SURFACE'
      READ (*,*) D
      WRITE(*,*) 'ENTER WIDTH OF TIBIA AT LEVEL OF OSTEOTOMY'
      READ(*,*)  WC
      WRITE(*,*) 'FNTER LENGTH OF TIBIA'
      READ(*,*) TL
      WRITE(*,*) 'ENTER LENGTH OF FEMUR'
      READ(*,*) FL
      WRITE(*,*) ' ENTER WIDTH OF TIBIA PLATEAU'
      READ(*,*) WP
      WRITE(*,*) ' ENTER TILT OF TIBIAL PLATEAU'
      READ(*,*) TP
      WRITE(*,*) 'TIBIAL PLATEAU OFFSET'
      READ(*,*) PO
C
C     CONVERT ANGLE VALUES TO RADIANS:
C
      PI = 4* ATAN(1.)
      CVN = PI / 180.
      TF = TF * CVN
      PO = PO*CVN
      TP = TP * CVN
C     CALCULATE ANGULAR OFFSET BETWEEN A VERTICAL REFERENCE
C     FRAME AND THE MECHANICAL AXES OF THE FEMUR AND TIBIA.
      DIFF = 1
      AA = ABS(TF/5)
      DO WHILE (DIFF .GT. .01)
      EQ1 = FL * SIN(ABS(TF) - AA)
      EQ2 = TL * SIN(AA)
      DIFF = EQ1 - EQ2
      AA = AA + .01 * CVN
      END DO
C     CALCULATE OFFSET OF MECHANICAL AXES.
      FMAO = PI/2. - (ABS(TF) - AA)
      TMAO = PI/2. + AA
      XL = WC / 2.
      A1 = ATAN(XL/D)
      XL2 = D / COS(A1)
      XL1 = SQRT(XL2 * XL2 + TL*TL - (2 * TL * XL2 * COS(A1) ) )
      X1 = TL * TL - XL2 * XL2 - XL1 * XL1
      ATL = ACOS(X1 / (-2 * XL1 * XL2) )
C
C     CASE 1) CONVENTIONAL APPROACH:
C
      ATLP = ATL - ABS(TF)
C
C     RESULTANT CORRECTION IS TMA:
C
      AW = ABS(TF)
      TLP = SQRT(XL1 * XL1 + XL2 * XL2 - 2 * XL1 * XL2 * COS(ATLP) )
```

```
      A1P   ACOS( (XL1 * XL1 - TLP*TLP - XL2*XL2) / (-2*TLP*XL2) )
      ATMA  A1P - A1
      TFP   ATMA - ABS(TF)
C
C     ANGULAR OFFSET OR UNDERCORRECTION FROM NEUTRAL ALIGNMENT:
C
      UC  ATMA - ABS(TF)
C
C     IF TFP < 0  THEN VARUS OR UNDERCORRECTED KNEE ALIGNMENT.
C     IF TFP > 0  THEN VALGUS OR OVERCORRECTED KNEE ALIGNMENT.
C
      WRITE(*,*) 'Case 1):'
      WRITE(*,*) 'TF', TF / CVN ,' DEG'
C
      WRITE(*,*) 'RESULTANT ANGULAR CORRECTION ', ATMA/CVN ,' DEG'
      WRITE(*,*) ' UNDERCORRECTION (UC)' ,UC/CVN ,' DEG'
C
C     CASE 2) MODIFIED APPROACH:
C
      A1PP = A1 + ABS(TF)
      X2 = 2 * XL2 * COS(A1PP)
      X3 = - 2 * XL2 * COS(A1PP)
      X4 = 4 * (XL2 * XL2 - XL1 * XL1)
      TLPP = ( X2 + SQRT(X3 * X3 - X4) ) / 2
      ATLPP = ACOS( (XL1*XL1 + XL2*XL2 - TLPP*TLPP) / (2 * XL1 * XL2) )
C
C     DEGREEE OF WEDGE CORRECTION :
C
      AWPP = ATL - ATLPP
C
C     DEGREE OF ADDITIONAL CORRECTION FROM CONVENTIONAL APPROACH:
C
      AC = AWPP - AW
C
C     LEG LENGTH  AND JOINT ANGLE ADJUSTMENTS:
C
      SLL = FL * SIN(FMAO) + TL * SIN(TMAO)
      SLLP = FL + TLPP
      SLLRED = (SLLP - SLL)/ SLL * 100.
      DELTAH = ABS(FMAO - PI/2)
      DELTAA = AWPP - DELTAH
C
C     TIBIAL PLATEAU TILT:
C
      TPP = TP + DELTAH
      WRITE(*,*) ' CASE 2) NEUTRAL ORIENTATION:'
      WRITE(*,*) 'ADDITIONAL CORRECTION FROM CONVENTIONAL CASE:
     + ', AC/CVN ,'DEG'
      WRITE(*,*) 'DEGREE OF WEDGE CORRECTION ' , AWPP/CVN ,' DEG'
      WRITE(*,*) 'RESULTANT STANDING LEG LENGTH ', SLLP ,' mm'
      WRITE(*,*) 'RELATIVE CHANGE IN LEG LENGTH', SLLRED ,' %'
      WRITE(*,*) 'REQUIRED HIP ROTATION: ', DELTAH / CVN   ,' DEG'
      WRITE(*,*) 'REQUIRED ANKLE ROTATION: ', DELTAA  / CVN  ,' DEG'
      WRITE(*,*) 'TIBIAL PLATEAU TILT FROM HORIZONTAL: '
     +, TPP/ CVN ,' DEG'
C
C     CONTINUE FOR CALCULATION OF OVERCORRECTED ALIGNMENT CASES.
C
      CALL CASE1 ()
C
```

```
      CALL CASE2 ()
      WRITE(*,*) ' CONTINUE (Y - 1/N   2)'
      READ(*,*) ANSW
      IF (ANSW .EQ. 1) GOTO 100
      END
C
C
C
      SUBROUTINE CASE1 ()
C
C     CASE 1) CONVENTIONAL APPROACH OVERCORRECTED CASE:
      COMMON A1, CVN, TF, XL1, XL2, ATL, AW, DELTAH, DELTAA
      COMMON FMAO, TMAO, PI, TP, FL, TL, WP, PO
      WRITE(*,*) 'ENTER OVERCORRECTION: (DEG) '
      READ(*,*) OC
      OC = OC * CVN
      ATLOC = ATL - ABS(TF) - OC
C
C
C     RESULTANT CORRECTION IS ATMA:
C
      AWOC = ABS(TF)+ OC
      TLPOC = SQRT( XL1*XL1 + XL2*XL2 - 2*XL1*XL2*COS(ATLOC) )
      A1OC = ACOS( (XL1*XL1-TLPOC*TLPOC-XL2*XL2)/(-2*TLPOC*XL2) )
      ATMAOC = A1OC - A1
C
C     ANGULAR OFFSET OR UNDERCORRECTION FROM A
C     PRE-SELECTED OVERCORRECTED VALGUS ALIGNMENT:
C
      UCOC = ABS(ATMAOC - ABS(TF) - OC)
      TFOC = OC - UCOC
C
C     IF TFP < 0  THEN VARUS OR UNDERCORRECTED KNEE ALIGNMENT.
C     IF TFP > 0  THEN VALGUS OR OVERCORRECTED KNEE ALIGNMENT.
C
      WRITE(*,*) 'Case 1) OVERCORRECTED:'
      WRITE(*,*) 'TF', TF / CVN ,' DEG'
C
      WRITE(*,*) 'RESULTANT ANGULAR CORRECTION ', ATMAOC/CVN ,' DEG'
      WRITE(*,*) ' UNDERCORRECTION (UC) ' ,UCOC/CVN ,' DEG'
      WRITE(*,*) 'RESULTANT VALGUS TF ALIGNMENT ',TFOC/CVN, ' DEG'
      RETURN
      END
C
C
C
      SUBROUTINE CASE2 ()
      COMMON A1, CVN, TF, XL1, XL2, ATL, AW, DELTAH, DELTAA
      COMMON FMAO, TMAO, PI, TP, FL, TL, WP, PO
C
C     CASE 2): OVERCORRECTED ORIENTATION
C
C
C
      WRITE(*,*) 'ENTER AMOUNT OF OVERCORRECTION IN DEGREES'
      READ(*,*) OC
      OC = OC* CVN
      A1PPP = A1 + ABS(TF) + OC
      X2 = 2 * XL2 * COS(A1PPP)
      X3 = - 2 * XL2 * COS(A1PPP)
```

```
      X4 = 4 * (XL2 * XL2 - XL1 * XL1)
      TLPPP = ( X2 + SQRT(X3 * X3 - X4) ) / 2
      ATLPPP = ACOS( (XL1*XL1 + XL2*XL2 - TLPPP*TLPPP) / (2*XL1*XL2) )
C
C     DEGREEE OF WEDGE CORRECTION :
C
      AWPPP = ATL - ATLPPP
C
C     AMOUNT OF ADDITIONAL CORRECRTION:
C
      AC = AWPPP - (AW + OC)
C
C     LEG LENGTH  AND JOINT ANGLE ADJUSTMENTS:
C
      ASLPPP = PI - OC
      SLL = FL * SIN(FMAO) + TL * SIN(TMAO)
      SLLPPP = SQRT(FL*FL + TLPPP*TLPPP - 2*FL*TLPPP*COS(ASLPPP) )
      SLLREDP = (SLLPPP - SLL) / SLL * 100.
      ALLH = ACOS((SLLPPP*SLLPPP+FL*FL-TLPPP*TLPPP)/(2*SLLPPP*FL))
      ALLA = ABS(OC - ALLH)
      DLTHPPP = ALLH + DELTAH
      DLTAPPP = AWPPP - DLTHPPP
C
C     TIBIAL PLATEAU TILT:
C
      TPPP = TP + DLTHPPP
C
C     LOCATION OF LOAD VECTOR RELATIVE TO MEDIAL MARGIN:
C
C
      LL = FL * SIN(ALLH) / SIN(PI - (PO+ ABS(TF) + ALLH) )

C
      SHIFT = (LL + WP/2) / WP * 100.
C
      WRITE(*,*) ' CASE 2) OVERCORRECTED ORIENTATION:'
      WRITE(*,*) 'RESULTANT WEDGE CORRECTION: ' , AWPPP / CVN ,' DEG'
      WRITE(*,*) 'ADDITIONAL CORRECTION FROM CONVENTIONAL CASE: '
     + , AC/CVN , 'DEG'
      WRITE(*,*) 'RESULTANT STANDING LEG LENGTH: ', SLLPPP ,' mm'
      WRITE(*,*) 'RELATIVE CHANGE IN LEG LENGTH: ', SLLREDP ,' %'
      WRITE(*,*) 'REQUIRED HIP ROTATION: ', DLTHPPP / CVN ,' DEG'
      WRITE(*,*) 'REQUIRED ANKLE ROTATION: ', DLTAPPP  / CVN ,' DEG'
      WRITE(*,*) 'TIBIAL PLATEAU TILT ', TPPP / CVN ,' DEG'
      WRITE(*,*) 'PERCENT LATERAL SHIFT ', SHIFT ,' %'
      RETURN
      END
```

```
C
C       PROGRAM FOR DOME OR (BARREL VAULT) OSTEOTOMY METHOD:
C           CONVENTIONAL AND MODIFIED APPROACHES
C
      COMMON D5, D, R, CVN, TF, AD, DAH
      COMMON FMAO, TMAO, PI, TP, DF, WP, PO, TL
  100 WRITE(*,*) 'ENTER TIBIOFEMORAL ANGLE'
      READ(*,*) TF
       TF = TF * (-1.)
      WRITE(*,*) 'ENTER DEPTH OF OSTEOTOMY CUT FROM TIBIAL SURFACE'
      READ (*,*) D
      WRITE(*,*) 'WIDTH OF CUT'
      READ(*,*) WC
      WRITE(*,*) 'ENTER RADIUS OF OSTEOTOMY'
      READ(*,*)  R
      WRITE(*,*) 'ENTER LENGTH OF TIBIA'
      READ(*,*) TL
      WRITE(*,*) 'ENTER LENGTH OF FEMUR'
      READ(*,*) DF
      WRITE(*,*) ' ENTER WIDTH OF TIBIAL PLATEAU'
      READ(*,*) WP
      WRITE(*,*) ' ENTER TILT OF TIBIAL PLATEAU'
      READ(*,*) TP
      WRITE(*,*) 'TIBIAL PLATEAU OFFSET'
      READ(*,*) PO
C
C     CONVERT ANGLE VALUES TO RADIANS:
C
      PI = 4* ATAN(1.)
      CVN = PI / 180.
      TF = TF * CVN
      PO = PO*CVN
      TP = TP * CVN
C     CALCULATE ANGULAR OFFSET BETWEEN VERTICAL
C     PLANE AND MECHANICAL AXES OF THE FEMUR AND TIBIA.
      DIFF = 1
      AA = ABS(TF/5)
      DO WHILE (DIFF .GT. .01)
      EQ1 = DF * SIN(ABS(TF) - AA)
      EQ2 = TL * SIN(AA)
      DIFF = EQ1 - EQ2
      AA = AA + .01 * CVN
      END DO
C     CALCULATE INITIAL OFFSET OF MECHANICAL AXES.
      FMAO = PI/2. - (ABS(TF) - AA)
      TMAO = PI/2. + AA
C
      A4 = PI - ABS(TF)
      D4 = SQRT(DF**2 + D**2 - 2* DF * D *COS(A4))
C
C     DOME TF ANGLE:
C
      ATFD = ACOS( (D**2 + D4**2 - DF**2) /( 2*D*D4) )
      AD = ATFD
C
C     CASE 1) CONVENTIONAL METHOD:
C
      D5 = TL - D - R
      A6P = PI - AD
      D6P = SQRT( (D+R)**2 + D5**2 - (2*(D+R)*D5*COS(A6P)) )
```

```
      A5P = ACOS(( (D+R)**2 + D6P**2 - D5**2) / (2*(D+R)*D6P) )
C
C     RESULTANT CORRECTION IS TMA:
C
      TMAD = A5P
C
C     RESULTANT LOWER LIMB ALIGNMENT:
C
      TFP = TMAD - ABS(TF)
C
C     ANGULAR OFFSET OR UNDERCORRECTION FROM NEUTRAL ALIGNMENT:
C
      UC = ABS(TFP)
C
C    IF TFP < 0  THEN VARUS OR UNDERCORRECTED KNEE ALIGNMENT.
C    IF TFP > 0  THEN VALGUS OR OVERCORRECTED KNEE ALIGNMENT.
C
      WRITE(*,*) 'Case 1):'
      WRITE(*,*) 'RESULTANT ANGULAR CORRECTION ', TMAD/CVN ,' DEG'
      WRITE(*,*) ' UNDERCORRECTION (UC)' ,UC/CVN ,' DEG'
C
C     CASE 2) MODIFIED APPROACH:
C
      A5PP =  ABS(TF)
      X1 = 2 * (D+R) * COS(A5PP)
      X2 = 4 * ( (D+R)**2  - D5**2)
      D6PP = ( X1 + SQRT(X1**2  - X2) ) / 2
      A6PP = ACOS( (D5**2 +(D+R)**2 - D6PP**2) / (2 * (D+R) * D5) )
C
C     DEGREEE OF ROTATION CORRECTION :
C
      ADPP = PI - A6PP
C
C     DEGREE OF ADDITIONAL CORRECTION FROM CONVENTIONAL APPROACH:
C
      ACD = ADPP - AD
C
C     LEG LENGTH  AND JOINT ANGLE ADJUSTMENTS:
C
      SLL = DF * SIN(FMAO) + TL * SIN(TMAO)
      SLLPP = DF + D6PP
      SLLRED = (SLLPP - SLL)/ SLL * 100.
      DAH = ABS(FMAO - PI/2)
      DAA = ADPP - DAH
C
C     TIBIAL PLATEAU TILT:
C
      TPP = TP + DAH

      WRITE(*,*) ' CASE 2) NEUTRAL ORIENTATION:'
      WRITE(*,*) 'ADDITIONAL CORRECTION FROM CONVENTIONAL CASE:
     + ', ACD/CVN ,'DEG'
      WRITE(*,*) 'DEGREE OF ROTATIONAL CORRECTION ' , ADPP/CVN ,' DEG'
      WRITE(*,*) 'RESULTANT STANDING LEG LENGTH ', SLLPP ,' mm'
      WRITE(*,*) 'RELATIVE CHANGE IN LEG LENGTH', SLLRED ,' %'
      WRITE(*,*) 'REQUIRED HIP ROTATION: ', DAH / CVN    ,' DEG'
      WRITE(*,*) 'REQUIRED ANKLE ROTATION: ', DAA  / CVN  ,' DEG'
      WRITE(*,*) 'TIBIAL PLATEAU TILT FROM HORIZONTAL: '
     +, TPP/ CVN ,' DEG'
C
```

```
C     CALCULATE THE OVERCORRECTED ALIGNMENT CONDITIONS:
C
      CALL CASE1 ()
C
      CALL CASE2 ()
      WRITE(*,*) ' CONTINUE (Y = 1/N = 2)'
      READ(*,*) ANSW
      IF (ANSW .EQ. 1) GOTO 100
      END
C
C
C
      SUBROUTINE CASE1()
C
C     CASE 1) CONVENTIONAL APPROACH OVERCORRECTED CASE:
C
      COMMON D5, D, R, CVN, TF, AD,DAH
      COMMON FMAO. TMAO, PI, TP, DF, WP, PO, TL
      WRITE(*,*) 'ENTER OVERCORRECTION; (DEG) '
      READ(*,*) OC
      OC = OC * CVN
      A6OC = PI-AD-OC
      D6POC = SQRT( (D+R)**2 +D5**2 - 2*(D+R)*D5*COS(A6OC) )
      A5POC = ACOS( ((D+R)**2 + D6POC**2 - D5**2) / (2*(D+R)*D6POC) )
      TMADOC = A5POC
      UCOC = ABS(TMADOC - ABS(TF) - OC)
C
C
C     RESULTANT CORRECTION IS TMA:
C
C     ANGULAR OFFSET OR UNDERCORRECTION FROM OVERCORRECTED ALIGNMENT:
C
      TFPOC = OC - UCOC
C
C     IF TFP < 0  THEN VARUS OR UNDERCORRECTED KNEE ALIGNMENT.
C     IF TFP > 0  THEN VALGUS OR OVERCORRECTED KNEE ALIGNMENT.
C
      WRITE(*,*) 'Case 1) OVERCORRECTED:'
      WRITE(*,*) 'TF', TF / CVN ,' DEG'
      WRITE(*,*) 'RESULTANT ANGULAR CORRECTION ', TMADOC/CVN ,' DEG'
      WRITE(*,*) ' UNDERCORRECTION (UC)' , UCOC/CVN , ' DEG'
      WRITE(*,*) ' RESULTANT TF ANGLE: ', TFPOC/CVN, 'DEG'
      RETURN
      END
C
C
C
      SUBROUTINE CASE2 ()
      COMMON D5, D, R, CVN, TF, AD,DAH
      COMMON FMAO, TMAO, PI, TP, DF, WP, PO, TL
C
C     CASE 2): OVERCORRECTED ORIENTATION
C
      WRITE(*,*) 'ENTER AMOUNT OF OVERCORRECTION IN DEGREES'
      READ(*,*) OC
      OC = OC* CVN
      A5PPOC = ABS(TF) + OC
      X1 = 2 * (D+R) * COS(A5PPOC)
      X2 = 4 * ((D+R)**2 - D5**2 )
      D6PPOC = ( X1 + SQRT(X1**2 - X2) ) / 2
```

```
      A6PPOC   ACOS( (D5**2 +(D+R)**2 - D6PPOC**2) / (2*(D+R)*D5) )
C
C     DEGREEE OF ROTATIONAL CORRECTION :
C
      ADPPOC = PI - A6PPOC
C
C     AMOUNT OF ADDITIONAL CORRECRTION:
C
      ACDOC = ADPPOC - AD - OC
C
C     LEG LENGTH  AND JOINT ANGLE ADJUSTMENTS:
C
      SLL = DF * SIN(FMAO) + TL * SIN(TMAO)
      SLLOC = SQRT(DF**2 + D6PPOC**2 - 2*DF*D6PPOC*COS(PI - OC) )
      SLLREDP = (SLLOC - SLL) / SLL * 100.
      DAHOC = ACOS((SLLOC**2+DF**2-D6PPOC**2)/(2*SLLOC*DF))
      DAAOC = ABS(OC - DAHOC)
      THROT = DAHOC + DAH
      TAROT = ADPPOC - THROT
C
C     TIBIAL PLATEAU TILT:
C
      TPPOC = TP + THROT
C
C     LOCATION OF LOAD VECTOR RELATIVE TO MEDIAL MARGIN:
C
C
      LL = DF * SIN(DAHOC) / SIN(PI - (PO+ ABS(TF) + DAHOC) )

C
      SHIFT = (LL + WP/2) / WP * 100.
C
      WRITE(*,*) ' CASE 2) OVERCORRECTED ORIENTATION:'
      WRITE(*,*) 'RESULTANT ROTATIONAL CORRECTION: ' ,ADPPOC/CVN,' DEG'
      WRITE(*,*) 'ADDITIONAL CORRECTION FROM CONVENTIONAL CASE: '
     + , ACDOC/CVN , 'DEG'
      WRITE(*,*) 'RESULTANT STANDING LEG LENGTH: ', SLLOC ,' mm'
      WRITE(*,*) 'RELATIVE CHANGE IN LEG LENGTH: ', SLLREDP ,' %'
      WRITE(*,*) 'REQUIRED HIP ROTATION: ', THROT / CVN ,' DEG'
      WRITE(*,*) 'REQUIRED ANKLE ROTATION: ', TAROT  / CVN ,' DEG'
      WRITE(*,*) 'TIBIAL PLATEAU TILT ', TPPOC / CVN ,' DEG'
      WRITE(*,*) 'PERCENT LATERAL SHIFT ', SHIFT ,' %'
      RETURN
      END
```